Novel conductive alkaline polymer membranes for fuel cells

Thesis submitted for the degree of

Doctor of Philosophy

University of Strathclyde

Gregory A. D. Mann

Department of Chemical and Process Engineering

University of Strathclyde, Glasgow

2017

This thesis is the result of the author's original research. It has been composed by the author and has not been previously submitted for examination which has led to the award of a degree.

Signed:

Date:

Abstract

A series of anion exchange membranes synthesised from poly (2, 6-dimethyl-1, 4-phenylene oxide) (PPO) have been investigated for water electrolysis applications. The prepared membranes were characterised using electrochemical impedance spectroscopy, infrared spectroscopy and thermal gravimetric analysis.

Initial membranes showed very low ionic conductivity and poor stabilities (> 60 ^{o}C). Improvements to these membranes were sought by investigating the chloromethylation of PPO as well as chemical cross-linking. Cross-linking of the membranes produced a small increase in stability however these membranes remained unstable at temperatures above 70 ^{o}C. Increasing the chloromethylation reaction time to 6 hours proved to be the only way of increasing both ionic conductivity and stability, however membrane stabilities at 90 ^{o}C were still poor. Eventually a membrane stable at 90 ^{o}C for 1100 hours was prepared using a quaternised PPO and polysulphone (PS) blend.

Reproducibility of the chloromethylated PPO (CMPPO) required to synthesise the membranes proved difficult. Thick polymer gels were observed which could not be used to make any membranes. A membrane was successfully prepared from a "semi gel" batch of CMPPO which showed the highest observed ionic conductivity (IC) whilst being stable at 90 ^{o}C. Improvements in stability without any loss of IC were achieved using secondary polymers as well as cross-linking agents. Investigation of a commercially available water soluble, poly(diallyldimethylammonium chloride) (polyDADMAC) proved to be ineffective due to the inability to render the materials insoluble in water. Selected membranes (based on ionic conductivity and stability) were tested for water electrolysis applications, with some of the membranes showing evolution of a small amount of oxygen and/or hydrogen.

Acknowledgments

Although the primary author of this thesis is myself, it does not do justice to the number of other people who have directly or indirectly played a part during the completion of this work.

Firstly, a thanks to Professor Shanwen Tao for the opportunity to carry out this work.

A thanks also to my colleagues in the fuel cell group, Chris, Pete, Lei, Ibrahim, Ai-Lien, Ken and Rong. Everybody showed a willingness to help each other out even if it meant a delay to their own work proceeding. This certainly made the process of working much easier. However, a special thank you is reserved for Dr. Vitor Magueijo who has put a lot of long hours into the revision of this thesis. A job that he did not ask for and despite already having a large workload, has performed admirably.

To the laboratory technicians, led by Jim Murphy, thank you for helping make the running of experiments smoother. I can recall a number of times when I was in need of a specific piece of glassware which was found from amongst the numerous stock cupboards.

To my fellow PhD colleagues within the department, sharing an office space with you all was a lot of fun. My office space in particular was a nice and relaxed atmosphere, making stressful days just that bit easier.

To Mum and Dad, I know you have been more keen than anyone for this PhD to be finished, but finally here it is done. Thank you for getting me to this stage in my life.

A final thanks to Jessica Smith, my best friend and other half. Always my biggest fan, ever so keen to help despite knowing full well that there was nothing more than encouragement you could offer.

Thanks again everyone.

Contents

Abstract 3

Acknowledgments 4

Contents 5

List of figures 12

Abbreviations 27

Chapter 1: Introduction 28

1.1 The need for renewable energy 28

1.2 Fuel cell technology 28

1.3 Types of fuel cell technology 30

1.3.1 Polymer electrolyte membrane fuel cell (PEMFC) 30

1.3.2 Alkaline fuel cell (AFC) 31

1.3.3 Phosphoric acid fuel cell (PAFC) 31

1.3.4 Direct methanol fuel cell (DMFC) 32

1.3.5 Molten carbonate fuel cell (MCFC) 33

1.3.6 Solid oxide fuel cell (SOFC) 34

1.3.6 Advantages and disadvantages 35

1.4 Polymer Electrolyte Membrane Fuel cells 37

1.4.1 Polymer Electrolyte Membrane materials 37

1.4.2 Catalyst activity 38

1.4.2 Catalyst contamination 43

1.4.3 Membrane degradation 47
1.5 Alkaline Fuel cells 52
1.5.1 AFC (liquid electrolyte) 52
1.5.2 Alkaline PEMFCs 54
1.5.3 Transport mechanisms in anion exchange membranes (AEMs) 56
1.5.4 Stability of AEMs 58
1.5.5 Overcoming stability issues of AEMs. 60
1.5.5.1 Crosslinking 60
1.5.5.2 Interpenetrating polymer networks (IPN) 62
1.5.5.3 Co-polymerisation 65
1.5.5.4 Replacement of the trimethylammonium group 66
1.6 Performance of various AEMs from the literature 72
1.7 Implementation of AEMs in water electrolysis 78
1.8 The challenges of the alkaline fuel cell 81
1.9 – Chapter 1 references 82
Chapter 2 – Aims 91
2.1 – Chapter 2 references 95
Chapter 3 – Experimental 96
3.1 – Experimental details 96
3.1.1 Chloromethylation 96
3.1.2 Quaternisation 99

3.1.3 Ion exchange 101

3.1.4 Cross-linking 102

3.1.5 Porous membranes 102

3.1.6 Treatment of porous membranes with water soluble polymers 103

3.1.7 Mixed membrane preparations 103

3.1.8 Cross-linkeded mix membrane preparation 104

3.1.9 Heat treatment 104

3.2 – Testing 104

3.2.1 Electrochemical impedance spectroscopy 104

3.2.2 Membrane preparation 105

3.2.3 Electrode preparation 105

3.2.4 Cell preparation 105

3.2.5 Infrared spectroscopy 106

3.2.6 Thermal gravimetric analysis 107

3.3 – Electrochemical impedance spectroscopy 107

3.4 – Infrared spectroscopy 117

3.5 – Thermal gravimetric analysis 124

3.6 – Chapter 3 references 126

Chapter 4 – Preparation of quaternised poly(2,6-dimethyl-1,4-phenylene oxide) (QAPPO), analysis and optimisation 127

4.1 – Chloromethylation of poly(2,6-dimethyl-1,4-phenylene oxide) (PPO) and AEM preparation 127

4.2 – Chloromethylation of PPO for one hour at 50 °C 130

4.3 – Chloromethylation of PPO for four hours at 50 °C 136

4.4 – Cross-linking of QAPPO (4hr, 50 °C) using diethylamine 140

4.5 – Cross-linking of QAPPO (4hr, 50 °C) using propylamine 144

4.6 – Cross-linking of QAPPO (4hr, 50 °C) using diaminopropane 148

4.7 – Conclusions on the chloromethylation of PPO for 4hrs at 50 °C 149

4.8 – Increase in chloromethylation reaction temperature to 60 °C 150

4.9 – Chloromethylation of PPO for four hours at 55 °C 152

4.10 – Chloromethylation of PPO for six hours at 50 °C 154

4.11 – Conclusions on the chloromethylation of PPO for 6hrs at 50 °C 159

4.12 – Overall conclusions for all batches of CMPPO and QAPPO AEMS 160

4.13 – Chapter 4 references 162

Chapter 5 – Improvements to stability using a quaternised poly(2,6-dimethyl-1, 4-phenylene oxide)/polysulphone blend, (QAPPO/QAPS) 163

5.1 – Chloromethylation of PPO and PS for 4.5 hours at 50 °C 164

5.2 – Production of AEMs from a CMPPO/CMPS ionomer mix 164

5.3 – Improvements to QAPPO/QAPS ionic conductivity 176

5.4 – Conclusions for the QAPPO/QAPS AEM series 181

5.5 – Chapter 5 references 182

Chapter 6 – Use of "semi gel" CMPPO to produce quaternised poly (2,6-dimethyl-1,4-phenylene oxide AEMs 183

6.1 – Rationale for the preparation of "semi gel" QAPPO AEMs 183

6.2 – Improving the stabiity of "semi gel" QAPPO AEMs 189

6.2.1 – Addition of a second polymer to the "semi gel" QAPPO AEM 191

6.2.1.1 – Polyvinylidene fluoride (PVDF) doped AEM 192

6.2.1.2 – Polyvinyl chloride (PVC) doped AEM 196

6.2.1.3 – Poly(vinylbenzyl chloride) (PVBC) doped AEM 199

6.2.2 – "Semi gel" QAPPO supported with a polytetrafluoroethylene filter 202

6.2.3 – 1, 4-diazabicyclo[2.2.2]octane (DABCO) cross-linking agent 207

6.3 – Conclusions for QAPPO prepared from "semi gel" CMPPO 213

6.7 – Chapter 6 references 215

Chapter 7 – Synthesis of AEMs using commercially available quaternised polymers 216

7.1 – Chapter rationale 216

7.2 – Preparation of porous polyvinylidene fluoride/polyDADMAC AEMs 219

7.3 – Polyvinylidene fluoride or polytetrafluoroethylene/polyDADMAC membranes prepared by polymer blending before casting 223

7.3.1 Preparation of polyvinylidene fluoride/polyDADMAC blend membranes 223

7.3.2 Preparation of polytetrafluoroethylene/polyDADMAC blend membranes……224

7.4 – Preparation of polyvinyl alcohol/polytetraethylene/polyDADMAC blend AEMs..... 228

7.4.1 Repeat of the preparation of polytetraethylene/polyDADMAC blend membranes..... 228

7.4.2 Preparation of polyvinyl alcohol/polytetrafluoroethylene/polyDADMAC blend AEMs..... 230

7.5 – Attempts to improve the ionic conductivity and stability of polyDADMAC containing membranes..... 232

7.5.1 Increasing the ionic conductivity by increasing the polyDADMAC content of the membranes..... 233

7.5.2 Increasing the ionic conductivity by using a higher molecular weight polyDADMAC..... 235

7.6 – Increasing the membrane stability by cross-linking of AEMs with glutaraldehyde..... 238

7.7 – Conclusions for use of pre-made quaternised polymers in synthesis of AEMs 245

7.8 – Chapter 7 references..... 247

Chapter 8 – Implementation of AEMs for the electrolysis of water..... 248

8.1 – Performance of QAPPO (4hr, 50 ^{o}C) propylamine cross-linked AEM in a water electrolysis cell..... 251

8.2 – Performance of QAPPO/QAPS AEM in a water electrolysis cell 254

8.3 – Performance of “semi gel” QAPPO/PVDF 5% AEM in a water electrolysis cell 257

8.4 – Performance of “semi gel” QAPPO/QAPVBTMACl 5% AEM in a water electrolysis cell 262

8.5 – Chapter 8 references 264

Chapter 9 – Conclusions 265

9.1 – QAPPO AEM synthesis 266

9.2 – QAPPO/QAPS blend AEMs 267

9.3 – Use of a “semi gel” batch of CMPPO in AEM preparation 269

9.4 – Modification of water soluble polymeric materials for use as AEMs 270

9.5 – Performance of selected AEMs in water electrolysis applications 272

9.5.1 Water electrolysis performance of the QAPPO (4hr, 50 oC) propylamine cross-linked AEM 272

9.5.2 Water electrolysis performance of the QAPPO/QAPS AEM 273

9.5.3 Water electrolysis performance of the “semi gel” QAPPO/PVDF 5% AEM 273

9.5.4 Water electrolysis performance of the QAPPO/QAPVBOH 5% AEM .. 274

9.6 – Chapter 9 references 275

Chapter 10 – Future work 276

Appendix A – Additional IR spectra 279

List of figures

Chapter 1 - Introduction

Figure 1.1: *General schematic of a fuel cell*……29

Figure 1.2: *Schematic of a molten carbonate fuel cell*….....33

Figure 1.3: *Schematic of a solid oxide fuel cell*……...34

Figure 1.4: *Comparison of the advantages and disadvantages of various types of fuel cell*……...36

Figure 1.5: *Chemical structure of Nafion*……...38

Figure 1.6: *Volcano plot summarising the catalytic activity of transition metals for the hydrogen oxidation reaction*……...39

Figure 1.7: *Volcano plot summarising the catalytic activity of transition metals for the oxygen reduction reaction*……...41

Figure 1.8: *Degradation of polymer backbones via radicals*…….....51

Figure 1.9: *Schematic of an AFC*…….……...53

Figure 1.10: *Chemical synthesis of QAPS*…….....55

Figure 1.11: *Proposed Grotthuss mechanism for transport of OH^- in AEM's*……...57

Figure 1.12: *Two direct nucleophilic displacement reactions present in AEM degradation*……...…….....59

Figure 1.13: *Two direct nucleophilic displacement reactions present in AEM degradation*……..……...59

Figure 1.14: *Chemical structure of cross-linked QAPS*……..……...60

Figure 1.15: *Two structures that can be formed using a semi-interpenetrating polymer network*…….……...62

Figure 1.16: *Chemical structure of quaternised chitosan*……...63

Figure 1.17: *Examples of OH^- conducting groups investigated as a replacement for conventional trimethylammonium groups. A) phosphonium; B) guanidinium; C) sulfonium; D) imidazolium; E) benzoimidazolium*……...……...67

Figure 1.18: *Phosphonium cation used by Yan et al*……...68

Figure 1.19: *Phosphonium cation used by Noonan et al*…….……...68

Figure 1.20: *Degradation of guanidinium groups*……...……...69

Figure 1.21: *Sulfonium cation used by Zhang et al*…….……...70

Figure 1.22: *Degradation mechanism for imidazolium cation*……...71

Figure 1.23: *Functionalised repeating unit contained within Choi et al's AEM*…...74

Figure 1.24: *Macromolecular cross-linker used by Lu et al*……...75

Figure 1.25: *Chloromethyl methyl ether*……..……...76

Chapter 2 - Aims

Figure 2.1: *Poly(2,6-dimethyl-1,4-phenylene oxide), PPO*…….……...92

Chapter 3 - Experimental

Figure 3.1: *Apparatus set-up for chloromethylation of PPO*……..……...98

Figure 3.2: *Apparatus set-up for the quarternisation of CMPPO*…….101

Figure 3.3: *Apparatus set-up for initial testing of AEMs*……...106

Figure 3.4: *Typical I-V curve for a fuel cell*……..……...108

Figure 3.5: *Nyquist plot*…….……...110

Figure 3.6: *Equivalent circuit model of the impedance from figure 3.5*…….....111

Figure 3.7: *Typical I-V curve for a fuel cell. (GDL = gas diffusion layer, An = Anode, Ca = Cathode, R = resistor, C = capacitor, L = inductor, Z_w = Warburg)* ……...113

Figure 3.8: *Ideal impedance plot for a fuel cell*…….…….……...115

Figure 3.9: *Observed impedance plot for a fuel cell*……....116

Figure 3.10: *The electromagnetic spectrum (wavelength (λ)/m)*……..……...117

Figure 3.11: *The electromagnetic spectrum (wavelength (λ)/m)*……..……...119

Figure 3.12: *Energy profile for variation in covalent bond length.*…….121

Figure 3.13: *Vibrational modes of a generalised non-linear molecule, AH_2X_2*.....122

Chapter 4 - Preparation of quaternised poly(2, 6-dimethyl-1, 4—phenylene oxide) (QAPPO), analysis and optimisation.

Figure 4.1: *Chloromethylation of poly (2,6-dimethyl-1,4-phenylene oxide, PPO*….128

Figure 4.2: *Resonance structure formed upon heating of paraformaldehyde and zinc chloride*….....128

Figure 4.3: *Mechanism for the chloromethylation of poly(2,6-dimethyl-1,4-phenylene, PPO*….....129

Figure 4.4: *Zoomed in part of lower portion of PPO infrared spectrum*……...130

Figure 4.5: *Chemical structure of PPO with colour co-ordinated bonds*….....131

Figure 4.6: *Zoomed in part of IR spectra comparison between PPO and CMPPO*...131

Figure 4.7: *Chemical structure of CMPPO with colour co-ordinated bonds*……....132

Figure 4.8: *Method of quaternisation of CMPPO to produce QAPPO*…….132

Figure 4.9: *Zoomed in part of IR spectra comparison between QAPPO membranes with different KOH treatment times*……...133

Figure 4.10: *Chemical structure of QAPPO with colour co-ordinated bonds*……...134

Figure 4.11: *Variation of IC with temperature for the QAPPO membrane prepared from a 1 hour batch of CMPPO. These AEMs were immersed in 1M KOH for 1 and 3 days*……...135

Figure 4.12: *Zoomed in part of IR spectra comparison between CMPPO at different stages in the chloromethylation reaction*……...136

Figure 4.13: *Zoomed in part of IR spectra comparison between QAPPO membranes immersed in 1M KOH for 1 and 3 days*……..137

Figure 4.14: *Variation of IC with temperature for the QAPPO membrane (4hr 50 °C) immersed in KOH for 1 and 3 days*….....138

Figure 4.15: *TG analysis comparison between QAPPO membranes (4hr 50 °C) immersed in 1M KOH for 1 (red) and 3 (black) days*….....139

Figure 4.16: *Method of the cross-linking of CMPPO using diethylamine*…….....140

Figure 4.17: *Zoomed in part of IR spectra comparison between cross-linked and noncross-linked QAPPO membranes 1M KOH treated for 1 day*……..141

Figure 4.18: *Variation of IC with temperature for the diethylamine cross-linked QAPPO membrane (chloromethylated for 4 hours at 50 °C)*…….142

Figure 4.19: *Variation of the IC with time for the diethylamine cross-linked QAPPO membrane (chloromethylated for 4 hours at 50 °C). This test was carried out at 90 °C* ……...143

Figure 4.20: *Variation of IC with time for the diethylamine cross-linked QAPPO membrane (chloromethylated for 4 hours at 50 °C) during a 220 hour loop run. This test was carried out at 90 °C*…….....……...144

Figure 4.21: *Dipropylamine (A) and propylamine (B) structures*….....145

Figure 4.22: *Variation of ionic conductivity with temperature for the propylamine cross-linked QAPPO membrane (chloromethylated for 4 hours at 50 °C)* ……..…….145

Figure 4.23: *Variation of the ionic conductivity with time for the propylamine cross-linked QAPPO membrane (chloromethylated for 4 hours at 50 ^{o}C). This test was carried out at 70 ^{o}C*……....146

Figure 4.24: *TGA comparison between diethylamine (black) and propylamine (red) cross-linked QAPPO membranes (chloromethylated for 4 hours at 50 ^{o}C)* ……...147

Figure 4.25: *Method of the cross-linking of QAPPO using diaminopropane*……....147

Figure 4.26: *Variation of ionic conductivity with temperature for the diaminopropane cross-linked QAPPO membrane (chloromethylated for 4 hours at 50 ^{o}C)* ….…….149

Figure 4.27: *Variation of ionic conductivity with temperature for all QAPPO membranes (cross-linked and noncross-linked) derived from the CMPPO batch chloromethylated for 4 hours at 50 ^{o}C*……..…....150

Figure 4.28: *Friedel-Crafts reaction schematic*……...151

Figure 4.29: *Variation of ionic conductivity with temperature for the QAPPO membrane (chloromethylated for 2.5 hours at 55 ^{o}C)* ……..……152

Figure 4.30: *Variation of ionic conductivity with temperature for the propylamine cross-linked QAPPO membrane (chloromethylated for 2.5 hours at 55 ^{o}C)* ….....153

Figure 4.31: *Variation of ionic conductivity with temperature for the QAPPO membrane (chloromethylated for 6 hours at 50 ^{o}C)* ……..……...154

Figure 4.32: *Variation of the ionic conductivity with time for the QAPPO membrane (chloromethylated for 6 hours at 50 ^{o}C). This test was carried out at 70 ^{o}C*……...155

Figure 4.33: *Variation of the ionic conductivity with time for the QAPPO membrane (chloromethylated for 6 hours at 50 ^{o}C). This test was carried out at 80 ^{o}C*….....156

Figure 4.34: *TGA comparison between 6 hour (black) and 4 hour (red) QAPPO membranes*….....157

Figure 4.35: *Variation of ionic conductivity with temperature for cross-linked QAPPO membranes (diethylamine and propylamine) derived from the CMPPO batch chloromethylated for 6 hours at 50 °C*……..……158

Figure 4.36: *Variation of ionic conductivity with temperature for all QAPPO membranes (cross-linked and noncross-linked) derived from the CMPPO batch chloromethylated for 6 hours at 50 °C*……..……....159

Figure 4.37: *Variation of ionic conductivity with temperature for all QAPPO membranes (noncross-linked only) derived from all CMPPO batches chloromethylated for 1, 4 and 6 hours at 50 °C*….....160

Chapter 5 – Improvements to stability using a quaternised poly(2, 6-dimethyl-1, 4—phenylene oxide)/polysulphone blend, QAPPO/QAPS

Figure 5.1: *Variation of ionic conductivity with temperature for the QAPPO/QAPS membrane (a 1:1 ratio of PPO and PS chloromethylated for 4.5 hours at 50 °C)* ..163

Figure 5.2: *Variation of ionic conductivity with time for the QAPS membrane prepared from 8 hour CMPS sample. The tests were performed at room temperature (black) and 60 °C (red)* ….....166

Figure 5.3: *Zoomed in part of infrared spectrum comparison between QAPPO (red) and QAPPO/QAPS (black). The QAPPO/QAPS (black) trace shows the addition of the S=O symmetric stretch at 1150 cm^{-1}*….....167

Figure 5.4: *Variation of ionic conductivity with temperature for the QAPPO/QAPS mix membrane*….....168

Figure 5.5: *Variation of ionic conductivity with time for the QAPPO/QAPS membrane. These tests was performed at 70 °C (black) and 80 °C (red)* ….....169

Figure 5.6: *Variation of ionic conductivity with time for the QAPPO/QAPS membrane. These tests was performed at 90 °C*….....170

Figure 5.7: *QAPPO (**1**) and QAPS (**2**)* ….....171

Figure 5.8: *Hypothesised molecule structure of the QAPPO/QAPS membrane with black and white chain representing QAPS and the red chain representing QAPPO*..171

Figure 5.9: *TGA comparison between the individual components of/and the QAPPO/QAPS membrane*….....172

Figure 5.10: *Variation of ionic conductivity with time for the QAPPO/QAPS membrane in 1M KOH. These tests was performed at 25 °C (black), 30 °C (red) and 40 °C (blue)* ….....173

Figure 5.11: *Variation of ionic conductivity with time for the QAPPO/QAPS membrane in 1M KOH. This test was performed at 60 °C*….....174

Figure 5.12: *Variation of ionic conductivity with time for the QAPPO/QAPS membrane in 1M KOH. This test was performed at 70 °C*….....175

Figure 5.13: *Variation of ionic conductivity with time for the QAPPO/QAPS membrane in 1M KOH. This test was performed at 80 °C*….....176

Figure 5.14: *Variation of ionic conductivity with temperature for the QAPPO/PS membrane loaded with 25% by weight ZrO_2*….....177

Figure 5.15: *Variation of ionic conductivity with temperature for the QAPPO/PS membrane loaded with 25% by weight SnO_2*….....178

Figure 5.16: *Variation of ionic conductivity with temperature for the QAPPO/PS membrane loaded with 20% by weight inorganic material. This 20% was made up of 10% ZrO_2 and 10% SnO_2*….....179

Figure 5.17: *Variation of ionic conductivity with time for the QAPPO/PS membrane loaded with 20% by weight inorganic material. This 20% was made up of 10% ZrO_2 and 10% SnO_2. This test was performed at 90 ^oC*….....180

Chapter 6: Use of "semi gel" batch of CMPPO to produce quaternised poly (2,6-dimethyl-1, 4-phenylene oxide)

Figure 6.1: *Variation of ionic conductivity with temperature for the "semi gel" QAPPO membrane*….....184

Figure 6.2: *Ionic conductivity comparison between "semi gel" QAPPO membrane and the other batches discussed in chapter 4*….....185

Figure 6.3: *Variation of ionic conductivity with time for the "semi gel" QAPPO membrane at 90 ^oC for 132 hours. (Long term stability test)* ….....186

Figure 6.4: *TGA comparison of the 6 hr and "semi gel" batches of CMPPO*….....187

Figure 6.5: *TGA comparison of the 6 hr and "semi gel" QAPPO AEMs*….....188

Figure 6.6: *Lower half of the infrared comparison of the "semi gel" QAPPO AEM before and after immersion in 1M KOH*….....189

Figure 6.7: *Lower half of the infrared comparison of the "semi gel" and 6 hr QAPPO AEMs*….....190

Figure 6.8: *Variation of the ionic conductivity of the "semi gel" QAPPO/PVDF 5% membrane with temperature*….....193

Figure 6.9: *Lower half of the infrared spectrum of the "semi gel" QAPPO/PVDF 5% membrane*….....194

Figure 6.10: *Variation of ionic conductivity with time for the "semi gel" QAPPO/PVDF 5% membrane. This test was performed at room temperature.* ….....195

Figure 6.11: *Variation of ionic conductivity with temperature for the "semi gel" QAPPO/PVDF 5% AEM (a comparison between the two heat cycles performed)*...195

Figure 6.12: *Variation of ionic conductivity with time for the "semi gel" QAPPO-PVDF 5% membrane. This test was performed at 90 °C*….....196

Figure 6.13: *Variation of ionic conductivity with temperature for the "semi gel" QAPPO- PVC 5% membrane. This data set was obtained after several heat cycles between 60 °C and 90 °C*….....197

Figure 6.14: *Variation of ionic conductivity with time for the "semi gel" QAPPO-PVC 5% membrane. This test was performed at 90 °C*….....198

Figure 6.15: *Chemical structure of QAPVBOH*….....199

Figure 6.16: *Variation of ionic conductivity with temperature for the "semi gel" QAPPO-QAPVBOH 5% membrane*….....200

Figure 6.17: *Variation of ionic conductivity with time for the "semi gel" QAPPO-QAPVBOH 5% membrane. These tests were performed at 70, 80 and 90 °C*….....201

Figure 6.18: *TGA comparison of the un-doped "semi gel "and 5% PVBOH doped QAPPO AEMs*….....202

Figure 6.19: *Variation of ionic conductivity with temperature for the "semi gel" QAPPO cast onto a porous PTFE filter*….....204

Figure 6.20: *Variation of ionic conductivity with time for the "semi gel" QAPPO cast onto a porous PTFE filter. This test was carried out at 60 °C for 24 hours*….....204

Figure 6.21: *Variation of ionic conductivity with time for the "semi gel" QAPPO cast onto a porous PTFE filter. This test was performed at 90 °C for 52 hours*….....205

Figure 6.22: *Lower half of the infrared spectrum comparison between the "semi gel" QAPPO membrane supported on PTFE (red) and the unmodified "semi gel" QAPPO AEM (black) (full spectrum in figure A.20 of appendix A)* ….....206

Figure 6.23: *Chemical structure of 1, 4-diazabicyclo[2.2.2]octane, DABCO*….....207

Figure 6.24: *Variation of ionic conductivity with temperature for the "semi gel" QAPPO AEM cross-linked with 10% and 20% DABCO compared to the uncross-linked "semi gel" QAPPO AEM*….....209

Figure 6.25: *Variation of ionic conductivity with time for the "semi gel" QAPPO cross-linked with DABCO (10%) compared to the uncross-linked AEM (figure 6.3). This test was performed at 90 °C for 500 hours*….....210

Figure 6.26: *Lower half of the infrared spectrum comparison of the "semi gel" QAPPO membrane cross-linked with different amounts of DABCO*….....211

Figure 6.27: *TGA comparison of the standard "semi gel" QAPPO and DABCO cross linked variants*….....212

Chapter 7 – Use of pre-made quaternised polymers in synthesis of AEMs

Figure 7.1: *Chemical structure of poly(acrylamide-co-diallyldimethylammonium chloride) (**A**) and poly(diallyldimethylammonium chloride), polyDADMAC (**B**)* ….217

Table 7.1: *Room temperature ionic conductivity results for PVDF/polyDADMAC membranes thermally treated at different temperatures*….....220

Figure 7.2: *TGA comparison plot of the PVDF/polyDADMAC membrane thermally treated at 190 °C for 10 minutes*….....221

Figure 7.3: *TGA comparison plots for PVDF/PolyDADMAC membranes treated at 190 ^{o}C, 170 ^{o}C and 150 ^{o}C for 10 minutes each. These membranes were prepared using porous PVDF films.* ….....222

Figure 7.4: *TGA comparison plot of the PVDF/polyDADMAC mix membrane treated at 190 ^{o}C for 10 minutes*….....224

Table 7.2: *Ionic conductivity results of PTFE-polyDADMAC blends treated at different temperatures*….....225

Figure 7.5: *Variation of IC with temperature for the PTFE/polyDADMAC blend membrane fired at 190 ^{o}C for 10 mins*….....226

Figure 7.6: *TGA plot comparing the PTFE/polyDADMAC blends thermally treated at 190 ^{o}C and 250 ^{o}C for 10 minutes to the untreated sample*….....227

Figure 7.7: *TGA plot of poly(diallyldimethylammonium chloride) (polyDADMAC)*208

Figure 7.8: *Variation of IC with temperature for the PTFE/polyDADMAC membranes fired at 300 ^{o}C for 20 and 30 minutes*….....229

Figure 7.9: *Variation of IC with temperature for the PTFE/PolyDADMAC membrane fired at 300 ^{o}C for 20 and 30 minutes respectively. This membrane was prepared using the modification to Huang et al's method described in the text*….....231

Figure 7.10: *Variation of IC with temperature for the 1:3 weight ratio PTFE/polyDADMAC membrane fired at 300 ^{o}C for 20 minutes. The 1:1 weight ratio PTFE/polyDADMAC membrane is also presented for comparison*….....233

Figure 7.11: *Variation of IC with time for the 1:3 weight ratio PTFE/polyDADMAC membrane fired at 300 ^{o}C for 20 minutes over the course of 24 hours. This test was performed at room temperature*….....234

Figure 7.12: *TGA comparison plot between the high and low molecular weight forms of PDADMAC*….....236

Figure 7.13: *Variation of IC with temperature for the PTFE/HMW-polyDADMAC membrane fired at 310 °C for 20 minutes compared to the low molecular weight derivative fired at 300 °C for 20 minutes*….....237

Figure 7.14: *Variation of IC with temperature for the PTFE/HMW-polyDADMAC membrane thermally treated at 310 °C for 20, 25 and 30 minutes*….....239

Figure 7.15: *Variation of IC with temperature for the PTFE/HMW-polyDADMAC membrane cross linked with glutaraldehyde and thermally treated at 300 °C for 20 minutes. The noncross-linked sample is also presented for comparison*….....239

Figure 7.16: *Variation of IC with time for the PVA/PTFE/polyDADMAC blend membrane cross-linked with glutaraldehyde and thermally treated at 300 °C for 20 minutes. This test was performed at room temperature*….....241

Figure 7.17: *Variation of IC with time for the PVA/PTFE/polyDADMAC blend membrane cross-linked with glutaraldehyde and thermally treated at 300 °C for 20 minutes. This test was performed at 40 °C*….....242

Figure 7.18: *Variation of IC with time for the PVA/PTFE/polyDADMAC blend membrane cross-linked with glutaraldehyde and thermally treated at 300 °C for 20 minutes. This test was performed at 50 °C*….....243

Figure 7.19: *Variation of IC with temperature for the PVA/PTFE/polyDADMAC membrane cross linked with glutaraldehyde at 60 °C and thermally treated at 300 °C for 20 minutes*….....243

Figure 7.20: *Variation of IC with time for the PVA/PTFE/PDADMAC blend membrane cross-linked with glutaraldehyde at 60 °C and thermally treated at 300 °C for 20 minutes. This test was performed at 60 °C*….....244

Chapter 8 – Implementation of AEMs for the electrolysis of water

8.1 – Performance of QAPPO propylamine cross-linked AEM in a water electrolysis cell

Figure 8.1: A - *I-V plot at room temperature.*

B – *Constant voltage stability test at room temperature.*

C – *Repeat I-V plot at room temperature*….....251

Figure 8.2: A - *I-V plot at 40 °C.*

B – *Constant voltage stability test at 40 °C.*

C – *Repeat I-V plot at 40 °C*….....252

Figure 8.3: A - *I-V plot at 60 °C.*

B – *Constant voltage stability test at 60 °C.*

C – *Repeat I-V plot at 60 °C*…….....253

Figure 8.4: A - *I-V plot at 80 °C.*

B – *Constant voltage stability test at 80 °C.*

C – *Repeat I-V plot at 80 °C*….....254

8.2 – Performance of QAPPO/QAPS AEM in a water electrolysis cell

Figure 8.5: A - *I-V plot at room temperature.*

B – *Constant voltage stability test at room temperature.*

C – *Repeat I-V plot at room temperature*….....255

Figure 8.6: A - *I-V plot at 40 °C.*

B – *Constant voltage stability test at 40 °C.*

C – *Repeat I-V plot at 40 °C*….....255

Figure 8.7: A - *I-V plot at 60 °C.*

B – *Constant voltage stability test at 60 °C.*

C – *Repeat I-V plot at 60 °C*….....256

Figure 8.8: A - *I-V plot at 80 °C.*

B – *Constant voltage stability test at 80 °C.*

C – *Repeat I-V plot at 80 °C*….....257

8.3 – Performance of "semi gel" QAPPO/PVDF 5% AEM in a water electrolysis cell

Figure 8.9: A - *I-V plot at room temperature.*

B – *Constant voltage stability test at room temperature.*

C – *Repeat I-V plot at room temperature*….....258

Figure 8.10: A - *I-V plot at 40 °C.*

B – *Constant voltage stability test at 40 °C.*

C – *Repeat I-V plot at 40 °C*….....258

Figure 8.11: A - *I-V plot at 60 °C.*

B – *Constant voltage stability test at 60 ^{o}C.*

C – *Repeat I-V plot at 60 ^{o}C*….....259

Figure 8.12: A - *I-V plot at 80 ^{o}C.*

B – *Constant voltage stability test at 80 ^{o}C.*

C – *Repeat I-V plot at 80 ^{o}C*….....260

Figure 8.13: *Water electrolysis of QAPPO-PVDF 5% under constant current of 400 mA cm^{-2} for 65 hours*….....261

8.4 – Performance of QAPPO/QAPVBOH 5% AEM in a water electrolysis cell

Figure 8.14: A - *I-V plot at room temperature.*

B – *Constant voltage stability test at room temperature.*

C – *Repeat I-V plot at room temperature*….....263

Figure 8.15: A - *I-V plot at 40 ^{o}C.*

B – *Constant voltage stability test at 40 ^{o}C.*

C – *Repeat I-V plot at 40 ^{o}C*….....263

Abbreviations

AEM	Anion exchange membrane
AFC	Alkaline fuel cell
APEMFC	Alkaline polymer electrolyte membrane fuel cell
CMPPO	Chloromethylated poly(2,6-dimethyl-1,4-phenylene oxide)
DABCO	(1,4-diazabicyclo[2.2.2]octane)
HOR	Hydrogen oxidation reaction
IC	Ionic conductivity
IR	Infra-red (spectroscopy)
IPN	Interpenetrating polymer network
KOH	Potassium hydroxide
PEMFC	Polymer electrolyte membrane fuel cell
PEM	Proton exchange membrane
polyDADMAC	Polydiallyldimethylammonium chloride
PPO	Poly(2,6-dimethyl-1,4-phenylene oxide)
PS	Polysulphone
PTFE	Polytetrafluoroethylene
PVC	Polyvinyl chloride
PVDF	Polyvinylidene fluoride
QAPPO	Quaternised poly(2,6-dimethyl-1,4-phenylene oxide)
QAPS	Quaternised polysulphone
ORR	Oxygen reduction reaction
TG	Thermal gravimetric (analysis)
TMA	Trimethylamine

Chapter 1: Introduction

1.1 The need for renewable energy

The modern world has become increasingly dependent on fossil fuels for its primary energy source. Increasingly large amounts of oil, natural gas and coal are used to provide us with electricity and heating for our homes and petrol for our vehicles all of which produces large quantities of harmful gases that damage the Earth's atmosphere. The Kyoto Protocol [1] was signed in 1997 and came into effect in February 2005. It is an international agreement from the world's leading economies to reduce the emission of a package of several greenhouse gases by 34% in 2020 and 80% in 2050 [1]. The protocol covers the emissions of carbon dioxide (CO_2), methane (CH_4), nitrous oxide (N_2O), hydrofluorocarbons (HFC's), perfluorocarbons (PFC's) and sulphur hexafluoride (SF_6). The total emission of the six greenhouse gases for the UK in 1990 was equivalent to 779,904,144 tonnes of CO_2 [1]. In 2012 statistics from the Department of Energy and Climate change within the UK government put the UK's total greenhouse gas emission at 581,100,000 tonnes of CO_2 equivalent [2, 3]. Although this amount equates to roughly a 25.5% overall reduction since 1990, the figure for 2012 is 3.2% higher than in 2011 [3]. Of this total amount, pure CO_2 emissions accounted for 474.1 million tonnes (82%) where 40% came from the energy sector and 24% from the transport sector [3].

1.2 Fuel cell technology

Part of the 25.5% reduction in the UK's CO_2 emissions since 1990 has been down to the development of nuclear and renewable energy sources such as wind, tidal and solar. However, these are mainly large-scale stationary power sources and do not address the

need for more mobile, small-scale forms of clean energy. Fuel cells have long been considered as the most logical replacement for internal combustion engines used in motor vehicles and other motorised equipment [4-10]. The world has seen a lot of recent development in electrical cars which are powered primarily by batteries. Both batteries and fuel cells are currently competing to be the primary power source for all electrical applications. The difference between a fuel cell and a battery is that a fuel cell can provide energy continuously as long as there is a constant supply of fuel, whereas a battery has a limited supply.

A fuel cell is an electrochemical device that converts chemical energy, in the form of a fuel, to electrical energy through a chemical reaction with oxygen or an other oxidising agent. The cell, Figure 1.1, is made up of four main components; anode, cathode, electrolyte and interconnect.

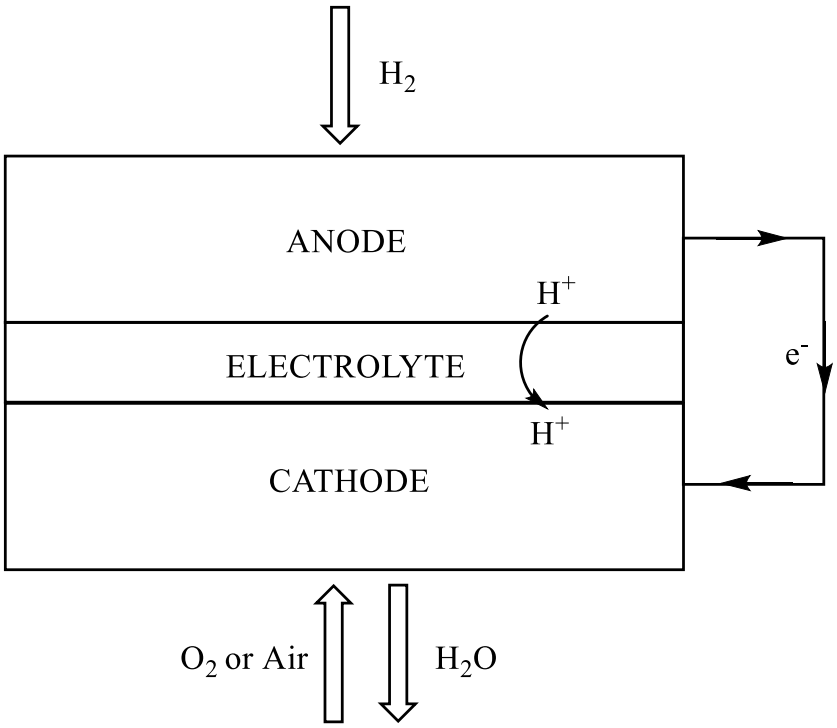

Figure 1.1: *General schematic of a fuel cell.*

The general principles of fuel cell operation are easy to understand and are shown in Equations 1.1 - 1.3.

$$\underline{\text{Anode:}}\ 2H_2 \rightarrow 4H^+ + 4e^- \quad \textbf{(1.1)}$$

$$\underline{\text{Cathode:}}\ O_2 + 4H^+ + 4e^- \rightarrow 2H_2O \quad \textbf{(1.2)}$$

$$\underline{\text{Overall cell reaction:}}\ 2H_2 + O_2 \rightarrow 2H_2O\ (+\text{Heat}) \quad \textbf{(1.3)}$$

Generation of electricity using a fuel cell is based on the formation of water from hydrogen and oxygen using equations 1.1 – 1.3. Gaseous hydrogen fuel is supplied to the anode where, in the presence of a catalyst, it is oxidised to protons (H^+) and electrons. The protons then pass from the anode to the cathode through a proton conducting electrolyte, while the electrons flow through the circuit. Once at the cathode, the H^+ ions and electrons react with either pure oxygen or simply air to create water.

1.3 Types of fuel cell technology

There are several different types of fuel cell. These fuel cells comprise different materials, operate at different temperatures and can utilise different fuels. Each fuel cell's operating conditions enable them to fulfil a wide range of potential roles.

1.3.1 Polymer electrolyte membrane fuel cell (PEMFC)

Polymer electrolyte membrane fuel cells are more commonly known as PEMFCs for short. Figure 1.1 above describes the workings of a PEMFC. This fuel cell generally uses a solid polymer electrolyte known as a proton exchange membrane at its core along with carbon electrodes coated with a platinum catalyst. These cells have an operating temperature range of 25 – 90 ^oC, with the optimum temperature being

between 60 ^{o}C and 80 ^{o}C. Because of this relatively low operating temperature their start up time is very fast and can produce high power densities of around 350 mW/cm^2 [11]. The US department of Energy has stated that PEM fuel cells have an average efficiency of 60% when used for motor applications, which is much higher than that of ~20% for an internal combustion engine [12]. Efficiencies of PEMFCs quoted in the literature put the figure somewhere between 45-60% [11].

1.3.2 Alkaline fuel cell (AFC)

Alkaline fuel cells or AFCs use a liquid alkali, normally potassium hydroxide (KOH) as the electrolyte instead of a solid membrane. They also work in a similar way to PEMFCs, instead of hydrogen being split at the anode, oxygen is reduced in the presence of water at the cathode to produce hydroxide ions, OH^-. It is these ions that then diffuse through the alkali media and react with hydrogen at the anode to produce water [13]. AFCs have a similar operating temperature and efficiency to PEMFCs (efficiency around 60-90 ^{o}C and 45-60 % respectively) but a much lower overall power density of only around 150 mW/cm^2 and lower general working lifetime [11, 14] primarily due to the liquid electrolyte.

1.3.3 Phosphoric acid fuel cell (PAFC)

Phosphoric acid fuel cells, or PAFCs, use phosphoric acid as a liquid electrolyte instead of a solid polymer to aid the transport of protons from the anode to the cathode. These fuel cells operate at temperatures slightly higher than PEMFC and AFCs, with normal working conditions of between 150-200 ^{o}C [15]. Despite the relatively high working temperature, PAFCs efficiency and power densities are not too dissimilar to

both PEM and AFCs (around 55% and 200 mW/cm^2) [11]. However recent work conducted by R. Lan *et al* has produced a PAFC operating at 250 ^oC and achieving a peak power density of 350 mW/cm^2 [16].

1.3.4 Direct methanol fuel cell (DMFC)

Direct methanol fuel cells or DMFCs use a solid polymer electrolyte as seen in PEMFCs however instead of using hydrogen as a fuel, liquid methanol is fed directly into the cell [17]. Methanol is viewed as being safer to store and handle and provides a higher power density than hydrogen for mobile applications [18]. Dilute methanol is oxidised in the presence of water and a platinum catalyst at the anode to produce protons and CO_2. The carbon dioxide is evolved from the cell and the protons travel across the proton exchange membrane in the same way as in PEMFCs. The same oxygen reduction reaction is observed at the cathode and water is formed, replacing the water used at the anode (Equations 1.4 – 1.6).

$$\underline{\text{Anode:}}\ CH_3OH + H_2O \rightarrow 6H^+ + 6e^- + CO_2 \qquad \textbf{(1.4)}$$

$$\underline{\text{Cathode:}}\ 3/2O_2 + 6H^+ + 6e^- \rightarrow 3H_2O \qquad \textbf{(1.5)}$$

$$\underline{\text{Overall cell reaction:}}\ CH_3OH + 3/2O_2 \rightarrow 2H_2O + CO_2 \qquad \textbf{(1.6)}$$

A low efficiency and production of CO_2 mean that these fuel cells do not provide such a "green" source of energy as other non CO_2 producing cells. Due to these facts these fuel cells are primarily used as add-ons to other fuel cells. Ethanol can also be used as a potential fuel [19].

1.3.5 Molten carbonate fuel cell (MCFC)

Molten carbonate fuel cells or MCFCs come under the classification of intermediate temperature fuel cells as they operate at temperatures around 650 ^{o}C [20, 21]. As the name suggests MCFCs use a molten carbonate salt mixture as the electrolyte. This mixture is held within a porous ceramic matrix, usually different types of lithium aluminates.

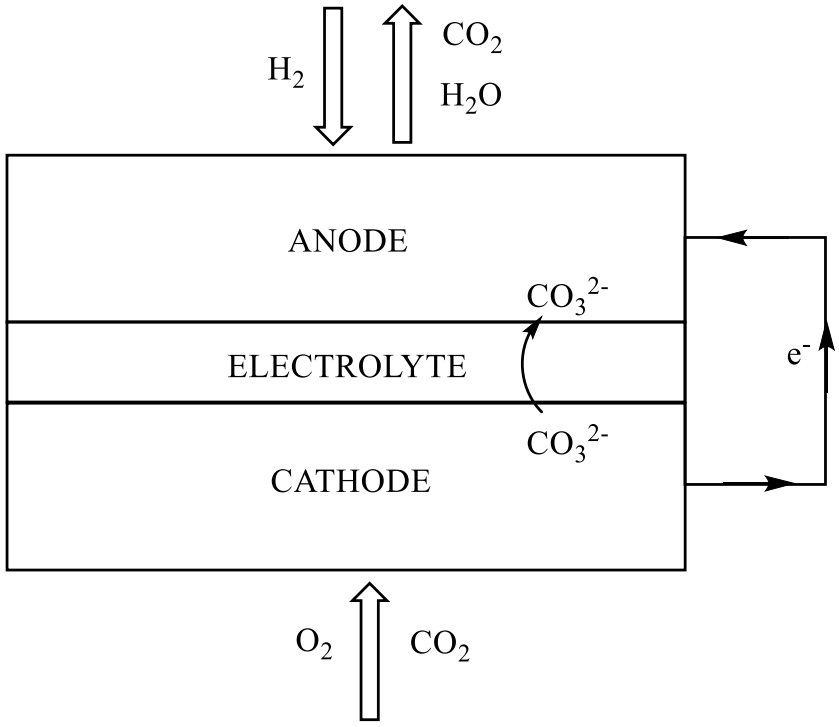

Figure 1.2: *Schematic of a molten carbonate fuel cell.*

Oxygen and carbon dioxide react at the cathode to produce mobile carbonate ions, which travel through the porous electrolyte and react with hydrogen at the anode to produce water and reform carbon dioxide (Figure 1.2). Subsequently this reformed CO_2 can be fed back into the cathode. It has been reported that efficiencies of MCFCs can reach 65% [11, 22] with more likely values of 50-60% [23]. Due to the operating

temperature being relatively high, the cell is not limited to solely using hydrogen gas. Other fuels are fed into the cell and are then naturally broken down to their component parts and hydrogen. This also removes the need for expensive platinum based catalysts.

1.3.6 Solid oxide fuel cell (SOFC)

Solid oxide fuel cells or SOFCs are classed as high temperature fuel cells as their operating temperature is around 800-1000 ^{o}C [18, 24, 25]. SOFCs use a non-porous solid ceramic electrolyte, most commonly yttria-stabilised zirconia (YSZ) [25].

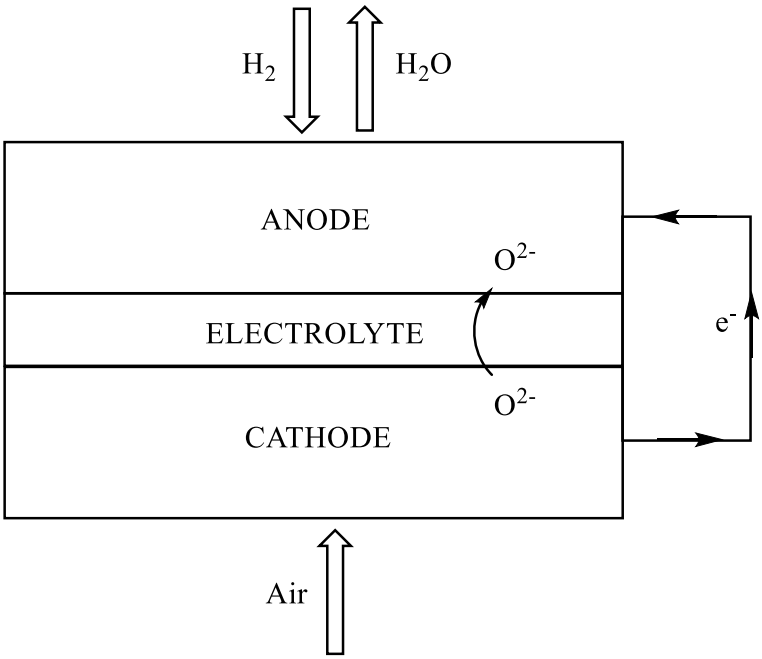

Figure 1.3: *Schematic of a solid oxide fuel cell.*

Oxygen from air is split at the cathode in the presence of a non-noble metal catalyst, which passes through the electrolyte and reacts with hydrogen at the anode to produce water (Figure 1.3). SOFCs have potential to be as efficient as MCFCs (around 60% [11]), with even the possibility to surpass that figure if equipment to make use of the large amount of waste heat is implemented (up to 80%).

1.3.6 Advantages and disadvantages

Fuel cell	Advantages	Disadvantages
Polymer electrolyte membrane fuel cell (PEMFC)	Low operating temperature. Short start-up time. High power density. Small, compact.	High cost due to use of platinum catalyst. Membrane thinning. CO poisoning of platinum catalyst.
Alkaline fuel cell (AFC)	Lower cost due to no need for platinum. Low operating temperature. Short start-up time. Small, compact.	Lower power density than PEMFCs. Poisoning of electrolyte by CO_2. Material durability issues.
Phosphoric acid fuel cell (PAFC)	More tolerant of impurities in fuel.	Expensive, needs platinum catalyst. Large and heavy. No more efficient than already installed power generators.
Direct methanol fuel cell (DMFC)	Higher energy density than hydrogen. Easier to store methanol.	Roughly 3-4 years behind in development. Low power densities.
Molten carbonate fuel cell (MCFC)	Use any fuel, no need for reformer. High efficiency and power density.	High temperature. Long start-up time. Large, no mobile applications.
Solid oxide fuel cell (SOFC)	Use any fuel, no need for reformer. High efficiency and power density.	High temperature. Long start-up time. Large, no mobile applications.

Figure 1.4: *Comparison of the advantages and disadvantages of various types of fuel cell.*

Figure 1.4 above shows the advantages and disadvantages of the various fuel cell technologies currently in use. It can be observed there is a clear distinction between size, power density and cost. PEMFC and AFCs are both relatively small, compact and operate at low temperatures, however PEMFCs suffer crippling costs due the need for platinum catalysts [26, 27] and the liquid KOH electrolytes present in AFCs can easily be poisoned by CO_2 impurity in the air supply [28, 29].

PAFCs may be more tolerant of fuel impurities but like PEMFCs require platinum catalysts and furthermore suffer from low efficiencies. DMFC technology is a few years behind in terms of power outputs whereas MCFC and SOFCs require large-scale deployment and very high temperature operation.

It is clear that to achieve high power densities at a low relative cost, fuel cells must be quite large and operate at very high temperatures. Smaller fuel cells, with potential use as mobile sources of power are either very inefficient or very expensive. There is no low cost, high power density (of comparable power output as PEMFCs), portable fuel cell in the current market. [*]

[*] (When the words "portable fuel cell" are used it is in reference to both power sources for general household equipment such as computers as well as larger scale power generators used outside the home.)

1.4 Polymer Electrolyte Membrane Fuel cells

1.4.1 Polymer Electrolyte Membrane materials

As stated previously PEMFCs are viewed as being the eventual power source for vehicle and mobile applications [4-9]. From all the fuel cells that utilise a solid polymer membrane as the electrolyte, PEMFCs currently provide the highest power output whilst also being the smallest device. For a polymeric membrane to be a viable option for use in PEMFCs, it has to fulfil a number of criteria:

i. Thermally stable up to >100 ^{o}C due to the operating temperature of <100 ^{o}C.
ii. Mechanically stable; material is able to be hot pressed.
iii. Chemically stable; material is stable in highly acidic conditions due to the acidic mediums used in PEMFCs.
iv. Highly permeable to water but not hydrogen or oxygen
v. Highly proton conductive

A perfluorosulfonic membrane developed in the late 1960s by Walter Grot of DuPont and commercialised under the name Nafion is by far the most commercially useful membrane to date [7, 30, 31]. Nafion exhibits proton conductivities > 100 mS cm^{-1}, has a working temperature up to 100 ^{o}C and is highly permeable to water allowing for good ion conduction.

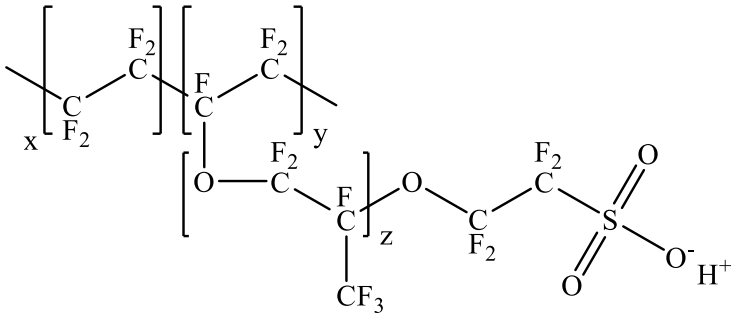

Figure 1.5: *Chemical structure of Nafion.*

Whilst Nafion performs exceptionally well in PEMFCs it has been found to perform very badly in DMFCs as it has high permeability to the fuel methanol, meaning the overall the cell is extremely inefficient [32-35].

1.4.2 Catalyst activity

Before discussing which metal catalyst is principally used in PEMFCs, it is important to understand what criteria the catalyst must match or match as much as possible in order to be deemed a good fit. Holton and Stevenson suggest four such criteria [36]:

i. *General activity* – The catalyst must be able to adsorb both H_2 and O_2 strongly enough so that the required reaction occurs. Conversely the adsorption must not be that strong that the products will not be released from the catalyst surface. This is also known as the Sabatier Principle.

ii. *Selectivity* – Preferably only one reaction should occur on the catalyst surface, producing one product and no side products.

iii. *General stability* – The catalyst must be able to withstand the general operating conditions of the fuel cell.

iv. *Poisoning resistance* – The catalyst must also be resistant to any impurities present in the fuels.

It is key to remember the difference between adsorbance and absorbance at this stage to avoid confusion. Adsorbance is where molecules are held on the surface of another solid. In this case H_2 and O_2 molecules are being held on the surface of the catalyst rather than being taken inside it. Figure 1.6 is a summary of a "volcano" plot which shows which transition metal is best suited for the hydrogen oxidation reaction, HOR [36, 37].

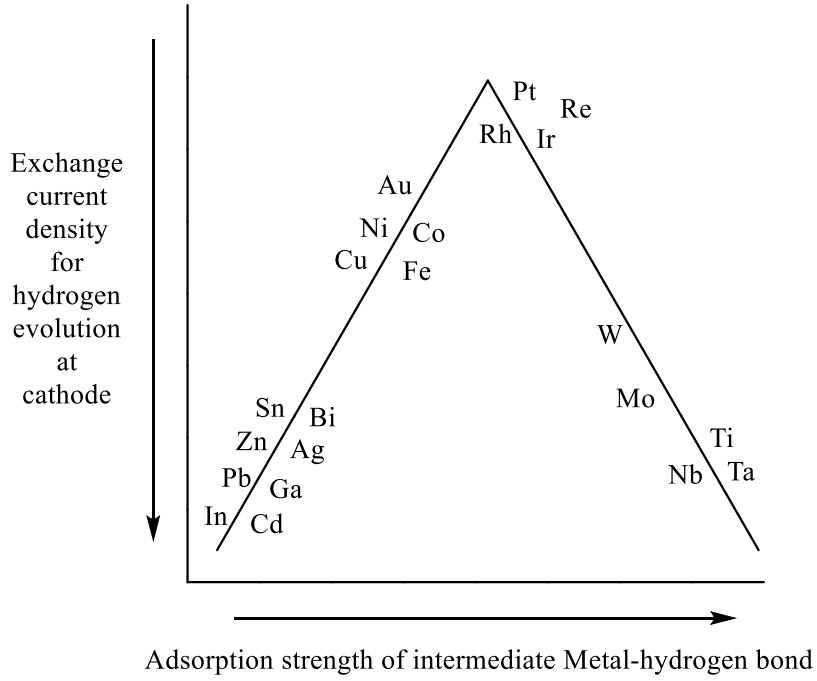

Figure 1.6: *Volcano plot summarising the catalytic activity of transition metals for the hydrogen oxidation reaction. [36]*

In this case the metal catalyst must be able to bind hydrogen sufficiently enough to undergo a reaction but not too tightly so that the reaction products are not released. This is known as the adsorption strength and it can be observed that platinum is the

most suitable metal when it comes to general catalytic activity. What happens at the anode and cathode during the HOR can be summarised in five key points [36]:

i. Hydrogen gas is fed into the anode and adsorbed onto the catalyst surface. The H-H bond is broken to give adsorbed atomic hydrogen.

$$\tfrac{1}{2}\, H_2 + * \rightarrow H^* \qquad \textbf{(1.7)}$$

where * represents the platinum catalyst active site.

ii. Adsorbed hydrogen loses an electron and is transferred to the membrane as H^+ ions.

$$H^* \rightarrow H^+ + e^- \qquad \textbf{(1.8)}$$

iii. Electrons flow to the cathode whereas the H^+ ions pass through the membrane.

iv. At the cathode, oxygen is adsorbed onto the catalyst surface. This bound oxygen is protonated by incoming H^+ ions from the anode and reduced by the electrons to form water.

v. The water molecule is then released from the catalyst surface.

Platinum's general catalytic activity for the hydrogen oxidation reaction is seen as the best fit. The hydrogen oxidation reaction with platinum is very fast with extremely small voltage losses meaning that relatively small platinum loadings are needed, around 0.05 mg cm^{-2} [36, 38]. The mechanism described above is the only mechanism

possible for platinum [39], so no by-products can be formed which satisfies the "selectivity" part of Holden's criteria. Also, with platinum being both acid and base stable, it is ideally suited for the acidic conditions of a PEMFC.

The same four point criteria can be applied for choosing the most suitable catalyst for the oxygen reduction reaction (ORR) occurring at the cathode. Figure 1.7 is the equivalent "volcano" plot for the activity of certain transition metals towards the ORR.

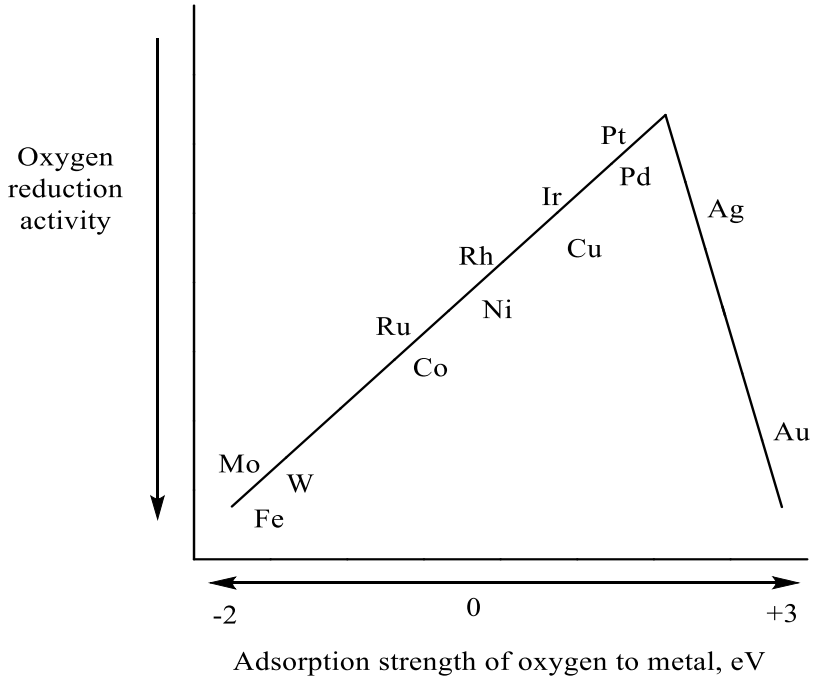

Figure 1.7: *Volcano plot summarising the catalytic activity of transition metals for the oxygen reduction reaction [36].*

From figure 1.7 it can be seen that platinum is the most suited catalyst choice. However unlike the HOR, platinum is not the ideal catalyst. The metals that sit on the left hand line tend to bind oxygen to their surface too strongly whilst the metals on the right

hand side of the line bind oxygen too weakly. It can be seen that in fact platinum binds oxygen slightly too strongly. The oxygen reduction reaction (ORR) via platinum is the limiting step in PEMFCs. It is comparatively slow, has multiple steps and is the source of more than half the voltage loss within the fuel cell [40]. Where the HOR is a simple one electron transfer, the ORR preferred dissociative pathway is via a four electron process which eventually forms water. The mechanism of the ORR at the cathode can be summarised in three key points [36, 41]:

i. Pure oxygen gas or air is fed into the cathode and adsorbed onto the catalyst surface.

$$\tfrac{1}{2}\, O_2 + * \rightarrow O^* \qquad \textbf{(1.9)}$$

ii. The surface bound oxygen is protonated with H^+ from the anode and reduced by an electron to give a surface bound hydroxyl molecule.

$$O^* + H^+ + e^- \rightarrow OH^* \qquad \textbf{(1.10)}$$

iii. This hydroxyl is further protonated, reduced to give water and desorbed from the catalyst surface. This water is then forced from the cell due to hydrophobic nature of its surroundings.

$$OH^* + H^+ + e^- \rightarrow H_2O + {}^* \qquad \textbf{(1.11)}$$

However the ORR via platinum is not as selective as the HOR. A second ORR mechanism is possible via an associative pathway upon adsorption onto the catalyst surface.

$$O_2^* + H^+ + e^- \rightarrow HO_2^* \quad \textbf{(1.12)}$$

A third reaction mechanism can also occur which goes on to produce hydrogen peroxide. This plays a major role in degradation of the polymer membranes and will be discussed at a later point.

Whereas the HOR requires as little as 0.05 mg/cm^{-2} of platinum for the catalytic reaction to proceed, it has been reported that the cathode requires platinum loadings of as much as 0.4 mg/cm^{-2}; 8 times higher [42]. This has been estimated to equal somewhere in the region of 72-94 g of platinum per fuel cell stack when used in cars, albeit using 2005 data [43]. It has been reported that this amount has reduced to around 30 g per fuel cell stack in 2013 [44] with some reports of platinum reduction in the region of 80% over the last decade [45]. The highly acidic conditions required for proton generation and conduction during PEMFC operation apply to both the anode and the cathode making platinum the only real option for the ORR, despite it not being optimal.

1.4.2 Catalyst contamination

During fuel cell operation the components and materials within the cell will come into contact with a lot of impurities in the fuels needed to operate the cell. These impurities can include carbon monoxide (CO)/dioxide (CO_2), hydrogen sulphide (H_2S), ammonia

(NH_3), methane (CH_4), nitrogen and sulphur oxides (NO_x/SO_x) as well as metal ions such as $Fe^{2/3+}$ and Cu^{2+} [46-54]. NO_x and SO_x are present in the air from vehicle exhaust fumes and can enter the cell if air is used as the source of oxygen. The metal ions can be inadvertently introduced into the cell via the elemental composition of some of the individual parts of the cell. Finally the rest of compounds are mainly produced in the reformation of hydrogen from natural gas.

These compounds can affect the fuel cells operation in one of three ways [47, 52]:

i. Introduce kinetic losses by changing the reaction mechanism.
ii. Increase ohmic losses by increasing the cell resistance.
iii. Decrease the membrane's ionic conductivity by degrading the active site availability.

Contaminants such as CO, CO_2, H_2S, CH_4, NO_x and SO_x all affect the platinum catalyst whereas NH_3 and metal cations both affect the membrane structure directly and indirectly via the formation of hydrogen peroxide, H_2O_2.

<u>CO/CO_2 poisoning:</u>

Both compounds have a similar effect on the platinum catalyst, in that they bind very strongly to the catalyst, reducing the number of active sites available for hydrogen oxidation or oxygen reduction [41, 47-49, 53, 54]. Over time the power output of the cell will decrease as more and more of the platinum catalyst is rendered ineffective. What makes CO and CO_2 poisoning extremely harmful to PEMFCs is that it is very difficult to eliminate without replacing all of the platinum within the cell. Such an outcome would prove very expensive.

CO can poison platinum in a number of ways which are discussed below. Firstly CO can simply be adsorbed on the surface of the platinum catalyst:

$$CO + Pt \rightarrow Pt - CO^* \quad \textbf{(1.13)}$$

This CO will stay strongly bound to the platinum site, reducing the number of sites available. The CO can bind in one of two ways depending on whether there are two adjacent available platinum active sites, either linearly or bridged. (**1.14** and **1.15**)

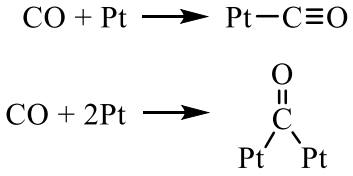

Secondly a CO molecule can directly replace a pre-adsorbed hydrogen. This bound H is ejected and replaced by a free CO molecule within the cell, once again blocking the site.

$$2CO + 2Pt - H^* \rightarrow 2Pt - CO^* + H_2 \quad \textbf{(1.16)}$$

CO_2 on the other hand does not directly bond to the platinum active sites. It is actually converted to CO by an existing Pt – H* site, resulting in the same power loss.

$$2Pt + H_2 \rightarrow 2Pt - H^* \quad \textbf{(1.17)}$$

$$CO_2 + 2Pt - H^* \rightarrow Pt - CO^* + H_2O + Pt \quad \textbf{(1.18)}$$

H_2S/SO_2 poisoning

H_2S is a common impurity in both the hydrogen and air needed for PEMFCs to operate [41, 46, 47, 55]. Like CO and CO_2, H_2S binds very strongly to the platinum catalyst but what makes it different is where as some PEMFCs can tolerate up to a certain level of CO/CO_2, only trace amounts of H_2S are needed to cause a severe performance drop. More importantly the developed platinum alloy catalysts shown to be tolerant towards CO/CO_2 have been proven to have no tolerance towards H_2S. Two poisoning mechanisms have been proposed, forming platinum sulphide (**1.19**) and platinum hydrogen sulphide (**1.20** and **1.21**) complexes respectively:

$$1)\quad Pt + H_2S \rightarrow Pt - S^* + H_2 \qquad \textbf{(1.19)}$$

$$2)\quad Pt + H_2S \rightarrow Pt - H_2S^+ \qquad \textbf{(1.20)}$$

$$Pt + HS^- + H^+ \rightarrow Pt - HS^{*-} + H^+ \qquad \textbf{(1.21)}$$

The formed platinum hydrogen sulphide (**1.21**) reacts further producing an electrochemical potential:

$$Pt - HS^{*-} + H^+ \rightarrow Pt + H_2S \qquad \textbf{(1.22)}$$

$$Pt + H^+ \rightarrow Pt^+ - H^* \qquad \textbf{(1.23)}$$

Which in turn forms the more potent platinum sulphide:

$$2Pt + H_2S \rightarrow Pt - SH^* + Pt - H^* \qquad \textbf{(1.24)}$$

$$Pt - SH^* \rightarrow Pt - S^* + H^+ + e^- \qquad \textbf{(1.25)}$$

Once platinum sulphide is formed it is reported that the fuel cell is irreversibly damaged and performance will dramatically decrease [46].

The presence of an SO_2 impurity has a similar affect to H_2S, in that the damaging Pt – S* complex is formed as shown below. Formed Pt – SO* is also shown to have a damaging effect on oxygen reduction at the cathode.

$$Pt + SO_2 + 2H^+ + 2e^- \rightarrow Pt - SO^* + H_2O \quad \textbf{(1.26)}$$

$$Pt - SO^* + 2H^+ + 2e^- \rightarrow Pt - S^* + H_2O \quad \textbf{(1.27)}$$

On February 27th 2017, the price of platinum on the wholesale market was $969 or £772 /oz (Johnson Matthey). Poisoning of the platinum catalyst by CO, CO_2, H_2S or SO_2 usually requires the platinum catalyst to be replaced or in some cases the entire fuel cell to be replaced at great cost. It is inconceivable to replace the platinum catalyst even once during the lifetime of a PEMFC, hence, with the current price of platinum, for the fuel cell to ever really be "cost effective" it must move away from the catalytic dependence on platinum.

1.4.3 Membrane degradation

NO_x, NH_3 and certain cation contaminants do not affect fuel cell performance by reducing the capability of the catalyst, but by attacking the proton exchange membrane instead. Both NO_x and NH_3 form ammonium ions, NH_4^+ in the following ways [47]:

$$NO_2 + 8H^+ + 7e^- \rightarrow NH_4^+ + 2H_2O \quad \textbf{(1.28)}$$

$$NH_3 + H^+ \rightarrow NH_4^+ \quad \textbf{(1.29)}$$

Due to the need for acidic conditions within PEMFCs for Nafion or Nafion type membranes to function, the formation of NH_4^+ is promoted due to high levels of H^+ ions within the cell. This means that even a small amount of NO_2 and NH_3 contaminant within the fuel can form enough NH_4^+ ions to pose a problem. NH_4^+ hinders or even prevents the conduction of H^+ through the membrane [47]. It has even been considered to affect the ionomers used to bind the catalyst layers to the electrodes.

The main reason for degradation of the proton exchange membrane is down to free radicals that form within the cell during operation. The formation of these radicals (•) is reportedly due to the formation of hydrogen peroxide via a free radical reaction between the hydrogen fuel and small traces of oxygen at the anode [39, 51, 52]

$$H_2 \rightarrow 2H\bullet \quad \textbf{(1.30)}$$

$$H\bullet + O_2 \rightarrow HO_2\bullet \quad \textbf{(1.31)}$$

$$HO_2\bullet + H\bullet \rightarrow H_2O_2 \quad \textbf{(1.32)}$$

Or even the incomplete reduction of oxygen at the cathode:

$$O_2 + 2H^+ + 2e^- \rightarrow H_2O_2 \quad \textbf{(1.33)}$$

The formed H_2O_2 can then react with metal cations such as Fe^{2+} or Cu^{2+}, to form hydroxyl radicals, which in turn can create peroxide radicals:

$$H_2O_2 + M^{2+} \rightarrow M^{3+} + OH\bullet + OH^- \quad \textbf{(1.34)}$$

$$OH\bullet + H_2O_2 \rightarrow HOO\bullet + H_2O \quad \textbf{(1.35)}$$

The polymer membranes are then very susceptible to these formed radicals and any terminal H bond can be the point at which the degradation can start. Linden *et al* [56] give a generalised explanation for how the radicals form on the polymer chain, denoted *P*.

$$P\text{-}H + HO\bullet \rightarrow P\bullet + H_2O \quad \textbf{(1.36)}$$

$$P\bullet + O_2 \rightarrow PO_2\bullet \quad \textbf{(1.37)}$$

$$PO_2\bullet + P\text{-}H \rightarrow POOH + P\bullet \quad \textbf{(1.38)}$$

It can then be seen that with the addition of oxygen the polymer membrane can be split in two which eventually leads to full collapse of the entire membrane structure. The generalised reaction mechanism proposed by Linden *et al* [56], figure 1.8, has been applied by researchers to Nafion, particularly by Curtin *et al* [57] who observed membrane thinning and the appearance of fluoride ions in the product water produced by the cell during full testing [39, 57]. When a membrane starts to degrade there is a chance that holes might start appearing throughout the membrane structure. There are several proposed mechanisms for the degradation of Nafion all including a series of three reactions (equations 1.39 – 1.41). Rf represents the rest of the polymer not involved in these reactions.

$$Rf - CF_2COOH + *OH \rightarrow Rf - CF_2* + CO_2 + H_2O \quad \textbf{(1.39)}$$

$$Rf - CF_2* + *OH \rightarrow Rf - CF_2OH \rightarrow Rf - COF + HF \quad \textbf{(1.40)}$$

$$Rf - COF + H_2O \rightarrow Rf - COOH + HF \quad \textbf{(1.41)}$$

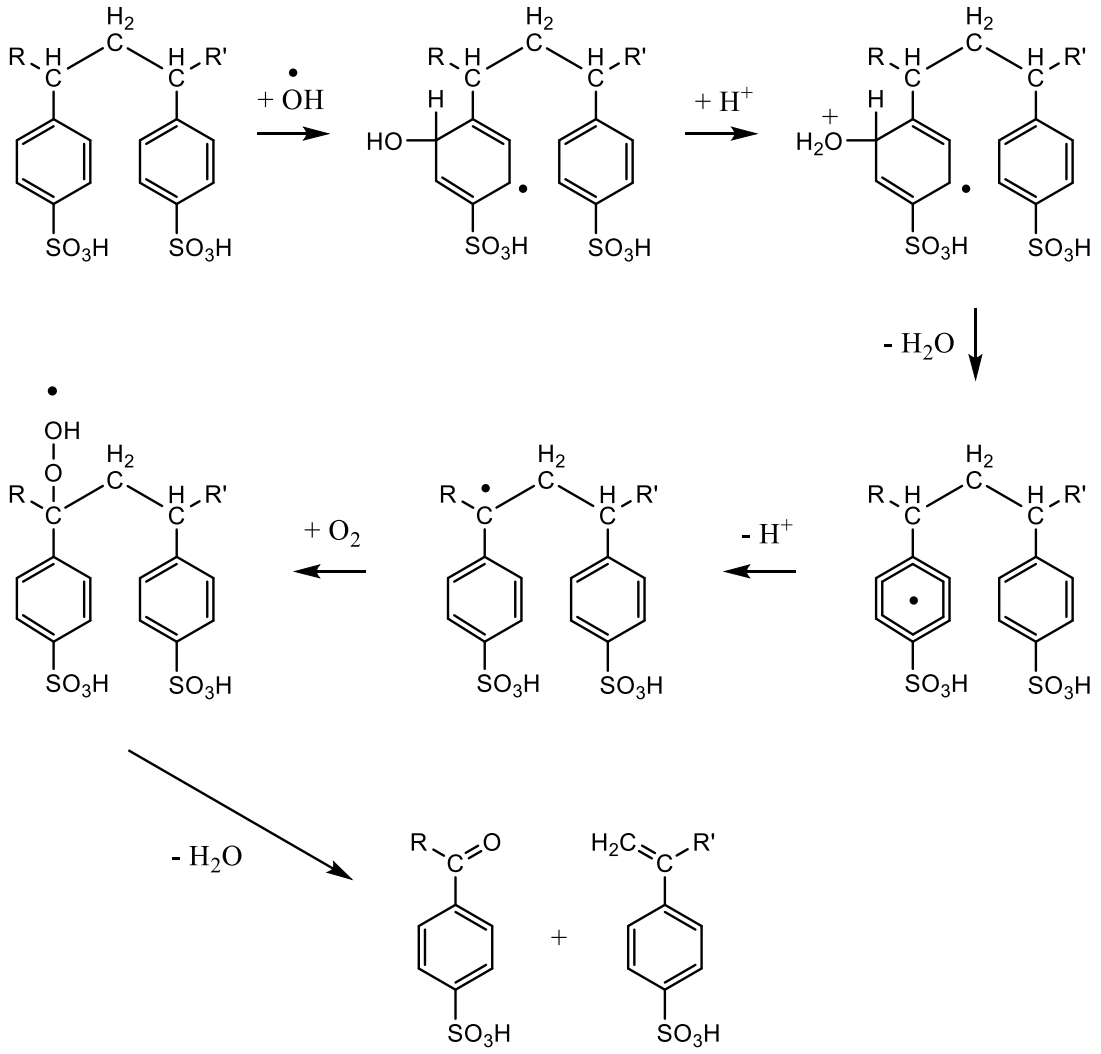

Figure 1.8: *Degradation of polymer backbones via radicals [56].*

To summarise, PEMFCs provide good overall power outputs but suffer from a number of critical drawbacks that are currently slowing their development. These problems revolve mainly around the use of platinum as the catalyst from the HOR and ORR within the cell. Although the HOR catalytic mechanism is quick and selective, the ORR via platinum is the opposite and can produce chemical by-products that attack

the polymer membrane within the cell. Platinum is also very sensitive to a number of fuel impurities, all of which have been discussed. Many researchers have posed the questions ‘why not use an alternative catalyst?’ with the repeated answer being that the acidic environment needed for PEMFCs and the acid based polymer membranes used, mean that platinum is the only metal catalyst that is stable enough to work for prolonged periods of time.

1.5 Alkaline Fuel cells

1.5.1 AFC (liquid electrolyte)

As described in a previous section, AFCs use a liquid electrolyte instead of a solid electrolyte (usually potassium hydroxide, KOH). Although the processes occurring in an AFC are different to those that occur in a PEMFC, the overall cell reaction is the same.

$$\underline{\text{Cathode:}}\ O_2 + 2H_2O + 4e^- \rightarrow 4OH^- \quad \textbf{(1.42)}$$

$$\underline{\text{Anode:}}\ 2H_2 + 4OH^- \rightarrow 4H_2O + 4e^- \quad \textbf{(1.43)}$$

$$\underline{\text{Overall cell reaction:}}\ 2H_2 + O_2 \rightarrow 2H_2O\ (+ \text{Heat}) \quad \textbf{(1.44)}$$

AFC technology relies on initially reducing oxygen instead of oxidising hydrogen, with the oxygen reduction reaction, ORR being kinetically faster under alkaline conditions [58, 59]. The AFC alkaline conditions and the inherently faster kinetics of the oxygen reduction reaction [60, 61] mean that non-noble metals can be used, regardless of the fact that they are less catalytically active than platinum. While the HOR remains the same, the ORR proceeds slightly differently to that in the PEMFC. The four electron transfer described earlier still happens but the mechanism that produces the harmful hydrogen peroxide, no longer occurs [58, 62].

$$O_2 + H_2O + 2e^- \rightarrow HO_2^- + OH^- \quad \textbf{(1.45)}$$

$$HO_2^- + H_2O + 2e^- \rightarrow 3OH^- \quad \textbf{(1.46)}$$

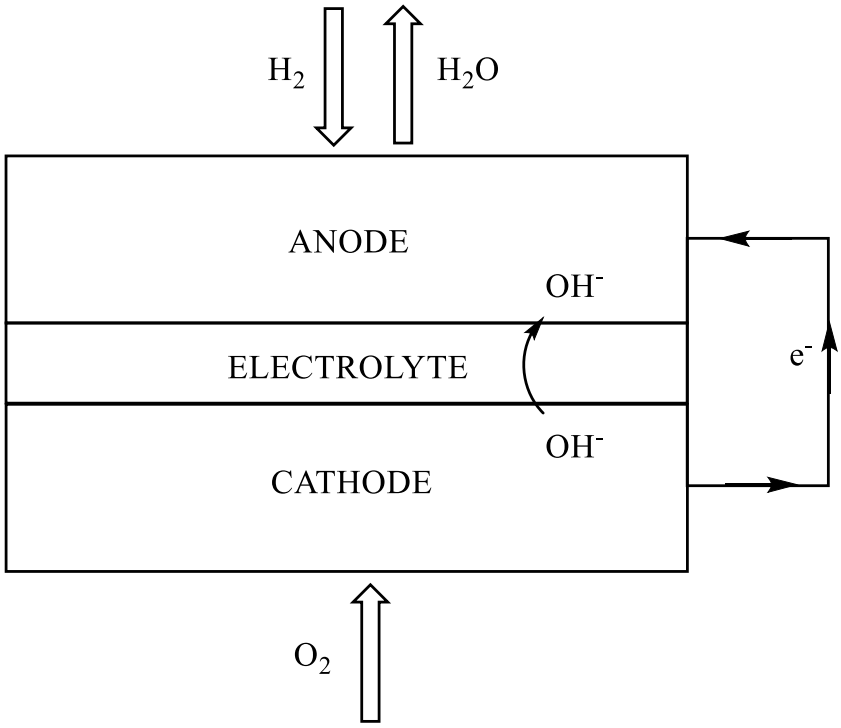

Figure 1.9: *Schematic of an AFC.*

As a consequence a lot of research has been devoted to the development of novel non-rare earth metal ORR catalysts for AFCs with varying degrees of success [63-82]. Lu *et al* state that even though alkaline polymer electrolyte fuel cells have the potential to eliminate the need for platinum catalysts, and hence reduce cost, most prototypes that have been developed still use platinum to some extent [30, 83-86].

Whilst the use of alternative catalyst materials is desirable, AFCs still demonstrate significant drawbacks. It has been reported that alkaline electrolytes are prone to carbonation if air is used as the source of oxygen [83, 87, 88] which eventually leads to the whole fuel cell failing. The mechanism behind this is that the precipitation of carbonates not only uses up available OH^- ions, reducing the ionic conductivity, but also will block up various pathways and inner workings of the fuel cell.

$$CO_2 + 2OH^- \rightarrow CO_3^{2-} + H_2O \quad \textbf{(1.47)}$$

Al Saleh *et al* investigated the effects of CO_2 impurities on AFC performance. They reported that at higher temperatures (70 ^oC +) there was no degradation in AFC (KOH) performance over a 200 hour period while at lower temperatures, the AFC did suffer some performance loss [89]. It has been suggested that the reasoning behind the loss of performance is to do with the solubility of the formed potassium carbonate: at 100 ^oC the reported solubility of K_2CO_3 in water is 156 g/100mL, whereas at 25 ^oC it is only 112 g/100 mL i.e. at lower temperatures the potassium carbonate will precipitate out of solution more readily than at higher temperatures. A lot of work has been published both supporting and contesting the idea that the presence of CO_2 and potassium carbonate within AFCs is detrimental to the health of the cell. However what is agreed is that the liquid electrolyte is the cause of most of the health issues of AFCs.

1.5.2 Alkaline PEMFCs

To get around these health problems and also the fact that alkaline electrolytes are not as conductive as Nafion, a lot of research has been performed [90-93]. It was discovered by Lu *et al* that by attaching an alkaline electrolyte, a quaternary ammonium cation, to a polymer base, it eliminated the chance of any CO_2 present in the air to react and form potassium carbonate [83]. This class of materials is now known as anion exchange membranes, AEMs. More specifically Lu *et al* developed a high performance alkaline polymer called quaternary ammonium polysulphone, QAPS

(**G**) (Figure 1.10), which is stable up to 120 ^{o}C and therefore well placed above the thermal range of this type of fuel cell [83].

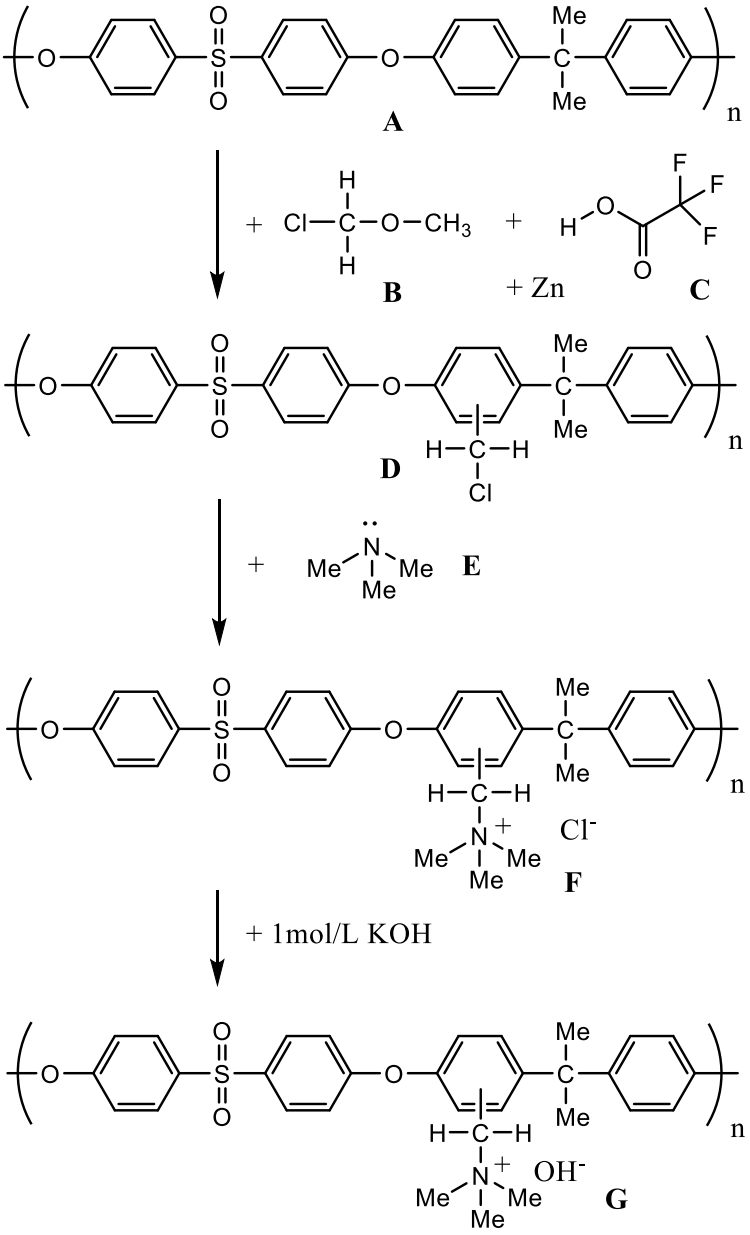

Figure 1.10: *Chemical synthesis of QAPS.*

The QAPS membrane was synthesized in a three step process from polysulphone (Figure 1.10). The first step involved the reaction of polysulphone (**A**) with chloromethyl methyl ether (**B**), using trifluoroacetic acid (**C)** and zinc as catalysts to produce chloromethylated polysulphone (**D**). The chloromethylated polysulphone (**D**) was then dissolved in DMF to form a 10% by weight solution, and treated with trimethylamine (**E**) to form chlorinated quaternary ammonium polysulphone, QAPS (**F**). To replace the chloride ion, the entire membrane was immersed in 1 mol KOH in order to yield the QAPS-OH membrane (**G**). Following this synthetic work, the same group published detailed data from a number of tests, most notably regarding the ionic conductivity of the QAPS membrane [94]. More specifically, they state that the QAPS membrane tested was stable in air below 120 ^{o}C, and that the ionic conductivity was stable at 20 mS cm^{-1} at 75 ^{o}C for 120 hours [95]. Immediately it can be seen that the conductivities observed from an alkaline AEM are one order of magnitude lower than that of Nafion (>10 mS cm^{-1} as compared to >100 mS cm^{-1}).

1.5.3 Transport mechanisms in AEMs

For a material to be a viable AEM for use in alkaline PEMFCs, it has to fulfil a number of criteria:

i. Thermally stable up to at least 120 ^{o}C;
ii. Mechanically stable; material is able to be hot pressed;
iii. Chemically stable; material is stable in water or alkaline conditions;
iv. Highly permeable to water but not hydrogen or oxygen;
v. Highly conductive to OH^{-} ions.

There are four accepted mechanisms for the transport of OH^- ions through a polymer membrane: a) surface site hopping, b) diffusion c) convection and d) the Grotthuss mechanism [96] with no one mechanism accepted to be providing the majority of the OH^- transport. For AEMs, the Grotthuss mechanism is believed to be responsible for a significant proportion of OH^- transport [60]. In the Grotthuss mechanism, it is believed that the transport of OH^- ions through an AEM involves a network of hydrogen bonded water molecules as seen in figure 1.11. With the addition of the blue water molecule a hyper-coordinated water molecule is formed as seen on the right hand side of figure 1.11. Subsequent bond rearrangements mean that the OH^- is shifted along the chain. This process can then be repeated with the approach of another water molecule to the nearly repositioned OH^- ion until the ion reaches the end of the chain.

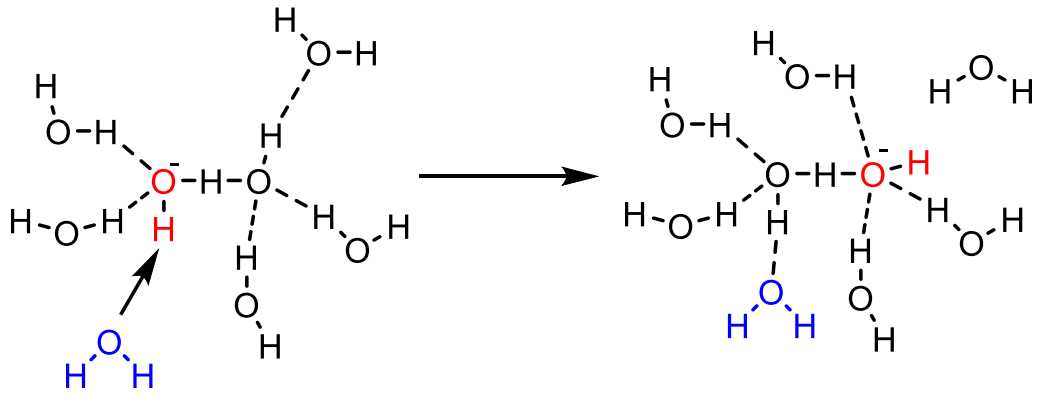

Figure 1.11: *Proposed Grotthuss mechanism for transport of OH^- in AEMs. Adapted from [96] and [97].*

Alternatively the OH^- can simply hop from one quaternary ammonium group to another and diffusion occurs when a concentration gradient is present. However, the

convection mechanism can be created as a consequence of the Grotthuss mechanism, as when the OH^- ions are shifted through the AEM, water molecules are pulled along with them. This in turn will then create a convection flow through the membrane [96], which is beneficial to overall OH^- conduction.

1.5.4 Stability of AEMs.

It is agreed that alkaline polymer electrolyte membrane fuel cell (APEMFCs) power densities are much lower than those observed in PEMFCs. This fact is partly due to the diffusion coefficient of OH^- ions being four times lower than that of H^+ ions [28, 98]. This means that to achieve the same power density as a PEMFC, four times as many OH^- ions must be conducted through an AEM than H^+ ions would be in an equivalent cell. It is clear that point (v) from section 1.5.3 is a key factor when designing an AEM.

Unfortunately, as alkaline electrolyte membranes get more conductive they become more prone to water uptake leading to increased swelling which will eventually cause the membrane to disintegrate [94]. The membrane disintegration is further increased at the high temperatures needed to operate this type of fuel cell. This degradation is caused by two main reactions both involving the OH^- ions present in the cell as shown in Figure 1.12, with both routes demonstrating a direct nucleophilic displacement of the ammonium group [26, 99, 100]. Route 1 occurs when an OH^- ion attacks the carbon atom adjacent to the ammonium group. Subsequently, the ammonium group is lost and a hydroxyl bond is formed, leaving the polymer membrane without any OH^- conducting groups. Route 2 instead involves a nucleophilic attack on a carbon atom

on the ammonium group. The carbon-nitrogen bond is broken, the nitrogen loses its positive charge, and an alcohol molecule (methanol) is formed. It has been reported that the peak degradation temperature for this trimethylammonium group is 60 ºC [101].

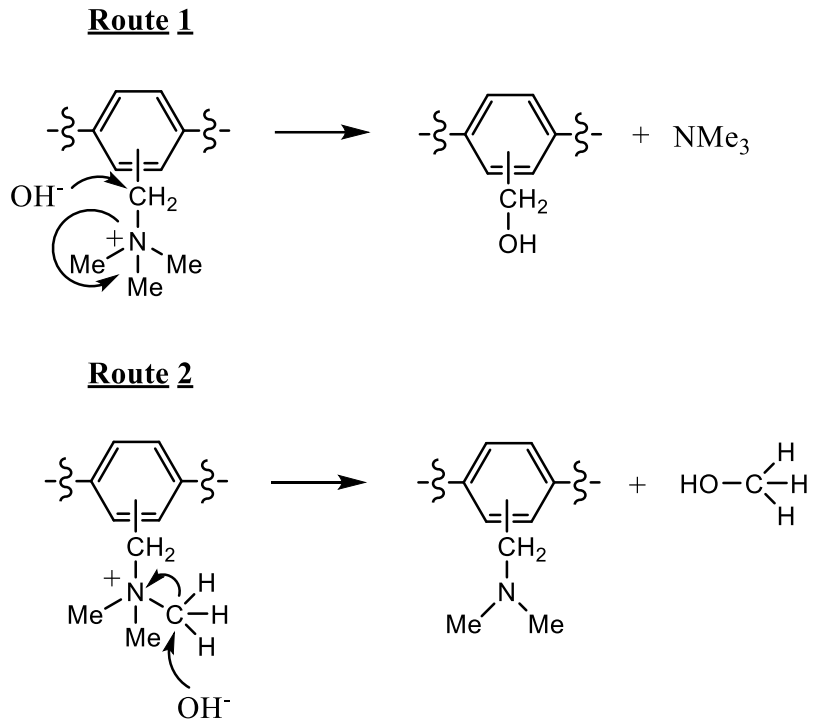

Figure 1.12: *Two direct nucleophilic displacement reactions present in AEM degradation.*

Figure 1.13 also shows a third displacement mechanism that occurs when β hydrogens are present on the polymer molecule. The OH^- ion extracts one of these β hydrogens as shown and the resulting displacement of the ammonium group and electron rearrangement results in an alkene being formed with water as a by-product.

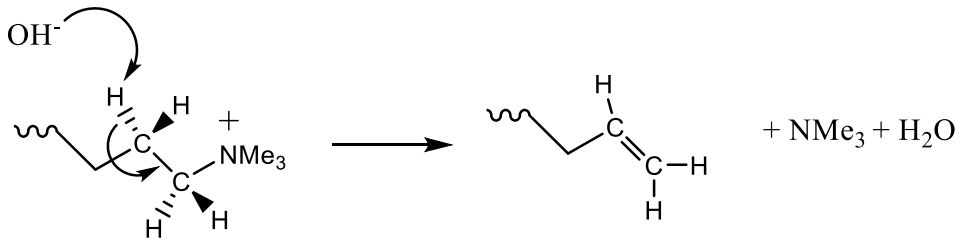

Figure 1.13: *Two direct nucleophilic displacement reactions present in AEM degradation.*

1.5.5 Overcoming stability issues of AEMs.

1.5.5.1 Crosslinking

It is completely impractical to have a fuel cell membrane that needs changing every few days. A method therefore needed to be developed that could produce a membrane "en-masse" that is stable, conductive and resistant to swelling. Two reactions are occurring within the reaction vessel during the chloromethylation reaction, functionalisation and cross-linking. The functionalisation reaction chloromethylates the benzene rings along the polymer chain and cross-links are formed from some of the chloromethylated sites. The chloromethylation and cross-linking reactions should occur in a 50:50 mix to achieve a highly conductive and highly stable membrane. However it is very difficult to get a good balance between the two, as favouring good conductivity will have a detrimental effect towards stability and vice versa. J. Pan and co-workers have developed a self-crosslinked QAPS membrane (figure 1.14) that is totally insoluble in water and has little or no swelling even at 90 ^{o}C [102].

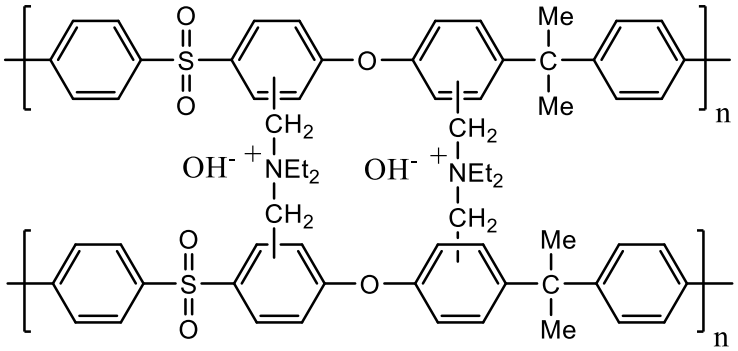

Figure 1.14: *Chemical structure of cross-linked QAPS [102].*

The cross-linked membrane was synthesised exactly like the Lu *et al* QAPS membrane [83] described above but with one additional step. Before casting, the ionomer solution was stirred with diethylamine (which was added as 30% of the benzyl chloride group) for 4 hours at 40 ^{o}C. The difference between this membrane and a standard QAPS membrane is the addition of a cross-linking agent (diethylamine) that acts as both an OH^- conductor and the cross-linker. These cross-links are present in addition to base quaternary ammonium groups. Pan *et al* reports a peak conductivity of 42 mS cm^{-1} at 90 ^{o}C and no degradation over a period of 500 hours at the same temperature [102].

F. Zhang and co-workers investigated the use of imidazole as a potential cross-linking agent [103]. Similar to the Pan *et al* cross-linking method [102], Zhang *et al* simply added 1-methyl-imidazole in slight excess to the polysulphone ionomer solution and stirred for 12 hours at room temperature. Zhang *et al* reported a peak ionic conductivity of 20.7 mS cm^{-1} [103] which was only observed at 20 ^{o}C; no other temperatures were investigated. Also this membrane was reported to have a swelling ratio and water uptake of 25.5% and 92.8% respectively [103]. The swelling ratio is the degree by

which the material increases in size when immersed in a solvent and the water uptake represents the amount of water that the material absorbs relative to its starting mass. As Zhang *et al* stated, these results were reasonable and a stability assessment was considered in which the membrane was submerged in 3M NaOH at 60 ^{o}C for 24 hours. This alkaline medium is of course more aggressive than that of water however it provides a good insight into the overall strength of synthesised membranes. Zhang *et al* discovered that after treatment the membrane's overall conductivity had decreased by 23.3% but the overall mechanical strength was unchanged. Zhang *et al* also observed a small peak power output of 16 mW cm^{-2} when used for fuel cell testing [103].

1.5.5.2 Interpenetrating polymer networks (IPN)

A technique has been developed to enhance the thermal stability of AEMs by combining AEMs with a second polymer structure or a semi-interpenetrating polymer network [95, 96, 104]. A downside to this technique however, is that the final ionic conductivities are slightly lower than the unmodified AEM. An example will be described later in this section. Figure 1.15 above illustrates this technique. Essentially, one polymer acts as the ion conductor (red line) and the other polymer network acts as a stabiliser (blue and black lines). Two different structures (dense and loose) can be formed simply by changing the reaction conditions [95].

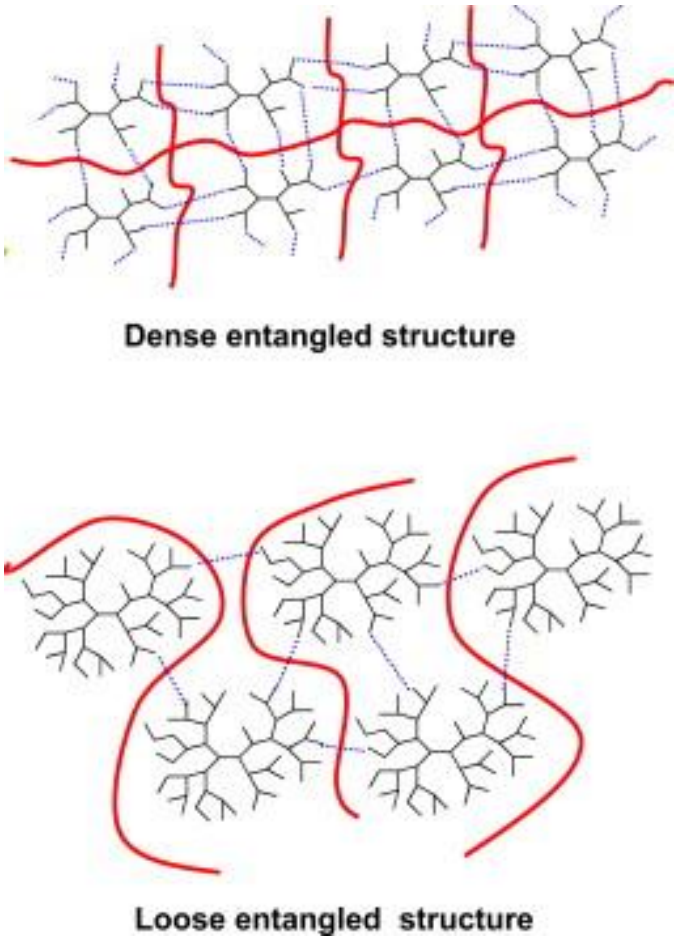

Figure 1.15: *Two structures that can be formed using a semi-interpenetrating polymer network [95].*

Chitosan based membranes have gained some attention in recent years [104, 105]. Chitosan is a linear polysaccharide that when dry is totally unconductive. However, when it is hydrated and quaternized (figure 1.16) chitosan shows some good conductive character. Chitosan has garnered so much attention because it is cheap to buy, produces excellent quality membranes and it can be modified very easily.

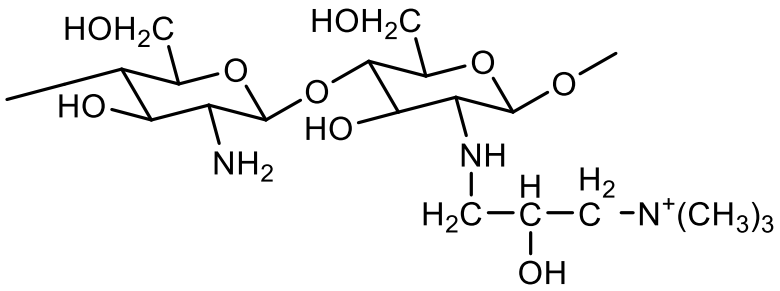

Figure 1.16: *Chemical structure of quaternised chitosan.*

Like the polysulphone based membranes described earlier, cross-linking between the chitosan chains occur on the same NH_2 group as quarternisation. Again there is the difficulty in producing membranes that are both conductive and strong. Schmitt *et al* highlights this fact in their research into chitosan membranes cross-linked with iodobutane [106]. The synthesised membranes were extremely fragile and only showed conductivities in the 1 – 10 mS cm^{-1} range.

As an example J. Wang and co-workers synthesised chitosan-polystyrene hybrid membranes [104]. In total 6 membranes were synthesised all with different percentage content of polystyrene ranging from 0% - 38% (Table 1.1). The standard quaternized chitosan membrane exhibited a conductivity of 55 mS cm^{-1}; however this membrane degraded very rapidly within 100 hours of testing. Subsequent testing showed a maximum tensile stress of 13 MPa which decreased dramatically to 2.5 MPa after only 96 hours [104]. However, by adding 21% by weight polystyrene to the reaction mixture, Wang *et al* were able to synthesise a stable membrane that achieved a reasonably stable conductivity of around 20 S cm^{-1} for nearly 300 hours. This membrane was also then able to withstand a tensile stress of around 20 MPa for 168 hours in 10 M KOH at room temperature. In short Wang and co-workers demonstrated

that the mechanical stability can be enhanced with the addition of a second polymer to create a semi-interpenetrating polymer network.

% weight of polystyrene in membrane	**Ionic conductivity at 75ºC ($mS\ cm^{-1}$)**
0	55
8	52
14	37
21	27
29	15
38	7

Table 1.1: *Ionic conductivity results for the membrane obtained by Wang et al [104].*

1.5.5.3 Co-polymerisation

Researchers have also investigated increasing the stability of the selected polymer that forms the backbone of all anion exchange membranes. Instead of using just a single polymer, multiple polymer blocks are used to form a co-polymer. The advantages of co-polymers are that you can tailor the properties of the material you want, combining the strengths of two polymers whilst decreasing the weaknesses. The synthesised product, whether it is made up of 2 or even three different base monomers will have roughly a combined set of physical properties and predictable structure.

Xu *et al* synthesised one such co-polymer membrane from three monomers: methyl methacrylate, ethyl methacrylate and vinyl benzyl chloride [107]. It is the vinyl benzyl chloride that ultimately acts as the OH^- ion conductor with the methacrylate elements providing the structural stability. As a consequence the membrane's first mass loss transition in the TGA plot, normally attributed to the loss of the OH^- conducting groups, was not observed until 200 ^oC, well above the operating temperature of alkaline fuel cells [107]. The synthesis method also does not have an adverse effect on the ionic conductivity (15 mS cm^{-1} – 50 mS cm^{-1} from 25 – 90 ^oC [107]) as chemical cross-linking or use of IPNs can sometimes do.

A different form of co-polymer can be achieved by a technique called grafting. It is essentially a co-polymerisation technique similar to the one described before, however monomers that may otherwise not react, can now be used since gamma radiation is usually the main energy source for the reaction. Mamlouk *et al* prepared a series of AEMs from low and high density polyethylene, using the radiation grafting technique [108]. The highest conductivity observed by Mamlouk *et al* was around 110 mS cm^{-1}, a figure that is not too far off the ionic conduction of Nafion. The highest peak power density observed was 823 mW cm^{-2} which is by far the highest reported power density for a APEMFC, even being of similar power to that of Nafion based PEMFCs [108].

1.5.5.4 Replacement of trimethylammonium group

The stability problems of the trimethylammonium group used for OH^- conduction in AEM's has already been discussed in section 1.5.4. The trimethylammonium (TMA) group can undergo direct nucleophilic displacement or β-H elimination with a peak

degradation temperature of 60 ^{o}C being reported [101]. A number of other groups containing a quaternary ion have been investigated to access their stability relative to that of TMA (Figure 1.15).

A) Phosphonium group

The phosphonium group is analogous that that of TMA, where simply the N atom is replaced with a P atom. Phosphonium ions have been investigated due to their higher basicity and higher ionic conduction [109].

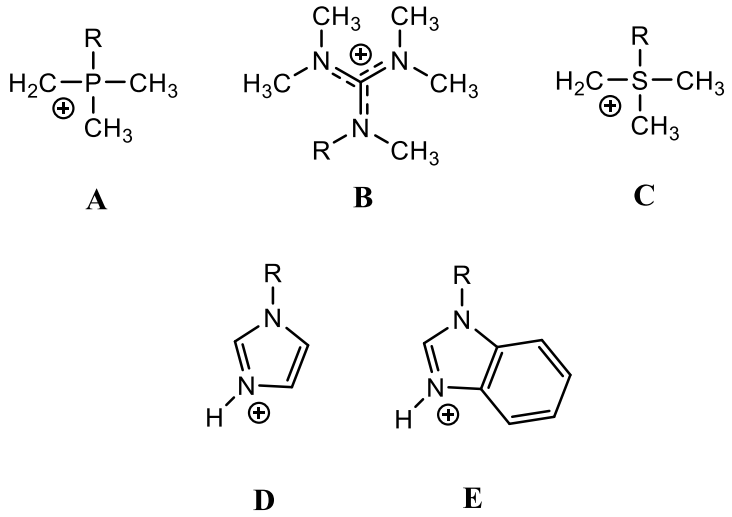

Figure 1.17: *Examples of OH^- conducting groups investigated as a replacement for conventional trimethylammonium groups. A) phosphonium; B) guanidinium; C) sulfonium; D) imidazolium; E) benzoimidazolium.*

However, generally the structure of the phosphonium ion is different to that of the structure seen in figure 1.17. Yan *et al* reported that simple aliphatic phosphonium groups suffer from stability problems similar to TMA groups, whereas the synthesised group shown in figure 1.18 was stable in 10 M KOH for 48 hours [110]. This in part is due to the methoxyphenyl groups being stronger electron donors and extremely

bulky preventing any nucleophilic OH^- attack on the phosphorus atom. The membrane that incorporated this phosphonium ion was also shown to be completely insoluble in water [110].

A slightly different phosphonium cation prepared by Noonan *et al* [111] (figure 1.19) has been shown to be better. When compared to a traditional TMA cation, 100% of the prepared cation was present after 20 days in 1M NaOH at 80 ^oC compared to less than 40% for TMA [111]. The AEM incorporating this group also displayed a stable ionic conductivity of 0.025 S cm^{-1} for 140 days at 22 ^oC [111].

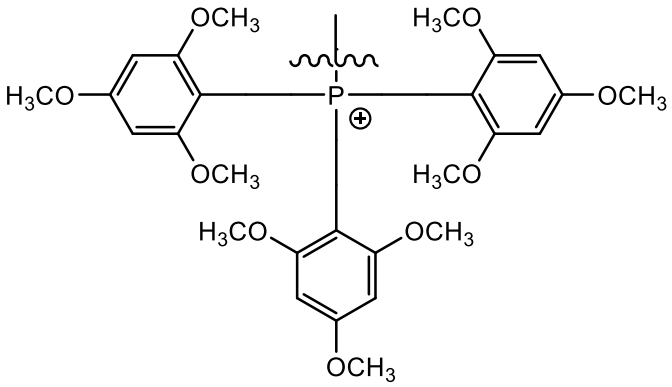

Figure 1.18: *Phosphonium cation used by Yan et al [109, 110].*

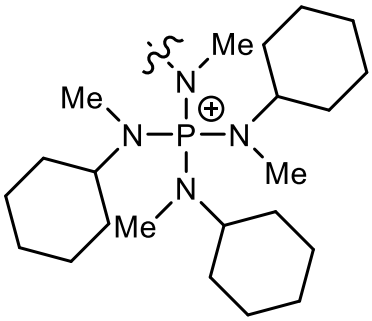

Figure 1.19: *Phosphonium cation used by Noonan et al [111].*

B) Guanidinium group

Guanidinium salts have been investigated for potential use as ionic liquids [112]. Similar to phosphonium groups, guanidinium groups have a higher basicity than TMA. This can be seen by looking at their relative pKa values. TMA has a pKa of 10.8 whereas pentaalkylguanidine has a pKa of 13.8. It is then theorised that OH^- ions will move more freely through any AEM synthesised with the guanidinium group [113]. Zhang *et al* conducted a study which compared TMA and guanidinium functionalised AEMs. They reported that the guanidinium functionalised AEMs exhibited a much higher IC than those functionalised with TMA; 42 mS cm^{-1} and 18 mS cm^{-1} respectively at 60 ^oC [113]. A higher of IC of 30 mS cm^{-1} at 90 ^oC [114] was observed by Sherazi *et al*. However, Li *et al* have reported that AEMs functionalised with guanidinium ions show poor stability to high concentrations of OH^- ions [115]. After immersing the AEM in 1M NaOH for 10 days at 60 ^oC, the membrane became brittle and showed extremely low ICs (8.8 mS cm^{-1} at 30 ^oC [115]). Both Sherazi *et al* and Li

et al report that the reduction in IC observed in strong alkaline solutions is caused by OH^- degradation of the guanidinium groups (figure 1.20) [114, 115].

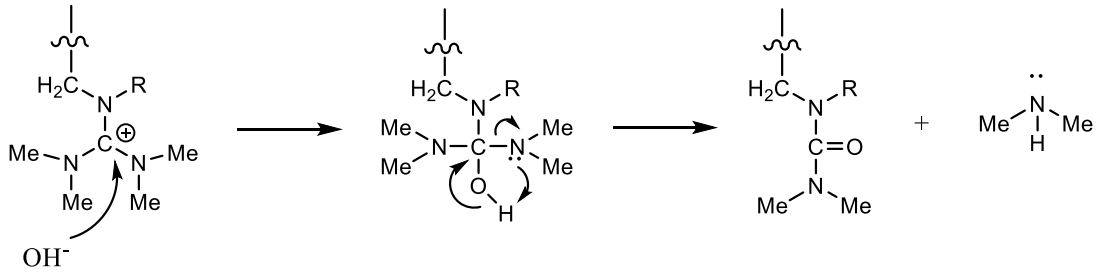

Figure 1.20: *Degradation of guanidinium groups [114, 115].*

C) Sulfonium group

Sulfonium groups behave in a similar way to phosphonium groups. Simple aliphatic substituted sulfonium groups suffer from stability problems, however like that seen with phosphonium groups, the addition of aryl substituents increases both the thermal and chemical stability [116]. Figure 1.21 shows the sulfonium group incorporated onto an AEM synthesised by Zhang *et al*.

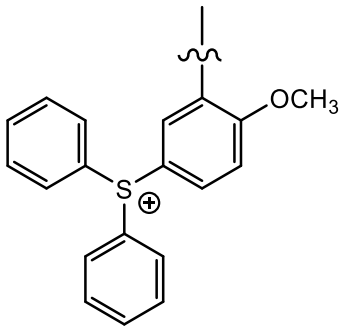

Figure 1.21: *Sulfonium cation used by Zhang et al [116].*

This AEM exhibited much higher thermal stability than the TMA derivative, with the first weight loss occurring at 242 ^{o}C as opposed to between 140-170 ^{o}C for the TMA derivative [116]. Zhang *et al* reports that the IC is slightly lower than that observed for AEMs functionalised with phosphonium groups [116], however the AEM did not show any reduction in conductivity when tested for 30 days in 1 M KOH at room temperature. This performance is similar to that observed with phosphonium functionalised AEMs [109-111].

D) Imidazolium group

Imidazolium functionalised AEMs have also been investigated as a replacement for TMA derivatives. This is due to the fact that the heterocyclic ring containing a pi electron configuration was thought to provide added stability [117]. However it has been shown that both imidazolium groups are not stable under prolonged alkaline exposure with imidazolium based AEMs IC steadily decreasing over time [118, 119]. The instability of the imidazolium groups lies on the carbon atom between the two nitrogen atoms, labelled the C-2 position (figure 1.22).

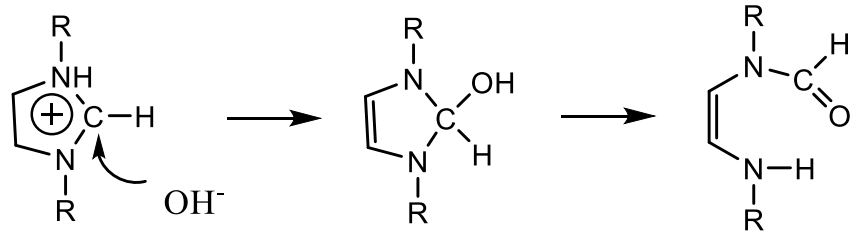

Figure 1.22: *Degradation mechanism for imidazolium cation [117, 120-122].*

In a similar way to that already discussed for the phosphonium and sulfonium ions, it has been reported that imidazolium ions exhibited an increase in stability if a bulky group is used to protect the C-2 atom [117, 123]. Both Yang and Lin *et al* have produced AEMs with bulky substituents on the C-2 atom of the imidazolium group which support these results. However the IC of these membranes are relatively low, just reaching the 10^{-2} S cm^{-1} range [117, 123].

1.6 Performance of various AEMs from the literature

Whereas Nafion can be used as the "go to" membrane when evaluating PEMFC materials due to its superior properties, there is no such membrane available for APEMFCs despite the vast amount of research conducted over the last 5-10 years [124]. A brief summary (Table 1.2) of various AEMs is shown below, including ionic conductivities and peak power densities where available.

Membrane	Ionic conductivity (mS cm^{-1})		Peak power density (mW cm^2)	Reference
	25 °C	60-90 °C		
Polysulphone (PS)	31	73 at 90 °C	-	[125]
Polysulphone – polytetrafluoroethylene (PS-PTFE)	17.5	27.5 at 70 °C	315 at 50 °C	[126]
Polysulphone – polytetrafluoroethylene – DABCO (PS-PTFE-DABCO)	25	51 at 55 °C	103-146 at 50 °C	[127]
Polystyrene – poly (ethylene-ran-butylene) (PSEBS)	-	18.6 at 60 °C	74.25 at 60 °C	[128]
Polyvinyl benzyl chloride – polytetrafluoroethylene (PVBC-PTFE)	16.5 32	22 at 60 °C 50 at 80 °C	162 at 25 °C 348 at 60 °C	[129] [130]
Poly (ethylene oxide) – graphene oxide (PEO-GO)	86	134 at 60 °C	53 at 60 °C	[131]
Poly (methyl vinyl ether-alt-maleic anhydride) (PMVMA)	19	27 at 65 °C	115 at 35 °C	[132]
Poly (ether ether ketone) (PEEK)	14.6	-	48.01 at 50 °C	[133]

Membrane	**Ionic conductivity (mS cm^{-1})**		**Peak power density (mW cm^2)**	**Reference**
	25ºC	**60-90ºC**		
Poly (tetraphenyl phthalazine ether sulfone) (PTPEKS)	51.2	-	100 at 80 ºC	[134]
Alkaline modified Nafion	41	110 at 80 ºC	-	[135]
	32	-	58.87 at 90 ºC	[136]
Poly (arylene ether sulfone)	65	0.087 at 80 ºC	-	[137]
	30	0.04 at 60 ºC	-	[138]
	23	0.036 at 60 ºC	-	[139]
	10	0.08 at 70 ºC	-	[140]
	50	-	-	[141]
Poly (2,6-dimethyl phenylene oxide) – Silica	8.5	-	-	[142]
	12	35 at 90 ºC	32 at 50 ºC	[143]
Polypropylene – polyethylene	17.5	-	27 at 25 ºC	
Poly (vinyl alcohol) – quaternized hydroxyethylcellulose ethoxylate (PVA-QHECE)	3	7.5 at 90 ºC	4.6 at 25 ºC	[144]

Table 1.2: *Summary of some AEM ionic conductivities and peak power densities from the last 5-10 years.*

As highlighted in previous sections AEMs conduct OH^- ions via quaternary ammonium cations. These cations are introduced in the polymer backbone via the various chemical reactions already discussed.

One downside to the synthesis method is that there is no way of judging where the quaternary ammonium ions will be placed along the polymer chains. This in turn can potentially create an uneven pathway for the OH^- to travel through the AEM and therefore slow down ionic conduction. Choi *et al* [145] synthesised an AEM that was comprised of a poly(aryl ether sulfone) block paired with a modified polymer block containing four quaternary ammonium ions. Figure 1.23 below shows the repeating unit containing the quaternary ammonium ions.

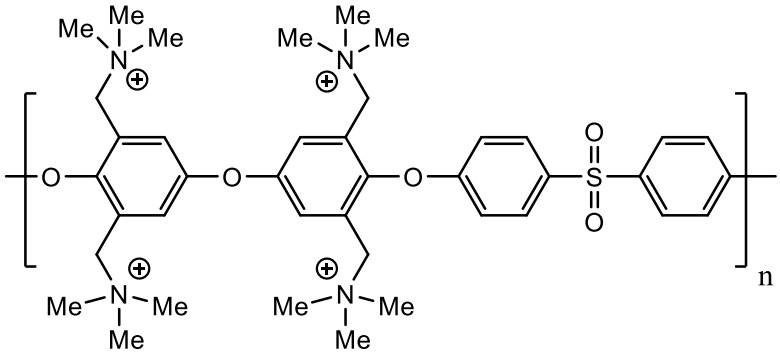

Figure 1.23: *Functionalised repeating unit contained within Choi et al's AEM [145].*

Choi *et al* indicated that this structure would be beneficial as effectively a channel for OH^- conduction would be created [145] i.e. with the increased number of quaternary ammonium groups also, the conduction of OH^- ions would be quicker as the travel distance between each quaternary ammonium cation is reduced.

The AEMs stability was reported to be unaffected by the increase in quaternary ammonium groups per repeat unit. However the AEM showed an increase in water uptake, ion exchange capacity and ionic conductivity. Choi *et al* reported peak conductivities of 111 mS cm^{-1} [145], a figure that is within the range of those observed for Nafion.

Lu *et al* [146] discuss the use of a different type of cross linking agent, one that is macromolecular in basis. They discuss that cross-linking on a macromolecular scale, like those discussed in section 1.5.5.1, tend to lead to AEMs with lower than expected ICs, because cross-linking requires a site that would otherwise be used for quarternisation. Lu *et al* also discuss that IPNs that are not complete suffer from non-uniformity which can lead to phase separations [146]. However they have designed an AEM that makes use of a macromolecular cross-linker prepared from polyvinyl alcohol and 4-dimethylaminobenzaldehyde, as shown in figure 1.24, as well as being a part IPN.

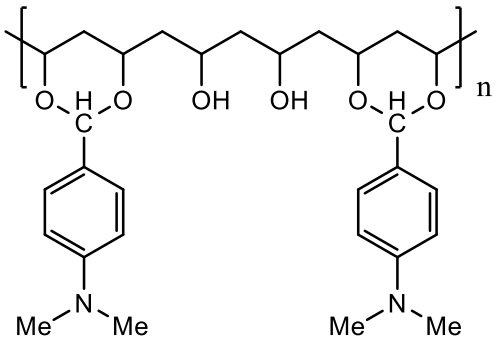

Figure 1.24: *Macromolecular cross-linker used by Lu et al [146].*

Once the cross-linking reaction has been performed, it can be seen that the quarternisation site that has been used for cross-linking will be replaced by the quaternary ammonium ion formed between N atom in figure 1.24 and the polyvinyl benzyl chloride that Lu *et al* used as the initial polymer substrate. The authors reported an increase in IC with increasing temperature, up to 50 S cm^{-1}. More importantly it was reported that the water uptake and swelling ratio of the AEM's did not increase with increasing temperature [146]. High water uptakes and swelling ratio can eventually lead to IC loss and membrane degradation.

The main synthetic routes to AEMs utilise chloromethyl methyl ether, CMME (figure 1.25) as the chloromethylating agent [83, 147]. CMME is highly toxic and carcinogenic to humans [148-150].

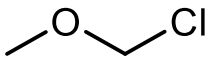

Figure 1.25: *Chloromethyl methyl ether.*

An attempt has been made to move away from using harmful reagents such as CMME and even the organic solvents used as reaction mediums [151]. The AEMs were prepared by mixing the polymer components and a cross-linker together and casting them in a controlled environment. The AEMs were then soaked in TMA and 1M KOH respectively to ensure they were OH^- conductive. All synthesised AEMs showed an increase in IC with increasing temperature, with a peak IC of 76 mS cm^{-1} at 70 ^oC

[152]. However the authors report that further work is needed to optimise the stability of AEMs prepared from solvent free strategies [152].

It has also been reported that Nafion does not perform particularly well in DMFC applications, due to a high methanol crossover which leads to a drastically lower fuel cell efficiency [32-35]. Abuin *et al* looked into preparing an alternative membrane for DMFC applications with the prospect of replacing Nafion [153]. A commercialised polysufone was used as the backbone and the AEM's were synthesised using similar techniques to those already discussed in this chapter. The reported IC of 14 mS cm^{-1} at 20 ^{o}C [153] is a lot lower than those observed for Nafion (100 mS cm^{-1} and higher). However, Abuin *et al* reported that the methanol permeability coefficient was lower than that observed for Nafion. The author then goes on to state that this can be attributed to the calculated activation energy of methanol permeation being higher for the synthesised membrane (32 kJ mol^{-1}) than that reported for Nafion (25 kJ mol^{-1}) [153]. In simple terms the membrane that Abuin *et al* created presents a stronger barrier to methanol crossover, which in theory will increase the overall efficiency of the fuel cell.

1.7 Implementation of AEM's in water electrolysis

For a portable device or even a car to be powered by a hydrogen fuel cell it needs to have a constant supply of both hydrogen and oxygen. The logistics of having separate hydrogen and oxygen fuel tanks is part of the reason why the commercialisation of these types of fuel cells has not occurred as rapidly as other developments. In theory, oxygen can come from air but hydrogen cannot be accessed so simply. Hydrogen is advantageous as it is clean, water is the only product of its combustion, it is relatively

easy to produce and it is available everywhere in the world [154]. Hydrogen is also extremely flammable, explosive and difficult to store without significant pressurisation. An alternative to gaseous hydrogen is to use solid state hydrogen storage materials. These materials release hydrogen after undergoing chemical reactions but as of yet are not efficient enough at producing a steady flow of hydrogen.

Electrolysis of water can be performed using any of the three main fuel cell devices known as electrolysers [155]. Water electrolysis is the decomposition of water into hydrogen and oxygen gas when an electrical current is passed through it [156, 157] (equations 1.46 – 1.48) The three types of electrolyser are:

1) Steam electrolysis [158] – performed at high temperatures.
2) PEM electrolyser [154] – making use of Nafion and platinum catalysts which are therefore expensive.
3) Alkaline electrolyser [155] – which as stated earlier make use of non-precious metal catalysts, alkaline electrolytes and solid alkaline membranes.

A hydrogen fuel cell produces water as its main product, which in theory could then be fed directly into a water electrolysis cell, producing hydrogen and oxygen which can then be fed back into the original cell.

$$\underline{\text{Cathode:}}\ 2H_2O + 2e^- \rightarrow H_2 + 2OH^- \quad \textbf{(1.46)}$$

$$\underline{\text{Anode:}}\ 4OH^- \rightarrow O_2 + 2H_2O + 4e^- \quad \textbf{(1.47)}$$

$$\underline{\text{Overall cell reaction:}}\ 2H_2O \rightarrow 2H_2 + O_2 \quad \textbf{(1.48)}$$

Lu *et al* reported the first implementation of the use of an alkaline polymer electrolyte in a water electrolysis cell [159]. The same QAPS membrane [83] as detailed in section 1.5.2 was used along with electrodes containing non-precious metal catalysts: a Ni-Mo cathode and Ni-Fe anode. A constant current was applied to the cell and the output voltage measured. At 70 ^{o}C Lu *et al* observed an increase in voltage with an increase in current density applied to the cell. Ideally one would like to see a drop in voltage as the current increases, as higher voltages can degrade the fragile OH^- conducting groups, however this work demonstrated the capability for alkaline membranes to be used in water electrolysis cells.

The main concern with alkaline water electrolysis is that it comes with a big power cost [155, 160]. Methanol has been proposed as an alternative fuel for obtaining hydrogen for portable devices. This is because only a voltage above 0.4 V is needed to electrolyse methanol as compared to above 1.2 V for water [160].

Equation 1.49 – 1.51 show the overall cell reaction in the electrolysis of methanol-water. The cathode reaction is the same as the one that occurs in the electrolysis of water, with the anode reaction somewhat different.

$$\underline{\text{Cathode:}}\ 2H_2O + 2e^- \rightarrow H_2 + 2OH^- \quad \textbf{(1.49)}$$

$$\underline{\text{Anode:}}\ CH_3OH + 6OH^- \rightarrow CO_2 + 5H_2O + 6e^- \quad \textbf{(1.50)}$$

$$\underline{\text{Overall cell reaction:}}\ CH_3OH + H_2O \rightarrow CO_2 + 3H_2 \quad \textbf{(1.51)}$$

Instead of oxygen being formed as the final product, carbon dioxide is instead formed, which can lead to questions as to whether the electrolysis of methanol is in fact a

"green energy source". Regardless of this, using a PVBC based polymer membrane, Tuomi *et al* have shown the reduction in energy required to run the cell over a water electrolyser. These authors stated that for every 10 mA cm^{-1} of current applied, this equated to around 30 ml/hour of hydrogen produced, meaning an overall efficiency of more than 90% [160].

1.8 The challenges of the alkaline fuel cell

Over the course of this introduction a number of key development issues with the APEMFC have been assessed. Firstly, the solid membranes used do not possess the same level of stability and conductivity as seen in their PEM counterparts. This restricts the fuel cell operation to lower temperatures where degradation is lower, which in turn has an impact on the already lower performance. Secondly, although non-noble metal catalysts can be used instead of platinum, again their performance comes nowhere near that of platinum based catalysts. Finally when both these points are combined, the results are a fuel cell that overall has a drastically lower power output than standard PEMFC. These are the challenges that face researchers in the development of new materials for alkaline fuel cells.

1.9 – Chapter 1 references

[1]. U. Nations, (1997).

[2]. *UK Department of Energy and Climate Change*, Annual Statement of Emissions for 2012, (2014).

[3]. *UK Department of Energy and Climate Change*, 2012 UK Greenhouse Gas Emissions - Final Figures, (2014).

[4]. M. Z. Jacobson, W. G. Colella and D. M. Golden, *Science*, (2005), **308**, 1901-05.

[5]. J. Wee, *Renewable and Sustainable Energy Reviews II*, (2007), **11**, 1720-38.

[6]. B. C. H. Steele and A. Heinzel, *Nature*, (2001), **414**, 345-52.

[7]. L. Gubler and G. G. Scherer, *Desalination*, (2010), **210**, 1034-37.

[8]. L. Carrette, K. A. Friedrich and U. Stimming, *Fuel Cells*, (2001), **1**, 5-39.

[9]. M. Li and K. Scott, *Electrochemica Acta*, (2010), **55**, 2123-28.

[10]. R. Farrauto, *Applied Catalysis B: Environmental*, (2005), **56**, 3–7.

[11]. S. J. Peighambardoust, S. Rowshanzamir and M. Amjadi, *International Journal of Hydrogen Energy*, (2010), **35**, 9349-84.

[12]. N. L. Garland, *US Department of Energy Fuel Cell Technologies Program*, 18th World Hydrogen Energy Conference, Essen, Germany, (2010).

[13]. G. Mulder, *Reference Module in Chemistry, Molecular Sciences and Chemical Engineering*, (2013), Alkaline Fuel Cells - Overview, 321-28.

[14]. M. Schulze and E. Gulzow, *Reference Module in Chemistry, Molecular Sciences and Chemical Engineering*, (2013), Alkaline Fuel Cells - Overview Performance and Operational Conditions, 353-61.

[15]. A. J. Appleby, *Reference Module in Chemistry, Molecular Sciences and Chemical Engineering*, (2013), Phosphoric Acid Fuel Cells - Overview, 533-47.

[16]. R. Lan, X. Xu, S. Tao and J. T. S. Irvine, *Journal of Power Sources*, (2010), **195**, 6983-87.

[17]. G. Crawley, *Fuel Cell Today*, (2007).

[18]. G. Couture, A. Alaaeddine, F. Boschet and B. Ameduri, *Progress in Polymer Science*, (2011), **36**, 1521– 57.

[19]. A. Brouzgou, A. Podias and P. Tsiakaras, *Journal of Applied Electrochemistry*, (2013), **43**, 119–36.

[20]. A. Kulkarni and S. Giddey, *Journal of Solid State Electrochemistry*, (2012), **16**, 3123–46.

[21]. A. L. Dicks, *Reference Module in Chemistry, Molecular Sciences and Chemical Engineering*, (2013), Molten Carbonate Fuel Cells - Overview, 446-53.

[22]. D. Sanchez, B. Monje, R. Chacartegui and S. Campanari, *International Journal of Hydrogen Energy*, (2013), **38**, 394-405.

[23]. A. Moreno, S. McPhail and R. Bove, *Italian National Agency for New Technologies, Energy and the Enviroment*, International Status of Molten Carbonate Fuel Cell (MCFC) Technology, (2008).

[24]. Y. Zhao, C. Xia, L. Jia, Z. Wang, H. Li, J. Yu and Y. Li, *International Journal of Hydrogen Energy*, (2013), **38**, 16498-517.

[25]. P. I. Cowin, C. T. G. Petit, R. Lan, J. T. S. Irvine and S. Tao, *Advanced Energy Materials*, (2011), **1**, 314–32.

[26]. J. R. Varcoe and R. C. T. Slade, *Fuel Cells*, (2005), **5**, 187-200.

[27]. D. Valade, F. Boschet, S. Roualdes and B. Ameduri, *Journal of Polymer Science, Part A: Polymer Chemistry*, (2009), **47**, 2043-58.

[28]. E. Agel, J. Bouet and J. F. Fauvarque, *Journal of Power Sources*, (2001), **101**, 267-74.

[29]. C. Sollogoub, A. Guinault, C. Bonnebat, M. Bennjima, L. Akrour, J. F. Fauvarque and L. Ogier, *Journal of Membrane Science* (2009), **335**, 37–42.

[30]. V. Neburchilov, J. Martin, H. Wang and J. Zhang, *Journal of Power Sources*, (2007), **169**, 221-38.

[31]. Y. F. Liang, X. L. Zhu and X. G. Jian, *Solid State Ionics*, (2008) **179**, 1940–45.

[32]. H. Ahmad, S. K. Kamarudin, U. R. Hasran and W. R. W. Daud, *International Journal of Hydrogen Energy*, (2010), **35**, 2160-75.

[33]. Z. G. Shao, X. Wang and I. M. Hsing, *Journal of Membrane Science*, (2002), **210**, 147-53.

[34]. H. A. Every, M. A. Hickner, J. E. McGrath and T. A. Z. Jr, *Journal of Membrane Science*, (2005), **250**, 183-88.

[35]. K. Ramya and K. S. Dhathathreyan, *Journal of Membrane Science*, (2008), **311**, 121-27.

[36]. O. T. Holton and J. W. Stevenson, *Platinum Metals Reviews*, (2013), **57**, 259–71.

[37]. J. M. Jaksic, N. M. Ristic, N. V. Krstajic and M. M. Jaksic, *International Journal of Hydrogen Energy*, 1998, **12**, 1121-56.

[38]. H. A. Gasteiger, J. E. Panels and S. G. Yan, *Journal of Power Sources*, (2004), **127**, 162–71.

[39]. R. Borup, *Chemistry Reviews*, (2007), **107**, 3904-51.

[40]. E. Antolini, J. R. C. Salgado and E. R. Gonzalez, *Journal of Power Sources*, (2006), **160**, 957–68.

[41]. N. Zamel and X. Li, *Progress in Energy and Combustion Science*, (2011), **37**, 292-329.

[42]. I. E. L. Stephens, A. S. Bondarenko, U. Grønbjerg, J. Rossmeislc and I. Chorkendorff, *Energy and Enviromental Science*, (2012), **5**, 6744-62.

[43]. H. A. Gasteiger, S. S. Kocha, B. Sompalli and F. T. Wagner, *Applied Catalysis B: Environmental* (2005), **56**, 9–35.

[44]. D. Carter, *Fuel Cell Today*, (2013).

[45]. *US Department of Energy: Hydrogen and Fuel Cell Technologies FY-14 Budget*, (2013).

[46]. V. A. Sethuraman and J. W. Weidner, *Electrochimica Acta*, (2010), **55**, 5683–94

[47]. X. Cheng, Z. Shi, N. Glass, L. Zhang, J. Zhang, D. Songa, Z. Liu, H. Wang and J. Shen, *Journal of Power Sources*, (2007), **165**, 739–56.

[48]. V. Mehta and J. S. Cooper, *Journal of Power Sources*, (2003), **114**, 32-53.

[49]. W. Schmittinger and A. Vahidi, *Journal of Power Sources*, (2008), **180**, 1-14.

[50]. S. Bose, T. Kuila, T. X. H. Nguyen, N. H. Kim, K. Lau and J. H. Lee, *Progress in Polymer Science*, (2011), **36**, 813–43.

[51]. J. Wu, X. Z. Yuan, J. J. Martin, H. Wang, J. Zhang, J. Shen, S. Wu and W. Merida, *Journal of Power Sources*, (2008) **184**, 104–19.

[52]. A. Collier, H. Wang, X. Z. Yuan, J. Zhang and D. P. Wilkinson, *International Journal of Hydrogen Energy*, (2006), **31**, 1838 – 54.

[53]. A. Rodrigues, J. C. Amphlett, R. F. Mann, B. A. Peppley and P. R. Roberge, *Royal Military College of Canada*.

[54]. J. J. Baschuk and X. Li, *International Journal of Energy Research*, (2001), **25**, 695-713.

[55]. R. Mohtadi, W.-K. Lee and J. W. V. Zee, *Applied Catalysis B: Environmental*, (2005), **56**, 37-42.

[56]. L. A. Linden, J. F. Rabek, H. Kaczmarek, A. Kaminska and M. Scoponi, *Coordination Chemistry Reviews*, (1993), **125**, 195-217.

[57]. D. E. Curtin, R. D. Lousenberg, T. J. Henry, P. C. Tangeman and M. E. Tisack, *Journal of Power Sources*, (2004), 41-48.

[58]. H. Meng and P. K. Shen, *Electrochemistry Communications*, (2006), **8**, 588–94.

[59]. F. Bidault, D. J. L. Brett, P. H. Middleton and N. P. Brandon, *Journal of Power Sources*, (2009), **187**, 39-48.

[60]. K. N. Grew and W. K. S. Chiu, *Journal of Electrochemical Society*, (2009), **156**, 13831-35.

[61]. J. Wang, S.Li and S. Zhang, *Macromolecules*, (2010), **43**, 3890-96.

[62]. N. A. Karim and S. K. Kamarudin, *Applied Energy*, (2013), **103**, 212-20.

[63]. H. Qin, S. Lao, Z. Liu, J. Zhu and Z. Li, *International Journal of Hydrogen Energy*, (2010), **35**, 1872-78.

[64]. H. Qin, Z. Liu, S. Lao, J. Zhu and Z. Li, *Journal of Power Sources*, (2010), **195**, 3124-29.

[65]. H.-J. Zhang, Q.-Z. Jiang, L. Sun, X. Yuan and Z.-F. Ma, *Electrochimica Acta*, (2010), **55**, 1107-12.

[66]. F. Brushett, *Journal of the American Chemistry Society*, (2010), **132**, 12185-87.

[67]. A. Nakamura, *ECS Transactions*, (2010), **33**, 1817-21.

[68]. J. Ma, Y. Liu, P. Zhang and J. Wang, *Electrochemistry Communications*, (2008), **10**, 100-02.

[69]. J. Ma, J. Wang and Y. Liu, *Journal of Power Sources*, (2007), **172**, 220-24.

[70]. J. Wu, Y. Wang, D. Zhang and B. Hou, *Journal of Power Sources*, (2011), **196**, 1141-44.

[71]. K. R. Lee, K. U. Lee, J. W. Lee, B. T. Ahn and S. I. Woo, *Electrochemistry Communications*, (2010), **12**, 1052-55.

[72]. L. Qu, Y. Liu, J.-B. Baek and L. Dai, *American Chemical Society NANO*, (2010), **4**, 1321-26.

[73]. L. Tang, Y. Wang, Y. Li, H. Feng, J. Lu and J. Li, *Advanced Functional Materials*, (2009), **19**, 2782-89.

[74]. B. Seger and P. Kamat, *Journal of Physical Chemistry C Letters*, (2009), **113**, 7990-95.

[75]. Y. Xin, J. Liu, Y. Zhou, W. Liu, J. Gao, Y. Xie, Y. Yin and Z. Zou, *Journal of Power Sources*, (2011), **196**.

[76]. R. Lan and S. Tao, *Journal of Power Sources*, (2011), **196**, 5021-26.

[77]. S. Ewing, R. Lan, X. Xu and S. Tao, *Fuel Cells*, (2009), **10**, 72-76.

[78]. Z. Chen, J. Choi, H. Wang, H. Li and Z. Chena, *Journal of Power Sources*, (2011), **196**, 3673-77.

[79]. D. Kubo, K. Tadanaga, A. Hayashi and M. Tatsumisago, *Journal of Power Sources* (2013) **222**, 493-97.

[80]. A. Morozan, B. Jousselme and S. Palacin, *Energy and Enviromental Science*, (2011), **4**, 1238-54.

[81]. F. Jaouen, E. Proietti, M. Lefevre, R. Chenitz, J.-P. Dodelet, G. Wu, H. T. Chung, C. M. Johnston and P. Zelenay, *Energy and Enviromental Science*, (2011), **4**, 114-30.

[82]. L. Zeng, T. S. Zhao, L. An, G. Zhao, X. H. Yan and C. Y. Jung, *Journal of Power Sources*, (2015), 275, 506-15.

[83]. S. Lu, J. Pan, A. Huang, L. Zhuang and J. Lu, *Proceedings of the National Academy of Sciences*, (2008).

[84]. J. Fu, J. Qiao, X. Wang, J. Ma and T. Okada, *Synthetic metals*, (2010), **160**, 193-99

[85]. Y. Lao, J. Guo, C. Wang and D. Chu, *Journal of Power Sources*, (2010), **195**, 3765-71.

[86]. J. Park, S. Park, S. Yim, Y. Yoon, W. Lee and C. Kim, *Journal of Power Sources*, (2008), **178**, 620-26.

[87]. G. F. McLean, T. Niet, S. Prince-Richard and N. Djilali, *International Journal of Hydrogen Energy*, (2002), **27**, 507-26.

[88]. S. Suzuki, H. Muroyama, T. Matsui and K. Eguchi, *Electrochemica Acta*, (2013), **88**, 552– 58.

[89]. M. A. Al-Saleh, S. Gültekin, A. S. Al-Zakri and H. Celiker, *Journal of Applied Electrochemistry*, (1994), **24**, 575-80.

[90]. R. Lan and S. Tao, *Electrochemical & Solid State Letters*, (2010), **13**, B83-B86

[91]. R. Lan, S. Tao and J. T. S. Irvine, *Energy Environ. Sci*, (2010), **3**, 438-41.

[92]. A. L. Ong, A. Bottino, G. Capanelli and A. Comite, *Journal of Power Sources*, (2008), **183**, 62-68.

[93]. F. Zhang, H. Zhang, J. Ren and C. Qu, *Journal of Materials Chemistry*, (2010), **20**, 8139-46.

[94]. J. Pan, S. Lu, Y. Li, A. Huang, L. Zhuang and J. Lu, *Advanced Functional Materials*, (2010), **20**, 312-19.

[95]. P. Chu, C.-S. Wu, P.-C. Liu, T.-H. Wang and J.-P. Pan, *Polymer Chemistry*, (2010), **51**, 1386-94.

[96]. G. Merle, M. Wessling and K. Nijmeijer, *Journal of Membrane Science*, (2011), **377**, 1-35.

[97]. M. E. Tuckerman, D. Marx and M. Parrinello, *Nature*, (2002), **417**.

[98]. Y. Wang, J. Qiao, R. Baker and J. Zhang, *Chem. Soc. Reviews*, (2013), **42**, 5768--87.

[99]. J. Ni, C. Zhao, G. Zhang, Y. Zhang, J. Wang, W. Ma, Z. Liu and H. Na, *Chem. Commun.*, (2011), **47**, 8943–45.

[100]. T. Chakrabarty, S. Prakash and V. K.Shahi, *Journal of Membrane Science*, (2013), **428**, 86–94.

[101]. J. B. Edson, C. S. Macomber, B. S. Pivovar and J. M. Boncella, *Journal of Membrane Science*, (2012) **399- 400**, 49– 59.

[102]. J. Pan, Y. Li, L. Zhang and J. Lu, *Chem. Commun.*, (2010), **46**, 8597-99.

[103]. F. Zhang, H. Zhang and C. Qu, *Journal of Materials Chemistry*, (2011), **21**, 12744-52.

[104]. J. Wang, R. He and Q. Che, *Journal of Colloid and Interface Science*, (2011), **361**, 219-25.

[105]. Y. Wan, B. Peppley, K. A. M. Creber and V. T. Bui, *Journal of Power Sources*, **195**, 3785-93.

[106]. F. Schmitt, R. Granet, C. Sarrazin, G. Mackenzie and P. Krausz, *Carbohydrate Polymers*, (2011), **86**, 362-66.

[107]. H. Xu, J. Fang, M. Guo, X. Lu, X. Wei and S. Tu, *Journal of Membrane Science*, (2010), 354, 206-11.

[108]. M. Mamlouk, J. A. Horsfall, C. Williams and K. Scott, *International Journal of Hydrogen Energy*, (2012), **37**, 11912-20.

[109]. X. Yan, S. Gu, G. He, X. Wu, W. Zheng and X. Ruan, *Journal of Membrane Science*, (2014), **466**, 220-28.

[110]. S. Gu, R. Cai, T. Luo, Z. Chen, M. Sun, Y. Liu, G. He and Y. Yan, *Angew. Chem. Int. Ed.*, (2009), **48**, 6499 –502.

[111]. K. Noonan, K. M. Hugar, H. A. Kostalik, E. B. Lobkovsky, H. D. Abruña and G. W. Coates, *Journal of American Chemical Society*, (2012), **134**, 18161−64.

[112]. N. M. M. Mateus, L. C. Branco, N. M. T. Lourenço and C. A. M. Afonso, *Green Chemistry*, (2003), **5**, 347-52.

[113]. Q. Zhang, S. Li and S. Zhang, *Chemistry Communinations*, (2010), **46**, 7495-97.

[114]. T. A. Sherazi, S. Zahoor, R. Raza, A. J. Shaikh, S. A. R. Naqvi, G. Abbas, Y. Khan and S. Li, *International Journal of Hydrogen Energy*, (2015), **40**, 786-96.

[115]. W. Li, S. Wang, X. Zhang, W. Wang, X. Xie and P. Pei, *International Journal of Hydrogen Energy*, (2014), **39**, 13710-17.

[116]. B. Zhang, S. Gu, J. Wang, Y. Liu, A. M. Herring and Y. Yan, *RSC Advances*, (2012), **2**, 12683-85.

[117]. Y. Yang, J. Wang, J. Zheng, S. Li and S. Zhang, *Journal of Membrane Science*, (2014), **467**, 48-55.

[118]. O. I. Deavin, S. Murphy, A. L. Ong, S. D. Poynton, R. Zeng, H. Herman and J. R. Varcoe, *Energy and Enviromental Science*, (2012), **5**, 8584-97.

[119]. M. A. Hossain, Y. Lim, S. Lee, H. Jang, S. Choi, Y. Jeon, S. Lee, H. Jub and W. G. Kim, *Solid State Ionics*, (2014), **262**, 754-60.

[120]. W. Wang, S. Wang, X. Xie, Y. lv and V. K. Ramani, *Journal of Membrane Science*, (2014), **462**, 112-18.

[121]. W. Wang, S. Wang, X. Xie, Y. lv and V. Ramani, *International Journal of Hydrogen Energy*, (2014), **39**, 14355-61.

[122]. L.-C. Jheng, S. L.-C. Hsu, B.-Y. Lin and Y.-I. Hsu, *Journal of Membrane Science*, (2014), **460**, 160-70.

[123]. B. Lin, F. Chu, Y. Ren, B. Jia, N. Yuan, H. Shang, T. Feng, Y. Zhu and J. Ding, *Journal of Power Sources*, (2014), **266**, 186-92.

[124]. M. A. Hickner, A. M. Herring and E. B. Coughlin, *Journal of Polymer Science, Part B: Polymer Physics*, (2013), **51**, 1727–35.

[125]. G. Wang, Y. Weng, D. Chu, R. Chen and D. Xie, *Journal of Membrane Science*, (2009), **332**, 63-68.

[126]. Y. Zhao, J. Pan, H. Yu, D. Yang, J. Li, L. Zhuang, Z. Shao and B. Yi, *International Journal of Hydrogen Energy*, (2013), **38**, 1983-87.

[127]. X. Wang, M. Li, B. T. Golding, M. Sadeghi, Y. Cao, E. H. Yu and K. Scott, *International Journal of Hydrogen Energy*, (2011), **36**, 10022-26.

[128]. R. Vinodh and D. Sangeetha, *Journal of Applied Polymer Science*, (2013), 1930-38.

[129]. Y. Cao, K. Scott and X. Wang, *International Journal of Hydrogen Energy*, (2012), **37**, 12688-93.

[130]. Y. Zhao, H. Yu, D. Yang, J. Li, Z. Shao and B. Yi, *Journal of Power Sources*, (2013), **221**, 247-51.

[131]. Y. Cao, C. Xu, X. Wu, X. Wang, L. Xing and K. Scott, *Journal of Power Sources*, (2011), **196**, 8377-82.

[132]. Y. Cao, X. Wang and K. Scott, *Journal of Power Sources*, (2012), **201**, 226-30.

[133]. A. Jasti, S. Prakash and V. K. Shahi, *Journal of Membrane Science*, (2013), **428**, 470–79.

[134]. D. W. Seo, Y. D. Lim, M. A. Hossain, S. H. Lee, H. C. Lee, H. H. Jang, S. Y. Choi and W. G. Kim, *International Journal of Hydrogen Energy*, (2013), **38**, 579-87.

[135]. H. L. S. Salerno and Y. A. Elabd, *Journal of Applied Polymer Science*, (2013), 298-307.

[136]. H. Hou, S. Wang, W. Jin, Q. Jiang, L. Sun, L. Jiang and G. Sun, *International Journal of Hydrogen Energy*, (2011), **36**, 5104-09.

[137]. J. Wang, Z. Zhao, F. Gong, S. Li and S. Zhang, *Macromolecules*, (2009), **42**, 8711–17.

[138]. Q. Zhang, Q. Zhang, J. Wang, S. Zhang and S. Li, *Polymer*, (2010), **51**, 5407-16.

[139]. X. Li, Y. Yu and Y. Meng, *ACS Applied Materials & Interfaces*, (2013), **5**, 1414–22.

[140]. J. Zhou, M. Unlu, I. Anestis-Richard and P. A. Kohl, *Journal of Membrane Science*, (2010), **350**, 286-92.

[141]. M. Tanaka, M. Koike, K. Miyatake and M. Watanabe, *Polymer Chemistry*, (2011), **2**, 99-106.

[142]. Y. Wu, C. Wu, T. Xu, X. Lin and Y. Fu, *Journal of Membrane Science*, (2009), **338**, 51-60.

[143]. Y. Wu, C. Wu, J. R. Varcoe, S. Poynton, T. Xu and Y. Fu, *Journal of Power Sources*, (2010), **195**, 3069-76.

[144]. T. Zhou, J. Zhang, J. Qiao, L. Liu, G. Jiang, J. Zhang and Y. Liu, *Journal of Power Sources* (2013), **227**, 291-99.

[145]. J. Choi, Y.-J. Byun, S. Y. Lee, J. H. Jang, D. Henkensmeier, S. J. Yoo, S.-A. Hong, H.-J. Kim, Y.-E. Sung and J.-S. Park, *International Journal of Hydrogen Energy*, (2014), 39, 21223-30.

[146]. W. Lu, Z.-G. Shao, G. Zhang, Y. Zhao and B. Yi, *Journal of Power Sources*, (2014), **248**, 905-14.

[147]. K. H. Gopi, S. G. Peera, S. D. Bhat, P. Sridhar and S. Pitchumani, *International Journal of Hydrogen Energy*, (2014), **39**, 2659-68.

[148]. *Hazardous Substances Data Bank (HSDB)*, US EPA, CASRN: 107-30-2.

[149]. *US EPS Integrated Risk Info System (IRIS)*, CASRN: 107-30-2.

[150]. *Acute Exposure Guideline Levels for Selected Airborne Chemicals: Volume 11*, (2012), National Academy of Sciences.

[151]. X. Lin, M. Gong, Y. Liu, L. Wu, Y. Li, X. Liang, Q. Li and T. Xu, *Journal of Membrane Science*, (2013), 425-426, 190-99.

[152]. X. Lin, Y. Liu, S. D. Poynton, A. L. Ong, J. R. Varcoe, L. Wu, Y. Li, X. Liang, Q. Li and T. Xu, *Journal of Power Sources*, (2013), **233**, 259-68.

[153]. G. C. Abuin, E. A. Franceschini, P. Nonjola, M. K. Mathe, M. Modibedi and H. R. Corti, *Journal of Power Sources*, (2015), **279**, 450-59.

[154]. J. D. Holladay, J. Hu, D. L. King and Y. Wang, *Catalysis Today*, (2009), **139**, 244-60.

[155]. J. Hnat, M. Paidar, J. Schauer, J. Zitka and K. Bouzek, *Journal of Applied Electrochemistry*, (2011), **41**, 1043-52.

[156]. M. Carmo, D. L. Fritz, J. Mergel and D. Stolten, *International Journal of Hydrogen Energy*, (2013), **38**, 4901-34.

[157]. C. Mittelsteadt, T. Norman, M. Rich and J. Willey, *Electrochemical Energy Storage for Renewable Sources and Grid Balancing*, (2015), PEM Electrolyzers and PEM Regenerative Fuel Cells Industrial View, 159-81.

[158]. P. Mocoteguy and A. Brisse, *International Journal of Hydrogen Energy*, (2013), **38**, 15887-902.

[159]. L. Xiao, S. Zhang, J. Pan, C. Yang, M. He, L. Zhuang and J. Lu, *Energy and Environmental Science*, (2012), **5**, 7869-71.

[160]. S. Tuomi, A. Santasalo-Aarnio, P. Kanninen and T. Kallio, *Journal of Power Sources*, (2013), **229**, 32-35.

Chapter 2: Aims

The main aim of this work was to prepare polymeric anion exchange membranes for use in alkaline polymer electrolyte fuel cells. Membranes were synthesised, characterised and tested in water at varying temperatures for varying amounts of time. The obtained data could then be compared to similar membranes reported in the literature.

As the name suggest, polymeric anion exchange membranes feature one or several polymer materials at their core. The first aim was to find a polymer suitable for use in alkaline PEM fuel cells. Due to the operating conditions of APEMFCs the polymer must be thermally and mechanically stable up to 100 ^{o}C, be acid/base stable and more importantly be completely insoluble in water. Nearly all polymers are thermally stable well past 100 ^{o}C and show acid/base resistance, however there are a few which are soluble in water, like polyvinyl alcohol, PVA. Many different polymers have been reported in the literature as being suitable for AEM production. One of the first reported AEMs in the literature by Lu *et al* used polysulphone (PS) [1] but since then many other polymers have been used and reported. Recently poly(2,6-dimethyl-1,4-phenylene oxide), PPO, has gained attention due to its high mechanical strength and high stability in hydrolysing environments [2]. PPO also features a higher glass transition temperature (213 ^{o}C) than polysulphone (185^{o}C) and polyether ether ketone (PEEK) (143 ^{o}C). Therefore, for these reasons PPO was chosen to be the main polymer used for synthesis of AEMs. Other polymers would be considered/used depending on PPO's performance.

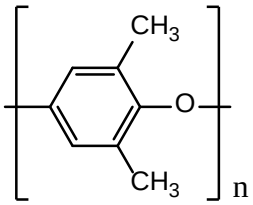

12

Figure 2.1: *Poly(2,6-dimethyl-1,4-phenylene oxide), PPO.*

During the introduction section, it was explained that the production of AEMs occurs in three stages, chloromethylation of polymer, quarternisation and ion exchange. The second aim of this work was to make use of a quick, easy and more importantly, a safe way of preparing AEMs. A lot of current AEMs use the highly toxic and carcinogenic [3-7], chloromethyl methyl ether as their chloromethylating agent [2, 8]. We decided to follow the trend of using the safer approach of paraformaldehyde and zinc chloride to chloromethylate the polymer. This would allow us to compare our data with AEMs made by a similar technique.

Trimethylamine, TMA, features heavily as the material of choice for inserting the quaternary ammonium group onto the polymer. However, as seen in the introduction section other quaternary ions have been discussed like imidazolium, guandinium, phosphonium and sulfonium. Although some of these quaternary ions have proven to be quite stable [9], they are expensive, can feature lengthy preparation processes and do not match the ease of insertion as trimethylamine. Therefore for these reasons TMA was chosen to be the quaternising agent.

A good AEM must primarily be a good conductor of OH^- ions as well as being stable in APEMFC working conditions. Ionic conductivity would be measured using electrochemical impedance spectroscopy, thermal and mechanical stability would be ascertained by thermal gravimetric analysis and structural information would be gained from infrared spectroscopy. These initial results would allow us to determine whether or not the AEM would be suitable for further testing.

The ionic conductivity of the AEMs was measured in water at temperatures from RT – 90 oC. An ionic conductivity (IC) > 10 mS cm^{-1} ideally over the full temperature range was required and anything < 10 mS cm^{-1} would need further work. If the membrane showed good conductivity at higher temperatures having started from < 10 mS cm^{-1}, it would be kept. By having this criteria, immediately any synthesised membrane with IC > 10 mS cm^{-1} is comparable to most AEMs reported in the literature. Initial loop tests in water at the temperature at which the highest IC was observed were performed for a couple of days to judge the relative stability of the membranes.

At this stage membranes would be categorised into two bands, IC's < or > 10 mS cm^{-1}. Any membrane with an IC below 10 mS cm^{-1} would be analysed to see whether the conductivity could be improved, by altering the chloromethylation process. Any membrane with conductivity above 10 mS cm^{-1} was tested for an extended period of time, again in water at the temperature at which the highest IC was observed. This time period would last for days, weeks, even months, depending on the performance of the membrane which would be measured every few hours by EIS, and checked every day.

Some high performing membranes would also be tested in harsher potassium hydroxide environments. Any issues with stability of the AEM's would be addressed with procedures already explained in the introduction, cross-linking, and the use of other polymers or even IPNs.

After all data had been collected, the final aim was to employ the best performing AEM's within actual H_2/O_2 fuel cells or water electrolysis cells. This would then allow us to evaluate each AEM and suggest further ways of improving the performance and/or stability.

2.1 – Chapter 2 references

[1]. S. Lu, J. Pan, A. Huang, L. Zhuang and J. Lu, *Proceedings of the National Academy of Sciences*, (2008).

[2]. G. Wang, Y. Weng, J. Zhao, D. Chu, D. Xie and R. Chen, *Polymers Advanced Technologies*, (2010), **21**, 554-60.

[3]. V. V. Shevchenko and M. A. Gumennaya, *Theoretical and Experimental Chemistry*, (2010), **46**, 139-52.

[4]. T. Chakrabarty, S. Prakash and V. K.Shahi, *Journal of Membrane Science*, (2013), **428**, 86–94.

[5]. *Hazardous Substances Data Bank (HSDB)*, US EPA, CASRN: 107-30-2.

[6]. *US EPS Integrated Risk Info System (IRIS)*, CASRN: 107-30-2.

[7]. *Acute Exposure Guideline Levels for Selected Airborne Chemicals: Volume 11*, (2012), National Academy of Sciences.

[8]. K. H. Gopi, S. G. Peera, S. D. Bhat, P. Sridhar and S. Pitchumani, *International Journal of Hydrogen Energy*, (2014), **39**, 2659-68.

[9]. W. Wang, S. Wang, X. Xie, Y. lv and V. Ramani, *International Journal of Hydrogen Energy*, (2014), **39**, 14355-61.

Chapter 3: Experimental and characterisation techniques

This chapter gives an in depth description of the synthesis methods employed in this thesis and the analytical and characterisation techniques used to analyse all prepared samples. The analytical techniques include electrochemical impedance spectroscopy, infra-red spectroscopy and thermal gravimetric analysis. All work was performed using equipment within the Fuel Cell group led by Professor Tao or belonging to the Chemical and Process Engineering department at the University of Strathclyde.

3.1 Experimental details

3.1.1 Chloromethylation

Chloromethylation of PPO (Sigma Aldrich) was carried out using the apparatus displayed in figure 3.1. All joints were greased with vacuum grease to keep a tight seal. Paraformaldehyde (Alfa Aesar, 97%) and 1, 2-dichloroethane (Alfa Aesar, 99+%) were placed in the three necked round bottomed flask along with a magnetic stirrer bar. This flask sat in an Asynt DrySyn single position heating block on top of a hot plate. This type of heating apparatus was used to reduce the chance of any water being accidently introduced to the system. In the centre socket a water jacket condenser was fitted and supported with a clamp stand. The water supply was connected to the bottom port and the exit pipe placed down the drain. Initially a stopper was placed in the right hand socket. In the left hand socket, the nitrogen gas line was placed along with the thermocouple for the hot plate. Both the nitrogen line and the thermocouple pierced a Nesco film layer placed over the neck of the socket. The end of the nitrogen gas line was placed in the solution so bubbles could be observed once the gas was turned on. This was performed to monitor the gas pressure throughout the synthesis.

With nitrogen gas bubbling, this solution was heated to 50 ^{o}C and left to stir for 30 minutes to allow the paraformaldehyde to de-polymerise. After 30 minutes, zinc chloride was added to the solution through the stoppered socket (**A** on figure 3.1) with the aid of a funnel. The stopper was re-attached and the solution left to stir for a further 30 minutes at 50 ^{o}C. At this point the reaction solution was more or less clear and colourless. To start the reaction PPO was then quickly added to the solution through a funnel via the same position as the zinc chloride. Once all PPO had been added, instead of a stopper the HCl gas line was inserted into socket **A**. HCl gas was produced in house by the reaction of sodium chloride and sulphuric acid.

$$NaCl\ (s)\ +\ c.\ H_2SO_4\ (l) \rightarrow\ NaHSO_4\ (s)\ +\ HCl\ (g) \qquad (\mathbf{3.1})$$

Immediately after the addition of the HCl gas the reaction solution started to turn a yellow colour and after about 30 minutes the solution was a dark orange/brown. The solution was left stirring at 50 ^{o}C for ca. 1 – 6 hours. The reaction was considered to be complete once a dark brown, slightly viscous solution was observed. The reaction was carefully watched and controlled as it proved to be very unstable. As the reaction proceeded the liquor seemed to get visibly thicker. Upon observing the thickening of the solution, small amounts of 1, 2-dichloroethane were added to the mixture to thin it out. It was even more imperative to carefully observe the reaction when this occurred as quite often this meant that the reaction has “overly cross-linked” and would eventually produce a viscous gel that would be very difficult to remove from the vessel.

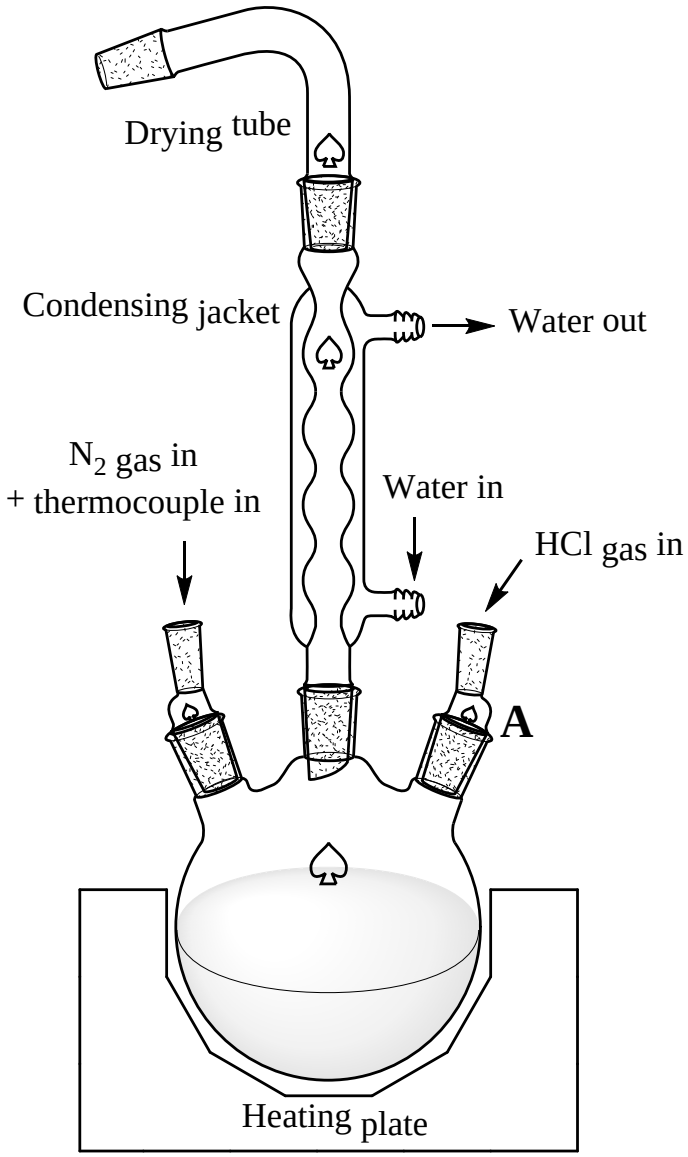

Figure 3.1: *Apparatus set-up for chloromethylation of PPO. The solution within the flask consisted of PPO, paraformaldehyde and $ZnCl_2$ all dissolved in 1, 2-dichloroethane.*

On occasions this viscous gel was formed and proved very difficult to obtain any chloromethylated product from it. Even if some chloromethylated product was obtained, upon trying to dissolve it again in another solvent, the same viscous gel

would be observed instead of a clear solution. This led to the whole batch being discarded and the reaction repeated. It was also noted that over time a precipitation build-up occurred on the ends of the two gas lines, which slowed the rate at which gas entered the system. This build-up occurred more on the nitrogen line and needed to be removed to allow the continued flow of nitrogen.

Once the reaction went to completion, the HCl gas line was disconnected and a stopper replaced in socket **A**. Any remaining salt and acid mixture was neutralised and disposed of immediately. The nitrogen gas was turned off at the cylinder and the remaining gas pressure in the regulator and pipe work was allowed to dissipate through the reaction vessel. The three neck round bottom flask was disconnected from the condenser and while the solution was still warm, poured into a beaker of methanol. Immediately a white precipitate was formed which was either a very fine powder or small clumps of white solid, depending on the success of the reaction. When small clumps of white solid were observed, this tended to indicate that the reaction product was slightly over crosslinked. Ideally the solid was allowed to precipitate in the methanol with gentle stirring overnight to maximise recovery. The white solid present was chloromethylated PPO, CMPPO. This powder was filtered through a Buchner funnel and washed with methanol and copious amounts of water, followed by drying at 60 ^{o}C for 24 hours.

3.1.2 Quarternisation

The quarternisation of CMPPO was carried out using the apparatus shown in figure 3.2. An amount of CMPPO, usually enough to form a 10% by weight solution was

dissolved in 1-methyl-2-pyrrolidinone (NMP) in a small glass sample vial. Depending on the variety of the CMPPO this could take a matter of 10 minutes at room temperature or 2-3 hours with the aid of heat. This was usually a very good indicator of whether the prepared membrane was going to be conductive and/or stable. A sample that was slightly over cross-linked tended to take a long time to dissolve, usually showed lower ionic conductivities. CMPPO in fine powder form was found to be highly conductive but the corresponding membranes were not particularly stable at high temperatures for long periods of time. On the other hand, chunks of solid were found to be not as conductive but were extremely stable at high temperatures for long periods of time.

Once the CMPPO was dissolved, a 30% aqueous solution of trimethylamine (TMA) was placed in a single neck round bottom flask (Figure 3.2). The flask was stoppered with a rubber bung with a plastic tube through the centre of it. This plastic tube acted as the gas pipe for the trimethylamine gas to reach the CMPPO solution. TMA is a gas at room temperature (boiling point of 3 ^{o}C) hence the TMA solution required low heat to produce a sufficient gas flow. The TMA solution was usually heated to about 25-28 ^{o}C. A small stirrer bar was placed in the vial of CMPPO solution and stirred at a slow rate. After a short time of heating, the TMA started bubbling slowly through the CMPPO solution. This continued for 30 minutes, making sure that the bubbling never exceeded roughly 1 bubble every 5 seconds. If the bubbling rate was excessive, the CMPPO solution turned a milky white colour and a solid precipitated out, which could not be dissolved again. The quarternisation reaction was complete once the

solution had thickened ever so slightly and turned a darker shade of brown. The glass tube was removed from the vial and the TMA solution removed from the heat.

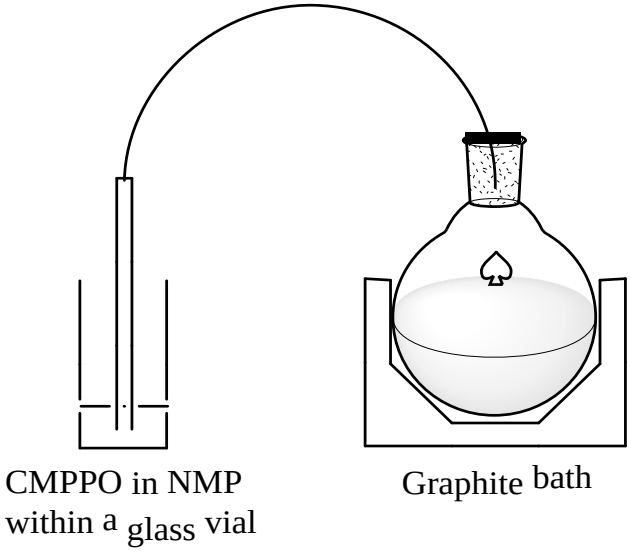

Figure 3.2: *Apparatus set-up for the quarternisation of CMPPO. The round bottom flask contains a 30% weight aqueous solution of trimethylamine (TMA).*

The now quaternised CMPPO, QAPPO, was allowed to stir for a further 15 minutes to ensure a complete reaction. The resulting solution was then cast in a small petri dish measuring 5.5 cm in diameter. This size of dish gave the optimal thickness for the membrane once dry. The QAPPO solution was dried in an oven at 60 ^{o}C for 24 hours and then further dried in a vacuum oven at 60 ^{o}C for another 24 hours.

3.1.3 Ion exchange

After drying, the polymer solution formed a solid membrane stuck to the bottom of the petri dish. The membrane could not be removed from the bottom of the dish simply by

trying to peel it off as it would invariably break very easily. An easier way to remove the membrane was developed by filling the petri dish with deionised water and leaving it for 10 minutes. This allowed the membrane to absorb water and remove itself from the bottom of the dish. At this current stage the QAPPO is in its chloride form, meaning the counter ion on the quaternary nitrogen atom is a chloride ion (Cl^-). For the membrane to be conductive the counter ion must be an OH^- ion. This was achieved by simply immersing the membrane in 1M potassium hydroxide for 24 hours.

3.1.4 Cross-linking

When a membrane formulation was selected as a candidate for cross-linking, one additional step was added to the membrane preparation procedure. First, the chloromethylation step was performed as described. The chloromethylated polymer was then dissolved in NMP and the cross-linking agent added to the solution and stirred for 4 hours at 45 ^oC. The cross-linking agent that was added depended on the type of cross-linked membrane that needed to be synthesised. Some examples of agents used, that will be discussed later on in the results chapter, are: diethylamine, propylamine, diaminopropane and 1, 4-diazabicyclo[2.2.2]octane. The cross-linking agent was always added in the amount equivalent to 30% of the benzyl chloride group on the membrane. The quarternisation, casting and ion exchange steps were performed as described in the previous sections.

3.1.5 Porous membranes

A second set of membranes were prepared using a prepared porous membrane as a support. A non-water soluble polymer, namely polyvinylidene fluoride (PVDF)

formed the “polymer base” analogous to PPO. These membranes differ from the AEMs described at the start of this chapter, in that the polymer base is not chloromethylated to provide the OH^- conduction. Instead it effectively acts as a support for a second quaternised polymer, poly(diallyldimethylammonium chloride) (polyDADMAC). The porous membrane base was prepared by firstly dissolving PVDF in NMP. An amount of salt, either granular or ground, was then added to the solution and stirred vigorously. To create the porous nature of the membrane the salt was then removed by soaking the membrane in warm deionised water.

3.1.6 Treatment of porous membranes with water soluble polymers

As explained in the previous section the porous PVDF membranes were made OH^- conductive by addition of a second polymer: poly(diallyldimethylammonium chloride) (polyDADMAC). The porous PVDF membrane was immersed in a dilute aqueous solution of polyDADMAC and sonicated for around 2 hours. The membrane was then taken out, the excess solution allowed to drip off and dried in a vacuum oven at 50 ^oC.

3.1.7 Mixed membrane preparations

A 50:50 mix of polytetrafluoroethylene (suspension in water) and poly(diallyldimethylammonium chloride) (20% weight in water) were mixed and cast onto a clean petri dish measuring 5.5 cm in diameter and dried at room temperature.

A second set of mix membranes were prepared with the addition of polyvinyl alcohol (PVA). PVA, PTFE and polyDADMAC were mixed in ratios of 1:1:1, 1:3:1 and 1:1:3

and cast onto a glass plate and dried in air. A frame was taped onto the glass plate to ensure that the solution did not flow off the sides.

3.1.8 Cross-linked mixed membrane preparation

Cross-linked versions of the mixed membranes prepared in section 3.1.7 were prepared as follows. PVA, PTFE and polyDADMAC were first mixed in ratios of 1:1:1, 1:3:1 and 1:1:3. Glutaraldehyde (30%) in acetone was added to the mixture followed by a small amount of dilute HCl. The mixture was finally heated at 40 ^{o}C for 20 mins – 1 hour, cast on a glass plate and dried at room temperature.

3.1.9 Heat treatment

The membranes described in sections 3.1.6, 3.1.7 and 3.1.8 were all subjected to heat treatment. Testable pieces of membrane (around 1 cm^2) were treated at various temperatures for varying amounts of time in a box furnace. Once cool, the membrane was immersed in a bath of 1 M KOH for 24 hours before testing.

3.2 Testing

3.2.1 Electrochemical impedance spectroscopy

As referred to in the objectives section, the main analytical method used to characterise the synthesised AEMs was electrochemical impedance spectroscopy, EIS. EIS allows the user to measure the relative ability of an AEM to conduct OH^- ions. Electrochemical impedance spectroscopy was performed using a Solartron Analytical SI 1260A impedance/gain-phase analyser controlled by SMaRT software over the

frequency range 1 MHz to 100 mHz. A more in-depth explanation of EIS is given in section 3.6. For now, this part will deal with how the synthesised AEM's were tested.

3.2.2 Membrane preparation

After the 24 hour immersion period in 1M KOH, each AEM was adequately washed with deionised water and kept hydrated until testing. A small piece measuring about 2 x 2 cm^2 was carefully cut from the membrane and set aside in a petri dish with deionised water.

3.2.3 Electrode preparation

Two pieces of carbon paper, each measuring 1 x 1 cm^2, were carefully cut and set aside. In a small glass vial, carbon black was mixed with isopropanol to make a thick paste. A small amount of PTFE emulsion was then added to the vial and mixed into the paste. This paste was then spread evenly over the two pieces of carbon paper to form a thick layer and allowed to dry.

3.2.4 Cell preparation

Figure 3.3 above shows the apparatus that was used for the EIS testing of the synthesised AEMs. Two equal lengths of silver wire were prepared and made into a U shape. The U bends were positioned in the centre of each PTFE plate and taped down at the edge so that the tape would not interfere with the test. The piece of membrane to be tested was patted dry with a paper towel to remove the excess surface water and sandwiched between the two prepared carbon electrodes. The membrane was then carefully placed on one of the silver wire U bends ensuring that the U bend was in

contact with the carbon paper. The second plate was placed on top of the membrane ensuring the second silver wire U bend was in contact with the respective carbon paper on the top side of the membrane assembly. The two PTFE plates was carefully and evenly screwed together making sure not to overtighten, as this would lead to the silver wires breaking the carbon paper electrodes and puncturing the membrane. Ideally the two pairs of silver wires should exit the jig on opposite sides, representing the two sides of the membrane. The combined testing apparatus (Figure 3.3) was then placed in a beaker of deionised water, ensuring the silver wires were long enough to reach the top of the beaker, where they were connected to the EIS analyser. The temperature was set to 25 ^{o}C and the system left to equilibrate for 15 minutes. The cell was then tested at varying temperatures between 25 and 90 ^{o}C.

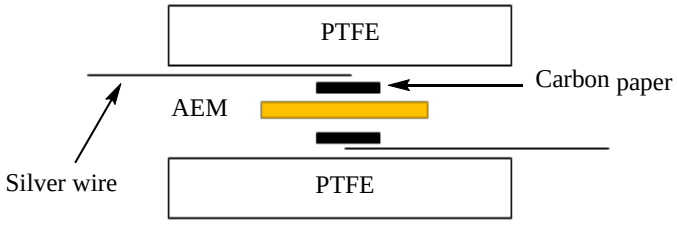

Figure 3.3: *Apparatus set-up for initial testing of AEMs.*

3.2.5 Infrared spectroscopy

Infrared spectroscopy was used to observe and confirm the chemical structure of all synthesised materials. A more in-depth explanation of IR spectroscopy is given in appendix B. IR spectroscopy was performed over the range of 600 – 4000 cm^{-1} and for 32 scans. Before the material was analysed it was thoroughly dried in a vacuum oven for 24 hours to remove any water.

3.2.6 Thermal gravimetric analysis

Thermal gravimetric analysis (TGA) was used to test the thermal stability of all synthesised materials. A more in depth explanation of TGA is given in appendix C. TGA was performed using a Stanton-Redcroft STA 1500 over the temperature range 25 – 600 ^{o}C. Before the material was analysed it was thoroughly dried in a vacuum oven for 24 hours to remove any water.

3.3 - Electrochemical impedance spectroscopy

The basis of electrochemical impedance spectroscopy is measuring the resistance of a material. Resistance is defined as the ability of a material to resist the flow of electrical current. Ohm's law describes resistance in terms of voltage (E) and current (I) with the unit Ohm, Ω.

$$R = \frac{E}{I} \qquad (3.2)$$

However this relationship can only be used for one material, an ideal resistor, whereas most other materials are more complex and do not necessarily follow Ohm's law. This means a more generalised term, impedance must be used. Impedance is the response to an alternating current which also has a frequency dependence [1]. A resistance however can be measured with a direct current and has no frequency dependence at all.

Figure 3.4 shows the ideal I-V curve for a fuel cell [2]. There are three sources of voltage loss that are associated with fuel cell operation and are represented by the different numbered portions of the curve on figure 3.4:

1. Blue – "Kinetic losses" – kinetics of HOR and ORR activation.
2. Yellow – "Mass transfer losses" – losses associated with the ionic conductivity through the membrane and formation of products.
3. Green – "Ohmic losses" – reactions limited by the diffusion of gases to and from electrodes.

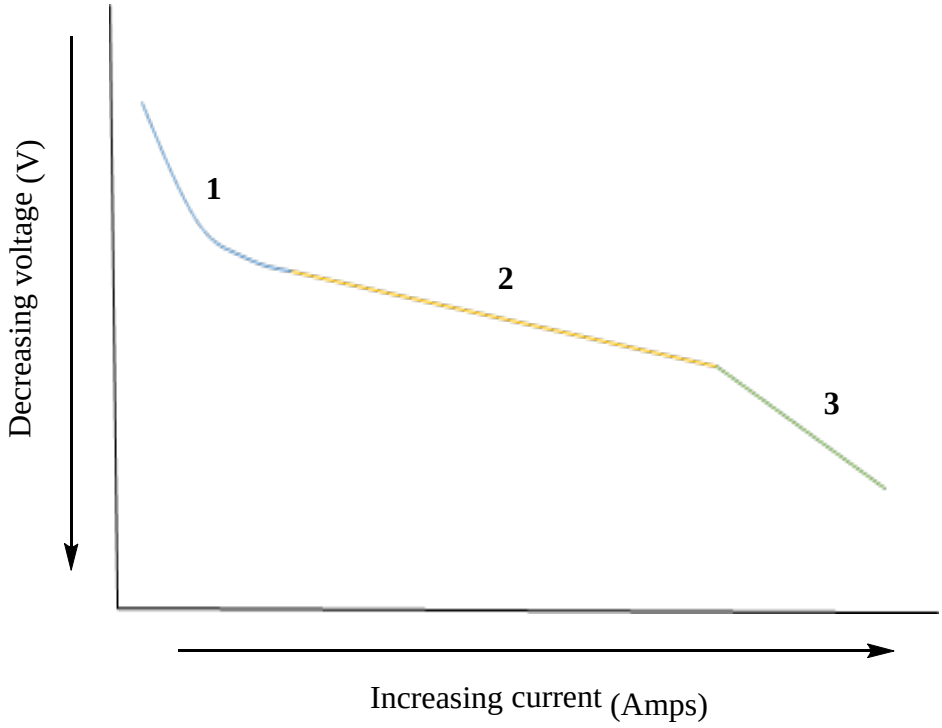

Figure 3.4: *Typical I-V curve for a fuel cell [2].*

Electrochemical impedance spectroscopy, EIS is a powerful tool used to analyse both fuel cells in general and its individual components. EIS can separate and quantify the

losses described allowing the user to identify them, as they appear at different AC frequencies. This allows the determination of specific materials properties such as ionic conductivity of AEMs.

EIS imposes a harmonic perturbation to a system that is in equilibrium. A small AC signal is applied by a frequency response analyser and the corresponding voltage and current through the cell is analysed to determine the impedance. The physiochemical processes shown in figure 3.4 all occur at characteristic time constants and at different frequencies. Therefore EIS measurements are performed over a range of frequencies (usually high to low) to ensure all the processes are identified. The AC signal is kept very small as to keep the response linear. In a linear system the response will also be linear just shifted in time. The impedance of the system can be derived from Ohm's law:

$$Z = \frac{E(t)}{I(t)} = \frac{Eo \sin(\omega t)}{Io \sin(\omega t + \varphi)} \qquad (\mathbf{3.3})$$

$$Z = Zo \frac{\sin(\omega t)}{\sin(\omega t + \varphi)} \qquad (\mathbf{3.4})$$

Where Z_o = impedance magnitude, φ = the phase shift, t = the time constant and ω = the frequency. The impedance can then be written as a complex number:

$$Z(\omega) = \frac{E}{I} = Zo \exp(j\varphi) \qquad (\mathbf{3.5})$$

$$Z(\omega) = Zo (\cos\varphi + j \sin\varphi) \qquad (\mathbf{3.6})$$

The impedance of the system is made up of a real and imaginary part, Z' and Z" respectively which can be plotted in graphical form as a Nyquist plot as seen in figure 3.5. The resistance of the system is represented by the real impedance, however the imaginary part can be comprised of other features such as capacitance and/or inductance. Inductance can be defined as the generation of an electromotive force from changes in electrical current within an electrical circuit. This is usually associated with the electrical equipment being used or the connections within the setup or fuel cell. However some of this charge is sometimes stored by the material, the amount of which is defined by the capacitance. Therefore it is not unusual to view the combined resistance and capacitance together:

$$Z(\omega) = R\frac{1 - i\omega\tau}{1 + \omega^2\tau^2} \qquad (\mathbf{3.7})$$

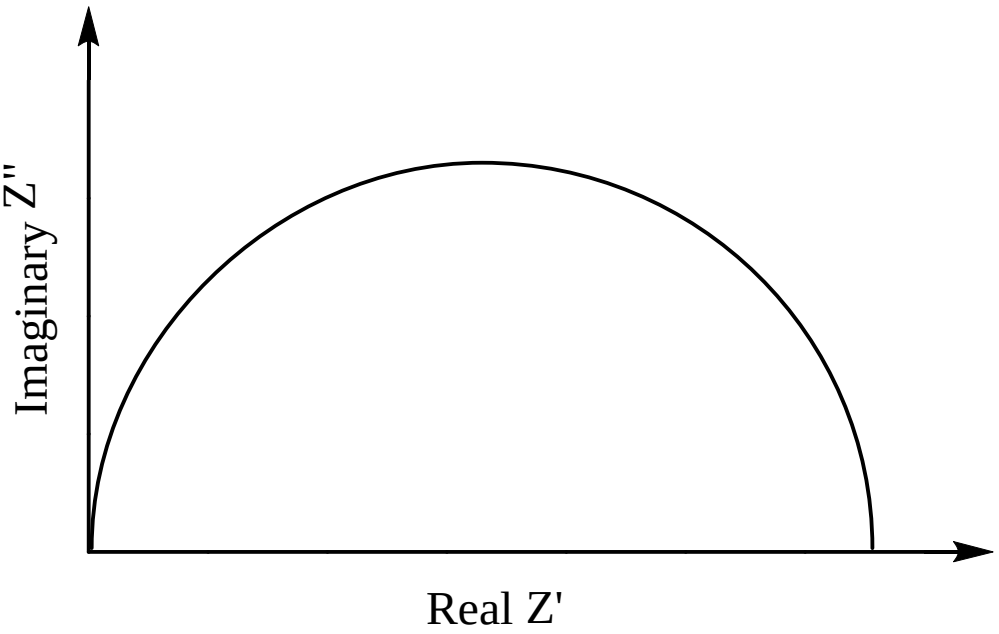

Figure 3.5: *Nyquist plot [3].*

The combination of these two elements lead to the semicircle observed in the Nyquist plot (figure 3.5). Different processes have different characteristic capacitances which means that they can be easily identified from the observed data. The physiochemical process that occur in a fuel cell as seen in figure 3.4 are observed as semicircles on the Nyquist plot.

Capacitance (F)	**Electrochemical process**
$10^{-9} – 10^{-5}$	Surface layer interaction
$10^{-7} – 10^{-5}$	Sample – electrode interface
10^{-4}	Electrochemical reaction

Table 3.1: *Capacitances of different electrochemical processes [2].*

The shape and number of these arcs indicate what physiochemical processes are occurring, however Nyquist plots contain no frequency data meaning they cannot be directly identified without fitting the equivalent circuit. Figure 3.5 is a representation of the impedance observed for the electrical circuit below in figure 3.6.

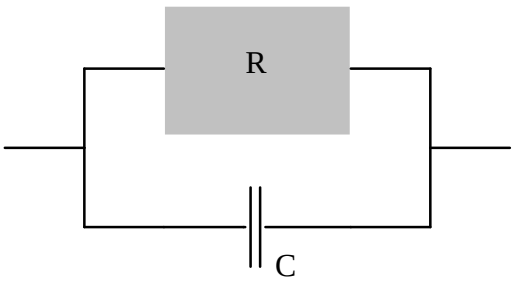

Figure 3.6: *Equivalent circuit model of the impedance from Figure 3.5 [2].*

The single semicircle represents a single time constant which is very rarely observed for fuel cell systems. Most fuel cell systems exhibit multiple semicircles with sometimes only part of the semicircle being visible on the Nyquist plot due to either existing outside the measured frequency range or due to overlap of multiple impedances. It is therefore common to see the corresponding Bode plots accompany any impedance data plotted in Nyquist form.

The data obtained from an EIS experiment can very difficult and complex to analyse. Therefore is it necessary to analyse the data by fitting it to what is known as an equivalent circuit model, comprised of equivalent circuit elements. This means that the data gets analysed in terms of common electrical components such as resistors, capacitors and inductors that represent the different working parts of the fuel cell. Again we have to remember that the fuel cell will not act in an “ideal” way, meaning a further two circuit elements are used, the constant phase element (CPE) and Warburg element.

Figure 3.7 shows a generalised equivalent circuit representing a typical single fuel cell [4]. Resistors are used to represent any pathway where ion or electron transport may occur, like to and from the anode and cathode as well as the through the electrolyte.

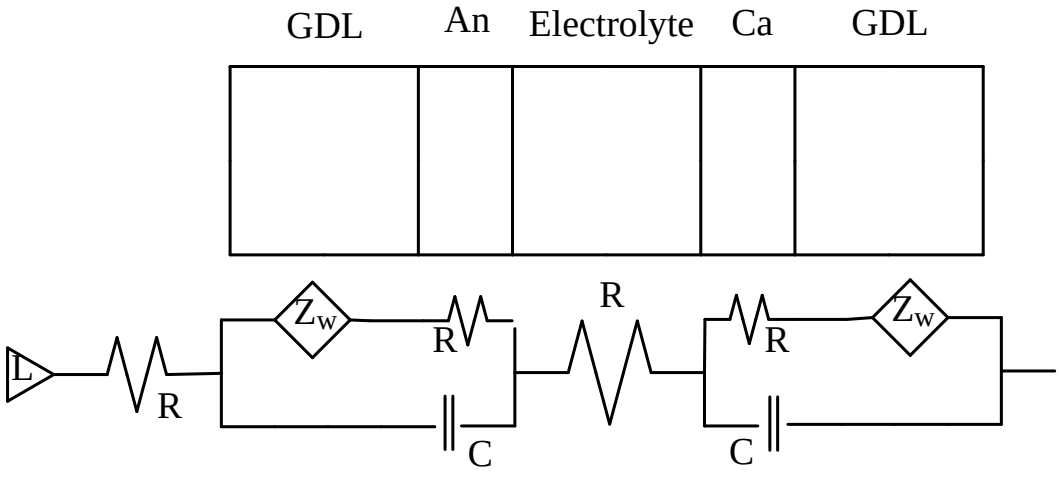

Figure 3.7: *Typical I-V curve for a fuel cell. (GDL = gas diffusion layer, An = Anode, Ca = Cathode, R = resistor, C = capacitor, L = inductor, Z_w = Warburg) [4].*

Both capacitors and inductors represent the electrochemical processes occurring including the adsorption and desorption of molecules onto and off the catalyst layers. The Warburg elements are used to represent actual mass transport through the cell, which includes to and from the electrodes. A Warburg impedance is also used to represent the mass transport that occurs through the electrolyte, with this semicircle appearing at low frequencies followed by an infinite 45^o slope, which is how it can be distinguished. The total impedance of the cell can be calculated similar to normal electrical rules. Elements present in series can be simply added together:

$$Z_{total} = Z_1 + Z_2 + Z_3 \ldots\ldots\ldots \qquad (\mathbf{3.8})$$

Whereas the impedance of any elements in parallel is calculated using the inverse of the sum of all resistances:

$$1/ Z_{total} = 1/ Z_1 + 1/ Z_2 + 1/ Z_3 \ldots\ldots\ldots \quad (\mathbf{3.9})$$

With respect to PEMFCs there are three main sources of resistance, the anode, cathode and electrolyte. The anode and cathode features overlap with each other but these can be separated by using a symmetrical fuel cell. However the cathode features tend to dominate the EIS spectra due to the fast HOR reaction occurring at the anode. The EIS spectra from PEMFCs show the three main "voltage losses" in three frequency areas. Figure 3.8 shows the ideal Nyquist impedance plot for a PEMFC.

High frequencies are where the ohmic resistances are observed. The first semicircle that is observed is within the medium frequency range and is associated with the kinetic losses of the fuel cell. Finally at lower frequencies the semicircle representing the resistance associated with mass transport through the electrolyte is observed (assuming an infinite diffusion length).

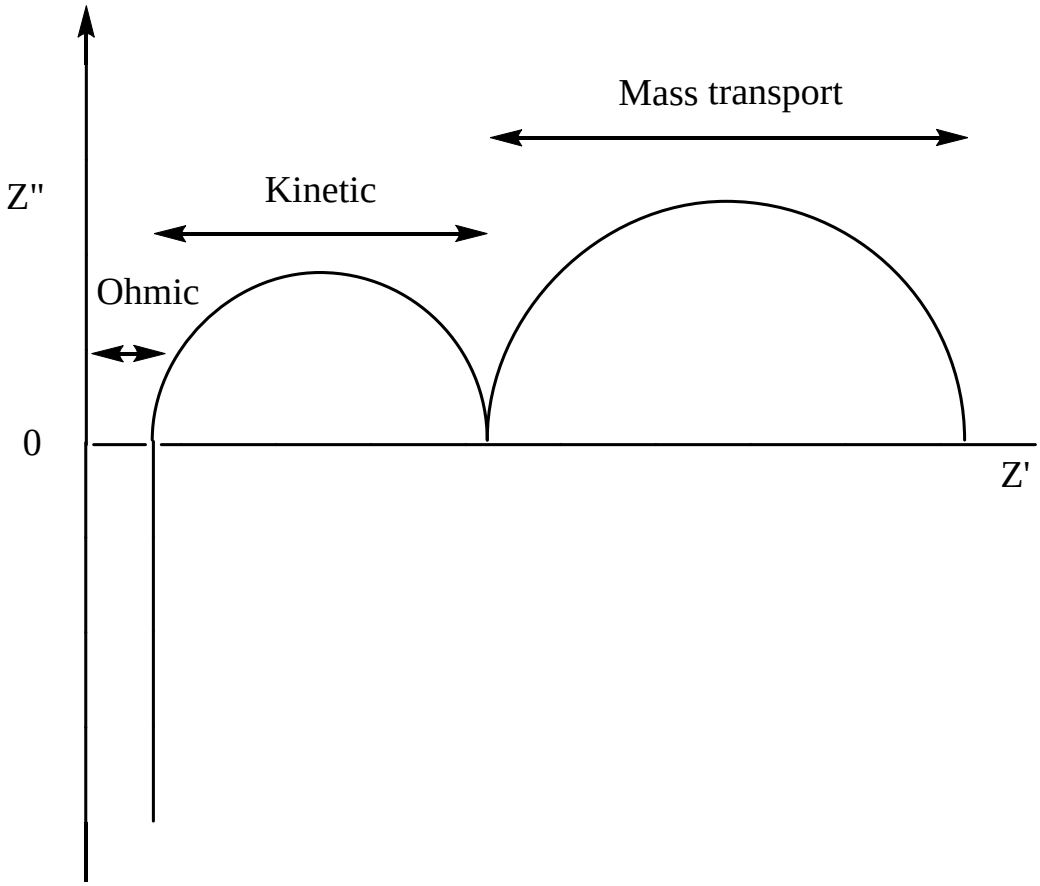

Figure 3.8: *Ideal impedance plot for a fuel cell.*

However this ideal plot is very rarely observed as shown in figure A.6. More often than not parts of or even entire semicircles are absent from the impedance plots. In PEMFCs diffusion of reactants to and from the electrodes as well as through the membrane occur. These processes are observed as a Warburg impedance, a 45^{o} line that stretches to infinity. Figure 3.9 below is an example of a commonly observed Nyquist impedance plot for a PEMFC. Only one semicircle is visible accompanied with a 45^{o} Warburg slope which would stretch to infinity.

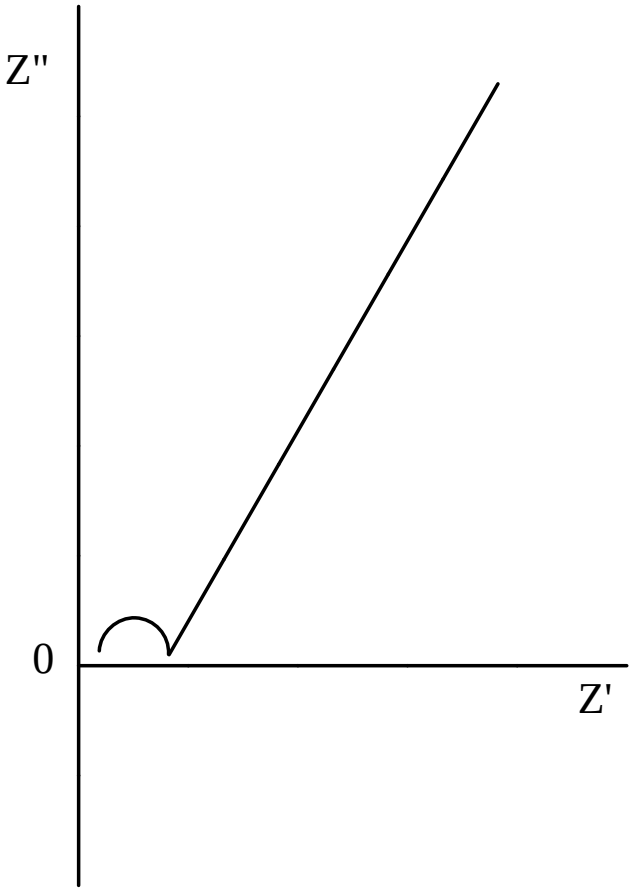

Figure 3.9: *Observed impedance plot for a fuel cell.*

To calculate the conductivity of an AEM, the resistance is read at the point where the Warburg slope begins or at the point where the line intersects the x axis if no identifying features can be observed. Ionic conductivity has the unit's S cm^{-1} and can be calculated using the formula:

Conductivity, $\sigma = (1/\rho) \times (\text{Thickness/Area})$

Where ρ represents the resistance in Ohms as described above. The thickness of the sample of AEM being tested was measured with callipers in mm.

3.4 – Infrared spectroscopy

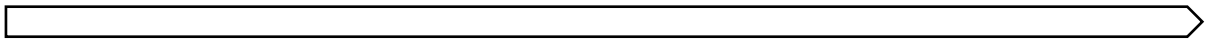

Radio	Microwave	Infra-red	Visible	Ultra-violet	X-ray	Gamma	Cosmic
10^{1} 10^{0}	10^{-2} 10^{-3}	10^{-5}	10^{-6}	10^{-7}	10^{-9}	10^{-11}	10^{-14}

Figure 3.10: *The electromagnetic spectrum (wavelength (λ)/m).*

Spectroscopy as a whole is the interaction of matter with radiation. Different wavelengths of light enable researchers to identify different properties of compounds and their characteristics. For instance, radio waves are used in nuclear magnetic resonance spectroscopy or NMR to look at changes in nuclear spin allowing one to identify the structure of the compound. NMR can also distinguish between different atoms of a compound even if they are the same i.e. hydrogen atoms, by analysing the surrounding chemical structure.

Infrared waves are the core of infrared spectroscopy or IR. They observe the changes in vibrational states of bonds within molecules. This technique is particularly good at identifying functional groups. The light waves of the UV-Visible range are used in electronic spectroscopy to measure the changes in the occupancy of valence orbitals of atoms within molecules. UV-Vis is mostly used to identify conjugated molecules. Finally X-rays are used in X-ray crystallography and X-ray diffraction to analyse the changes in occupancy of core orbitals of atoms within molecules, making this particularly useful for looking at crystal structures.

Infrared spectroscopy is the main identification method of scientists to determine the structures of organic molecules, which is done by observing the interaction of molecules with infrared radiation. The Infrared region can be split into three parts:

1) Near-infrared region (12800 - 4000 cm^{-1})

2) Mid-infrared region (4000 - 200 cm^{-1})

3) Far-infrared region (50 - 1000 cm^{-1})

IR spectroscopy deals with the mid-infrared range between 4000 – 200 cm^{-1} as most organic and inorganic characteristic adsorptions lie within this range.

Modern day IR spectrometers most commonly use Fourier transform techniques (FT-IR). A. A. Michelson is credited with proposing the workings of an FT-IR back in 1890's, however it was not widely used until sometime later during the development of the digital age [5]. The block diagram over the page (figure 3.11) details the basic workings of an FT-IR spectrometer. Light from an IR source is directed towards a beam splitter (black line) where ideally around 50% of this light is reflected and the other 50% passes through the beam splitter. It can be seen that effectively two light streams of different optical path lengths have been created. The red arrows represent one path which is reflected by the beam splitter to a fixed mirror, which in turn reflects the light back again. The other path, represented by the blue arrows, passes through the beam splitter and is reflected back to it this time by a moveable mirror. On returning to the beam splitter both light pathways are partially reflected towards the sample, with

the remaining light being transmitted back to the IR source. The light interacts with the sample and then the sum of the two beams is detected.

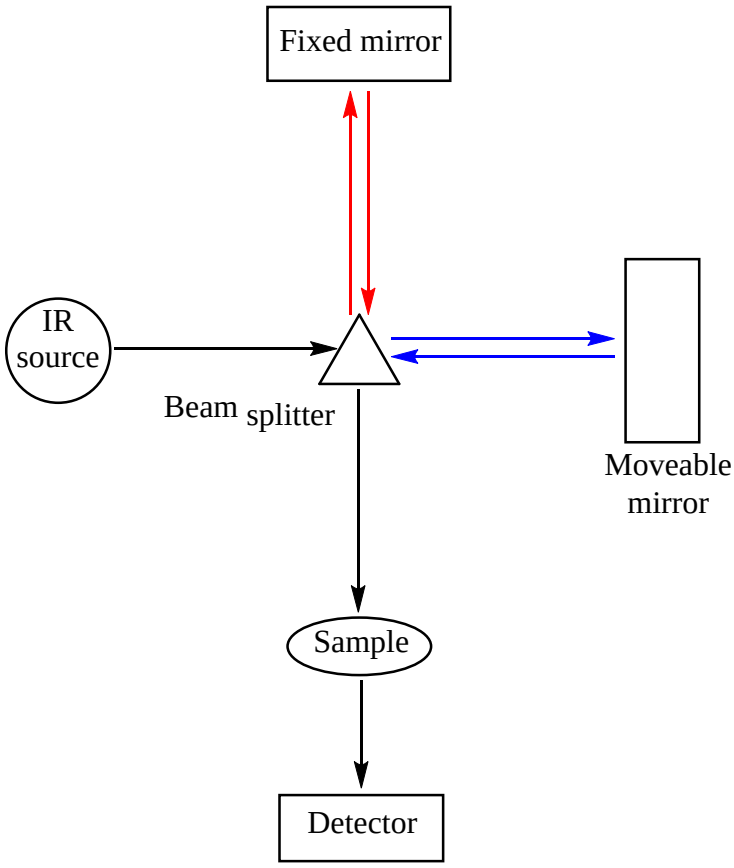

Figure 3.11: *Block diagram of an FT-IR.*

The data obtained from the detector can be represented by equation 3.10 below. The data gets treated mathematically with equation 3.11 to obtain a spectrum that we can analyse. The spectra are displayed using a unit of frequency called wavenumbers (cm^{-1}). These two equations (3.10 and 3.11) together are known as a Fourier pair, hence where the name Fourier Transform IR comes from.

$$I(\delta) = \int_0^{\infty} B(v)\cos(2\pi\delta v)\,dv \qquad (\mathbf{3.10})$$

$$B(v) = \int_{-\infty}^{+\infty} I(\delta)\cos(2\pi v\delta)\,d\delta \qquad (\mathbf{3.11})$$

However, the sample chamber is not a vacuum so it is reasonable to believe that anything present in the surrounding air will also be detected, for example any water vapour. This can then be incorporated into the spectrum and sometimes mask parts of the spectrum of the sample. To prevent this, the FT-IR is run without any sample present so what is obtained is a spectrum purely of the IR source plus any other inferences that may be present. This is known as the background spectrum. This is stored within the computer's memory and subsequently subtracted from the spectrum obtained when a sample is present.

As stated above, IR spectroscopy looks at the changes in vibrational states of bonds within molecules and their IR wavelengths are directly associated with these changes. All chemical bonds constantly vibrate to some extent whatever the temperature, but observable vibrations can only occur at certain energy levels, usually the n = 0 to n = 1 level as shown in figure 3.12. When exposed to infrared radiation, the molecules selectively absorb certain wavelengths of this radiation causing a change in the dipole moment. The frequency at which this peak is observed is determined by the vibrational energy gap and the intensity is related to the relative change in dipole moment i.e. the greater the change, the more intense the peak [6].

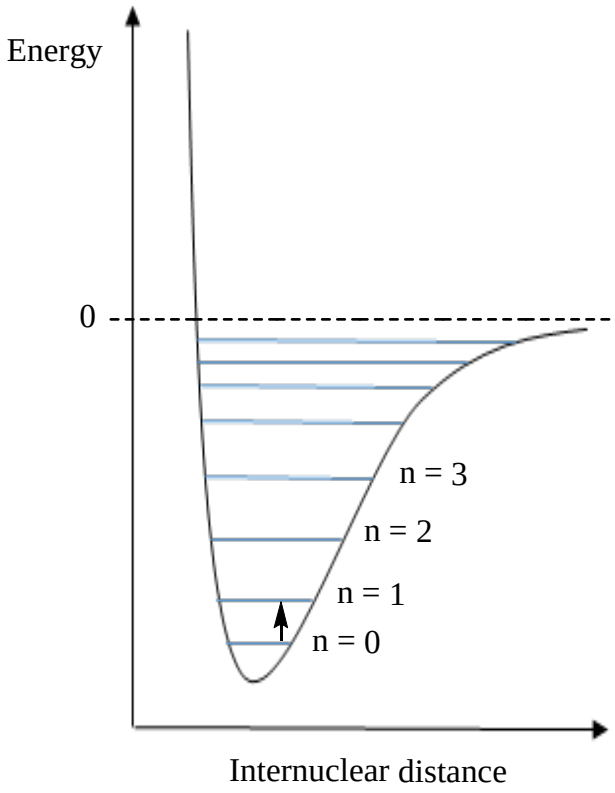

Figure 3.12: *Energy profile for variation in covalent bond length.*

Therefore, it can be seen that by analysing the infrared spectrum, structural information of a molecule can be discovered. Most molecules are infrared active except for a few diatomic molecules like O_2 and N_2. This is due to the fact that the molecule is symmetrical and therefore has no change in dipole moment. For a linear molecule that contains N atoms, where N is the number of atoms, the number of vibrational modes associated with it are equal to the equation:

$3N - 5$

e.g. HCN = (3 x 3) – 5 = 4 vibrational modes.

Where non-linear molecules it is equal to:

3N – 6

e.g. H_2O = (3 x 3) – 6 = 3 vibrational modes

For a generalised non-linear molecule AH_2X_2, there would be (3 x 5) – 6 = 9 vibrational modes, six of which are associated with the A – X bond and are as follows:

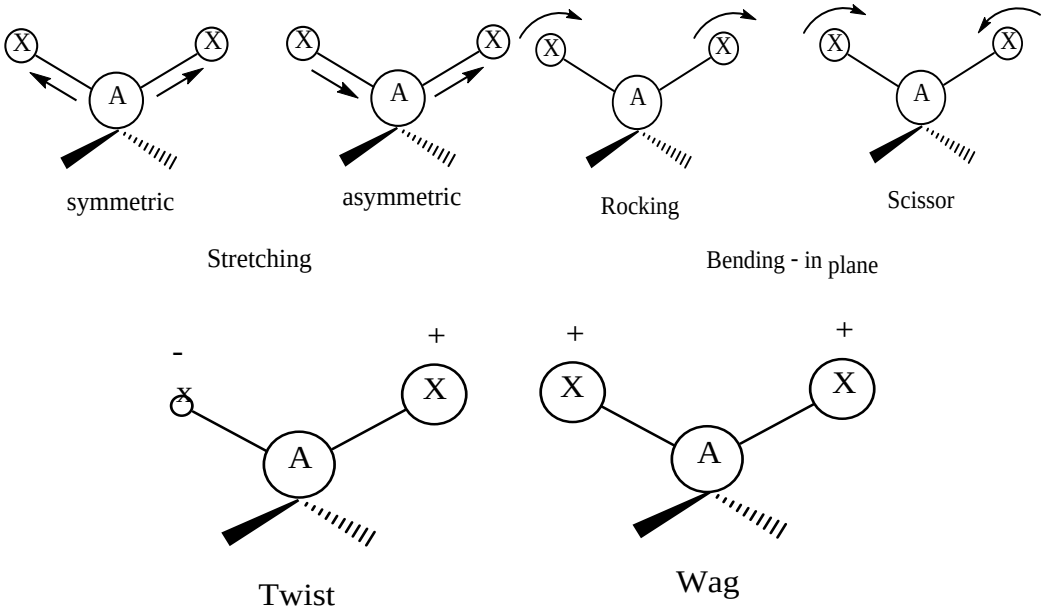

Figure 3.13: *Vibrational modes of a generalised non-linear molecule, AH_2X_2.*

As described earlier IR spectra are recorded using a unit of frequency called a wavenumber, with the unit cm^{-1}. These recorded frequencies can be characteristic of certain types of bond and even certain elements and functional groups. Table 3.2 below details just a few of the more characteristic bond types observed and their respective wavenumber.

500 – 1500 cm^{-1}	1500 – 2000 cm^{-1}	2000 – 2500 cm^{-1}	2500 – 4000 cm^{-1}
C – C C – O C – F C – Cl	C = C C = O	C≡C C≡N	O – H N – H C – H

Table 3.2: *Bond types and their characteristic IR frequencies.*

The frequency at which a bond appears in the spectrum is affected by the masses of the atoms involved and whether it is a single, double or even triple bond. The frequencies can be calculated and predicted by applying Hooke's law (equation 3.12) as it is a function of the force constant, F and the reduced mass of the elements that make up the bond.

$$\bar{\nu} = \frac{1}{2\pi c}\sqrt{\frac{F}{\mu}} \quad \text{where} \quad \mu = \frac{m_1 m_2}{m_1 + m_2} \qquad (\mathbf{3.12})$$

For example, C-O has a frequency of around 1100 cm^{-1}, C=O around 1700 cm^{-1} and the triple bound carbonyl around 2140 cm^{-1}. The triple bound carbonyl has a higher value of F acting on the bond, therefore the frequency will be higher. The same can be seen for differing reduced masses, with a C-Cl bond appearing at around 700 cm^{-1} but a lighter C-O bond appears at around 1100 cm^{-1}. In general the stronger the bond or lighter the atoms involved the higher the observed frequency on the spectrum.

IR bands do not appear in the same form on the spectrum. IR bands can be measured by their intensity, being either strong, medium or weak. What appearance the band

shows all depends the change in dipole moment when it is stretched. For example a C=C bond will be much weaker in appearance as opposed to a N=O bond. Bond symmetry can even cause an IR band to be completely absent from the spectrum.

IR spectroscopy was used in this work to analyse the polymeric materials synthesised and confirm the presence or absence of key functional groups needed for IC.

3.5 – Thermal gravimetric analysis

Thermal gravimetric analysis, TGA is a method of analysis which measures the changes in chemical and physical properties of materials [7, 8]. These measurements are usually functions of time or temperature. TGA measures the mass loss or even mass gain that occurs when the sample material is heated. These losses or gains can be attributed to three processes:

1. Material decomposition
2. Chemical reactions with other materials (not associated with material decomposition)
3. Release of absorbed species i.e. water

TGA can be especially useful for analysing polymers as they show distinct areas of decomposition. TGA uses a precision balance within a high temperature furnace. This balance records the mass change of the material from a constant mass. The temperature and temperature change must also be recorded accurately. The furnace within the TGA generally heats with a constant heating rate over time but can also heat until a constant

mass loss is achieved. Gases can be introduced into the furnace to create inert atmospheres to prevent unwanted reactions or conversely to stimulate reactions.

TGA measures the weight of the sample constantly as the temperature increases. As parts of the sample degrade or are removed, the weight decreases until either the temperature limit of the program is reached or the all reactions are complete. This enables a graph to be plotted of temperature against mass loss.

For most APEMFC materials, there are certain characteristic weight loss temperatures that can be attributed to certain processes happening within the chemical structure. These are mainly the loss of absorbed water, the trimethylammonium group and finally the complete breakdown of the polymer backbone.

3.6 – Chapter 3 references

[1]. E. Barsoukov and J. R. Macdonald, *Wiley-Interscience*, (2005).

[2]. P. I. Cowin and C. T. G. Petit, *Electrochemical Impedance: An Introduction*, (2010).

[3]. B. A. Boukamp, *"Electrochemical Impedance Spectroscopy"*, (2008).

[4]. *Electrochemical Impedance Spectroscopy (EIS): A Powerful and Cost Effective Tool for Fuel Cell Diagnostics* Scribner Associates Incorporated.

[5]. W. D. Perkins, *Topics in Chemical Instrumentation*, (1986), 63, A5-10.

[6]. D. Adams, *Heriot-Watt University IR Lecture Notes*, (2009).

[7]. S. P. Stodghill, *American Pharmaceutical Review*, (2010).

[8]. L. Froberg, *Presentation - "Thermal Analysis TGA/DTA"*.

Chapter 4 – Preparation of quaternised poly(2, 6-dimethyl-1, 4—phenylene oxide) (QAPPO), analysis and optimisation.

The four synthesis steps involved in the preparation of QAPPO have been described in chapter 3. The stability and ionic conductivity of these AEMs are governed by how successfully these four steps are performed. A number of factors related to the different steps of the synthesis were investigated. These were:

1. The amount of time the chloromethylation step was run for. Three runs were performed over 1, 4 and 6 hours.
2. The temperature the chloromethylation step was performed at; 50 ^{o}C or higher.
3. Use of chemical cross-linkers similar to that reported by Pan *et al* [1]. Other reagents with the potential to be cross-linkers were also investigated.
4. The length of time the ion-exchange step was run for. Whether 1 or 3 day immersion in 1M KOH was optimal and whether any adverse effects were observed on the AEMs.

4.1 – Chloromethylation of poly (2,6-dimethyl-1,4-phenylene oxide) (PPO) and AEM preparation

In this work poly (2,6-dimethyl-1,4-phenylene oxide) (PPO) was used as the base polymer as described in the aims section. The first production stage of the AEM involved the chloromethylation of the base polymer. One way to achieve this is to follow the method by Lu *et al* [2] discussed in section 1.5.2. This method involves dissolving PPO in a suitable solvent followed by addition of chloromethyl methyl ether and trifluoroacetic acid. However, it is well known that chloromethyl methyl ether is highly carcinogenic and toxic [3-7] therefore it is not best suited for large scale

production and a much safer chloromethylation method has been developed [8]. This safer method uses paraformaldehyde catalysed by zinc chloride and is shown in Figure 4.1.

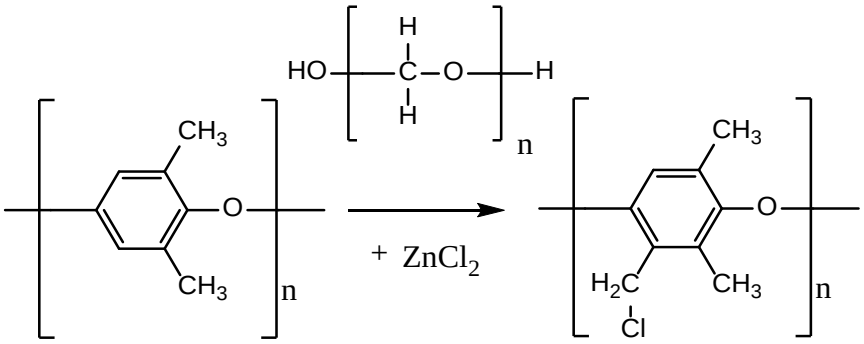

Figure 4.1: *Chloromethylation of poly (2,6-dimethyl-1,4-phenylene oxide), PPO.*

The reaction is a Blanc chloromethylation which involves the addition of a chloromethyl group onto the benzene ring within the polymer structure. Firstly, paraformaldehyde and zinc chloride are dissolved in 1,2-dichloroethane, heated to 50 ^{o}C and stirred for 30 mins. The heat depolymerises the paraformaldehyde producing the resonance structure seen in figure 4.2.

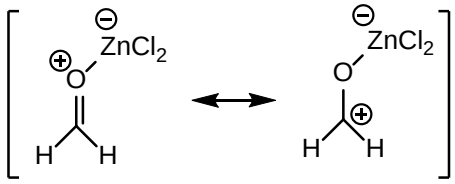

Figure 4.2: *Resonance structure formed upon heating of paraformaldehyde and zinc chloride.*

At the same time nitrogen and HCl gas are incorporated into the reaction vessel to saturate the solution and make it ready for the addition of the polymer. Figure 4.3 details the mechanism of the reaction. As soon as the polymer starts to be dissolved

into the solution, π electrons from the aromatic benzene rings attack the electrophilic carbon atom of the formaldehyde. The benzene ring reforms producing a benzyl alcohol which due to the presence of high concentrations of HCl gas, is immediately converted to chloride.

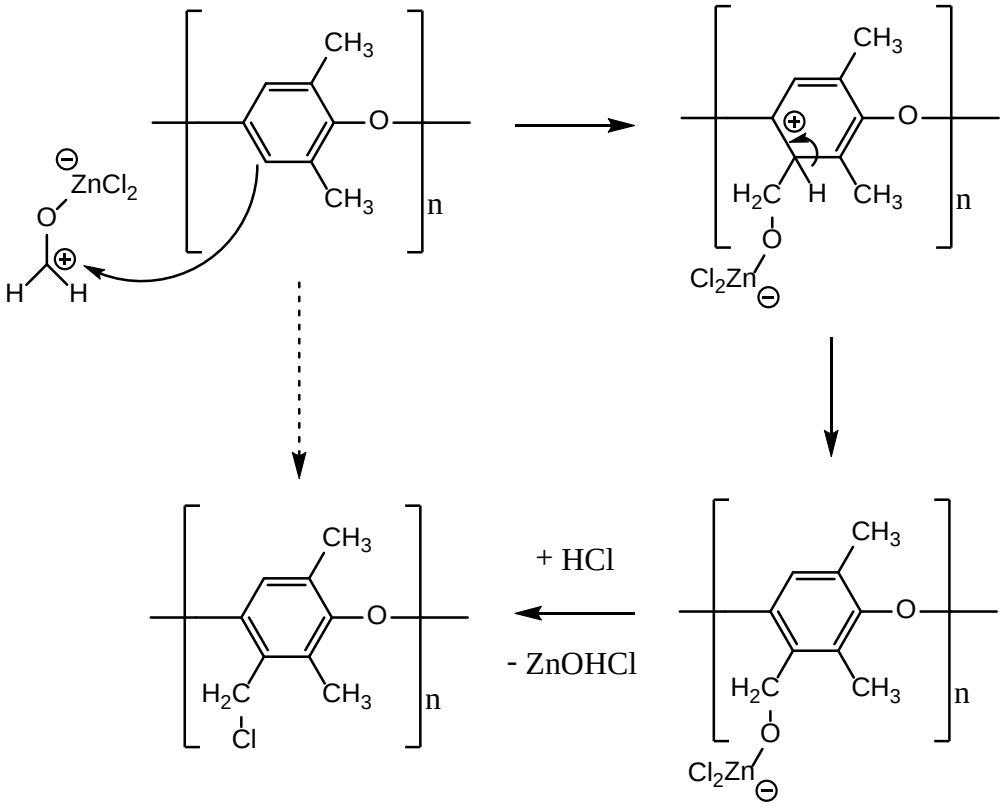

Figure 4.3: *Mechanism for the chloromethylation of poly(2,6-dimethyl-1,4-phenylene, PPO.*

4.2 – Chloromethylation of PPO for 1 hour at 50°C

As the optimum reaction time varies with which base polymer is used, the first reaction was run for 1 hour, to gauge the respective reactivity. The reaction liquor was brown in colour and produced clumps of solid, rather than a powder. These clumps of solid polymer were difficult to dissolve in NMP and needed the aid of heat to completely dissolve. This indicates that the reaction may not have proceeded to completion as CMPPO should be relatively soluble in NMP.

Figure A.1 of appendix A shows the full IR spectrum of the starting polymer, PPO. Figure 4.4 is a zoomed in view of the lower wavenumber portion of the spectrum.

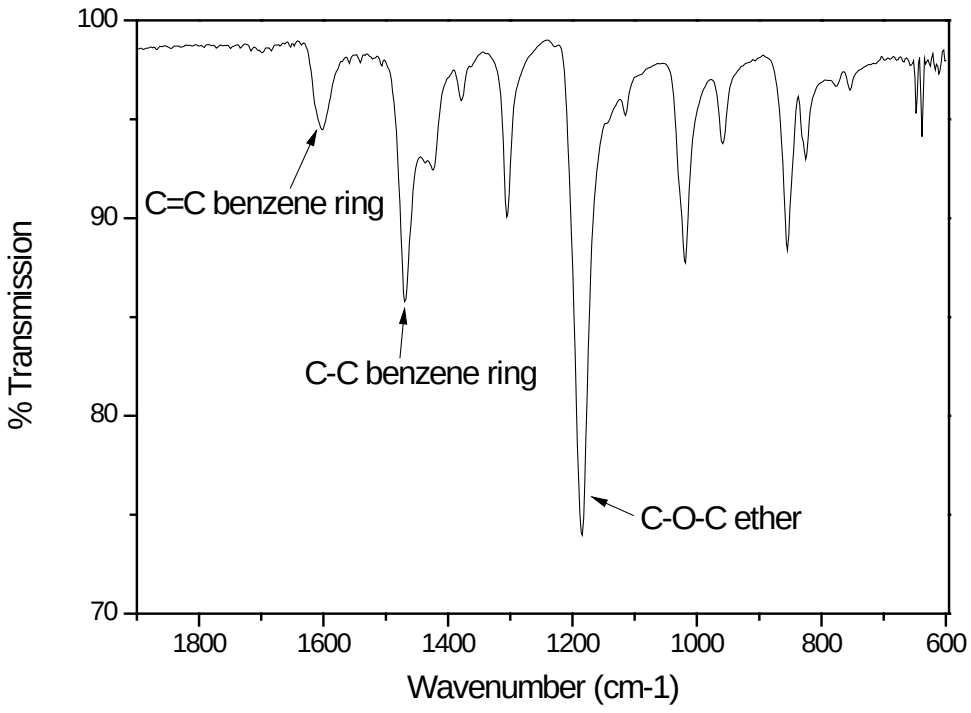

Figure 4.4: *Zoomed in part of lower portion of PPO infrared spectrum.*

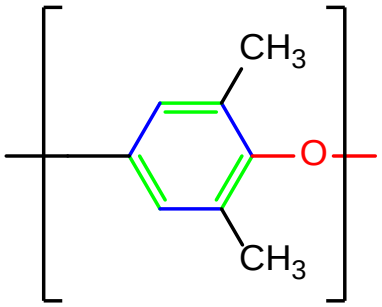

Figure 4.5: *Chemical structure of PPO with colour co-ordinated bonds.*

The characteristic C-O-C ether bond can be observed at just below 1200 cm^{-1} (red bonds in figure 4.5). The two peaks at 1500 cm^{-1} and 1600 cm^{-1} represent the C-C (blue bonds in figure 4.5) and C=C (green bonds in figure 4.5) portions of the benzene ring respectively. The small collection of peaks at just below 3000 cm^{-1} represent the C-H alkyl stretches of the methyl groups in PPO.

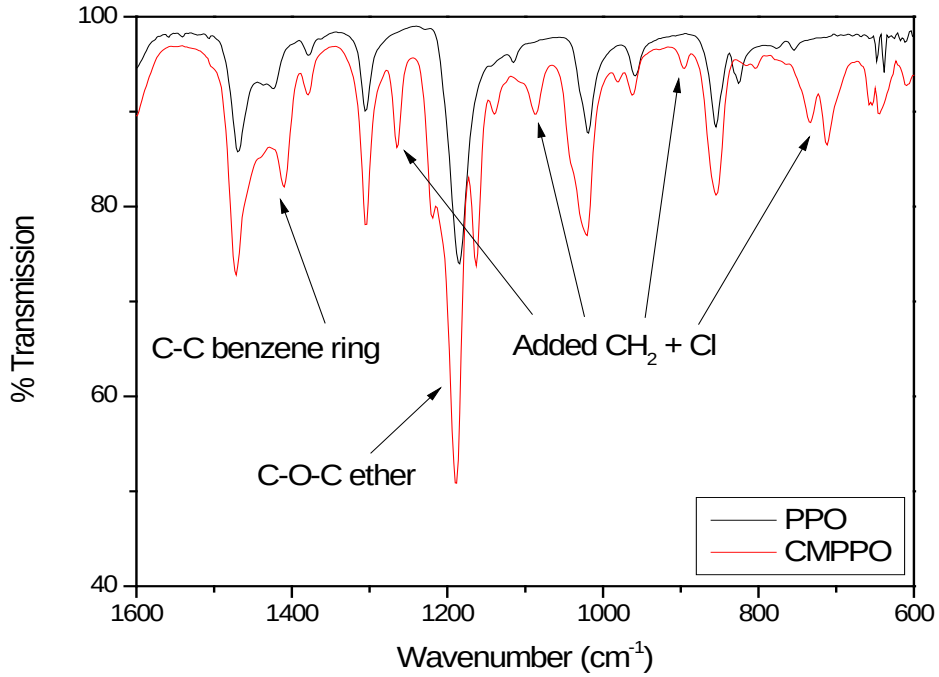

Figure 4.6: *Zoomed in part of IR spectra comparison between PPO and CMPPO.*

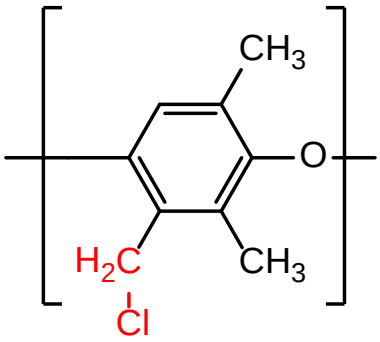

Figure 4.7: *Chemical structure of CMPPO with colour co-ordinated bonds.*

Figure 4.6 shows a zoomed in view of the lower portions of both the IR spectra of PPO (black) and the prepared CMPPO (red) (full spectrum in figure A.2 of appendix A). The main notable difference between the two spectra is the addition of the C-Cl band (red bonds in figure 4.7) at just above 700 cm^{-1} in the CMPPO spectrum. This indicates that to some degree the chloromethylation reaction was a success. Other bands have been labelled on the spectrum and they correspond to the added CH_2 group.

The quarternisation process replaces the Cl atom with a quaternary ammonium group as seen below in figure 4.8.

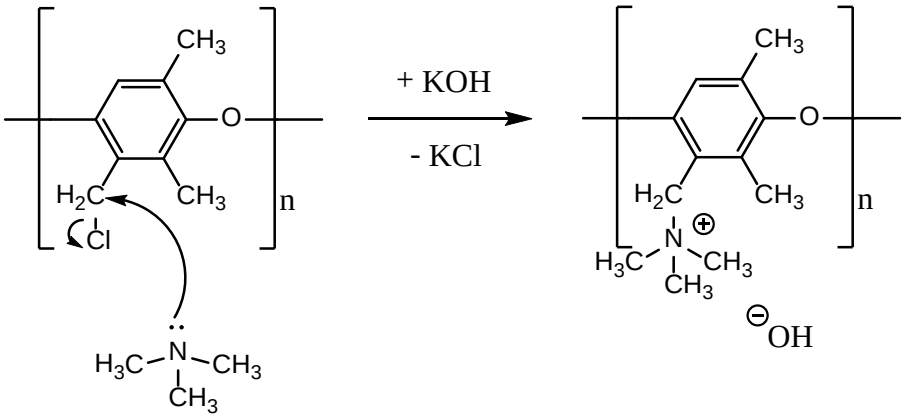

Figure 4.8: *Method of quaternisation of CMPPO to produce QAPPO.*

After quaternising the CMPPO in solution the membranes were immersed in 1M KOH for one and three days, to see whether there is any relative effect on membrane conductivity and structure. Figure 4.9 shows the zoomed in view of the lower portion of the IR spectrum obtained for the QAPPO membrane subjected to the respective KOH treatments. Firstly the sharp peak at 1000 cm^{-1} in the IR of CMPPO has been replaced with a collection of small peaks, one of which represents the C-N bond of the quaternary ammonium group (red bonds in figure 4.10). However, there still seems to be a band representing the C-Cl bond at just above 700 cm^{-1}, which indicates that the quarternisation reaction may not have been 100% completed. The appearance of the two infrared spectra in figure 4.9 (full spectrum in figure A.3 of appendix A) are similar suggesting no effect of KOH treatment time on the membrane structure.

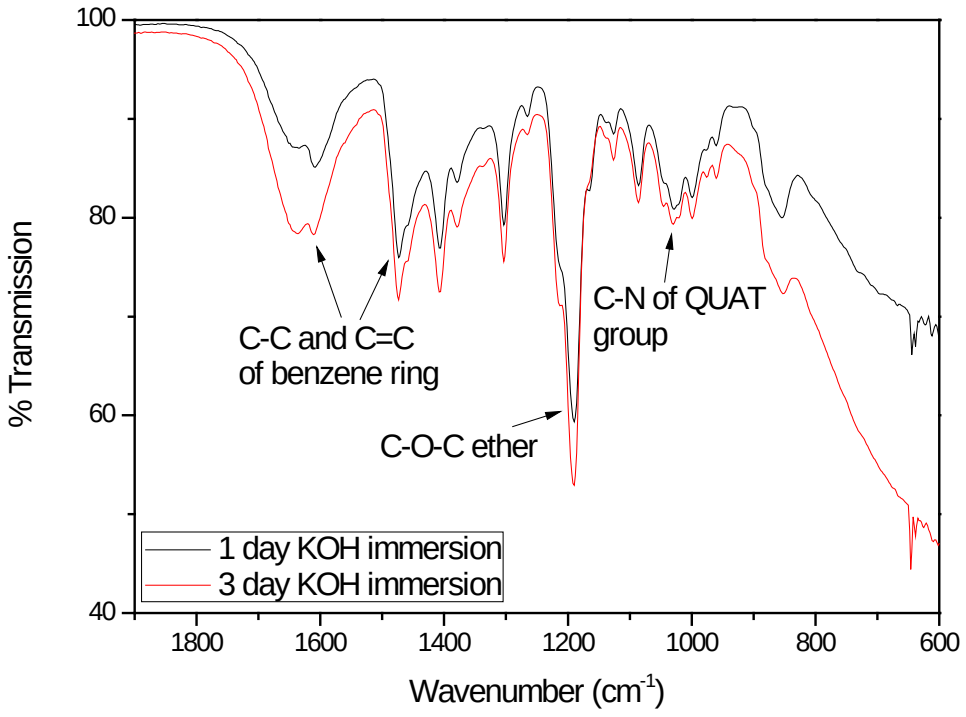

Figure 4.9: *Zoomed in part of IR spectra comparison between QAPPO membranes with different KOH treatment times.*

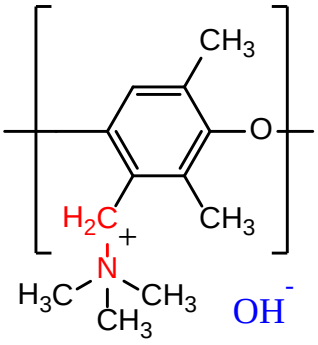

Figure 4.10: *Chemical structure of QAPPO with colour co-ordinated bonds.*

Figures 4.11 shows for different temperatures the ionic conductivities in water of two identical pieces of membrane synthesised from the "1 hour batch" of CMPPO, after immersion in 1M KOH for one and three days respectively. The membrane immersed for 1 day in 1M KOH showed higher conductivity than the 3 day version, however the AEMs conductivity very quickly decreased as the temperature increased. The membrane immersed for 3 days in 1M KOH, showed lower overall conductivity but an increase as the temperature increased.

Unfortunately, both membranes were highly unstable at temperatures above 60 ^{o}C. A one hour chloromethylation reaction therefore did not provide a thermally stable batch of CMPPO with good conductivity that can be used for membrane synthesis. The chloromethylation reaction was next run for four hours to compare the stability and ionic conductivity with relation to increased chloromethylation time.

The IC graphs detailing the variation of IC with temperature also contain error bars for the data set at each temperature. It can be seen that the most error is observed during the first two temperature experiments and then the error very quickly diminishes over

the rest of the testing. This is not surprising as initially the OH^- conduction pathway through the membrane is not optimal. As the membrane heats up further into the test, the conduction pathway starts become more facile, meaning less error is observed in the results.

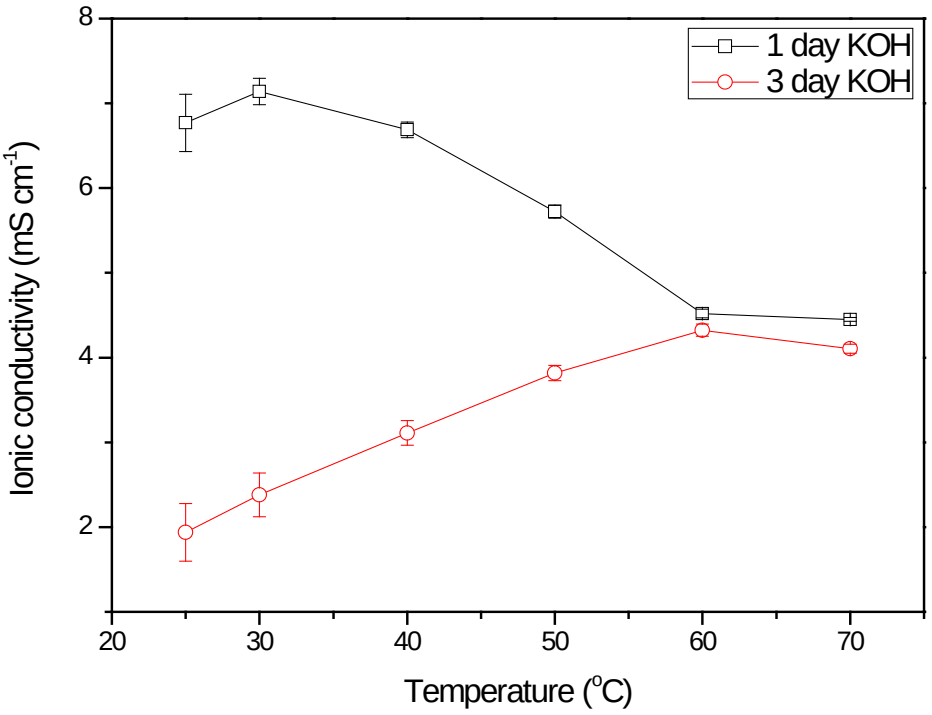

Figure 4.11: *Variation of IC with temperature for the QAPPO membrane prepared from a 1 hour batch of CMPPO. These AEMs were immersed in 1M KOH for 1 and 3 days.*

4.3 - Chloromethylation of PPO for 4 hours at 50 ºC

A four hour batch of CMPPO was synthesised without any problems. After each hour, a 1 ml sample was taken from the reaction liquor and precipitated in methanol to yield the CMPPO present at that stage of the reaction. The IR spectra of all samples are shown in figures A.4 – A.6 of appendix A, however the zoomed in view at lower wavenumber is shown in figure 4.12.

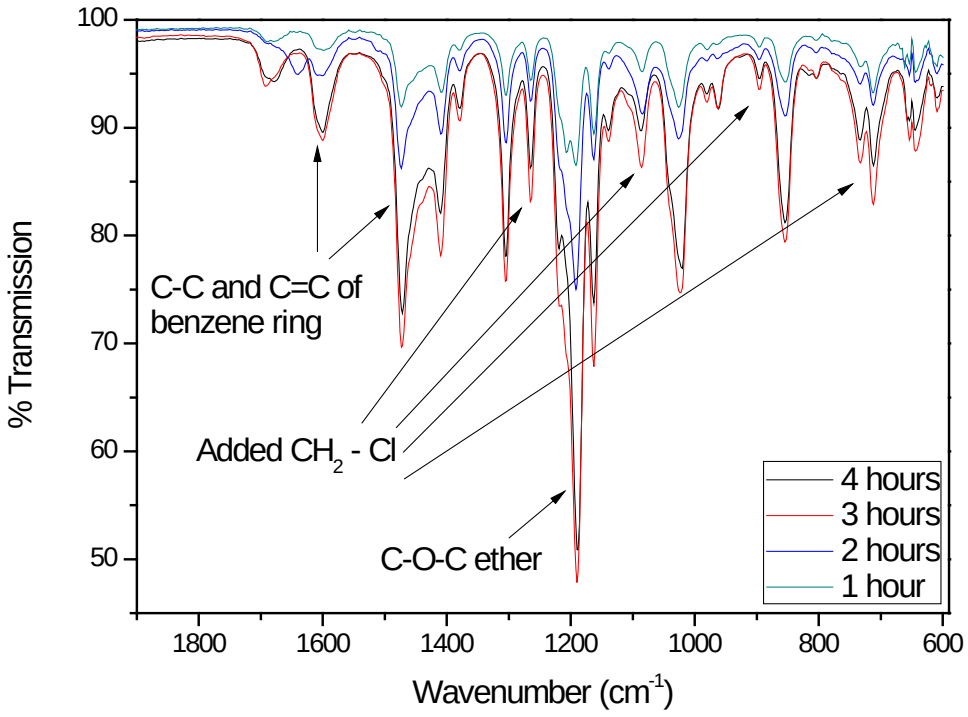

Figure 4.12: *Zoomed in part of IR spectra comparison between CMPPO at different stages in the chloromethylation reaction.*

It is observable that as the reaction proceeds further, the peaks associated with chloromethylation (C-Cl and CH_2) become more intense, indicating that the polymer is becoming increasingly chloromethylated. The peak, on the full spectra in appendix D, at 2300 cm^{-1} that appears to get more intense as the reaction time increases can be

attributed to either carbon dioxide picked up by the apparatus or an overtone band, although it may be a little high. Again there was no discernible difference in the IR spectra between the two KOH treatments. (Figure 4.13 with full spectra shown in figure A.8 of appendix A).

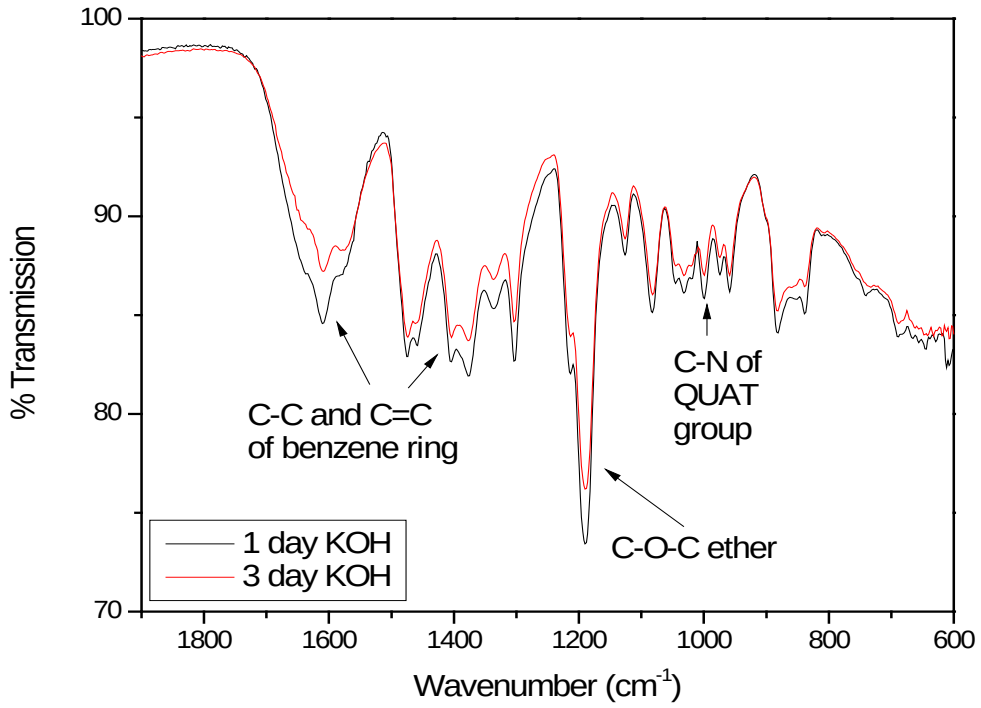

Figure 4.13: *Zoomed in part of IR spectra comparison between QAPPO membranes immersed in 1M KOH for 1 and 3 days.*

Figure 4.14 shows the ionic conductivities that were observed from 25-60 ^{o}C, for both the 1 and 3 day KOH treated membranes. At 60 ^{o}C both membranes produced a good conductivity of 11.8 and 11 mS cm^{-1}respectively. Again, it was noticed that the 1 day KOH treated membrane initially decreased in conductivity before increasing again at 60 ^{o}C. The 3 day treated membrane also follows the same pattern as for the CMPPO produced after one hour of chloromethylation (1 hour batch of CMPPO).

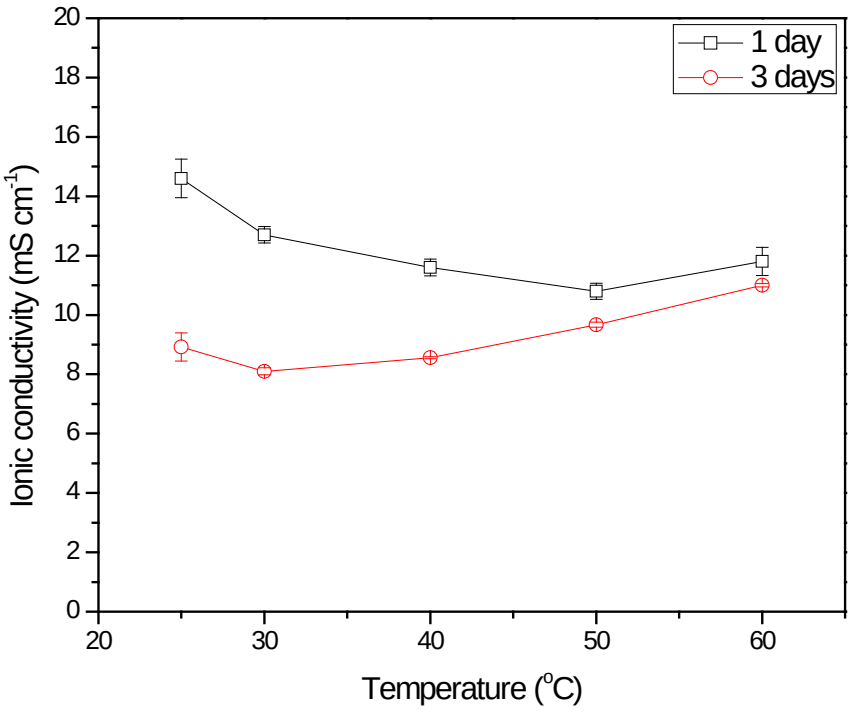

Figure 4.14: *Variation of IC with temperature for the QAPPO membrane (4 hr 50 °C) immersed in KOH for 1 and 3 days.*

The error bars associated with figure 4.14 closely follow those observed in figure 4.11 (large at the beginning of the test, smaller towards the end), which can be attributed to membrane stabilisation. Despite the good result in terms of IC, the membranes were again very unstable at 60 °C and quickly degraded. However from TGA experiments, it was easy to deduce that 1 day KOH treatment was the best out of the two treatments, despite its initial decrease in conductivity. This can be clearly seen in the TGA plots of both the membranes shown in Figure 4.15. TGA of AEMs usually show three weight losses represented by dips in the continuous line. The first loss at around 100 °C is attributed to the evaporation of any absorbed water in the membrane. The second loss at around 200 °C is the degradation of the quaternary ammonium ions and the

third loss usually occurs at the decomposition temperature of the polymer used. Figure 4.15 shows that both membranes exhibited the loss of absorbed water at about 100 ^{o}C, however the membrane treated in 1M KOH for 3 days continues to lose weight fairly rapidly and by 200 ^{o}C there is almost a 20% weight loss gap between the two KOH treatments. Therefore, the 3 day KOH treatment may have a positive effect of causing the conductivity to rise with increasing temperature; nevertheless, it defiantly also has a negative effect on the overall membrane stability.

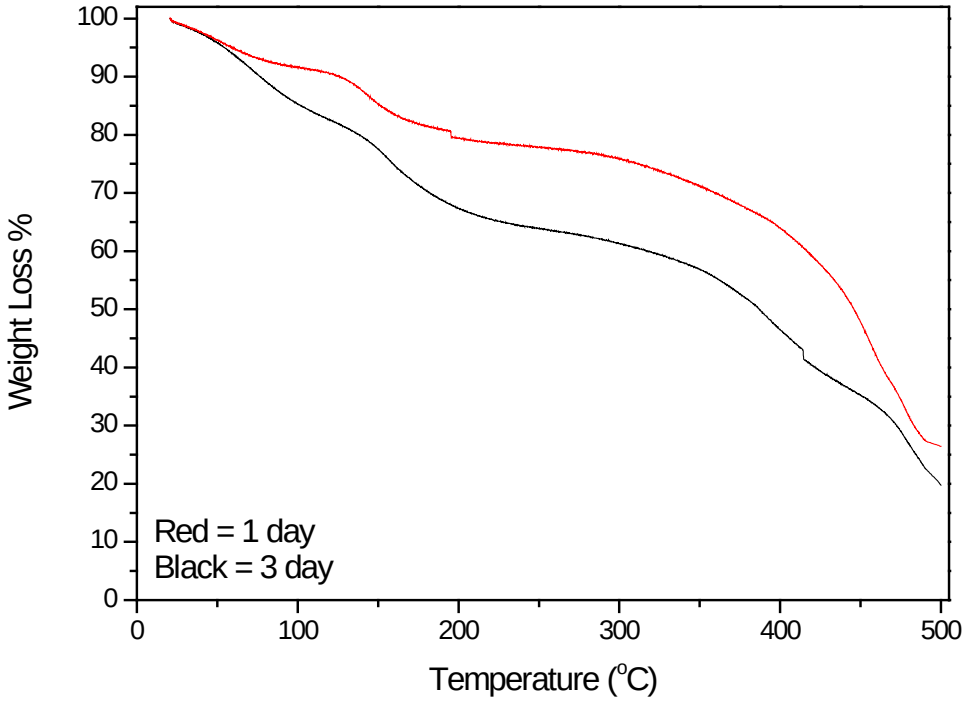

Figure 4.15: *TG analysis comparison between QAPPO membranes (4 hr 50 ^{o}C) immersed in 1M KOH for 1 (red) and 3 (black) days.*

4.4 – Cross-linking of QAPPO (4 hr, 50 ºC) using diethylamine

Another way of producing a more stable membrane is to use a chemical cross-linker. As explained earlier, there are many different chemicals that can be used to cross-link AEMs. Pan *et al* created a cross-linked membrane using diethylamine [1]. The synthesis of standard membranes involves two competing reactions; functionalisation and cross-linking. The key to a stable and highly conductive membrane is to get a 50/50 balance between the two processes. The cross-linking of membranes with diethylamine was achieved via the reaction in figure 4.16 below.

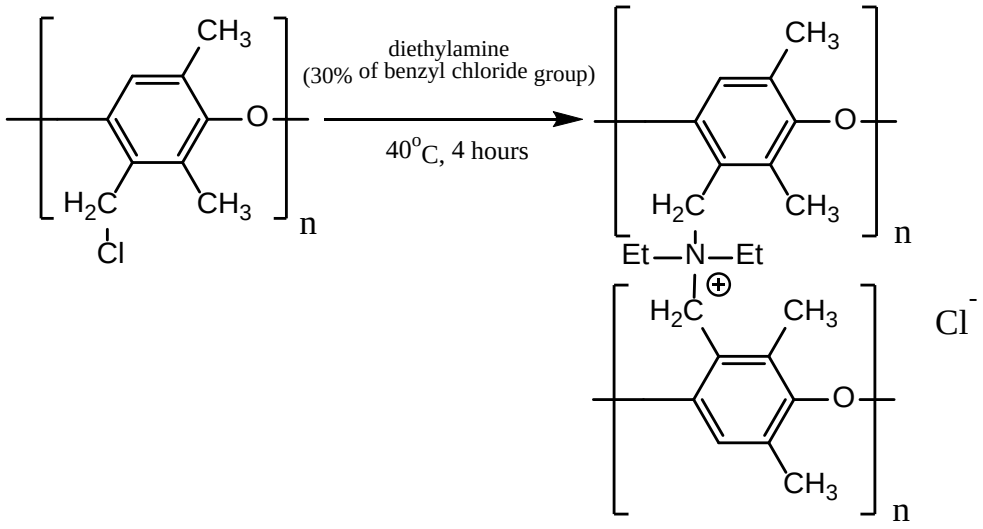

Figure 4.16: *Method of the cross-linking of CMPPO using diethylamine [1].*

The cross-linking agent diethylamine was added dropwise to the dissolved CMPPO solution before it was quaternised with trimethylamine. This was done to ensure that the cross-linking agent reacted fully with the CMPPO. Once the diethylamine was added to the CMPPO solution there was a noticeable colour change and viscosity increase. After these initial change to the solution, no other observed changes occurred over the rest of the 4 hour reaction time. Increases in cross-linker concentration were considered; however the attempts with higher cross-linker concentration produced

extremely brittle membranes. In fact, usually an extremely thick polymer solution was observed within the reaction vial that could not be cast. Figure 4.17 shows the IR spectra for cross-linked and noncross-linked QAPPO (Full spectrum of diethylamine cross-linked QAPPO shown in figure A.9 of appendix A).

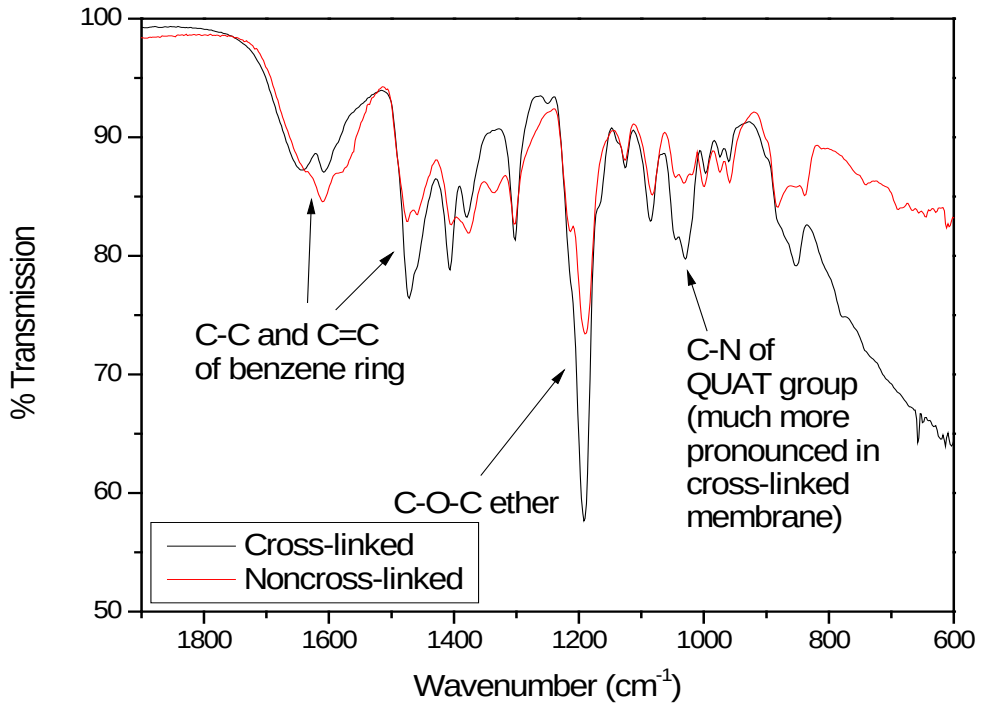

Figure 4.17: *Zoomed in part of IR spectra comparison between cross-linked and noncross-linked QAPPO membranes 1M KOH treated for 1 day.*

Figure 4.18 shows the ionic conductivity of the diethylamine cross-linked membrane produced from the 4 hr at 50 ^{o}C batch of CMPPO (including very small errors apart from at 60^{o}C which is relatively large compared to the rest of the test). The first observation about this membrane is the fact that it is stable up to 90 ^{o}C, something that was not observed with any other QAPPO membrane produced so far. The ionic

conductivity at low temperatures is very poor, but there is a steep rise with increasing temperature. The initial low IC is not surprising when implementing a cross-linking agent. Cross-links take up two sites which, further on in the reaction sequence, TMA groups attach to, thus providing sites for OH^- conduction. Although the cross-link provides a site for ionic conduction, overall there is a net loss of one site. The more cross-links there are, the greater the net loss of conduction sites and therefore the lower the IC of the AEM.

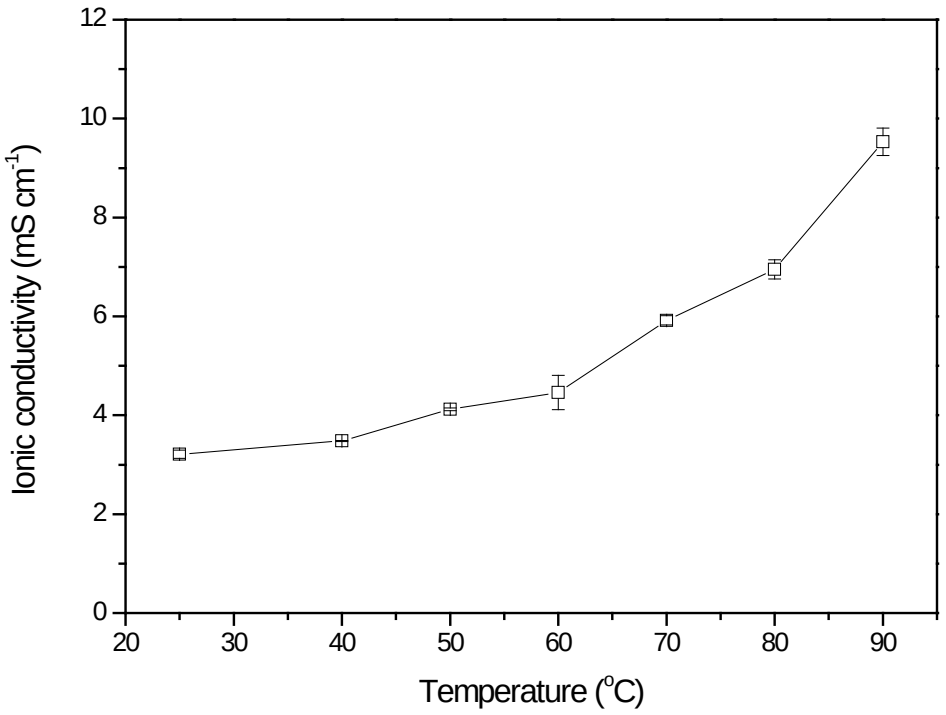

Figure 4.18: *Variation of IC with temperature for the diethylamine cross-linked QAPPO membrane (chloromethylated for 4 hours at 50 °C).*

Stability tests were performed on AEMs where impedance measurements were was taken at various intervals over a period of time. These tests are referred to as “loop” tests and allow the researcher to understand the long term ionic conductivity of any

AEM. During a 2.5 hour loop test at 90 ^{o}C the conductivity continued to increase, which indicated that it could increase even further. A further 10 loop run, which equated to another 5 hours, was performed on this membrane at 90 ^{o}C. From figure 4.19, after a further 5 hours of testing the conductivity was still rising, so the decision was made to test the membrane for a whole week to ascertain the peak conductivity of this membrane.

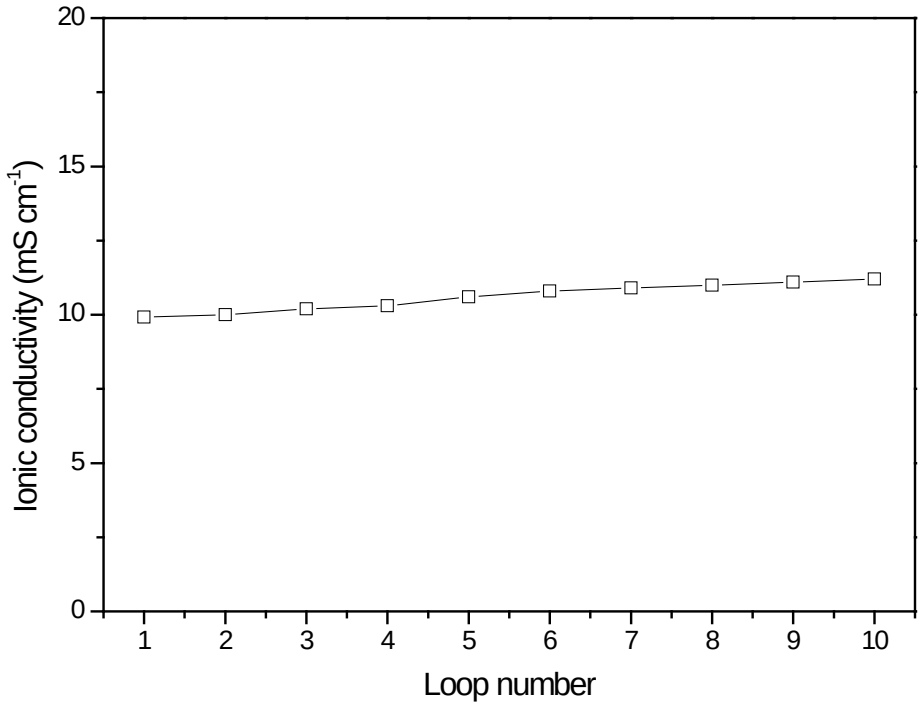

Figure 4.19: *Variation of the IC with time for the diethylamine cross-linked QAPPO membrane (chloromethylated for 4 hours at 50 ^{o}C). This test was carried out at 90^{o}C.*

The results of the week-long test can be seen in figure 4.20 where the ionic conductivity peaks at 20.2 mS cm^{-1} after ca. 11 hours, followed by a slow decline over time. The week-long test also showed that the membrane has an ionic conductivity of

10 mS cm^{-1} for 160 hours before dropping below this value. However, the IR comparison shown in figure D.10 of appendix D does not show any obvious reasoning for the decline in IC as both spectra (before and after testing) are very similar.

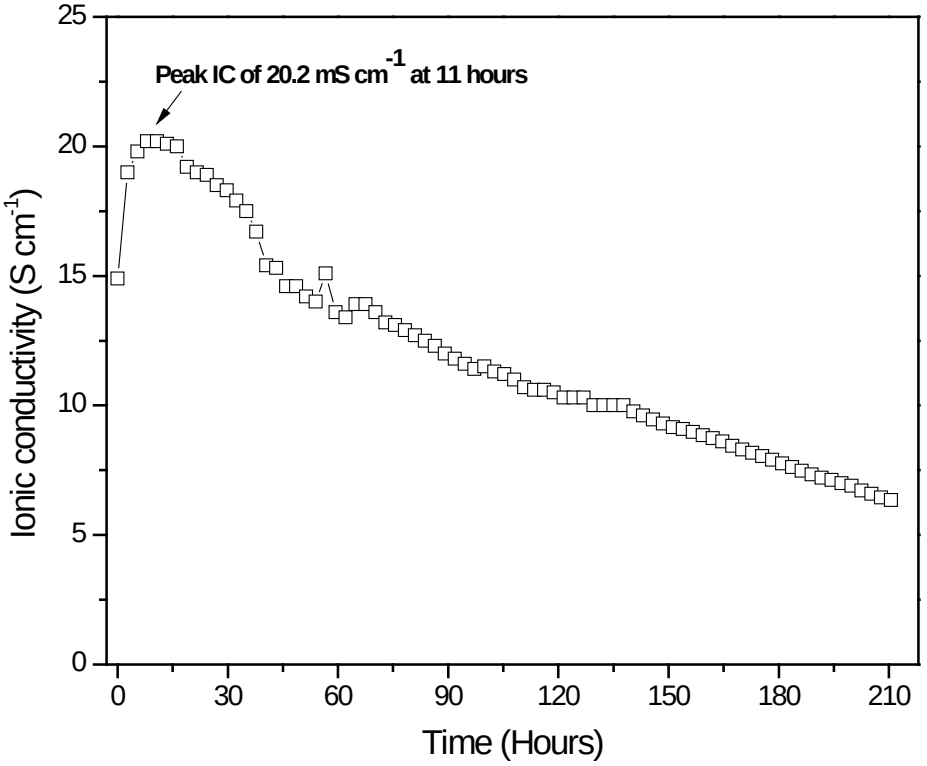

Figure 4.20: *Variation of IC with time for the diethylamine cross-linked QAPPO membrane (chloromethylated for 4 hours at 50 °C) during a 220 hour loop run. This test was carried out at 90 °C.*

4.5- Cross-linking of QAPPO (4 hr, 50 °C) using propylamine

After testing membranes cross-linked using diethylamine, it was decided to try a different cross-linker, propylamine. Different cross-linkers were used to investigate their effects on stabilisation or/and IC or whether all cross-linking agents provided the same effect regardless of material. Dipropylamine is highly toxic, flammable and

corrosive. These attributes render this molecule highly unsuitable for commercial use; hence the mono propylamine (B in figure 4.21) was used.

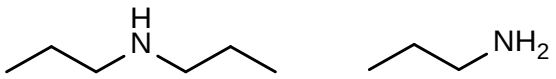

A **B**

Figure 4.21: *Dipropylamine (A) and propylamine (B) structures.*

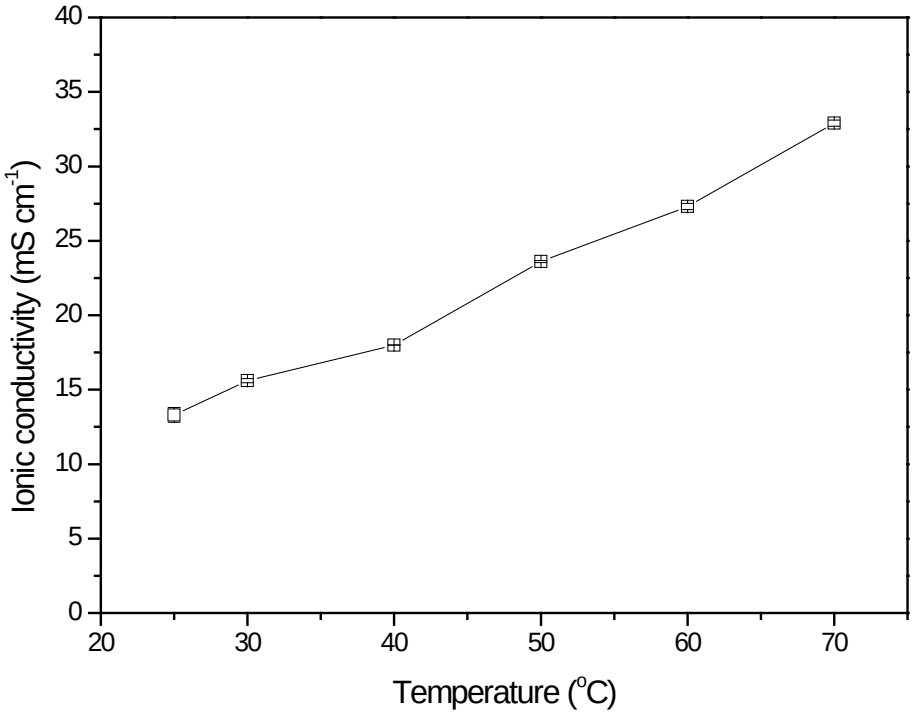

Figure 4.22: *Variation of ionic conductivity with temperature for the propylamine cross-linked QAPPO membrane (chloromethylated for 4 hours at 50 °C).*

Figure 4.22 shows the results observed for the propylamine cross-linked membrane synthesised from the 4 hour batch of CMPPO (including extremely small errors). The ionic conductivity increased rapidly with temperature to 32.9 mS cm^{-1} at 70 °C. The observed peak conductivity is almost double the value observed at 90 °C for the membrane cross-linked with diethylamine, and not far off from being three times

higher than the value observed for the noncross-linked membrane. This was unexpected as it was thought that the IC would reflect what had happened with the diethylamine derivative (an overall decrease in IC, but higher stability). However it can be seen that this was not the case. Again the plot suggested that the membrane had not equilibrated yet, so the AEM was tested for another 4 hours at 70 ^{o}C, with the following results (figure 4.23).

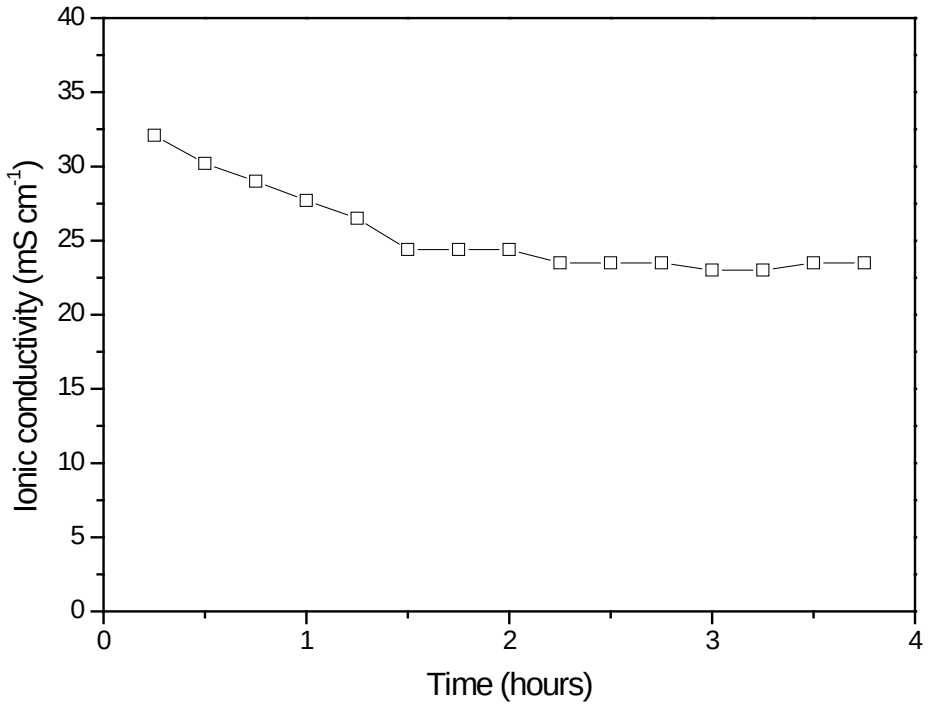

Figure 4.23: *Variation of the ionic conductivity with time for the propylamine cross-linked QAPPO membrane (chloromethylated for 4 hours at 50 ^{o}C). This test was carried out at 70 ^{o}C.*

After a promising start, the membrane ionic conductivity decreased and equilibrated at 23.5 mS cm^{-1}, nevertheless this result is still higher than that observed at 90 ^{o}C for

the diethylamine cross-linked membrane. To try to explain why the higher IC of this AEM, a TG analysis was performed on the two cross-linked AEMs (Figure 4.24).

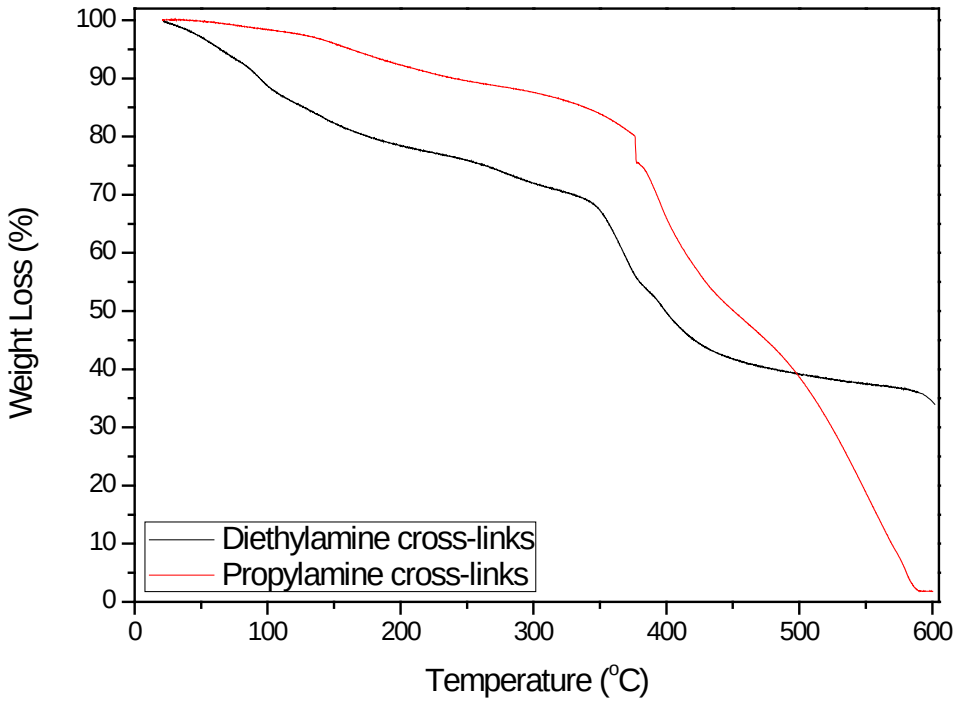

Figure 4.24: *TGA comparison between diethylamine (black) and propylamine (red) cross-linked QAPPO membranes (chloromethylated for 4 hours at 50 °C).*

The main source of membrane degradation is the free OH^- ions in solution. Noncross-linked membranes exhibit very poor mechanical strength and quickly degrade. This suggests that at temperatures of 60 °C or higher, the OH^- ions attack the quaternary ammonium groups. Cross-linking with diethylamine provides a steric barrier that the OH^- ions must overcome before they can attack the ammonium groups, hence why the diethylamine cross-linked membrane is stable up to 90°C and provides a higher conductivity. Therefore by increasing the steric bulk further with a propylamine, the

stability and conductivity will further increase as supported by the conductivity and thermal plots above.

4.6 - Cross-linking of QAPPO (4 hr, 50 ºC) using diaminopropane

After the propylamine cross-linker provided some very good results, another alkyl amine (diaminopropane) was used instead. This molecule keeps the same alkyl chain as propylamine, however it now incorporates two amine groups. As cross-linking occurs through the amine nitrogen, two quaternary nitrogen groups will be formed. The idea behind this was that the mechanical strength could be kept but the conductivity could increase due to the presence of twice the number of amine groups.

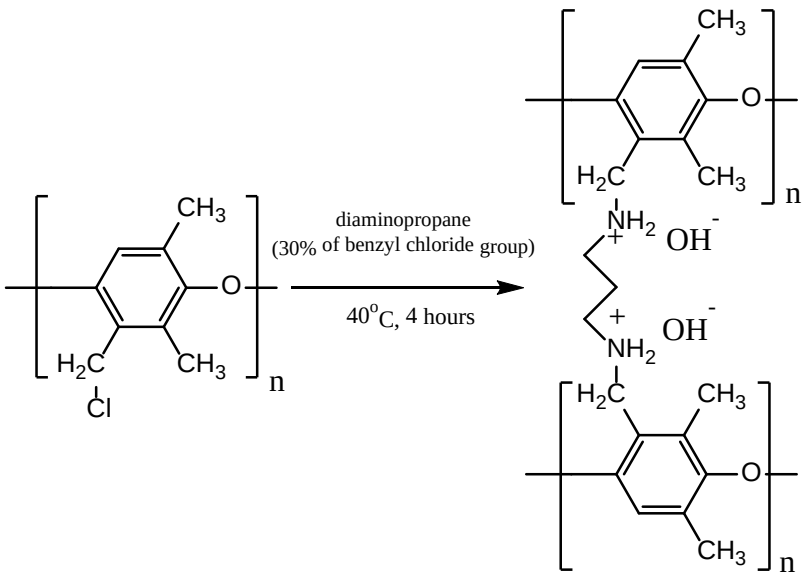

Figure 4.25: *Method of the cross-linking of QAPPO using diaminopropane.*

Figure 4.26 shows the IC results for the diaminopropane cross-linked membrane. Unlike both previous cross-linking experiments, there is a decrease in conductivity up to 60 ºC followed by a slight rise afterwards. This was not what was expected; however

all the data sits above 10 mS cm^{-1} and the membrane was completely stable up to 90 ^{o}C.

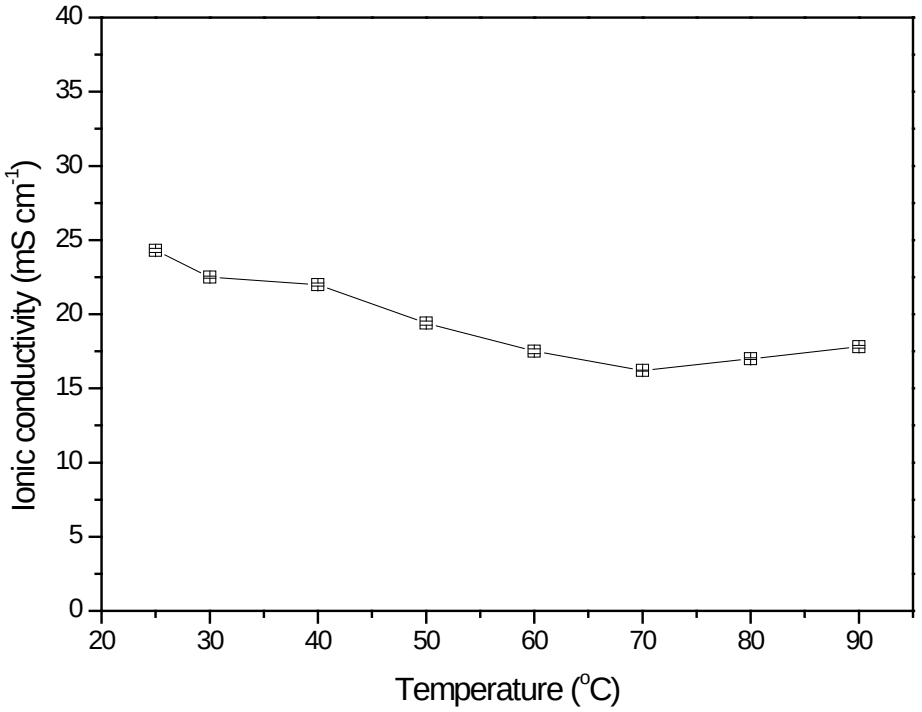

Figure 4.26: *Variation of ionic conductivity with temperature for the diaminopropane cross-linked QAPPO membrane (chloromethylated for 4 hours at 50 ^{o}C).*

4.7 – Conclusions on the chloromethylation of PPO for 4 hr 50 ^{o}C

Figure 4.27 shows the combined results of all membranes synthesised from the batch of PPO chloromethylated for 4 hours at 50 ^{o}C. By far the best results were observed when using propylamine as the cross-linking agent. The most exciting feature of this cross-linked membrane is that the ionic conductivity keeps increasing past 60 ^{o}C. Although this batch produced some good results in terms of ionic conductivity, the main conclusion that can be taken from these results is that stability issues dominate.

The noncross-linked membrane is highly unstable above 60 °C which does not provide a good base to build around. Additional efforts were therefore focused on producing a more thermally stable membrane that kept the same level of conductivity.

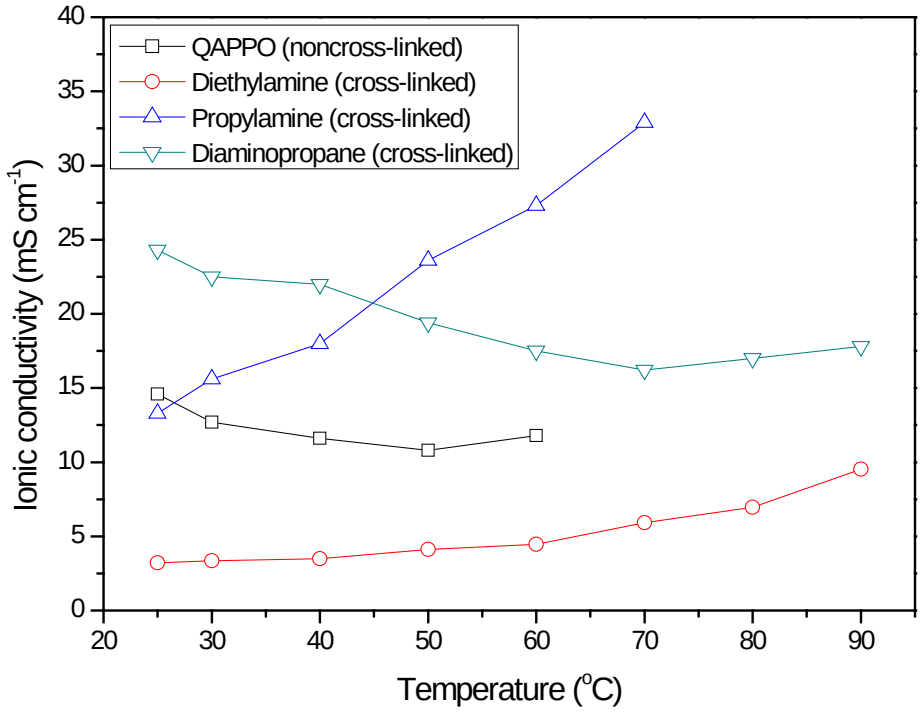

Figure 4.27: *Variation of ionic conductivity with temperature for all QAPPO membranes (cross-linked and noncross-linked) derived from the CMPPO batch chloromethylated for 4 hours at 50 °C.*

4.8 – Increase in chloromethylation reaction temperature to 60 °C

As discussed at the beginning of this chapter, one experimental change that was going to be investigated was the use of a higher reaction temperature during chloromethylation. Therefore, a higher reaction temperature of 60 °C was tested with the reaction time kept constant (4 hours). This experimental change yielded two failed chloromethylation attempts. After the start-up of the experiment, the reaction solution

almost immediately turned into a thick orange gel (IR spectrum shown in figure D.11 of appendix D). This same kind of gel was observed previously in a MSc project when working with polysulphone based membranes [9]. It has been reported that this polymer gel observed during the chloromethylation process is of no use for membrane synthesis, as it is an “over cross-linked” polymer [10, 11]. This gel, be very difficult to dissolve in any solvent during the membrane preparation stage and any membrane prepared would show very poor ionic conductivity. This is due to cross link bonds forming at each point where a chloromethylation has occurred. The number of sites available for quarternisation would be greatly reduced and thus the conductivity would also.

The gelation reaction, as it is called, is often described as “Friedel-Crafts” in type [10, 11].

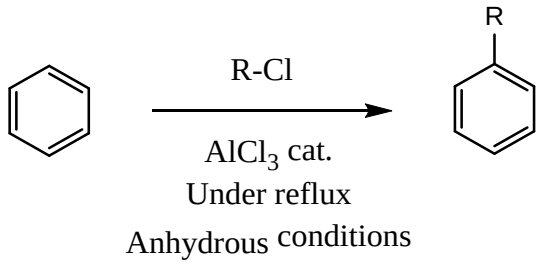

Figure 4.28: *Friedel-Crafts reaction schematic.*

A Friedel-Crafts alkylation involves an electrophilic aromatic substitution, where a carbocation acts as the electrophile. A catalyst, typically a metal chloride, removes the chlorine atom from a chlorosubstituted alkane, thus creating a carbocation. An electron pair from an aromatic ring will then attack this carbocation, forming a new carbon-carbon bond. Subsequent loss of H^+ then restores the benzene ring double bond

configuration. It is important to remember that the chloromethylation process needs to be balanced with the cross-linking reaction. High reaction temperatures seem to speed up the Friedel-crafts cross-linking reaction, as the chloromethylated PPO is susceptible to dechloroination and attack from unreacted PPO molecules.

4.9 – Chloromethylation of PPO for 4 hours at 55 ºC

As chloromethylation reactions at 60 ºC were proven difficult to complete, the temperature was reduced to 55 ºC. Again, a couple of attempts failed due to the formation of the thick gel; however, one reaction managed to reach 2.5 hours before showing signs of failure, i.e. reaction solution starting to thicken dramatically.

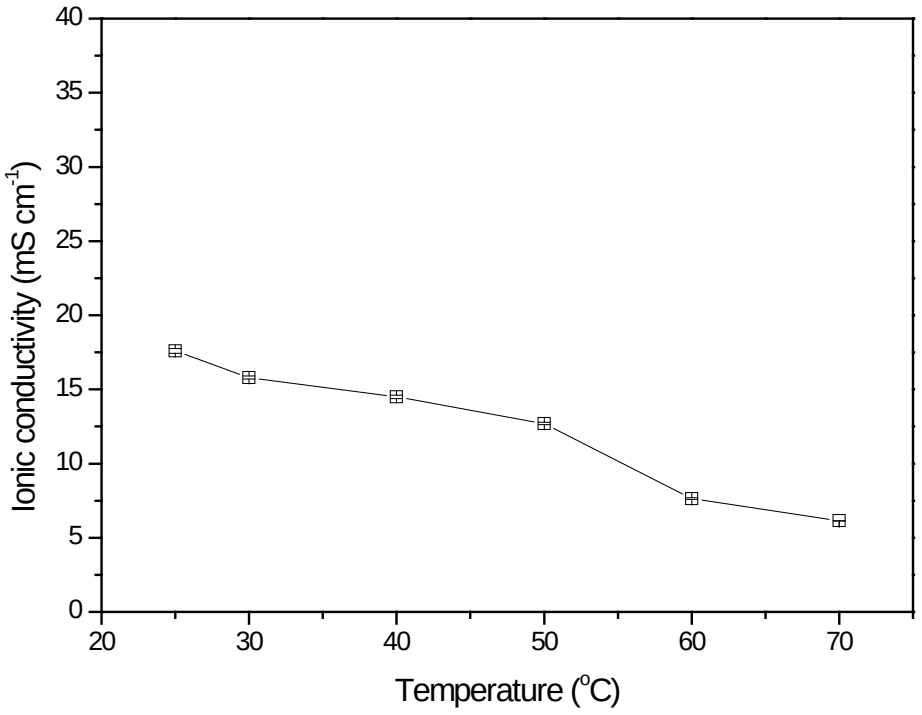

Figure 4.29: *Variation of ionic conductivity with temperature for the QAPPO membrane (chloromethylated for 2.5 hours at 55 ºC).*

Figure 4.29 shows the results observed for the membrane synthesised from the 2.5 hour at 55 ^{o}C batch of CMPPO.

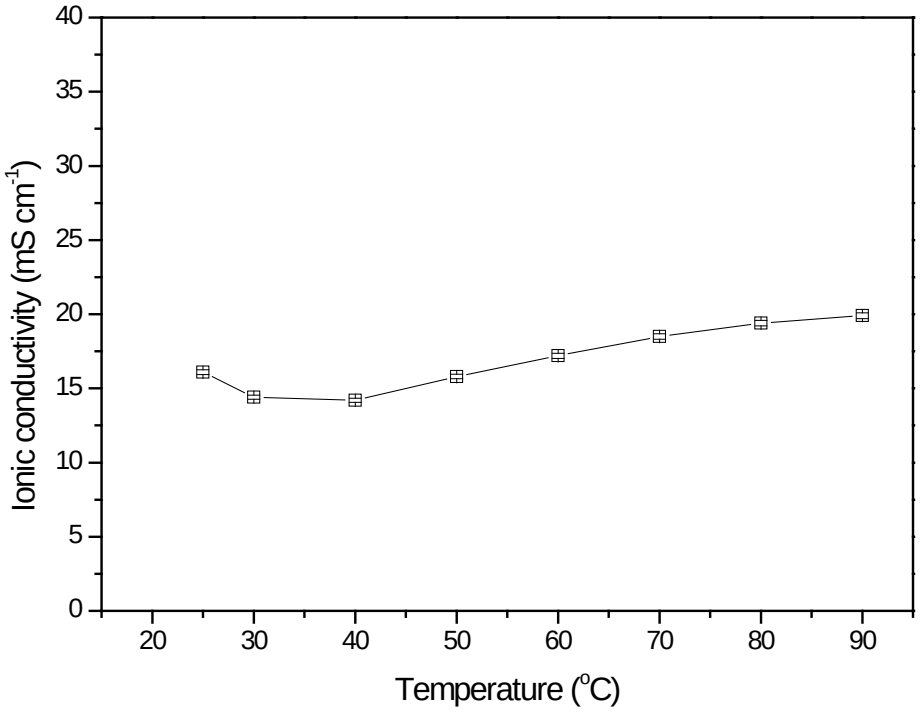

Figure 4.30: *Variation of ionic conductivity with temperature for the propylamine cross-linked QAPPO membrane (chloromethylated for 2.5 hours at 55 ^{o}C).*

The ionic conductivity of the membrane falls off very rapidly followed by complete dissolution into the testing water at 70 ^{o}C. Regardless of this fact, a propylamine cross-linked membrane was synthesised and tested yielding the results shown in figure 4.30. After a slight stabilisation period, this membrane followed the trend set by the 4 hour at 50 ^{o}C analogue shown in figure 4.22; however, its IC did not reach that of the 4 hour at 50 ^{o}C batch (> 30 mS cm^{-1} at 70 ^{o}C).

To conclude due to the poor performance of the standard membrane and the unpredictable nature of the chloromethylation reaction at temperatures above 50 ^{o}C, longer reaction times were attempted instead to synthesise stronger membranes.

4.10 – Chloromethylation of PPO for 6 hours at 50 ^{o}C

Previous chloromethylation reactions were performed for one and four hours. A 6 hour batch of CMMPO was synthesised without any problems. The IC plot of the synthesised noncross-linked membrane is shown in Figure 4.31.

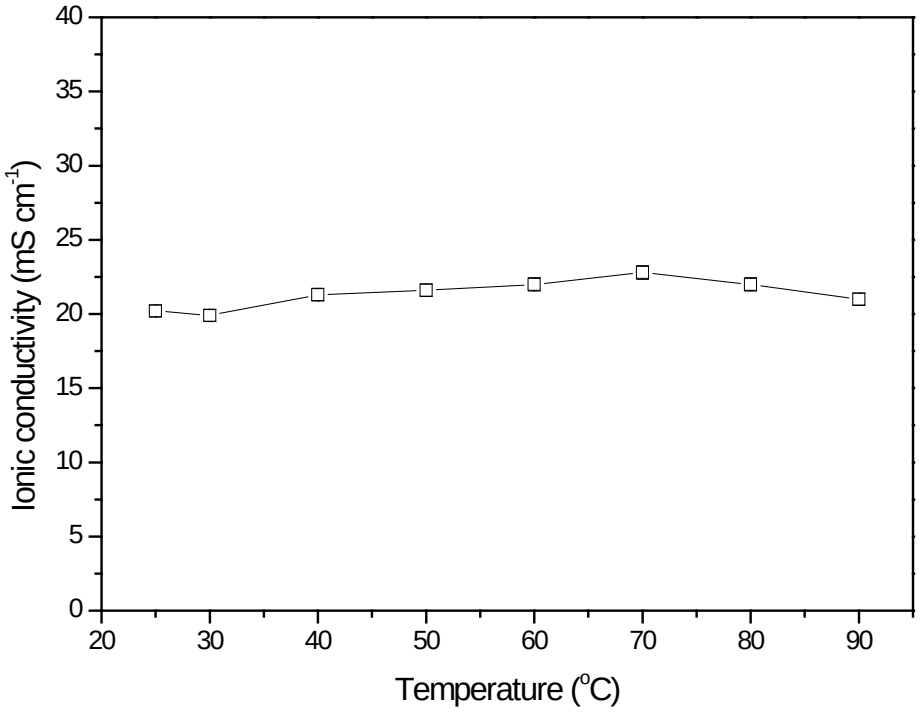

Figure 4.31: *Variation of ionic conductivity with temperature for the QAPPO membrane (chloromethylated for 6 hours at 50 ^{o}C).*

Unlike the previous synthesised noncross-linked membranes, this membrane was "testable" up to 90 ^{o}C, indicating that it is more stable. The IC peaked at 70 ^{o}C, rather

than 60 °C, before decreasing. At 60 °C, the 6 hour batch membrane showed a higher IC (22 mS cm^{-1}) than the IC recorded for the noncross-linked 4 hour batch membrane, (12 mS cm^{-1}). A stability test was performed on this membrane initially at 70 °C (Figure 4.32). The membrane showed a stable conductivity of between 21 and 22 mS cm^{-1} for 3 weeks or 500 hours. This was the first time that a membrane showed such stability over an extended period of time with a stable IC.

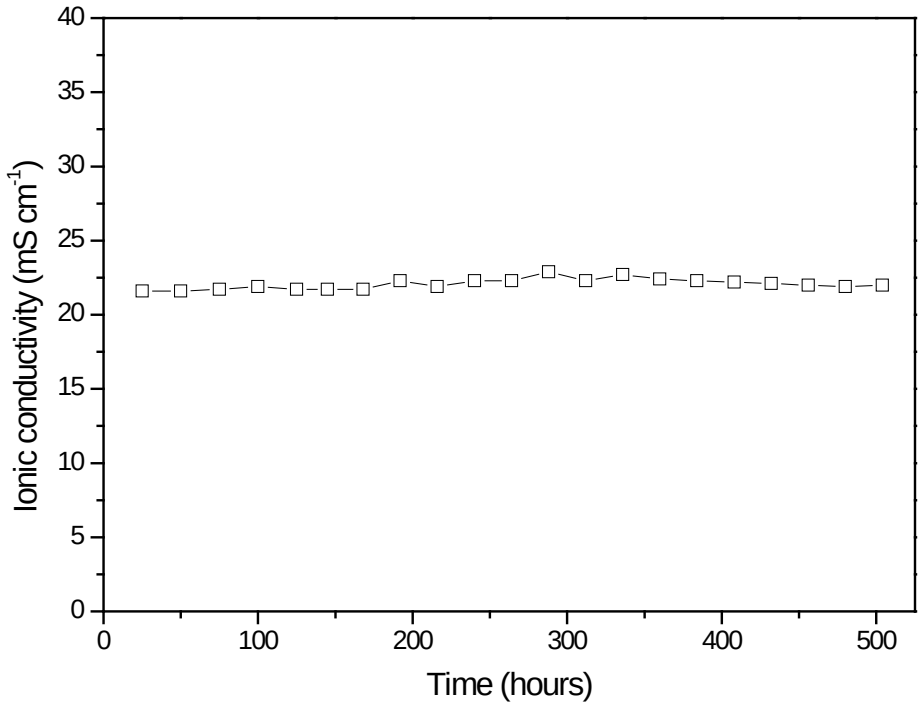

Figure 4.32: *Variation of the ionic conductivity with time for the QAPPO membrane (chloromethylated for 6 hours at 50 °C). This test was carried out at 70 °C.*

A second stability test was carried out at 80 °C. Figure 4.33 shows the results of this test, indicating that the membrane is not stable at 80 °C as it is at 70 °C. This was not entirely unexpected as the initial IC vs temperature conductivity test showed a decrease in conductivity between 70 °C and 80 °C.

Figure 4.34 shows the TGA plot for the 6 hour QAPPO membrane compared to that observed for the 4 hour QAPPO membrane. As explained earlier, the first weight loss at around 100 ^{o}C is attributed to absorbed water being evaporated and this can be seen on both curves.

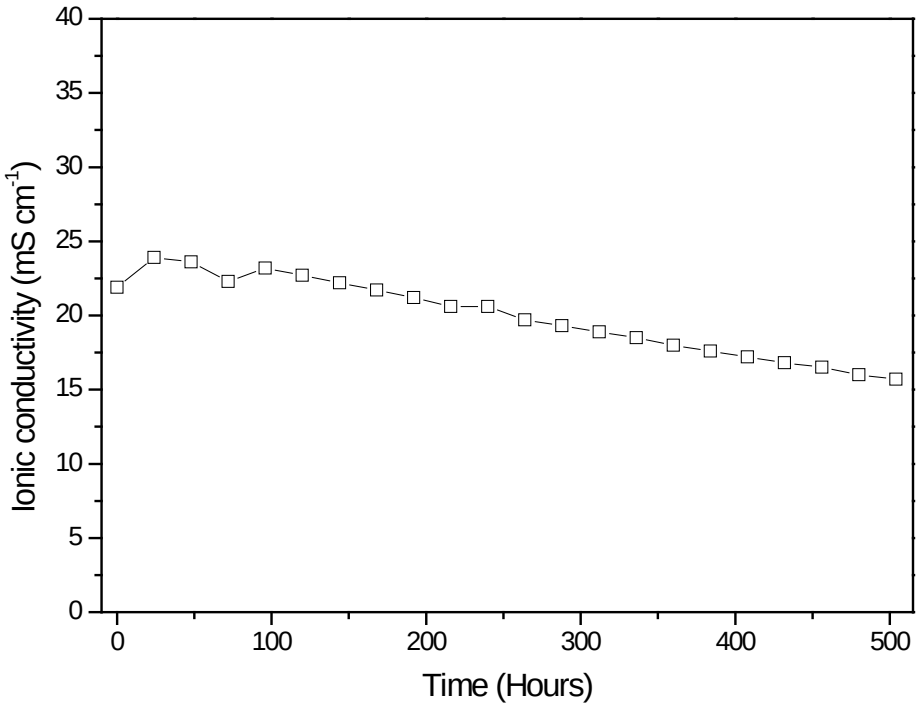

Figure 4.33: *Variation of the ionic conductivity with time for the QAPPO membrane (chloromethylated for 6 hours at 50 ^{o}C). This test was carried out at 80 ^{o}C.*

However the 6 hour QAPPO membrane shows a more dramatic loss as opposed to the 4 hour equivalent. It is known that as AEMs get more conductive, they absorb more water, which is an explanation for the greater initial weight loss exhibited by the 6 hour membrane. The second weight loss concerns the degradation of the quaternary ammonium ion, which can be seen at about 150 ^{o}C on the 4 hour curve. After the first weight loss, the 6 hour curve does not show a second weight loss until about 250 ^{o}C.

This evidence can explain why the membrane chloromethylated for 6 hours is more stable at elevated temperatures than the one chloromethylated for only 4 hours.

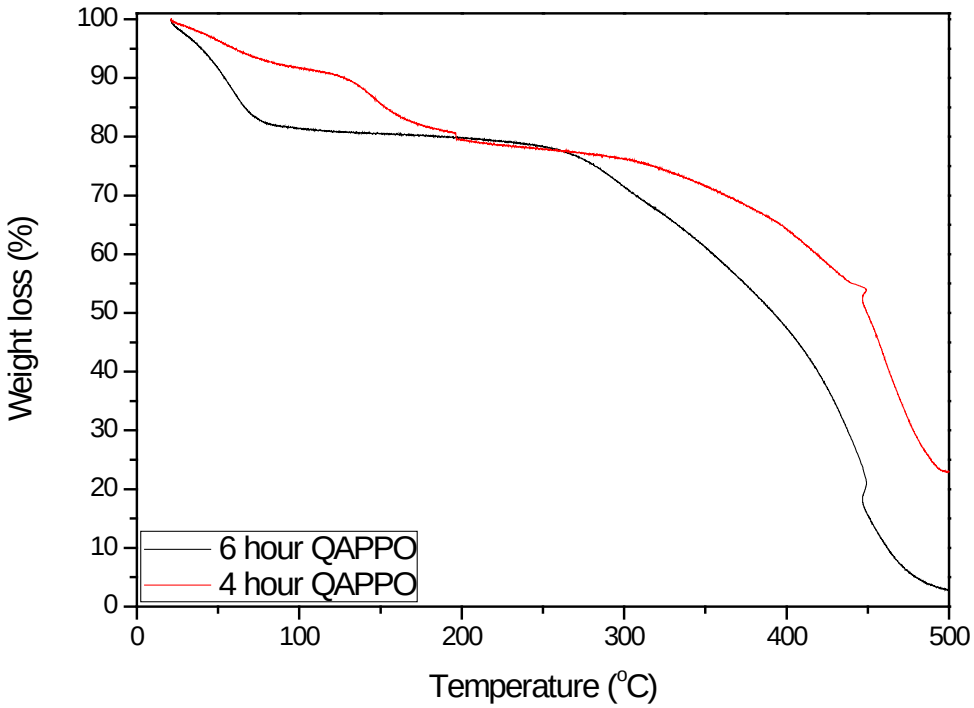

Figure 4.34: *TGA comparison between 6 hour (black) and 4 hour (red) QAPPO membranes.*

However it must be noted that the 6 hour membrane is still unstable at 80 ºC and with the working temperature of AEMs needing to be as close to 100 ºC as possible, improvements are still needed. Due to the successes observed when using propylamine and diethylamine as cross-linking agents, it was decided to test the respective cross-linked membranes performance. Figure 4.35 shows the results of the cross-linked membranes. Clearly, the propylamine derivative achieves the highest IC out of the two, with the IC of the diethylamine AEM not even reaching the IC displayed at room temperature by the propylamine cross-linked AEM.

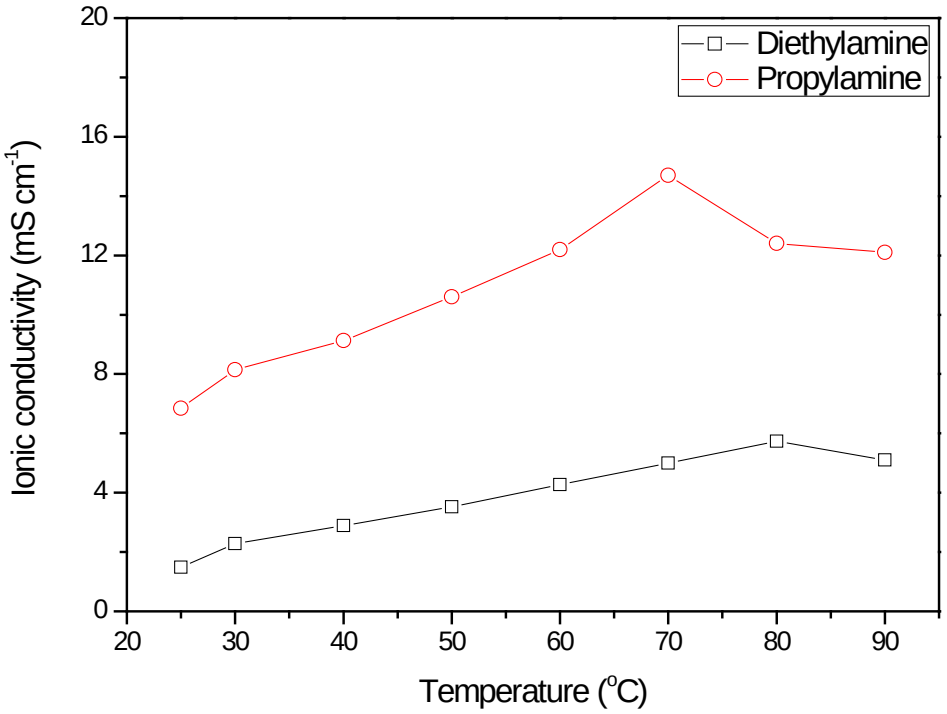

Figure 4.35: *Variation of ionic conductivity with temperature for cross-linked QAPPO membranes (diethylamine and propylamine) derived from the CMPPO batch chloromethylated for 6 hours at 50 °C.*

4.11 - Conclusions on the chloromethylation of PPO for 6 hrs 50 ºC

Figure 4.36 displays the combined results for all membranes synthesised from the batch of CMPPO chloromethylated for 6 hours. The noncross-linked membrane proved to have a quite reasonable performance which led us to believe that by cross-linking it, it would show the same increase in performance observed for the batch chloromethylated for 4 hours. However, this was not the case as the performance of both cross-linked analogues were not even of comparable quality. This inferred that further modification of the AEMs is not always the best course of action.

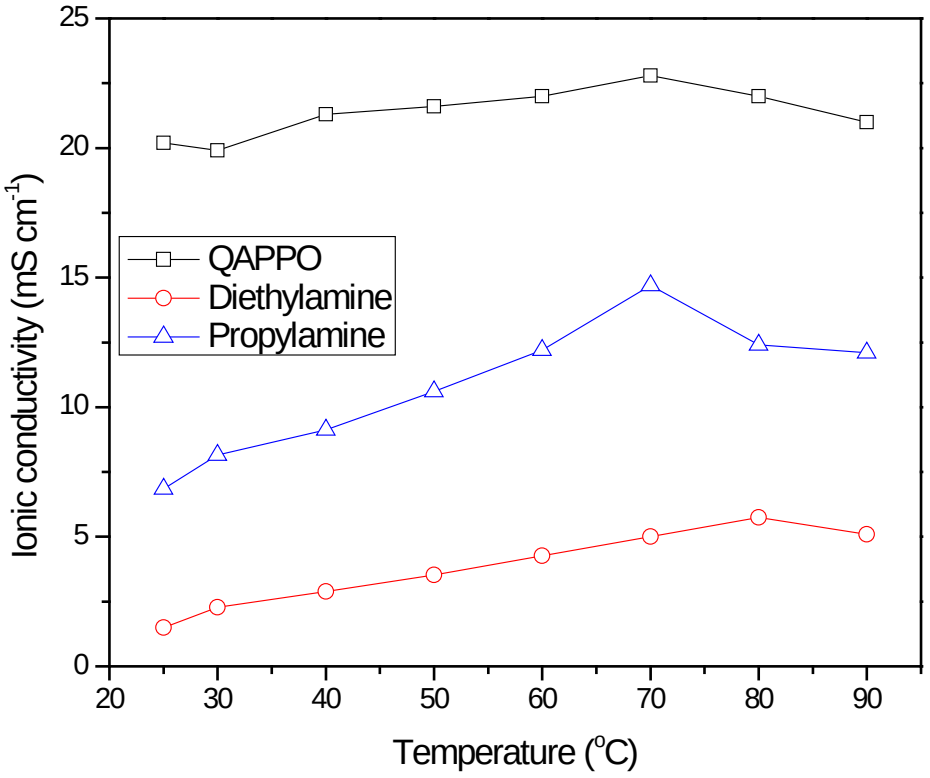

Figure 4.36: *Variation of ionic conductivity with temperature for all QAPPO membranes (cross-linked and noncross-linked) derived from the CMPPO batch chloromethylated for 6 hours at 50 °C.*

4.12 – Overall conclusions for all batches of CMPPO and QAPPO AEMs

Figure 4.37 compares the ICs observed for the three batches of QAPPO membranes derived from CMPPO samples with different chloromethylation times. It can be seen that as the reaction time during the CMPPO preparation step increases, the overall conductivity and stability also increases. Membranes prepared from a 1 hour batch of CMPPO have a very low IC (below 10 mS cm^{-1}) and are very unstable at past 60 ^{o}C.

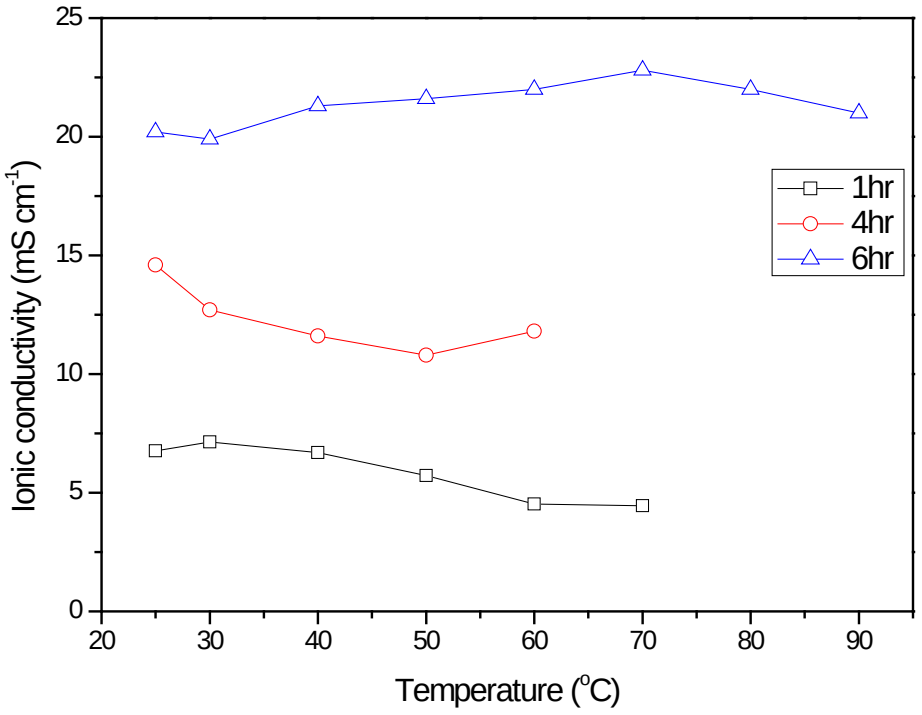

Figure 4.37: *Variation of ionic conductivity with temperature for all QAPPO membranes (noncross-linked only) derived from all CMPPO batches chloromethylated for 1, 4 and 6 hours at 50 ^{o}C.*

Increasing the reaction time to 4 hours had the effect of increasing the IC to above 10 mS cm^{-1}. However, these membranes were again unstable at temperatures over 60 ^{o}C. Chemical cross-linking with diethylamine lowered the overall IC (below 10 mS cm^{-1})

but the membrane was now stable for a short time at 90 ^{o}C. Chemical cross-linking with different reagents (propylamine and diaminopropane) showed differing effects. Propylamine cross-links produced a membrane whose IC was higher than 30 mS cm^{-1} and again stable at 90 ^{o}C, whereas diaminopropane cross-links did not produce membranes with higher IC.

Increasing the chloromethylation reaction temperature to both 55 ^{o}C and 60 ^{o}C produced reaction failures and unworkable thick polymer gels. One 55 ^{o}C preparation of CMPPO was successful but an unstable membrane was obtained. Increasing the reaction time further to 6 hours at 50 ^{o}C was the only way that a higher IC was observed along with a higher stability. The AEM was stable for 500 hours at 70 ^{o}C with an IC of 22 mS cm^{-1}. The 6 hour batch of CMPPO was used as the base material for the work discussed in the next chapter.

4.13 – Chapter 4: References

[1]. J. Pan, Y. Li, L. Zhang and J. Lu, *Chem. Commun.*, (2010), **46**, 8597-99.

[2]. S. Lu, J. Pan, A. Huang, L. Zhuang and J. Lu, *Proceedings of the National Academy of Sciences*, (2008).

[3]. *Hazardous Substances Data Bank (HSDB)*, US EPA, CASRN: 107-30-2.

[4]. *US EPS Integrated Risk Info System (IRIS)*, CASRN: 107-30-2.

[5]. *Acute Exposure Guideline Levels for Selected Airborne Chemicals: Volume 11*, (2012), National Academy of Sciences.

[6]. V. V. Shevchenko and M. A. Gumennaya, *Theoretical and Experimental Chemistry*, (2010), **46**, 139-52.

[7]. T. Chakrabarty, S. Prakash and V. K.Shahi, *Journal of Membrane Science*, (2013), **428**, 86–94.

[8]. E. Avram, E. Butuc, C. Luca and I. Druta, *Journal of Macromolecular Science, Part A: Pure and Applied Chemistry*, (1997), **34**, 1701-14.

[9]. G. Mann, *MSc Thesis: Alkaline polymer electrolyte membrane for fuel cell applications* 2010.

[10]. J. Wang, S.Li and S. Zhang, *Macromolecules*, (2010), **43**, 3890-96.

[11]. G. Wang, Y. Weng, D. Chu, R. Chen and D. Xie, *Journal of Membrane Science*, (2009), **332**, 63-68.

Chapter 5 – Improvements to stability using a quaternised poly(2, 6-dimethyl-1, 4—phenylene oxide)/polysulphone blend, QAPPO/QAPS

Chapter 4 identified that long term stability was the major issue for the synthesised AEMs. It was shown that the AEM synthesised from the 6 hour batch of CMPPO had the highest IC. Conversely, it was also shown to be less stable than the 4 hour AEM. As AEMs get more conductive, they become more prone to water uptake, which leads to increased swelling. Ultimately, the swelling will eventually cause the membrane to disintegrate [1], with this disintegration phenomenon being greater at the high temperatures needed to operate these kinds of fuel cells.

During the chloromethylation of PPO, two reactions occur within the synthesis solution; functionalisation and cross-linking. The functionalisation reaction is responsible for the chloromethylation of the benzene rings along the polymer chain. Cross-links are then formed between some of these chloromethylated sites. These reactions should occur in a 50:50 mix to achieve a highly conductive and highly stable membrane. However it is very difficult to get a good balance between the two, as leaning towards one reaction will always have a detrimental effect towards either conductivity or stability.

Previous research has highlighted the potential benefits of adding a small percentage of a different polymer to a conductive ionomer solution pre-casting [2]. These blended membranes were shown to be more stable at higher temperatures. The effect of adding a second polymer is comparable to that of cross-linking; an increase in stability is observed together with a reduction in overall IC. The optimal result would be to

increase the stability without any negative effect to IC. In this work, two different blending methods were employed:

1. Adding equal amounts of the two polymers before chloromethylation to get a true polymer blend.

2. Synthesising two separate chloromethylated polymers and mixing them together at the ionomer stage before quarternisation.

5.1 – Chloromethylation of PPO and PS for 4.5 hours at 50 ºC

Polysulphone was chosen to be the secondary polymer in this case as it was used in one of the first AEMs of this type [3]. A 1:1 ratio of PPO and PS were added to the reaction vessel and the normal reaction procedure was followed. Figures A.12 in appendix A show the IR spectrum of the CMPPO/PS sample compared to that of CMPPO (6 hr, 50 ºC). Figure A.13 in appendix A shows the zoomed in lower half of figure A.12 with the added S=O peaks from the incorporated PS. Figure 5.1 shows the conductivity observed for this polymer blend after quaternisation. This membrane's conductivity peaked at 70 ºC (13 mS cm^{-1}) followed by a decrease in conductivity as the temperature was further increased. During the longevity test at 70 ºC, this conductivity was not reproduced and the membrane very quickly disintegrated within one hour. This "one pot synthesis" of chloromethylating two polymers at once was abandoned at this point. The instability of the membrane is also the cause for the high amount of error observed on figure 5.1

5.2 – Production of AEMs from a CMPPO/CMPS ionomer mix

The main problem with the "one pot" chloromethylation synthesis described in section 5.1 is that there is no way of controlling the level of functionalisation per base polymer.

By purely mixing the two base polymers together in the reaction solution, one polymer could have a higher degree of functionalisation than the other which could lead to disjointed pathways for OH^- to travel through the membrane and ultimately lower the IC.

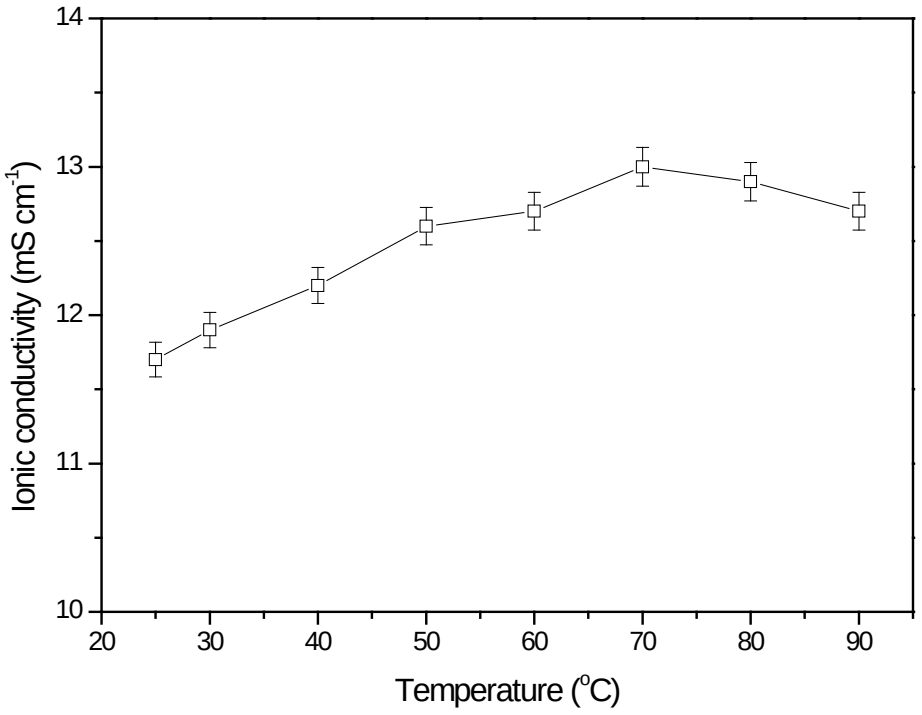

Figure 5.1: *Variation of ionic conductivity with temperature for the QAPPO/QAPS membrane (a 1:1 ratio of PPO and PS chloromethylated for 4.5 hours at 50 °C).*

By mixing two known conductive polymers at the ionomer stage it was believed that this would produce a better result. The two polymer samples that were selected were:

1. 6 hour CMPPO from previous chapter.
2. 8 hour CMPS from G. Mann MSc project [4]. (IRs of the CMPS and associated QAPS are shown in figures D.14 and D.15 respectively in appendix D)

The conductivity of the quaternised membrane prepared from the 6 hour CMPPO batch is known to be 20 mS cm^{-1} at 90 ^{o}C, as discussed in the previous chapter. The conductivity of the 8 hour CMPS batch was also known as it had been investigated previously [4]. The CMPS was prepared in the same manner as the CMPPO sample. The CMPS sample was different in appearance to the CMPPO sample, as it was made of hard clumps of polymer rather than a fine powder. The quaternised membrane synthesised from this sample was tested for extended periods of time at both room temperature and 60 ^{o}C, the results of which can be seen in figure 5.2.

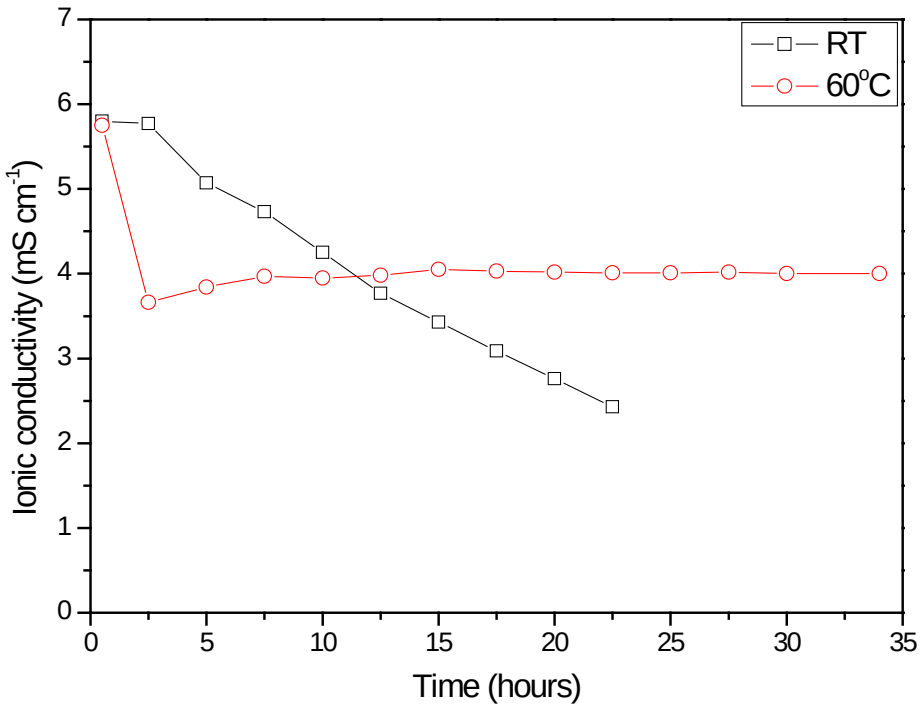

Figure 5.2: *Variation of ionic conductivity with time for the QAPS membrane prepared from 8 hour CMPS sample. The tests were performed at room temperature (black) and 60 ^{o}C (red).*

At room temperature the membrane IC shows a steady decrease over a 24 hour period. This conductivity is very poor as it is well below 10 mS cm^{-1}. A higher temperature stabilisation run was performed and after 35 hours the membrane was found to have a stable conductivity of 4 mS cm^{-1}. This performance at the time was undesirable, however its stability was noted as being excellent.

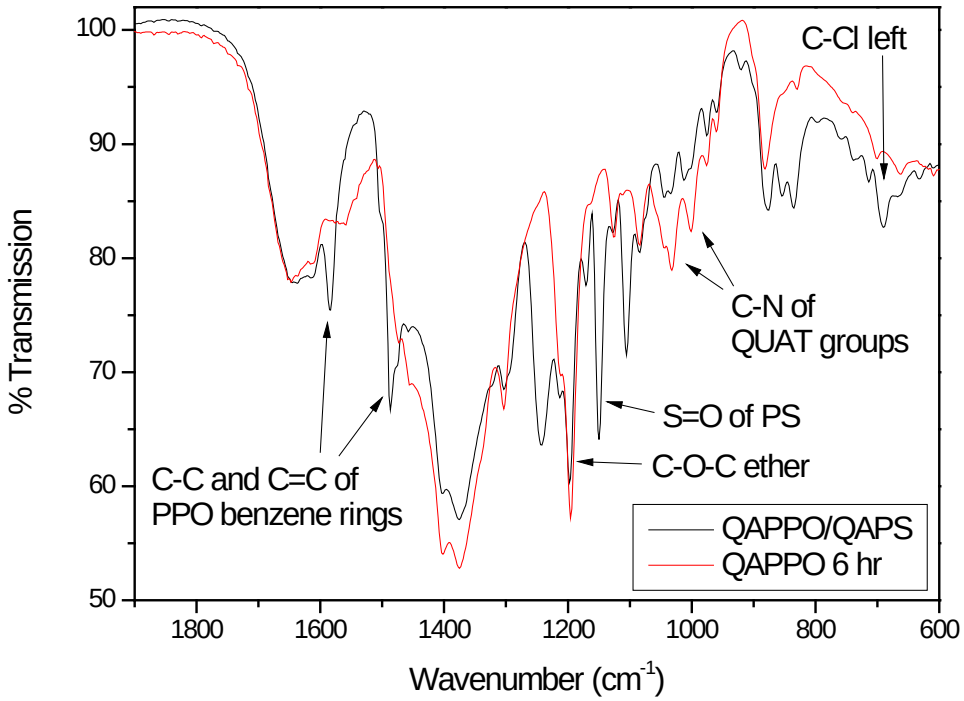

Figure 5.3: *Zoomed in part of infrared spectrum comparison between QAPPO (red) and QAPPO/QAPS (black). The QAPPO/QAPS (black) trace shows the addition of the S=O symmetric stretch at 1150 cm^{-1}.*

This CMPS sample was mixed in equal amounts with the 6 hour CMPPO sample from the previous chapter, quaternised and cast. An infrared comparison of the standard QAPPO and QAPPO/QAPS membrane is shown in Figure 5.3 (full spectrum of QAPPO/QAPS shown in figure D.16 and D.17 of appendix D). The spectra of the two

membranes are similar apart from the appearance of the S=O symmetric stretch at 1150 cm^{-1}. Figure 5.4 shows the conductivity result (along with associated error) for the PPO/PS ionomer mix membrane. Although the conductivity is only 20 mS cm^{-1} at 60 ^{o}C, it increases with increasing temperature up to 25 mS cm^{-1} at 90 ^{o}C. This increase is not large but there was no sign of degradation above 60 ^{o}C.

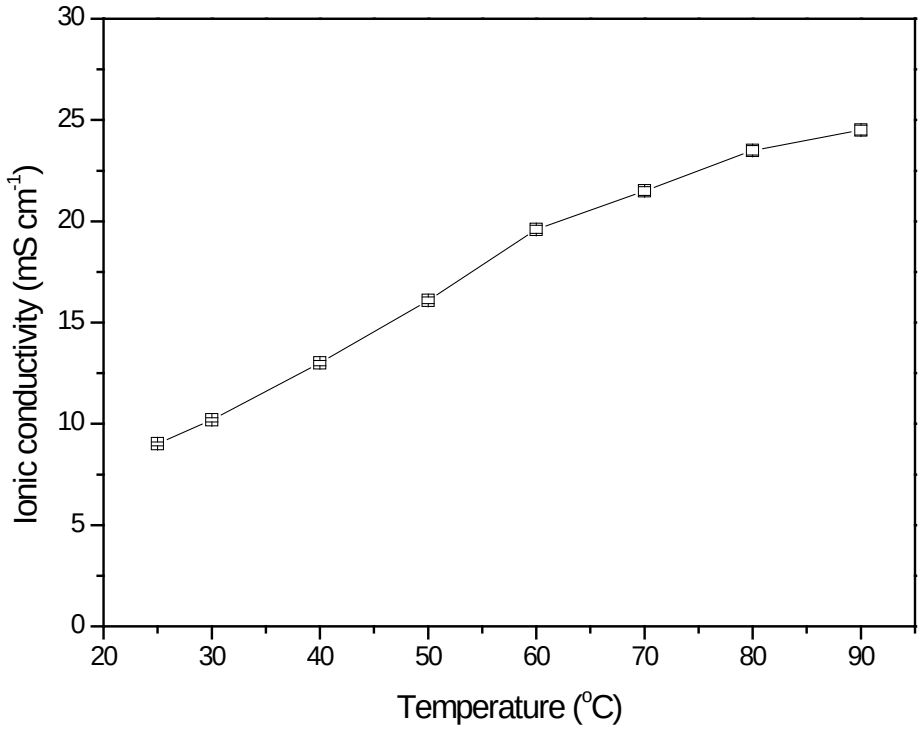

Figure 5.4: *Variation of ionic conductivity with temperature for the QAPPO/QAPS mix membrane.*

Figure 5.5 show the conductivity results for long term stability tests performed at 70 ^{o}C and 80 ^{o}C for 70 and 120 hours respectively. Firstly the membrane shows a slow decline in conductivity to around 13.3 mS cm^{-1} at 70 ^{o}C compared to the initial result seen in figure 5.4 which showed the IC at 25 mS cm^{-1} at 70 ^{o}C. Normally this would

indicate that the membrane is slowly breaking down and if left longer the downward trend would continue. However at 80 ^{o}C the conductivity actually stabilises roughly between 10 and 15 mS cm^{-1} for the full 120 hour period with no sign of physical degradation. The decrease in conductivity at the start can therefore be attributed to membrane stabilisation. This occurs when the polymer chains within the AEM work to align themselves and form a stable pathway for the OH^- ions to travel.

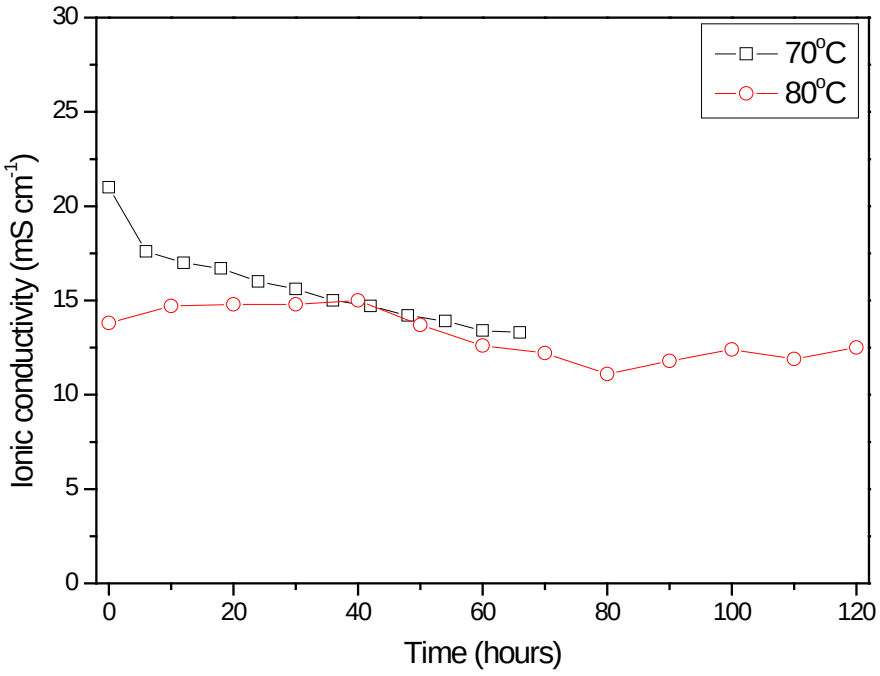

Figure 5.5: *Variation of ionic conductivity with time for the QAPPO/QAPS membrane. These tests was performed at 70 °C (black) and 80 °C (red).*

The temperature was further increased to 90 ^{o}C and figure 5.6 shows the observed results for an 1100 hour test. Firstly it shows that the membrane is stable at 90 ^{o}C for a prolonged amount of time. Secondly it appears to show two different levels of conductivity with initially the conductivity following that seen in figure 5.5 (15 mS

cm^{-1}). However around the 300 hour mark there is a small jump in conductivity to around 20 mS cm^{-1} which then slowly increases for the rest of the test. To attempt to explain this result, we need to look at the composition of the membrane itself. The membrane is comprised of a 50:50 mixture of QAPPO (**1**) and QAPS (**2**) shown in figure 5.7.

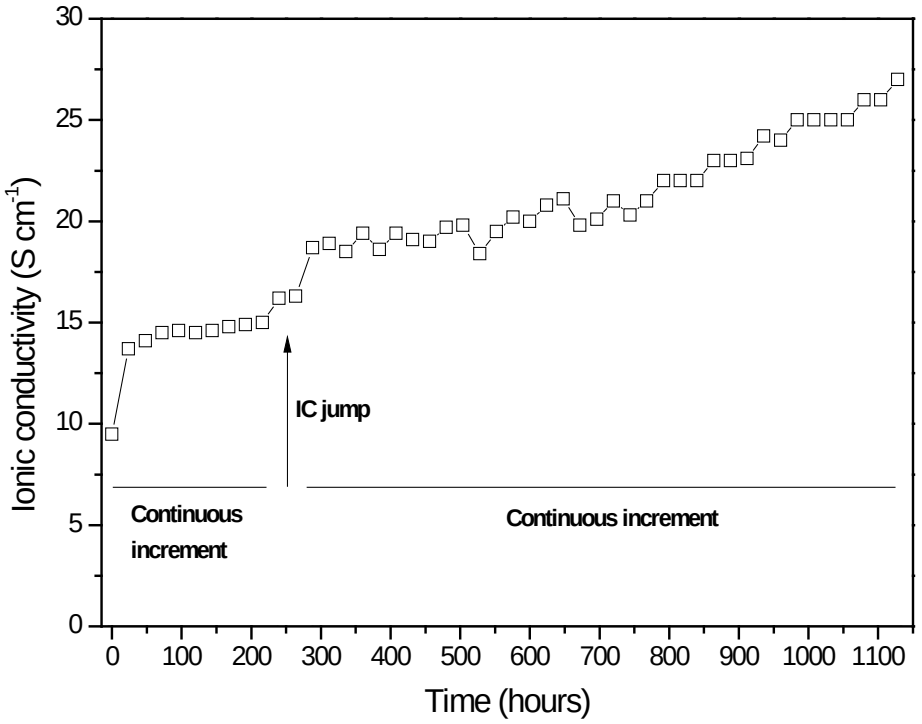

Figure 5.6: *Variation of ionic conductivity with time for the QAPPO/QAPS membrane. These tests was performed at 90 °C.*

It is easy to see that the polysulphone monomer of QAPS is a lot larger than that of QAPPO. There is potential for the QAPS chains to envelop the QAPPO structure in a way similar to that shown in figure 5.8.

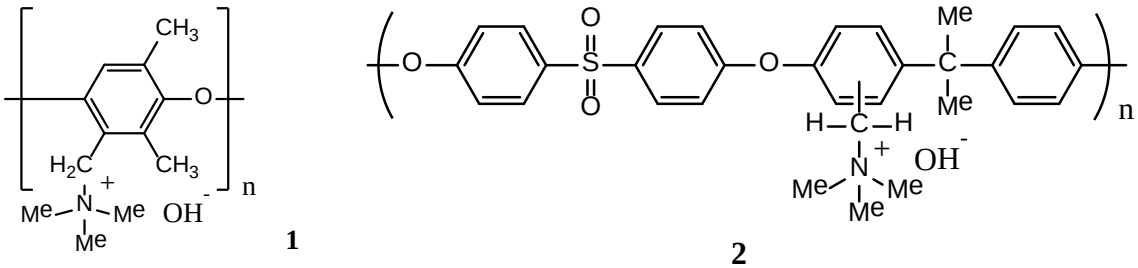

Figure 5.7: *QAPPO (**1**) and QAPS (**2**).*

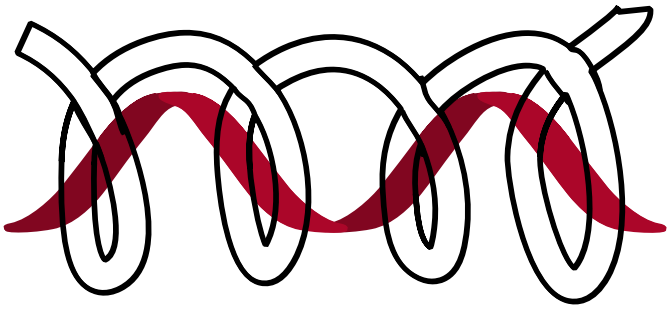

Figure 5.8: *Hypothesised molecule structure of the QAPPO/QAPS membrane with black and white chain representing QAPS and the red chain representing QAPPO.*

During previous testing the QAPS sample that was used in this work proved to be an ineffective OH^- conductor [4] so it is highly unlikely that much of the conductive ability observed is due to this polymer sample. The ionic conduction that was observed for the blended membrane must be due primarily to the QAPPO moiety, since the observed value is similar to the value observed for the standard unmodified QAPPO membrane. Figure 5.9 shows the TG analysis of the individual components (QAPPO and QAPS) compared to the actual blended membrane. The QAPPO component exhibits the characteristic weight loss below 100 ^oC, which one would associate with

a sample that was conductive but not that stable at temperatures nearing 100 ^{o}C. The QAPS sample on the other hand shows low weight loss until well over 300 ^{o}C, something characteristic of a sample that is stable but minimally conductive. The combined blended membrane curve initially mirrors that of the QAPS sample before exhibiting its first major weight loss at 150 ^{o}C.

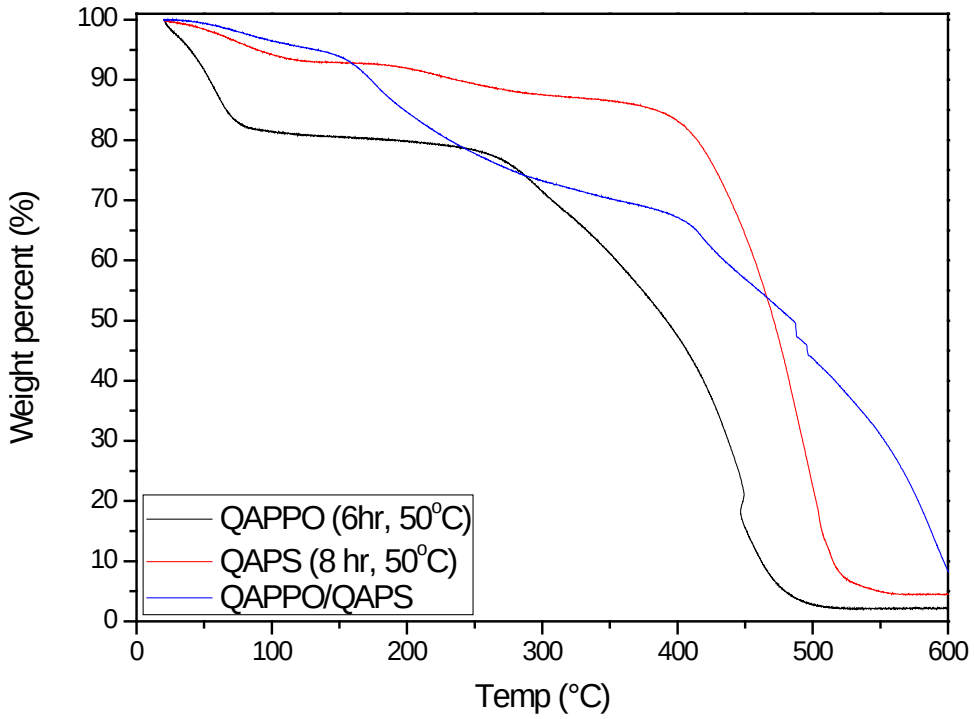

Figure 5.9: *TGA comparison between the individual components of/and the QAPPO/QAPS membrane.*

Figure 5.9 implies that the first weight loss of the QAPPO has been postponed by around 50-60 ^{o}C simply by adding in a second polymer (QAPS). A potential explanation for this observation could be attributed to the bulk of the PS component. As the PS molecule is proportionately larger in size than the PPO sample, it could be

obstructing any free OH^- ions from attacking any quaternary ammonium ions. However, due to its low conductive nature any IC loss from the PS sample would be very minimal. This idea could also go some way to explaining the steady increase in IC seen on figure 5.6. Initially the OH^- ion pathway through the membrane is not stable as they have to pass through a large bulky group. However as the experiment went on, the polymer chains aligned themselves into a more ordered state, meaning the pathway for OH^- conduction became less hindered.

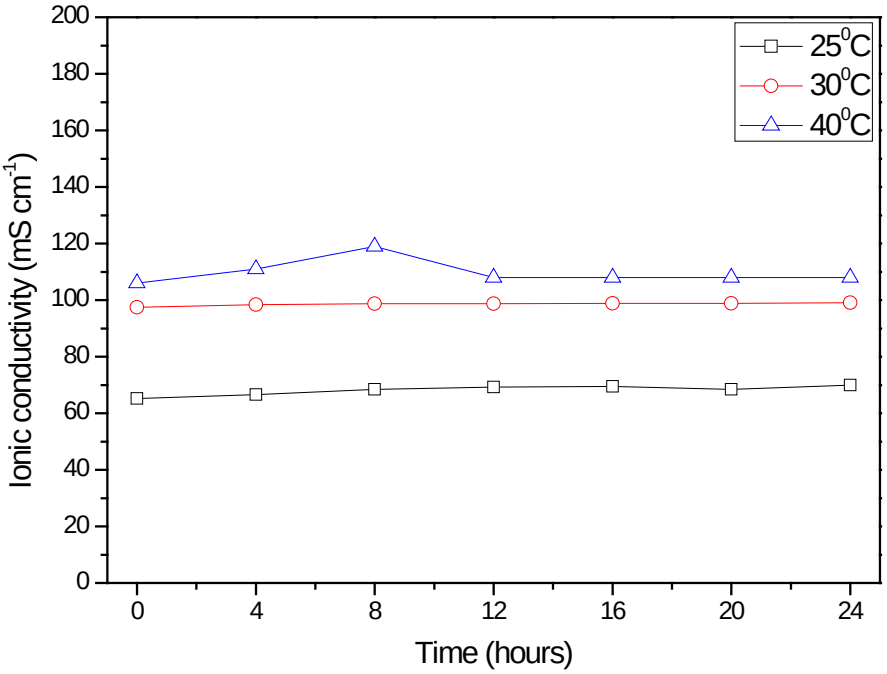

Figure 5.10: *Variation of ionic conductivity with time for the QAPPO/QAPS membrane in 1M KOH. These tests was performed at 25 °C (black), 30 °C (red) and 40 °C (blue).*

All impedance tests so far were performed in deionised water. However to access the stability of the membranes more fully, impedance tests were also performed in a strong

alkali medium of 1 M KOH. Figure 5.10 shows the results observed for the QAPPO/QAPS membrane tested in 1 M KOH between 25 ^{o}C and 40 ^{o}C.

It can be seen that the membrane is stable at all three temperatures for a period of 24 hours. It is also worth noting that the conductivity levels are now an order of magnitude higher (100 mS cm^{-1}) due to the fact that the test is being run in an alkali media. The temperature was further increased to 60 ^{o}C and figure 5.11 shows the IC observed for a total of 336 hours. For the duration of the test, the IC was stable at 130+ mS cm^{-1}; roughly 10 times higher than in deionised water.

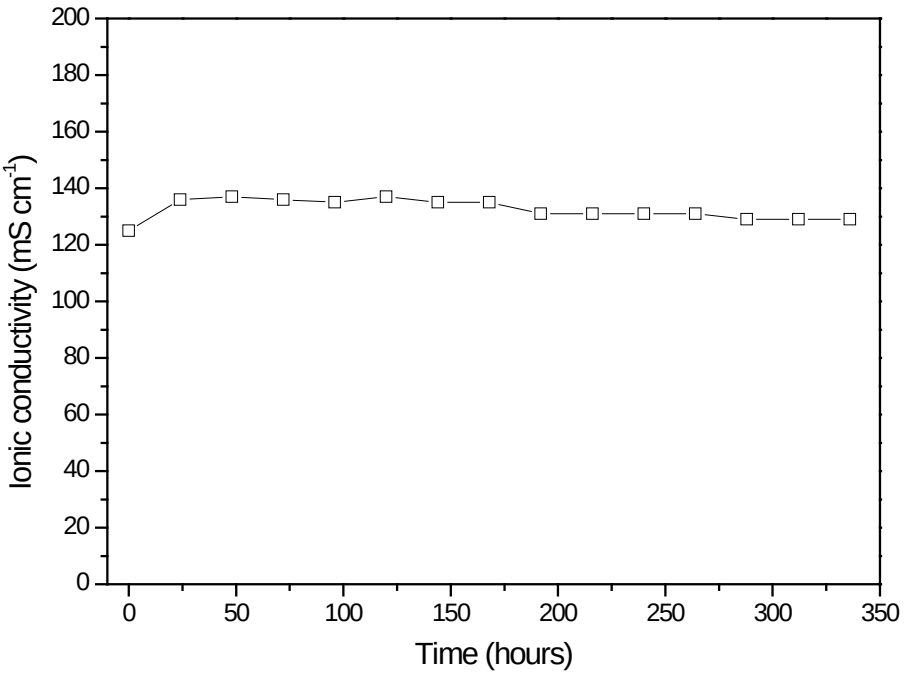

Figure 5.11: *Variation of ionic conductivity with time for the QAPPO/QAPS membrane in 1M KOH. This test was performed at 60 ^{o}C.*

When the temperature was increased to 70 ^{o}C, the IC of the QAPPO/QAPS membrane started to fall as shown in figure 5.12, stabilising again at 110 mS cm^{-1} towards the end of the test, a value still 10 times higher than the IC values observed in deionised water. At 80 ^{o}C, the membrane showed fairly consistent conductivities around 100 mS cm^{-1}; however after 144 hours, the ionic conductivity fell dramatically as the membrane started to show signs of complete degradation (figure 5.13).

At this point, it is worth noting that all the tests performed with the QAPPO/QAPS ionomer mix membrane (Figures 5.4 through to 5.13), were done using the same test piece cut from the master AEM. The membrane had been tested for a total of 2,178 hours at varying degrees of temperature and two different reaction mediums before failing.

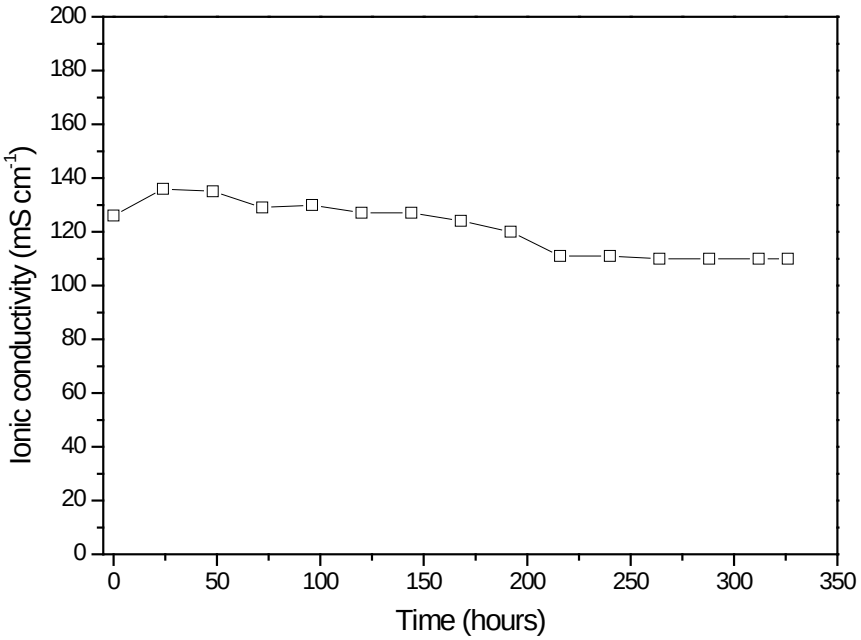

Figure 5.12: *Variation of ionic conductivity with time for the QAPPO/QAPS membrane in 1M KOH. This test was performed at 70 ^{o}C.*

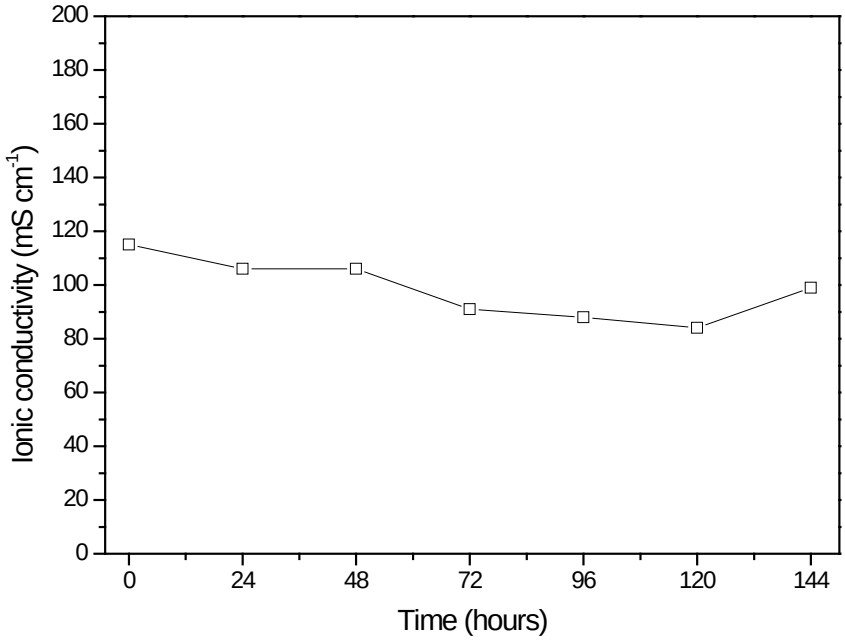

Figure 5.13: *Variation of ionic conductivity with time for the QAPPO/QAPS membrane in 1M KOH. This test was performed at 80 °C.*

5.3 – Improvements to QAPPO/QAPS ionic conductivity

The stability of the standard QAPPO membrane discussed in chapter 4 was greatly improved by the addition of a PS component. However, the IC did not increase and actually decreased slightly as expected. Therefore, the next aim was to try and improve the IC of the now stable AEM.

Polysulphone AEMs have been further developed to include inorganic materials within the membranes. Vinodh *et al* synthesised a polysulphone membrane that had been doped with increasing amounts of zirconium oxide, ZrO_2 [5]. A standard QAPS membrane was synthesised and then an amount of ZrO_2 was mixed into the solution, pre-casting. Vinodh *et al* added 2.5%, 5%, 7.5% and 10% by weight of ZrO_2 to

different QAPS membranes as well as keeping a standard QAPS for comparison measures. They observed that the ionic conductivity increased with increasing weight % of ZrO_2 added. The standard QAPS membrane produced an IC of 7.3 mS cm^{-1} however once 10% ZrO_2 was added the IC increased to 15.1 mS cm^{-1}. Peak fuel cell power densities of 140 mW cm^{-2} and 250 mW cm^{-2} were observed at RT and 60 ^oC respectively which is an increase of around 50 mW cm^{-2} at RT and around 100 mW cm^{-2} at 60 ^oC in comparison to the standard QAPS membrane.

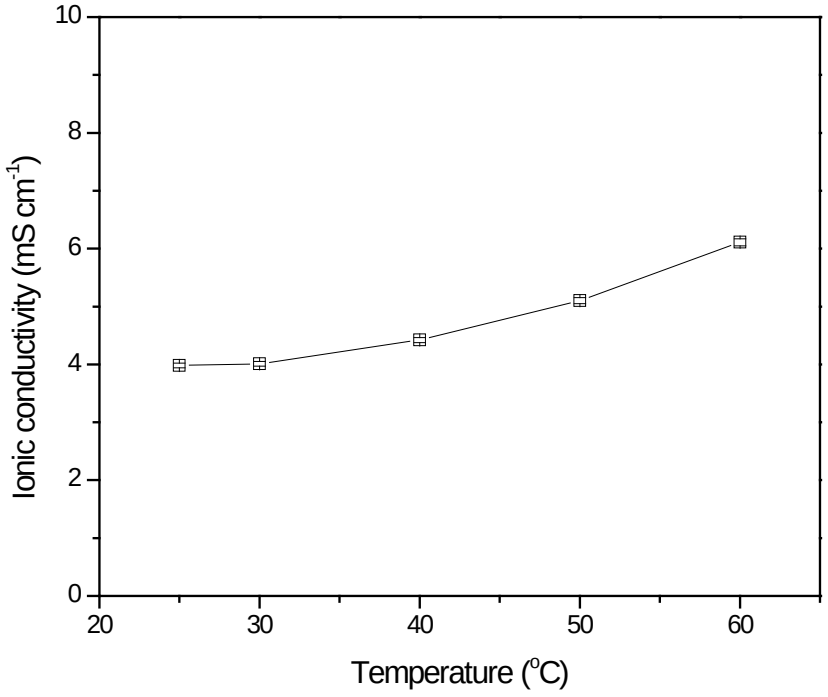

Figure 5.14: *Variation of ionic conductivity with temperature for the QAPPO/PS membrane loaded with 25% by weight ZrO_2.*

Attempts were made to try and increase the overall conductivity of the QAPPO/QAPS blend membrane that was stable for 1100 hours by adding small amounts of inorganic materials. Vinodh *et al* achieved the best results with 10% by weight ZrO_2 but did not

investigate any higher percentages. 25% by weight ZrO_2 was added to the QAPPO/QAPS membrane to investigate whether it would increase the overall IC. Figure 5.14 shows that the IC observed for this AEM. The IC for the standard QAPPO/QAPS AEM discussed in section 5.2 ranged from 10 mS cm^{-1} at room temperature to 25 mS cm^{-1} at 90 ^oC. From figure 5.14, it can be seen that the IC of the membrane loaded with ZrO_2 is much lower, 6.11 mS cm^{-1}, almost half of that observed from the QAPPO/QAPS membrane at room temperature. The idea was extended to using SnO_2 particles instead of ZrO_2 with the results shown in figure 5.15.

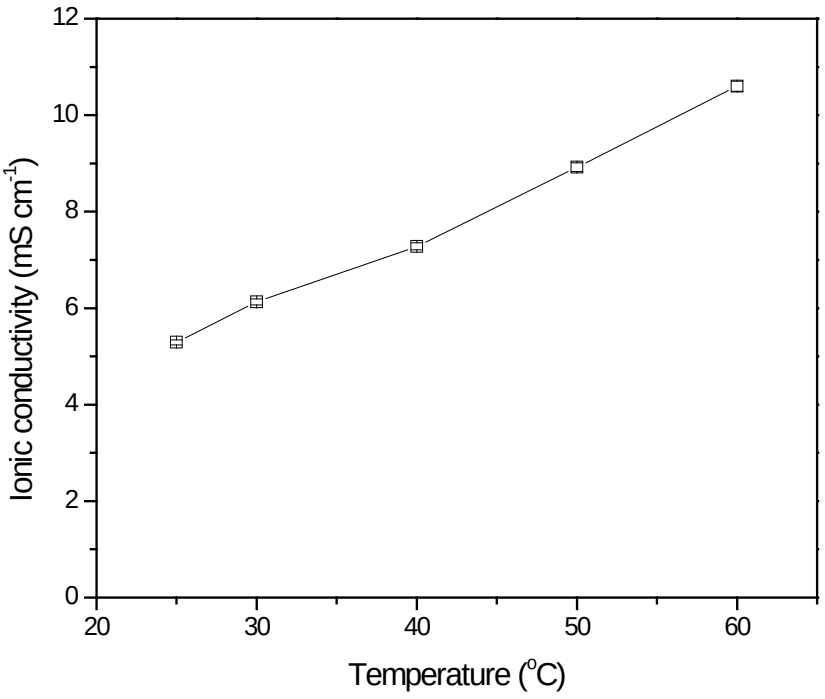

Figure 5.15: *Variation of ionic conductivity with temperature for the QAPPO/PS membrane loaded with 25% by weight SnO_2.*

Again the results were no higher than the standard polymer blend membrane. In fact both these AEMs suffered from stability issues above 60 ^{o}C, becoming very brittle upon addition of the large quantity of ZrO_2 and SnO_2 particles.

As an extension to this idea the total amount of inorganic material was reduced to 20% as 25% seemed to be adversely affecting the stability of the AEM. This 20% was made up of a combination of the two materials (10% for each). Figure 5.16 shows the IC observed for the obtained membrane, and it can be seen that the IC increases with temperature up to around 25 mS cm^{-1} at 90 ^{o}C.

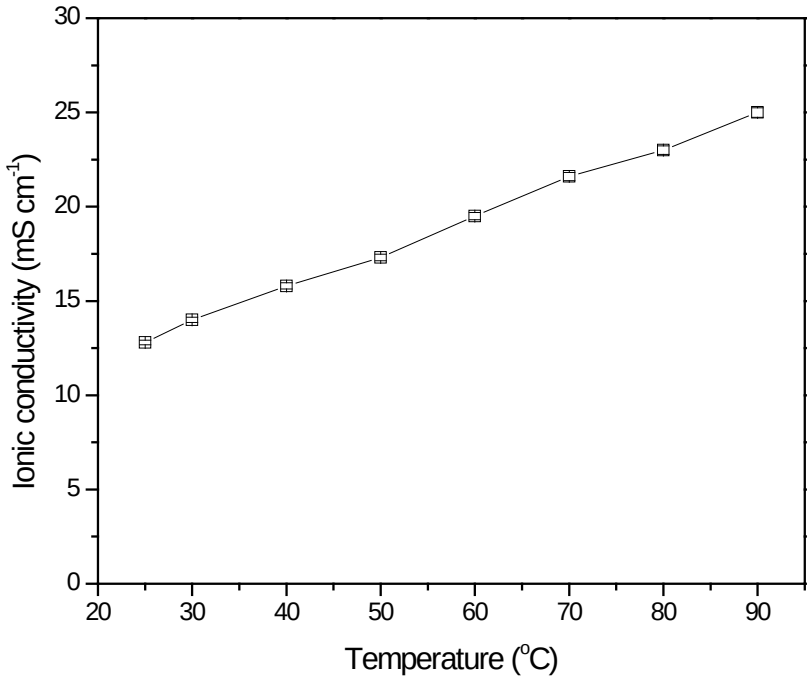

Figure 5.16: *Variation of ionic conductivity with temperature for the QAPPO/PS membrane loaded with 20% by weight inorganic material. This 20% was made up of 10% ZrO_2 and 10% SnO_2.*

This result is only slightly higher than the standard QAPPO/QAPS and standard QAPPO AEMs. The addition of the inorganic material had not resulted in a strong increase in the IC as hoped. In fact it had actually decreased the overall stability as now this membrane was proven to be unstable at 90 ^{o}C as figure 5.17 shows. One final point to make was that all AEMs synthesised with the addition of ZrO_2 or SnO_2 showed a better IC value than those reported by Vinodh *et al*, although the addition of inorganic materials proved to be ultimately detrimental.

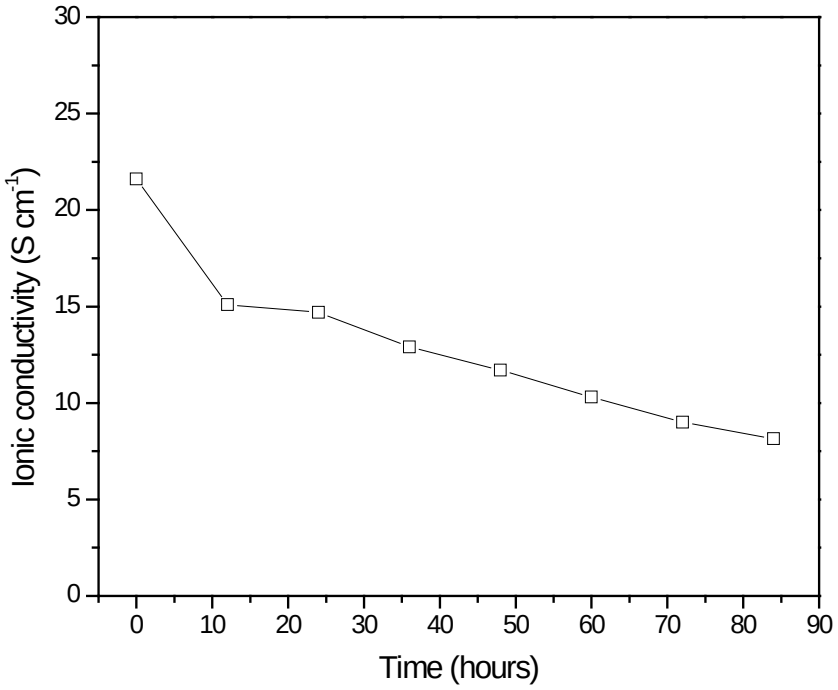

Figure 5.17: *Variation of ionic conductivity with time for the QAPPO/PS membrane loaded with 20% by weight inorganic material. This 20% was made up of 10% ZrO_2 and 10% SnO_2. This test was performed at 90 ^{o}C.*

5.4 – Conclusions for the QAPPO/QAPS AEM series

The overall aim of this part of work was to synthesise an AEM that was more stable at higher temperatures than the AEM prepared from the 6 hour batch of CMPPO. Two different methods were employed based on the idea of polymer blends.

Firstly, AEMs were synthesised from chloromethylated PPO and PS prepared together in the same reaction vessel. This produced membranes with a slightly lower conductivity (13 mS cm^{-1}) and a similar stability (stable to 70 ^{o}C). Secondly AEMs were synthesised from two separate chloromethylated PPO and PS samples (chloromethylated separately). The 6 hour CMPPO was mixed together with a chloromethylated sample prepared from PS during a MSc project. The IC performance of this CMPS sample was extremely low however it was stable at 90 ^{o}C. The AEM prepared from these two samples performed very well by showing an IC of on average 20 mS cm^{-1} for 1100 hours at 90 ^{o}C. This AEM was further tested for 888 hours in 1M KOH up to 80 ^{o}C before failing. Further improvements to the IC were attempted by using the idea developed by Vinodh *et al* of adding % by weight amounts of inorganic materials to the AEMs. This had a negative effect on this AEM, lowering both the conductivity and stability of the QAPPO/QAPS membrane.

This chapter has shown that stability can be improved by the addition of a secondary polymer. The next stage of this work focused again on increasing the IC of the AEMs. As concluded at the end of chapter 4, the only way of achieving AEMs with higher IC appeared to be by focusing on optimising the preparation of the chloromethylated components.

5.5 – Chapter 5: References

[1]. J. Pan, Y. Li, L. Zhang and J. Lu, *Chem. Commun.*, (2010), **46**, 8597-99.

[2]. J. Wang, R. He and Q. Che, *Journal of Colloid and Interface Science*, (2011), **361**, 219-25.

[3]. S. Lu, J. Pan, A. Huang, L. Zhuang and J. Lu, *Proceedings of the National Academy of Sciences*, (2008).

[4]. G. Mann, *MSc Thesis*, 2010.

[5]. R. Vinodh, M. Purushothaman and D. Sangeetha, *International Journal of Hydrogen Energy*, (2011), **36**, 7291-302.

Chapter 6: Use of "semi gel" CMPPO to produce quaternised poly (2,6-dimethyl-1, 4-phenylene oxide) AEMs

6.1 – Rationale for the preparation of "semi gel" QAPPO AEMs

Chapter 4 focused on improving AEM stability and chapter 5 discussed further stability improvements and improvements to ionic conductivity. During this work, multiple attempts to synthesise CMPPO were made with only a few successes. Chapter 4 discussed increasing the reaction temperature or reaction time as ways for producing more stable AEMs. Although in the end increasing the reaction time did produce a more stable membrane, several attempts were necessary to synthesise the CMPPO required.

The CMPPO synthesis stage proved to be the most difficult part of the AEM production process, with ten synthesis attempts performed to achieve one successful batch. Syntheses were deemed failures by the observation of a thick gel and the absence of any free liquid within the reaction vessel. This gel, if precipitated in methanol, would produce a white powder that would subsequently reform the gel upon the next stage of the synthesis. Thus no useable membrane were successfully produced from any CMPPO batch that yielded this gel. Any synthesis that yielded this thick gel was immediately terminated and the reaction products disposed of without either attempting to precipitate the solid or producing an AEM. This approach was wasteful in both time and chemicals.

There is no literature discussing at what point the reaction solution becomes unusable. The next attempt at synthesising CMPPO was watched very closely with the option

that if a noticeable change in the reaction solution was observed, it would immediately be removed from the heat and precipitated in methanol. The idea behind this was to answer the question: if the chloromethylation reaction is terminated quickly enough after the gel starts forming, could the batch of CMPPO still be used? An answer to this question could also potentially remove the time aspect of the reaction, with the "end" of the synthesis being determined by solution appearance (thickening) rather than by an arbitrary time figure.

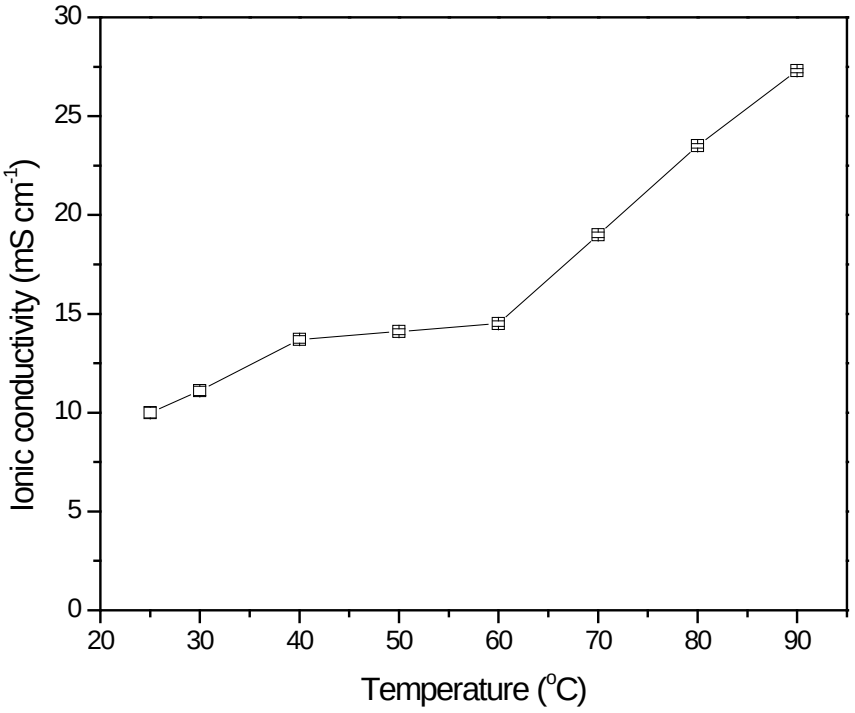

Figure 6.1: *Variation of ionic conductivity with temperature for the "semi gel" QAPPO membrane.*

Following the explained rationale, the gradual thickening of the solution was gauged semi-quantitatively by the speed at which the stirrer bar rotated and the size of the vortex it created. The reaction synthesis was meant to proceed for 8 hours, however,

due to the thickening of the solution it was terminated after only 1 hour. The obtained CMPPO was quite a fine powder rather than clumps of polymer as observed for the over-crosslinked gels. This powder was labelled “semi-gel” CMPPO, and Figure 6.1 shows the IC observed for the AEM produced from this material. The IC increases with temperature to 27.3 mS cm^{-1} at 90 ^{o}C. The “semi gel” QAPPO AEM did not show any visible signs of degradation on inspection after the test. This proves that even though a batch of CMPPO may appear over crosslinked, it did not mean that it was unusable. Figure 6.2 compares the IC of the AEM prepared from the “semi gel” batch of CMPPO to the IC of the batches discussed in chapter 4.

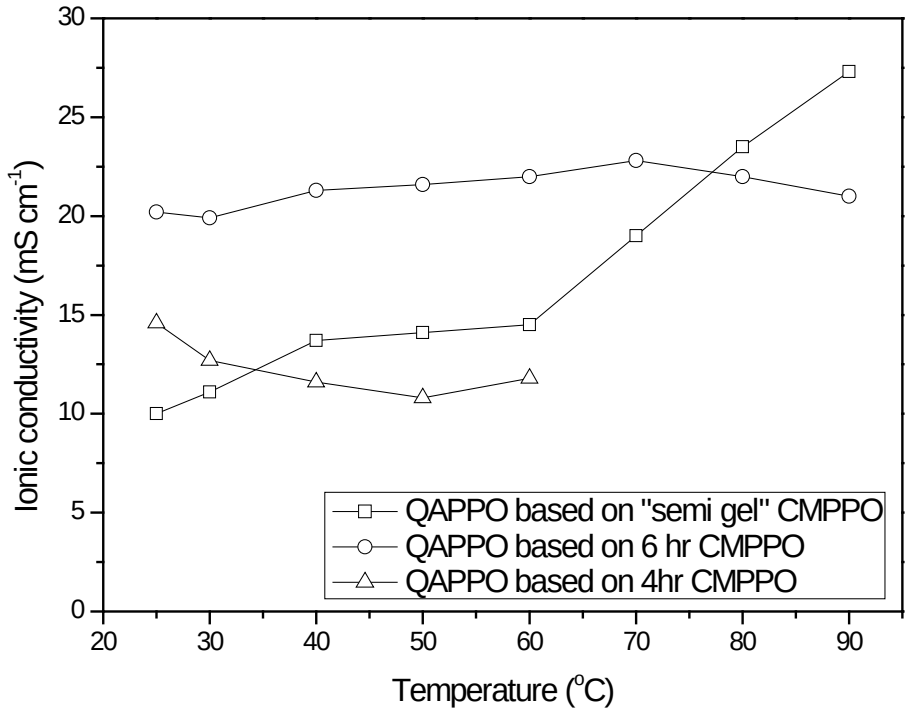

Figure 6.2: *Ionic conductivity comparison between “semi gel” QAPPO membrane and the other batches discussed in chapter 4.*

At room temperature it can be seen that the "semi gel" AEM performs worse than both the other two batches; however, as the temperature increases there is a continuous and sharp increase in IC up to a temperature of 90 ^{o}C, as opposed to increases and decreases. The 6 hour CMPPO AEM ionic conductivity peaked at 70 ^{o}C and actually decreased with increasing temperature from that point. The 6 hour CMPPO AEM produced a stable IC at 70 ^{o}C for 500 hours but degraded at 80 ^{o}C for the same time period. The only way to get the 6 hr CMPPO AEM to give a stable IC at 90 ^{o}C was to add a second polymer to obtain a blend as described in chapter 5. Figure 6.3 shows the observed IC for the "semi gel" AEM at 90 ^{o}C for 132 hours (long term stability test).

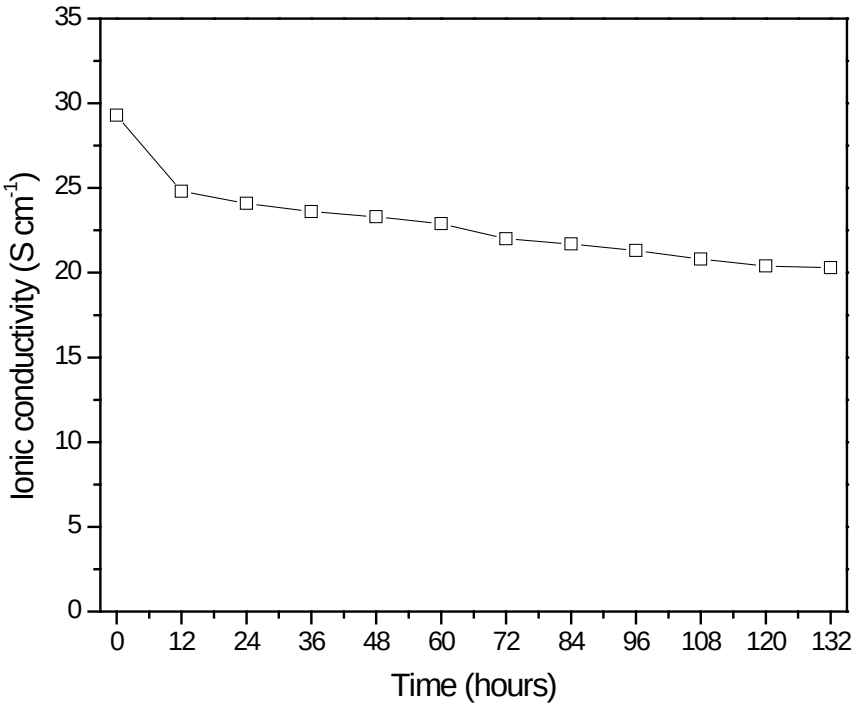

Figure 6.3: *Variation of ionic conductivity with time for the "semi gel" QAPPO membrane at 90 ^{o}C for 132 hours. (Long term stability test).*

Over this time period, the AEM has a very small decrease in IC, which could be attributed to membrane stabilisation. However due to lab constraints at the time, this test could not be extended further. In terms of temperature stability, Figure 6.4 shows that there is no real difference in the low temperature behaviour of the 6 hr and "semi gel" CMPPO samples. The "semi gel" batch of CMPPO showed a much lower high temperature tolerance than the 6 hr version, with the difference in total degradation temperature being almost 200 ^{o}C.

Figure 6.5 is able to explain the difference in stability between the 6 hr and "semi gel" standard AEMs.

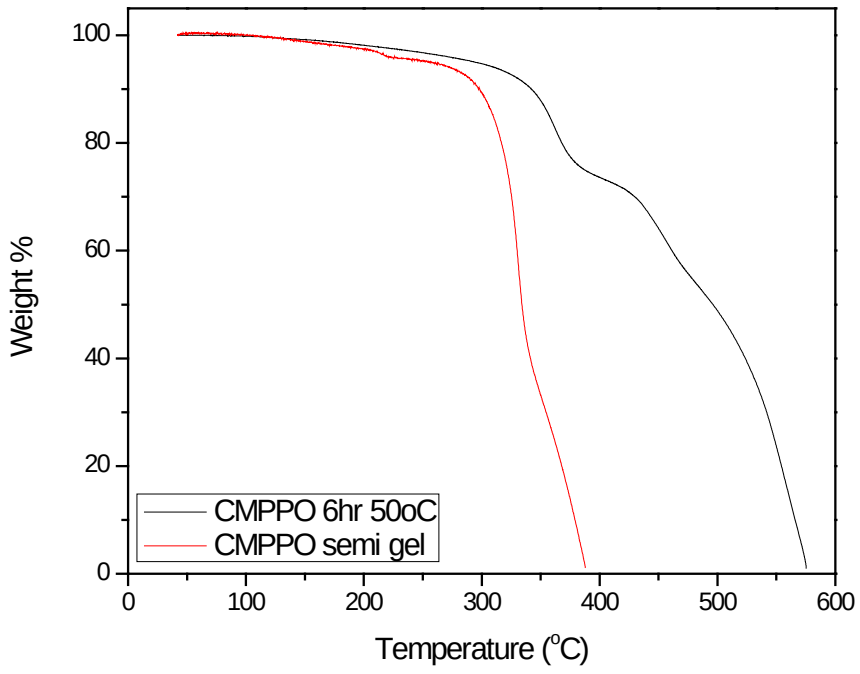

Figure 6.4: *TGA comparison of the 6 hr and "semi gel" batches of CMPPO.*

Decreases in ionic conductivity are associated with the loss of the quaternary ammonium groups which occur around 200 ^{o}C. From figure 6.5 it can be seen that up to 200 ^{o}C, the “semi gel” AEM loses almost 10% less weight than the 6 hr AEM. This observation implies that the “semi gel” QAPPO AEM has lost a smaller number of its quaternary ammonium groups compared to the 6 hr QAPPO AEM. This explains the higher IC observed for the “semi gel” QAPPO AEM by 90 ^{o}C.

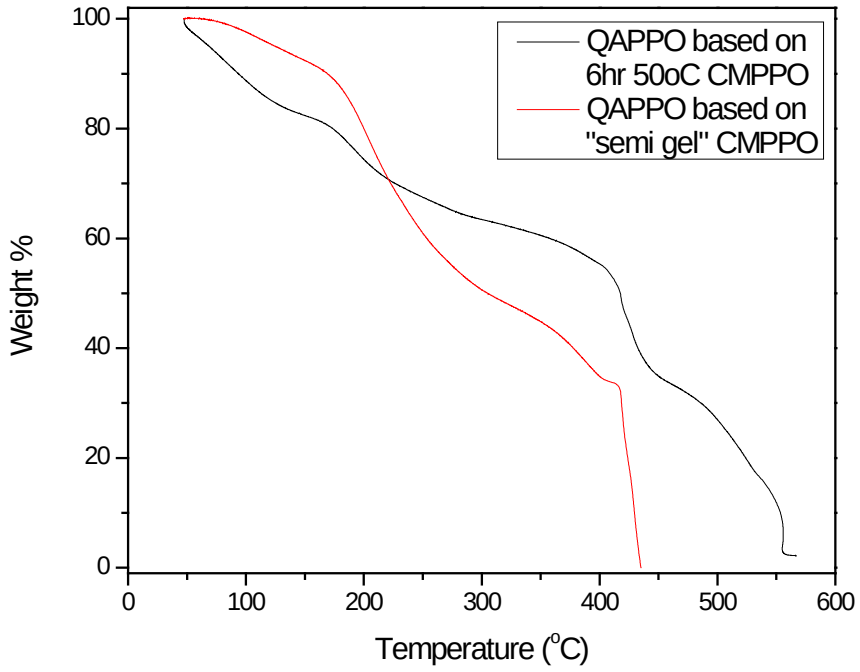

Figure 6.5: *TGA comparison of the 6 hr and “semi gel” QAPPO AEMs.*

Figures 6.6 and 6.7 give two IR comparisons of the “semi gel” QAPPO AEM. Firstly figure 6.6 shows that there is no difference in trace appearance between the pre and post KOH version of the “semi gel” QAPPO membrane (full IR comparison shown in figure A.18 of appendix A), which implies no major chemical structural change has occurred. Secondly, figure 6.7 shows that there is no significant differences between

the “semi gel” and 6 hr QAPPO AEMs implying that in terms of their general chemical structures they are the same. All the evidence presented so far in this section show that during the CMPPO preparation stage the reaction can be terminated just before a full gel is observed and a good performing AEM produced.

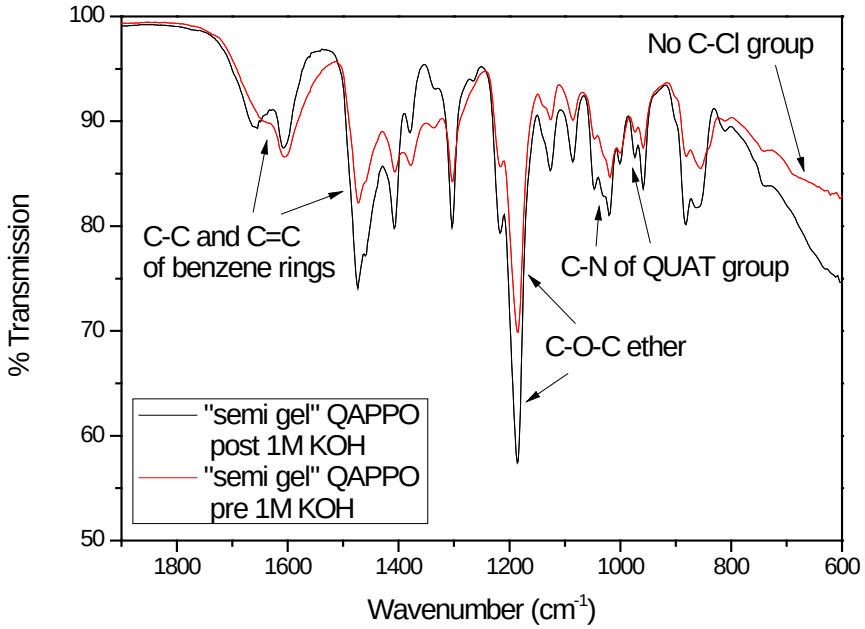

Figure 6.6: *Lower half of the infrared comparison of the “semi gel” QAPPO AEM before and after immersion in 1M KOH.*

6.2 – Improving the stability of “semi gel” QAPPO AEMs

The “semi gel” QAPPO AEM achieved a higher IC than all the previous unmodified QAPPO AEMs presented in chapters 4 and 5. This AEM appears to be unstable at 90 ^{o}C, but, as discussed in chapter 5, the addition of a second polymer typically has a stabilising effect. As seen in chapter 4 chemical cross-linking improves the stability of AEMs but this usually comes with a reduction in IC. Therefore, following the lessons learned from the research presented in chapters 4 and 5, an investigation was

performed to try and improve the stability of the “semi gel” QAPPO AEM without any reduction in IC.

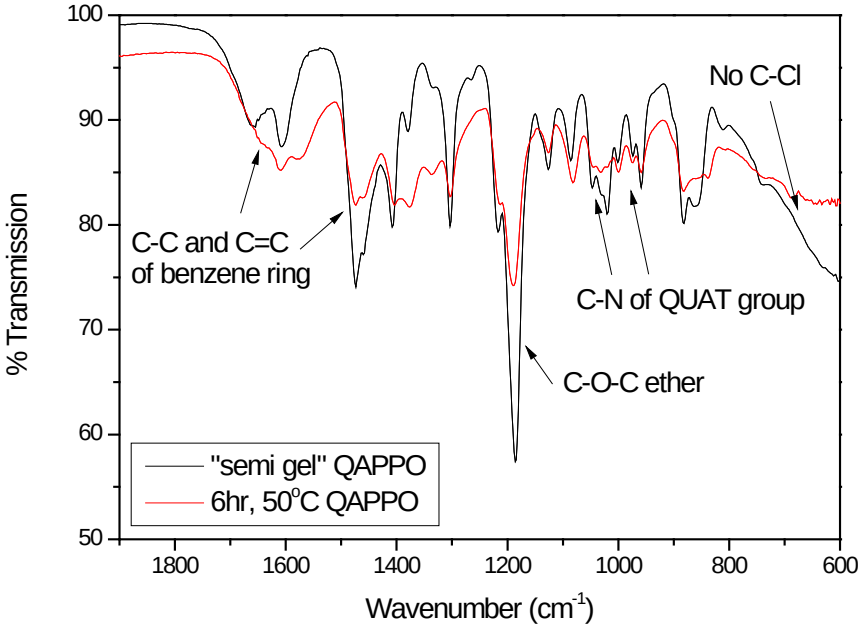

Figure 6.7: *Lower half of the infrared comparison of the “semi gel” and 6hr QAPPO AEMs.*

The “semi gel” batch of CMPPO was therefore used to create three modified AEMs via:

1) Addition of a secondary polymer (similar to the procedure used to produce the QAPPO/QAPS AEMs in chapter 5). However this time the secondary polymer was added without any modification before addition. The QAPS component of the QAPPO/QAPS AEM was shown be of very low IC so its contribution to the overall IC of the AEM was minimal. It was added purely for an increase in stability. Therefore it was decided to not to pre-quaternise the polymers during

this investigation as it would be unnecessary as only an increase in stability was being sought at this stage.

2) Support the QAPPO AEM with a pre-prepared porous PTFE filter [1-3]. Cao *et al* states that the introduction of the quaternary ammonium ions is the reason for the decrease in thermal stability and mechanical strength of the polymers [2]. There is a further decrease in mechanical properties upon ion exchange. By placing the QAPPO within the porous structure of a PTFE filter, the combined AEM would retain the mechanical strength of PTFE whilst still being OH^- conductive.
3) Addition of 1, 4-diazabicyclo[2.2.2]octane (DABCO) as a cross-linking agent.

6.2.1 – Addition of a second polymer to the "semi gel" QAPPO AEM

It was seen with the QAPPO/QAPS blend membrane in Chapter 5 that by adding a second polymer to the original conductive polymer, the overall stability of the final synthesised membrane was increased. Three different polymers were selected as the secondary component for the blends with "semi gel" CMPPO:

1) Polyvinylidene fluoride, PVDF – PVDF has a melting point of 171 ^oC so it is thermally stable at the operating temperatures of APEMFCs. PVDF is also insoluble in water and highly resistant to chemical attack from solvents, acids and bases.

2) Polyvinyl chloride, PVC – The melting point of PVC is 160 ^{o}C. PVC is highly resistant to acids and bases and insoluble in water. PVC is a very rigid polymer which can make the AEMs a lot less flexible and less prone to puncture.
3) Poly(vinylbenzyl chloride), PVBC – One polymer was added with a slightly different reasoning to that outlined above. Whilst the addition of PVBC to the AEM mix would aid in the overall stability, as it is present in chloride form, it would become quaternised. This AEM sample would be compared to the QAPPO/QAPS AEM discussed in chapter 5 in terms of overall IC but more importantly how much a second highly quaternised polymer affects the overall stability.

6.2.1.1 – Polyvinylidene fluoride (PVDF) doped AEM

A small amount of PVDF, 5% of the total weight of CMPPO used to create the AEM, was added during the dissolution of the CMPPO. Normal quarternisation and casting procedures followed. Figure 6.8 shows the IC observed for the obtained PVDF doped "semi gel" QAPPO AEM (QAPPO/PVDF 5%). The IC increased with increasing temperature up to 28.6 mS cm^{-1} at 90 ^{o}C. This conductivity observed at 90 ^{o}C is similar to the conductivity observed for the un-doped "semi gel" QAPPO AEM at the same temperature which was expected as the PVDF dopant was unmodified. This doped membrane was slightly more conductive than the QAPPO/QAPS AEM discussed in chapter 5.

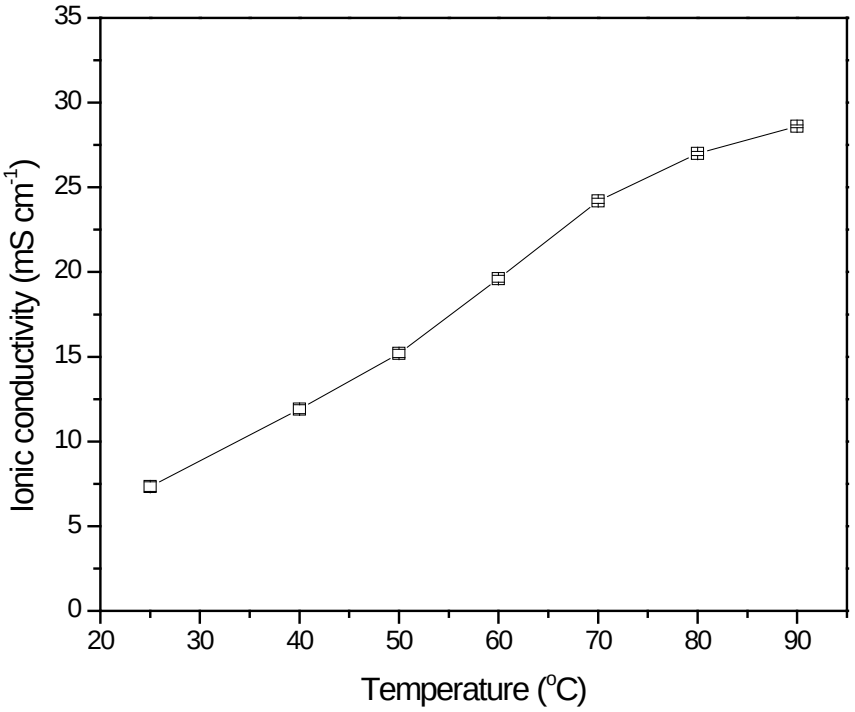

Figure 6.8: *Variation of the ionic conductivity of the "semi gel" QAPPO/PVDF 5% membrane with temperature.*

The IR spectrum of the PVDF doped "semi gel" QAPPO AEM is available in appendix A (figure A.19). Figure 6.9 shows a zoomed in section of the IR spectrum between 600 and 1900 cm^{-1}. The QAPPO peaks are similar to those described in previous chapters. The C – F stretch associated with PVDF typically occurs between 1000 – 1200 cm^{-1}, however there is no obvious peak on figure 6.9 that could be definitively labelled as the C- F stretch. A justification for this observation might be that due to the presence of broad C – H peaks it is highly likely that the C – F stretch peak has been masked. This AEM was tested for 24 hours at room temperature to test the stability of its IC and the results are shown in figure 6.10.

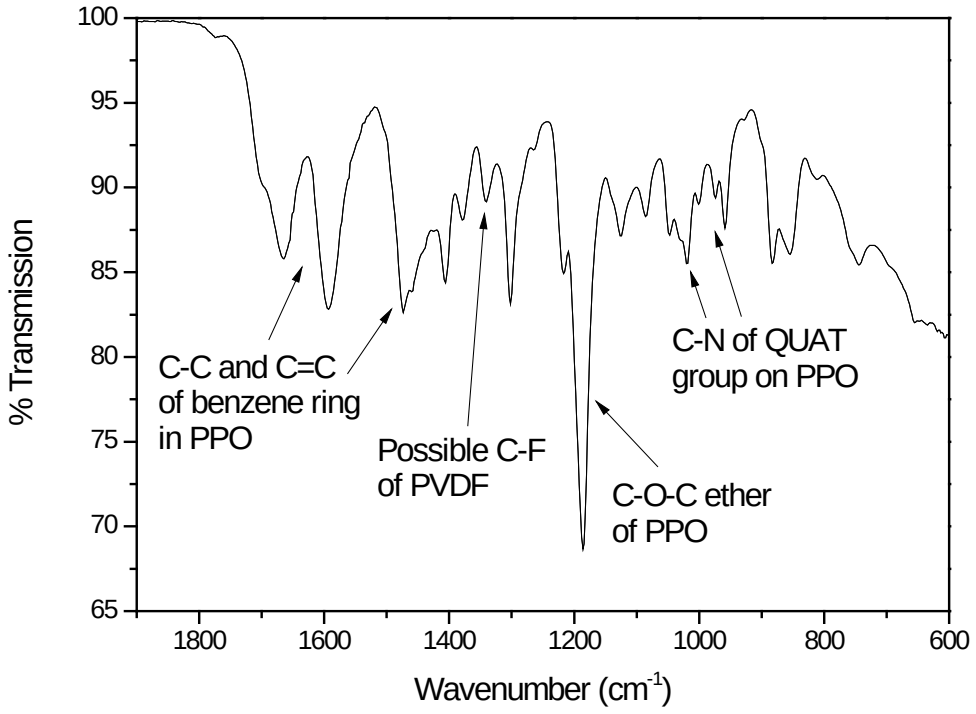

Figure 6.9: *Lower half of the infrared spectrum of the "semi gel" QAPPO/PVDF 5% membrane.*

Figure 6.10 shows values of IC two times higher than the value observed at room temperature in figure 6.8 (7.5 mS cm^{-1}). This can be attributed to membrane stabilisation, which occurs quicker at higher temperatures. As the AEM has already been put through a heat cycle up to 90 ^{o}C, it is not uncommon to observe a slightly higher IC at lower temperatures a second time around. This was confirmed by performing a second heat cycle test shown in figure 6.11. The IC at room temperature was just slightly higher than that seen in figure 6.10, however the IC at 90 ^{o}C was unaffected. This AEM was further tested at 90 ^{o}C for a longer period of time. Figure 6.12 shows that the membrane was stable at 90 ^{o}C for 500 hours with an ionic conductivity between 20 – 25 mS cm^{-1}, slightly lower than suggested by the initial test.

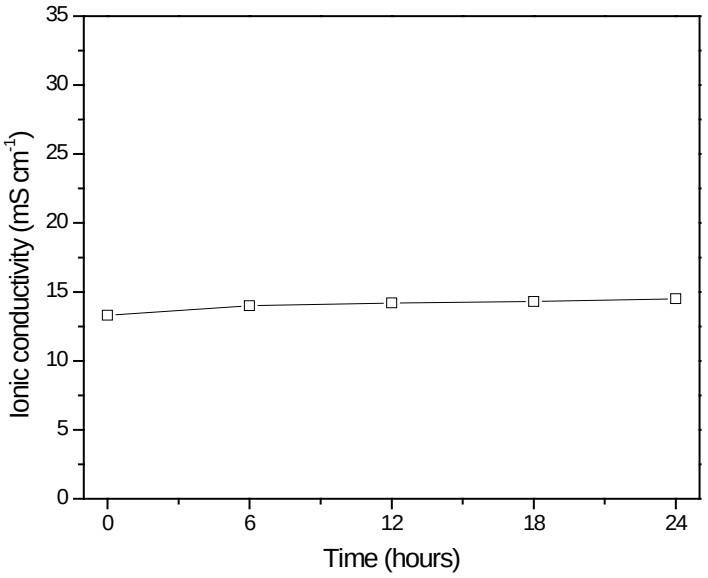

Figure 6.10: *Variation of ionic conductivity with time for the "semi gel" QAPPO/PVDF 5% membrane. This test was performed at room temperature.*

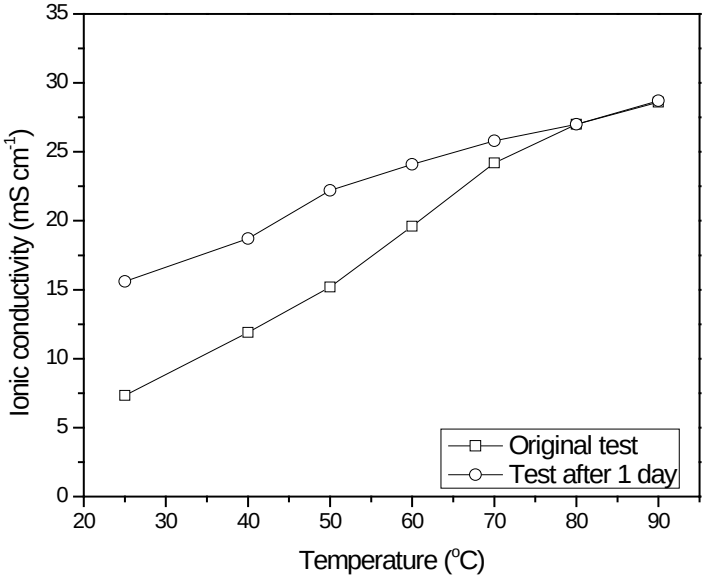

Figure 6.11: *Variation of ionic conductivity with temperature for the "semi gel" QAPPO/PVDF 5% AEM (a comparison between the two heat cycles performed).*

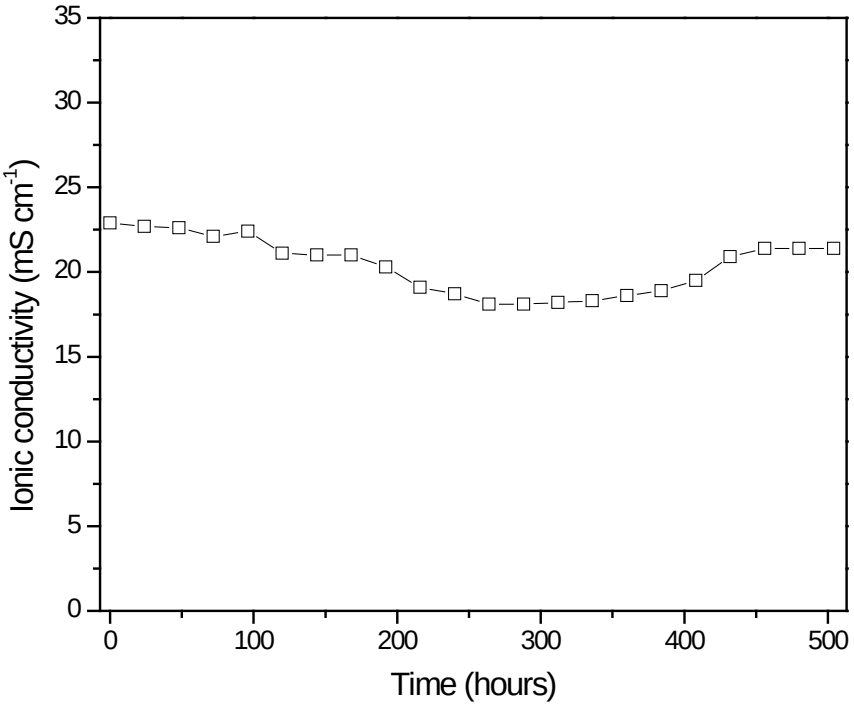

Figure 6.12: *Variation of ionic conductivity with time for the "semi gel" QAPPO-PVDF 5% membrane. This test was performed at 90 °C.*

Overall the "semi gel" QAPPO/PVDF 5% performed very similarly to the QAPPO/QAPS AEM (chapter 5). The addition of the small amount of PVDF had stabilised the performance of the AEM at 90 °C.

6.2.1.2 – Polyvinyl chloride (PVC) doped AEM

In exactly the same manner, 5% by weight PVC was added during the dissolution of CMPPO. Normal quarternisation and casting procedures followed. As expected the dry membrane was much more rigid and inflexible than all others prepared. When the AEM was immersed into 1M KOH to convert it to the OH^- form, there was also a lot less water uptake than seen with previous AEMs. Initially the impedance of the AEM

at room temperature was extremely high (between 20 and 30 Ω cm^{-1}). These impedance values when analysed show the IC of the QAPPO/PVC 5% being between 0.4 – 0.8 mS cm^{-1} (400 – 800 µS cm^{-1}). The AEM had to be heat cycled several times between 60 ^{o}C and 90 ^{o}C before any reasonable results were observed. Figure 6.13 shows the IC observed for the AEM between 60 ^{o}C and 90 ^{o}C after several heat cycles. The IC does increase with increasing temperature similar to previously discussed AEMs, however the IC is very low comparatively.

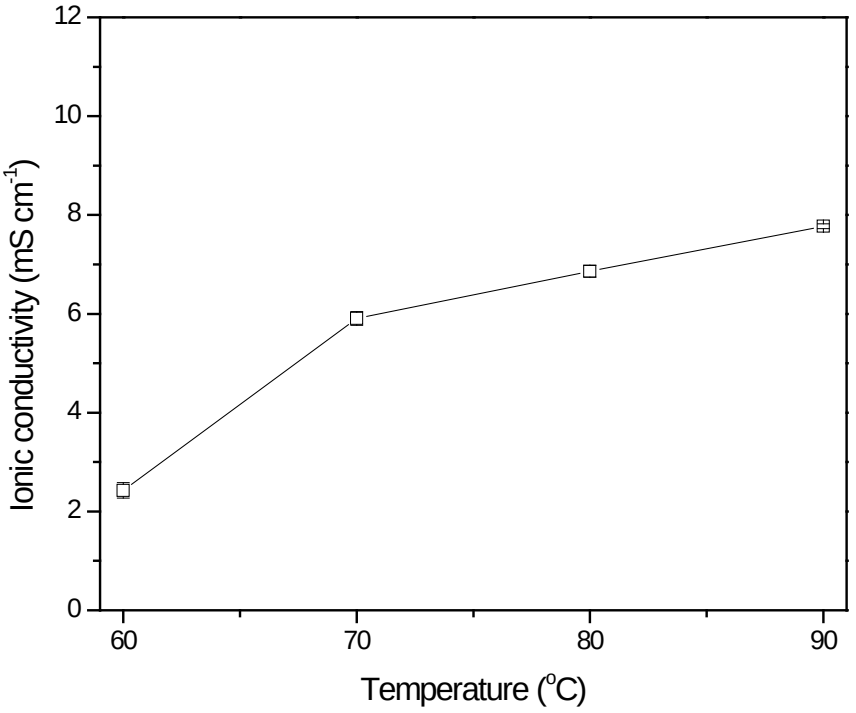

Figure 6.13: *Variation of ionic conductivity with temperature for the "semi gel" QAPPO- PVC 5% membrane. This data set was obtained after several heat cycles between 60 ^{o}C and 90 ^{o}C.*

The IC of the PVC doped AEM at 90 ^{o}C is only 0.8 mS cm^{-1} (800 µS cm^{-1}), roughly three times less than the value observed for the un-doped "semi gel" QAPPO AEM in

section 6.1 (25 mS cm^{-1} at 90 ^{o}C). In chapters 4 and 5, the addition of a second polymer component and membrane cross-linking, both produced reductions in IC (when compared with the un-doped, noncross-linked membranes) [4-6], however, neither produced such a dramatic drop in IC as the one seen with this PVC doped membrane. It was hypothesised that the membranes initial poor performance was due to it not being stabilised yet.

The IC was maintained for a period of 130 hours at 90 ^{o}C as shown in figure 6.14 and the IC did not improve with time. Therefore, overall the addition of 5% PVC to the "semi gel" QAPPO membrane had a severe detrimental effect to the ionic conductivity whilst imparting some degree of stability.

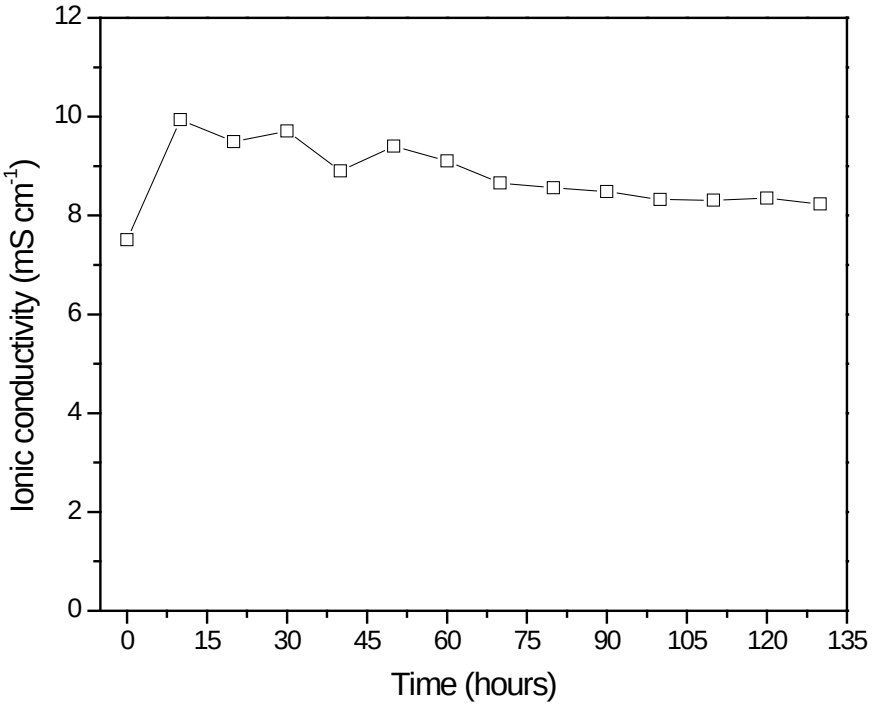

Figure 6.14: *Variation of ionic conductivity with time for the "semi gel" QAPPO-PVC 5% membrane. This test was performed at 90 ^{o}C.*

6.2.1.3 – Poly(vinylbenzyl chloride) (PVBC) doped AEM

Poly(vinyl benzyl chloride) (PVBC) was added to the "semi gel" CMPPO in the same percentage amount as PVDF and PVC were discussed in sections 6.2.1.1 and 6.2.1.2 However, in this case during the quarternisation and ion exchange stages the PVBC dopant was also converted to OH^- conducting form, quaternised poly(vinyl benzyl hydroxide), QAPVBOH shown in figure 6.15. The "semi gel" QAPPO/QAPVBOH AEM synthesised was akin to the QAPPO/QAPS AEM discussed in chapter 5. However, it was expected that the PVBC doped AEM would have a higher IC than both the "semi gel" QAPPO and QAPPO/QAPS AEMs. This expectation was due to the assumption that the PVBC dopant would have been quaternised to a much higher degree than the PS sample (PVBC was a reagent grade powder from Sigma Aldrich rather than a PS sample not well chloromethylated in house).

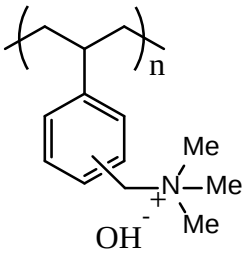

Figure 6.15: *Chemical structure of QAPVBOH.*

Figure 6.16 shows that the addition and quaternisation of PVBC yields higher values of IC over the entire ranges of temperature tested (RT – 90 ^oC), with a maximum value of 40 mS cm^{-1} observed at 90 ^oC. The un-doped "semi gel" QAPPO membrane exhibited an IC just under 30 mS cm^{-1} at 90 ^oC. This approximate 33% increment in IC must be attributable to the QAPVBOH component of the AEM. The AEM was

further tested at 70, 80 and 90 ºC for 24 hours each. Figure 6.17 shows the IC results for these three tests. The IC was fairly similar for all the tests fluctuating between 30 and 40 mS cm^{-1}. This confirmed the results of the initial heat cycle test and represents a small increase in IC on the standard "semi gel" QAPPO AEM. As the QAPPO/QAPVBOH AEM appeared to be stable at high temperatures the stability was investigated further using thermogravimetric (TG) analysis. Figure 6.18 compares the TG plot for this membrane to the standard "semi gel" QAPPO membrane. There is a larger initial drop in weight compared to the standard "semi gel" QAPPO AEM.

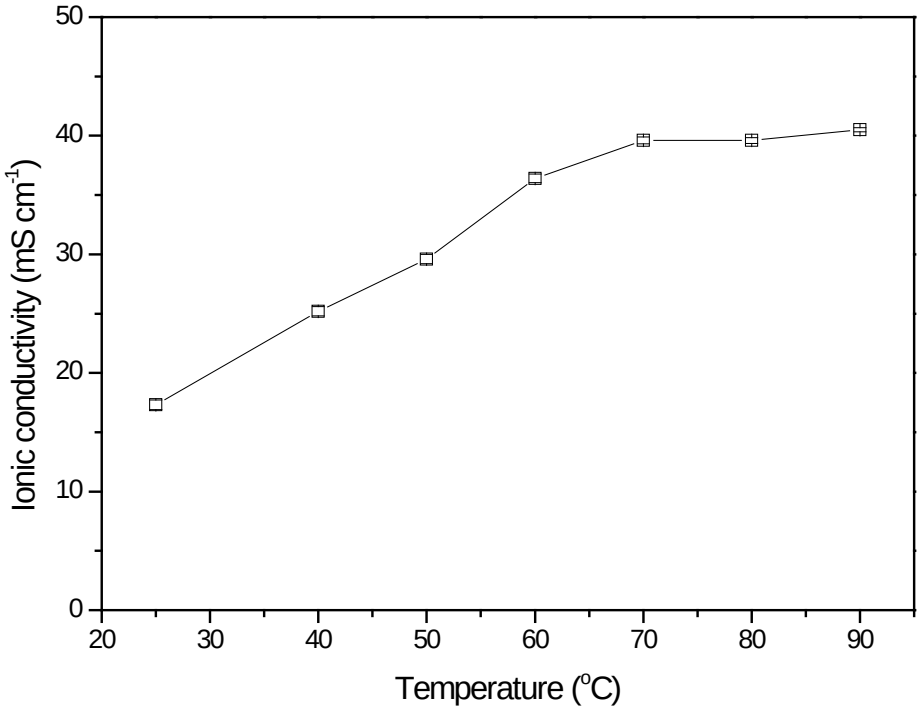

Figure 6.16: *Variation of ionic conductivity with temperature for the "semi gel" QAPPO-QAPVBOH 5% membrane.*

The weight loss up to 100 ºC is associated with the evaporation of bound water. As AEMs get more conductive, their water uptake also increases. As the

QAPPO/QAPVBOH AEM is more conductive than the un-doped “semi gel” QAPPO, it is expected that it absorbs more water and therefore shows a larger initial weight loss. The second weight loss associated with the degradation of the quaternary ammonium groups (around 200 ^{o}C for un-doped “semi gel QAPPO) has been postponed by 50-75 ^{o}C. Overall the final degradation temperature is over 100 ^{o}C higher than the un-doped “semi gel” QAPPO AEM.

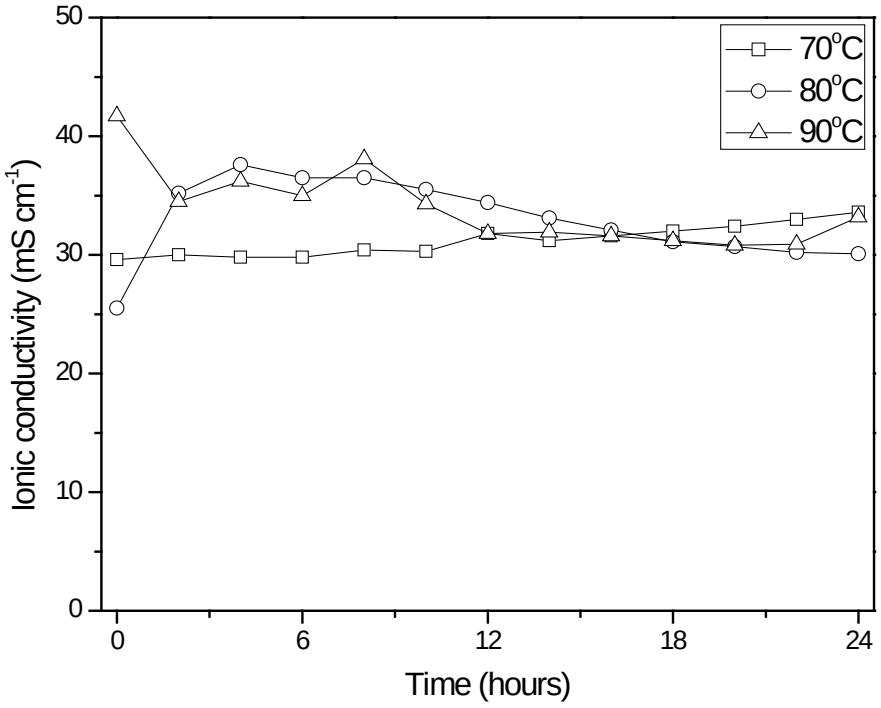

Figure 6.17: *Variation of ionic conductivity with time for the “semi gel” QAPPO-QAPVBOH 5% membrane. These tests were performed at 70, 80 and 90 ^{o}C.*

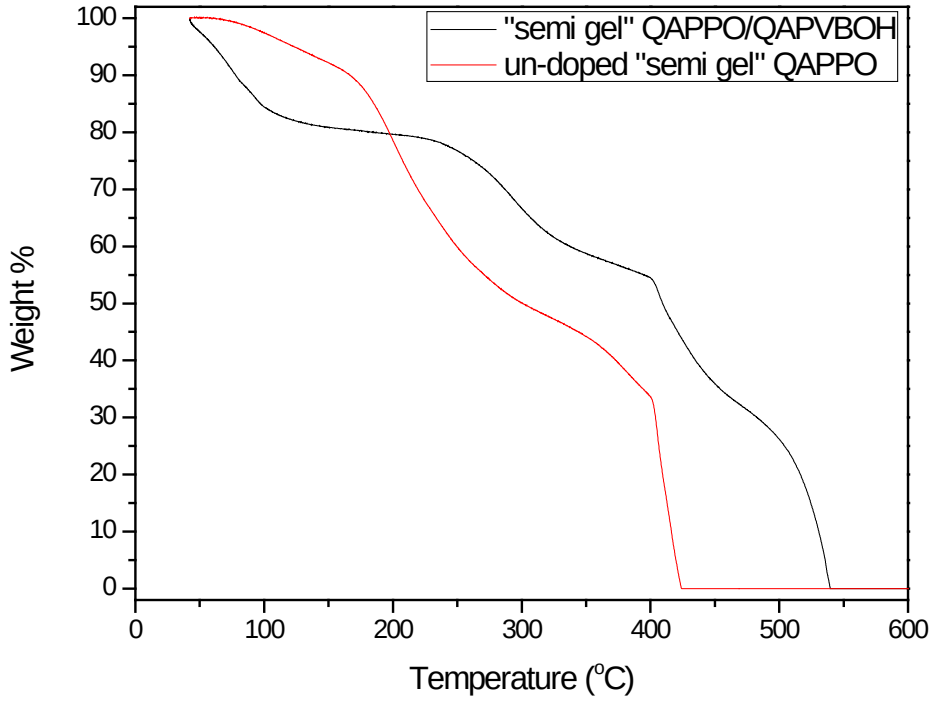

Figure 6.18: *TGA comparison of the un-doped "semi gel "and 5% PVBOH doped QAPPO AEMs.*

6.2.2 – "Semi gel" QAPPO supported with a polytetrafluoroethylene filter (PTFE)

The base polymeric materials used to prepare the AEMs presented in this thesis are mechanically strong. However the amine modification required to make them OH^- conductive has a negative effect on the mechanical properties [2, 7]. AEMs, instead of being rigid become soft and malleable with very little tensile strength. A research group lead by Professor Keith Scott at the University of Newcastle has attempted to address these issues by synthesising AEMs for both acid and alkaline fuel cells based on a porous PTFE filter [1-3]. The aims of their work was to produce an AEM with a high tensile strength whilst keeping a high level of ionic conductivity.

The group have reported two different ways of preparing these AEMs. Firstly they took poly (vinyl benzyl chloride), quaternised it and then diluted the solution to be kept as a stock. A porous PTFE filter was then sonicated in the polymer stock solution for a set time and then air dried. This process was repeated several times until the weight of the PTFE filter had increased by a certain percentage [2]. This weight increase represented the quaternised poly (vinyl benzyl chloride) within the pores of the PTFE filter. Cao *et al* reported that the OH^- conductive PTFE showed a threefold increase in tensile strength compared to the standard poly (vinyl benzyl chloride) AEM. The IC was also only slightly lower than the standard AEM at 22 mS cm^{-1} at 60 ^oC rather than 24 mS cm^{-1} [2]. Secondly a quaternised polysulphone solution was cast onto a porous PTFE filter rather than absorption into the pores [3]. The reported increase in tensile strength was not as high as the previous example, up to 32 MPa from 22 MPa, however the IC was in fact higher than the standard AEM, 50 mS cm^{-1} up from 40 mS cm^{-1} at 60 ^oC [3].

The first method that was applied to the "semi gel" QAPPO AEM was the method reported by Wang *et al* [3]. A "semi gel" QAPPO solution was prepared as normal but instead of casting into a petri dish, the solution was cast onto a porous PTFE filter and dried. Figure 6.19 shows the IC observed for this membrane. The IC was unexpectedly low having only just reached 10 mS cm^{-1} at 90 ^oC. Figure 6.20 confirms the low IC as the AEM showed stable conductivity of 9 mS cm^{-1} at 60 ^oC for 24 hours.

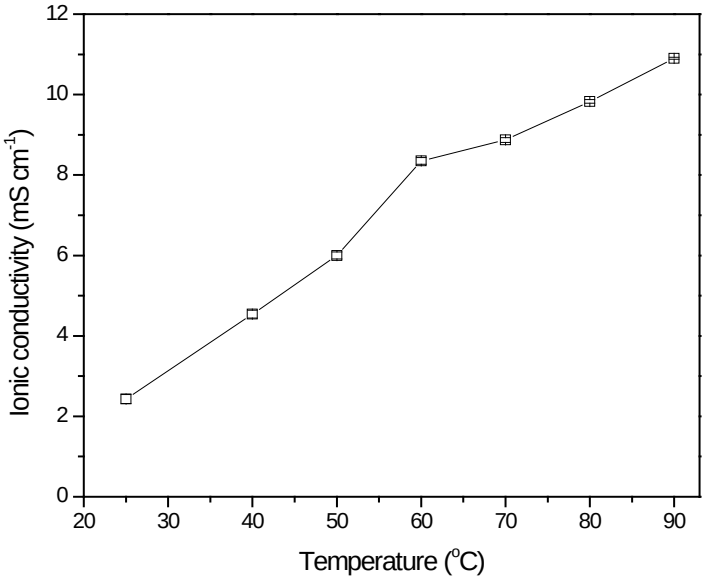

Figure 6.19: *Variation of ionic conductivity with temperature for the "semi gel" QAPPO cast onto a porous PTFE filter.*

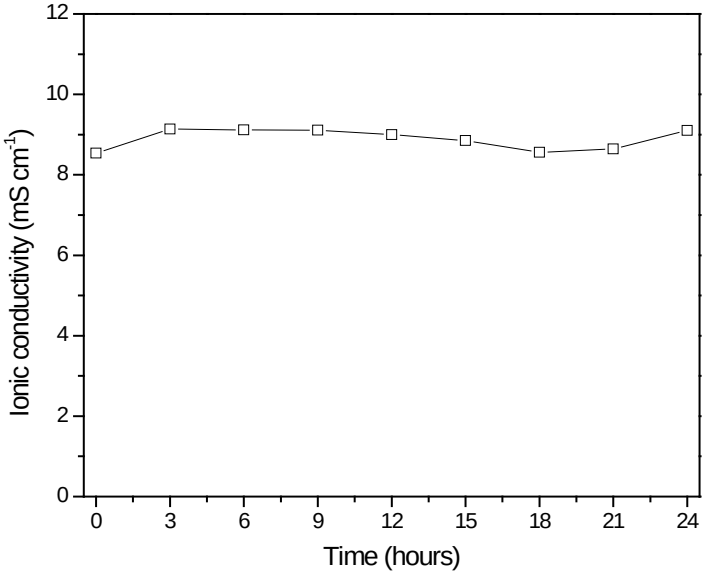

Figure 6.20: *Variation of ionic conductivity with time for the "semi gel" QAPPO cast onto a porous PTFE filter. This test was carried out at 60 °C for 24 hours.*

However at 90 ^{o}C, the “semi gel” QAPPO on the PTFE was shown to degrade in a similar fashion to the unmodified “semi gel” QAPPO AEM, over the course of 52 hours as seen in figure 6.21. The IC peaked immediately at the same level as was observed in the 60 ^{o}C test but then slowly decreased for the remainder of the test.

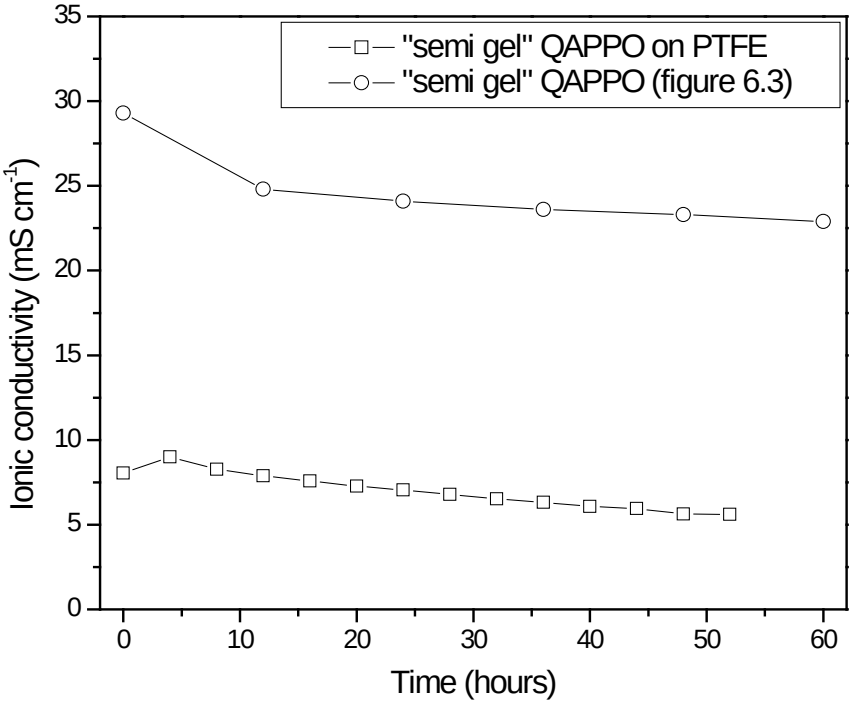

Figure 6.21: *Variation of ionic conductivity with time for the “semi gel” QAPPO cast onto a porous PTFE filter. This test was performed at 90 ^{o}C for 52 hours.*

There is a reason which can help explain the very low ionic conductivity of this sample. The “semi gel” QAPPO solution pre casting was not very viscous so when an attempt was made to cast it onto the PTFE filter the majority of the solution ran off the sides. To try and keep the solution within the boundaries of the PTFE filter the solution was cast inside a petri dish. However once dry it was clear that the loading of the “semi gel” QAPPO on the filter was not uniform, with a large proportion of it weighted to

the one side. The results imply that some “semi gel” QAPPO had made it into the pores of the PTFE filter as a low level on IC was being observed. However the results also show that the PTFE filter has had no effect on the stability of the “semi gel” QAPPO component.

The second series of PTFE supported “semi gel” QAPPO AEMs were prepared using the method proposed by Cao *et al* [2]. During the preparation of the AEMs discussed above it was observed that the N-methylpyrrolidone did not seem to penetrate the PTFE filter. Cao *et al* used a more polar solvent, toluene, in their research [2]. “Semi gel” QAPPO solution was prepared in toluene, this solution diluted by half and the filter soaked under sonication for 10 minutes then dried.

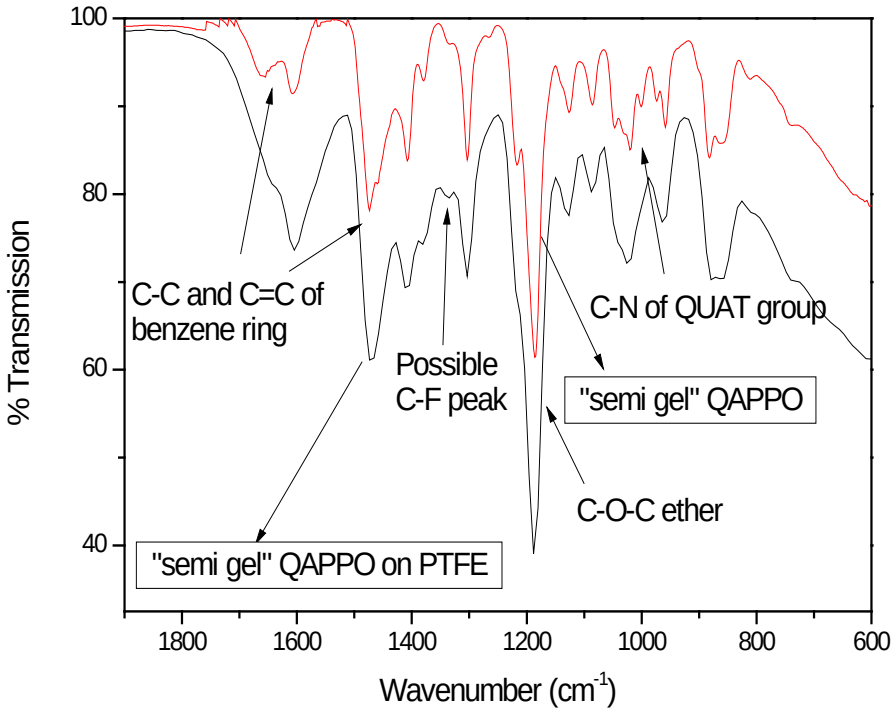

Figure 6.22: *Lower half of the infrared spectrum comparison between the “semi gel” QAPPO membrane supported on PTFE (red) and the unmodified “semi gel” QAPPO AEM (black) (full spectrum in figure A.19 of appendix A)*

Once the filter stopped showing any weight gains it was tested. Unfortunately these test results were extremely poor. At room temperature, a peak ionic conductivity of 1.36 μS cm^{-1} was observed which increased to 4.28 μS cm^{-1} at 60 ^{o}C which indicates only a minute amount of "semi gel" QAPPO was present in the pore structure. This was confirmed by comparing the IR spectrum to the IR obtained for the unmodified "semi gel" QAPPO, shown in figure 6.22. The IR matches the unmodified "semi gel" QAPPO AEM very closely confirming the presence within the PTFE. The peaks associated with the C – F bonds of the PTFE occur over the range 1000 – 1400 cm^{-1} which means they could be obscured by the QAPPO peaks. This method was repeated a number of times with no major change in the results.

The IC observed by Cao *et al* for their AEM only fractionally decreased when using this technical procedure [2]. However, here the IC decreases very dramatically and the stability of the "semi gel" QAPPO within the PTFE is not improved.

6.2.3 – 1, 4-diazabicyclo[2.2.2]octane (DABCO) cross-linking agent

In chapter 4 the cross linking agents diethylamine, propylamine and diaminopropane were employed to attempt to produce a high membrane stability without reducing the IC. Whilst these agents achieved some success in stabilising the AEMs, there was a reduction in IC for most cases. Diethylamine, propylamine and diaminopropane are all liquids at room temperature with the first two chemicals also having very low boiling points. 1, 4-diazabicyclo[2.2.2]octane, DABCO, is a solid at room temperature with a high melting point, 160 ^{o}C. Overall it is more stable to the temperatures used in this

type of fuel cell. DABCO has a cage structure based on anthracene and is shown in figure 6.23.

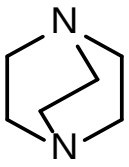

Figure 6.23: *Chemical structure of 1, 4-diazabicyclo[2.2.2]octane, DABCO.*

Cross-linking occurs via the nitrogen atom of the above mentioned reagents. When using diethylamine and propylamine all cross-linking occurs through a single N atom [8]. Diaminopropane theoretically, if it follows the principle of how diethylamine cross-links, allows for cross linkages to occur at both N atoms at either end of propane chain. DABCO therefore is potentially able to cross link in a similar fashion to diaminopropane.

DABCO was added to the “semi gel” CMPPO solution before quarternisation and casting, in the same weight percentage (30% of benzyl chloride group) as the other three cross linkers already discussed in chapter 4. Once cast and dry this AEM was extremely brittle due to excessive cross-linking. Extracting the cross-linked membrane from the casting dish proved very difficult and a complete membrane was not obtained. There were potentially testable pieces, however upon cell assembly these shattered under the pressure of the cell plates. The weight percentage of DABCO was reduced to 20% and 10% to reduce the amount of cross-linking, and the new AEM was prepared. Both of these weight percentages produced membranes that could be tested with figure 6.24 showing the results compared to the uncross-linked “semi gel” QAPPO AEM.

The 20% cross-linked membrane was less brittle than the 30% cross-linked sample however the 10% cross-linked membrane was much softer and malleable, more akin to the appearance of the uncross-linked "semi gel" QAPPO AEM. Despite a better appearance, the ionic conductivity of the 20% cross-linked "semi gel" QAPPO AEM was very poor compared to the standard "semi gel" QAPPO AEM. The IC value increased by a very minimal amount and was over 5 times less than the value observed for the uncross-linked AEM at 90 ^{o}C. However, the IC observed for the 10% cross-linked AEM was similar to the uncross-linked AEM with the peak IC at 90 ^{o}C being 24 mS cm^{-1} which is only slightly lower than the peak IC observed for the uncross-linked AEM (27 mS cm^{-1}).

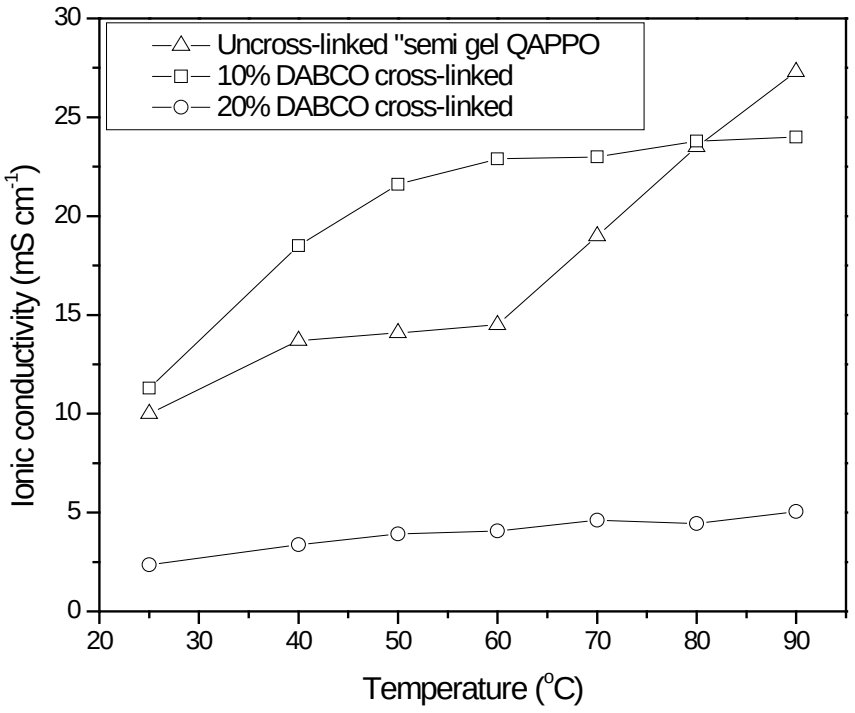

Figure 6.24: *Variation of ionic conductivity with temperature for the "semi gel" QAPPO AEM cross-linked with 10% and 20% DABCO compared to the uncross-linked "semi gel" QAPPO AEM.*

Considering all the cross-linking agents discussed in chapter 4 were added as 30% by weight, the results observed here for the 30% and 20% DABCO cross-linked AEMs were quite surprising. No AEMs prepared using diethylamine, propylamine or diaminopropane suffered from severe brittleness that the 30% DABCO cross-linked AEM showed in this section of work. Also none of the previous cross-linking agents had such a severe effect on IC as seen by the 20% DABCO cross-linked AEM. From the results it indicates that the DABCO cross-linking agent cannot be used in the same amount compared to diethylamine, propylamine and diaminopropane.

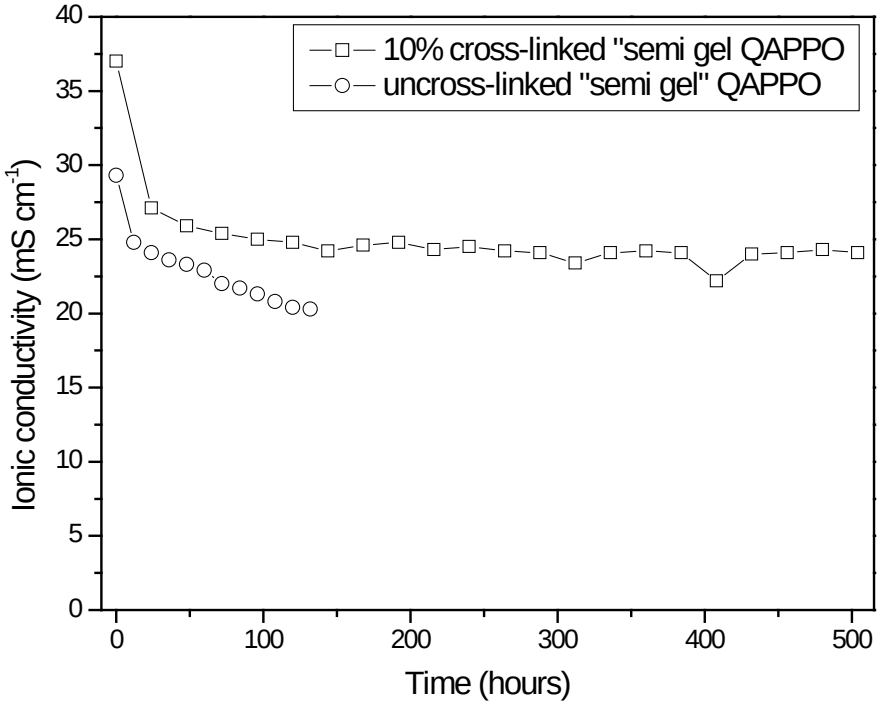

Figure 6.25: *Variation of ionic conductivity with time for the "semi gel" QAPPO cross-linked with DABCO (10%) compared to the uncross-linked AEM (figure 6.3). This test was performed at 90 °C for 500 hours.*

However as the 10% DABCO cross-linked AEM showed similar IC to that observed for the uncross-linked "semi gel" QAPPO AEM further testing was carried out. Figure 6.25 details the results of the 500 hour stability test performed on this AEM. The membrane was stable at an ionic conductivity of 25 mS cm^{-1}. The equivalent test performed on the standard "semi gel" QAPPO AEM shows a small decline in IC over a 132 hour period with a starting IC of a similar level. When cross-linking with DABCO the stability of the "semi gel" QAPPO has been increased without suffering any significant losses in IC.

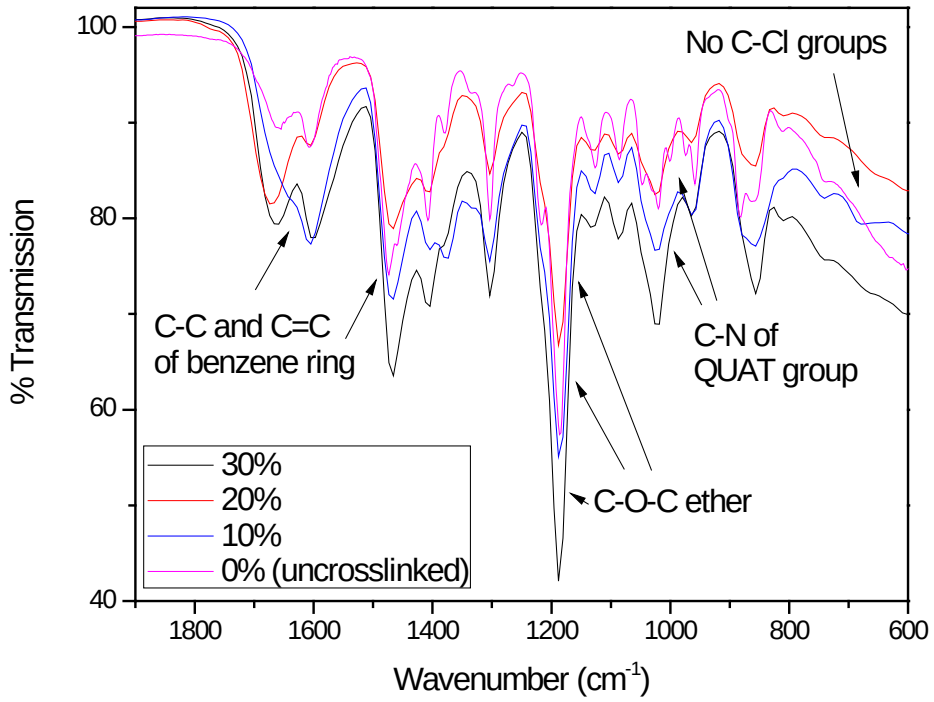

Figure 6.26: *Lower half of the infrared spectrum comparison of the "semi gel" QAPPO membrane cross-linked with different amounts of DABCO.*

Whilst the infrared spectra (full infrared spectrum comparison shown in figure A.20 of appendix A) of the DABCO cross linked AEMs shown in figure 6.26 do not show any clear structural differences that could help quantify the results observed, the thermogravimetric analysis does provide some key information. Figure 6.27 shows the TGA plots for the three cross linked variants compared to the standard "semi gel" AEM. The first observation that can be seen is that when a higher weight percentage cross linker is used, the thermal stability of the prepared AEM increases. The second inference can be taken from the individual traces that each AEM gives. The first loss at 100 ^{o}C associated with the loss of bound water is greatest in the uncross-linked and 10% cross-linked AEMs but very little in the 30% DABCO cross linked AEM.

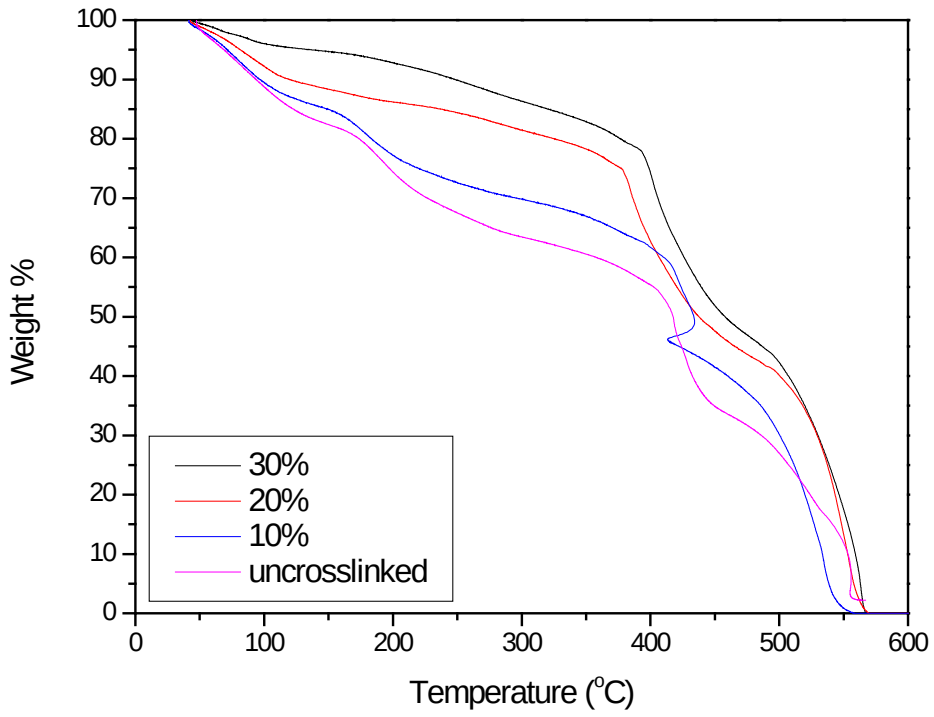

Figure 6.27: *TGA comparison of the standard "semi gel" QAPPO and DABCO cross linked variants.*

This validates the IC results discussed in this chapter. The more conductive a membrane the more water it uptakes, so as the uncross-linked and 10% cross-linked AEMs were the most conductive, it is to be expected that they would contain the most bound water. As the 30% cross linked variant was not even testable in terms of IC due to the membrane being brittle, it is also expected that this AEM would contain very little water. The 30% and 20% cross linked AEMs also have no second weight loss around 200 – 250 ^{o}C which is associated with the loss of the quaternary ammonium groups. This implies that there are not many quaternary ammonium groups present, meaning overall the membrane would have low IC which was the case for the 20% cross linked AEM.

6.3 – Conclusions for QAPPO prepared from "semi gel" CMPPO

Following rheological obstacles in the polymer chloromethylation synthesis, this chapter initially investigated the viability of using thick polymer gels to produce AEMs. Whilst the reaction solutions that yielded thick gel were found to be unusable, it was discovered that if a reaction solution was terminated quickly enough after the initial signs of a gel forming, then the resultant chloromethylated polymer could be used. One such "semi gel" CMPPO batch yielded a QAPPO AEM with an ionic conductivity of 27.5 mS cm^{-1} at 90 ^{o}C. This conductivity was the highest observed by any unmodified QAPPO membrane synthesised during this work; however, this membrane was shown to be not completely stable at 90 ^{o}C.

Chapters 4 and 5 discussed using cross-linking agents and secondary polymers as ways of improving the stability of the AEMs. Whilst both of these methods improved the

stability of the AEM drops in the ionic conductivity were observed. Attempts were made in this chapter to help improve the stability of the "semi gel" QAPPO AEM without any loss in ionic conductivity. PVDF, PVC and PVBC were added to the "semi gel" QAPPO AEM with differing results. The addition of PVDF increased the stability with a reduction in IC as observed in chapter 5. The addition of PVC had a severe detrimental effect on the IC whilst PVBC showed a small increase in IC (between 30 and 40 mS cm^{-1}) due to it being able to be quaternised. QAPPO was cast on or around a prepared porous PTFE filter according to work carried out by the Scott group [1-3]. These processes did not work and very low ionic conductivities were observed.

Finally, a cross linking agent different from the ones used in chapter 4 was employed, DABCO. This reagent produced very brittle AEMs when a 30% weight amount was used, but as the percentage amount was reduced, the brittleness of the AEMs decreased and the IC increased. An AEM with 10% cross linking agent produced 500 hours of stable IC only fractionally lower than that observed for the standard "semi gel" QAPPO membrane.

6.4 – Chapter 6 references

[1]. M. Li and K. Scott, *Journal of Power Sources*, (2011), **196**, 1894-98.

[2]. Y. Cao, K. Scott and X. Wang, *International Journal of Hydrogen Energy*, (2012), **37**, 12688-93.

[3]. X. Wang, M. Li, B. T. Golding, M. Sadeghi, Y. Cao, E. H. Yu and K. Scott, *International Journal of Hydrogen Energy*, (2011), **36**, 10022-26.

[4]. P. Chu, C.-S. Wu, P.-C. Liu, T.-H. Wang and J.-P. Pan, *Polymer Chemistry*, (2010), **51**, 1386-94.

[5]. G. Merle, M. Wessling and K. Nijmeijer, *Journal of Membrane Science*, (2011), **377**, 1-35.

[6]. J. Wang, R. He and Q. Che, *Journal of Colloid and Interface Science*, (2011), **361**, 219-25.

[7]. Y. Luo, J. Guo, C. Wang and D. Chu, *Journal of Power Sources*, (2010), **195**, 3756-71.

[8]. J. Pan, Y. Li, L. Zhang and J. Lu, *Chem. Commun.*, (2010), **46**, 8597-99.

Chapter 7 – Synthesis of AEMs using commercially available quaternised polymers

7.1 Chapter rationale

Chapter 4 demonstrated the difficulty in producing chloromethylated polymer of a consistent quality. This has led to AEMs of different stabilities and ionic conductivities. The main problem seems to lie with the chloromethylation reaction of the base polymer (PPO). The unpredictable nature of the "Friedel-Crafts type" reaction had led to chloromethylated products favouring either ionic conductivity or stability with very little middle ground.

There are commercially available polymers containing quaternary ammonium groups for example poly(vinylbenzylammonium chloride), PVBACl. The advantage of using a material of this type is that by knowing the molecular weight it is possible (at least hypothetically) to control the number of quaternary ammonium groups present in the AEM and therefore the ionic conductivity. Such materials, if cast, in theory could be used as an OH^- ion conducting film by treating it with KOH without any further modification. Unfortunately whilst this can be done, PVBACl is soluble in water meaning it would readily dissolve in the aqueous environment of alkaline polymer fuel cells.

Zeng *et al* have looked at a way of making PVBACl insoluble by using a thermal treatment [1]. The PVBACl film was subjected to a thermal treatment at 190 ^oC for 10, 30 and 60 minutes. Zeng *et al* found that over time the quaternary ammonium groups were being converted to tertiary amines. The samples thermally treated for 60 minutes had significantly more tertiary amine groups than the 10 minute treated

samples. This subsequent increase in tertiary amine groups had the consequence of making the water soluble polymer more hydrophobic, and thus more insoluble. In short, the PVBACl was being partially degraded (or modified) to remove some of its water solubility. As a result, Zeng *et al* found that the 60 minute treated samples performed worse in fuel cell tests than the 10 minute treated samples. In fact a membrane subjected to thermal treatment at 190 ^{o}C for 10 mins produced a surprisingly high peak power output of 210 mW^{-2} at 50 ^{o}C with H_2/O_2 fuels.

This thermal treatment method proposed by Zeng *et al* is not ideal as it relies on the partial destruction of the functional ion conductive group within the polymeric material and the authors conducted their research with a view to using the converted PVBACl as ionomers for the catalysis (catalyst layer) rather than as AEMs. Nevertheless, the approach by Zeng *et al* was deemed interesting and a decision was made to try and ascertain whether this method could be implemented for AEM synthesis.

Figure 7.1 details another two water soluble polymers that are commercially available pre-dissolved in water.

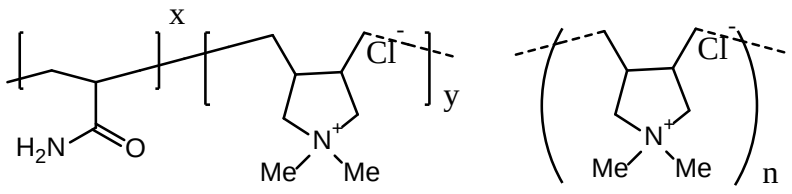

A **B**

Figure 7.1: *Chemical structure of poly(acrylamide-co-diallyldimethylammonium chloride) (**A**) and poly(diallyldimethylammonium chloride), polyDADMAC (**B**).*

These water soluble polymers present a potentially “greener” alternative to the AEMs discussed in chapters 4, 5 and 6. No lengthy synthesis would be required and no use of hazardous chemicals or problematic organic solvents such as chloromethyl methyl ether (CMME) and dichloromethane would be needed. Poly(acrylamide-co-diallyldimethylammonium chloride) has already been researched for use as a fuel cell electrode binder [2].

Based on published work with commercially available quaternised polymers, the preparation of a series of AEMs were proposed in three ways.

1. Preparing a porous membrane from PVDF and sodium chloride (salt). The salt would be removed from the membrane once dry by boiling in hot water. The AEM would be prepared by immersing the PVDF substrate in polyDADMAC solution.
2. Mixing the water soluble polymer with a suspension of water insoluble polymer material (PVDF or PTFE), casting and then drying. This dry AEM would then be thermally treated in a furnace before exchanging the counter ions in 1M KOH and testing.
3. Preparation of a porous PTFE membrane using method proposed by Huang *et al* [3]. A mix of PVA, PTFE and calcium carbonate, $CaCO_3$ was prepared. This mixture was cast into a film and then sintered at 360^{o}C. This thermal treatment degraded the PVA leaving a film of PTFE and $CaCO_3$. This film was then boiled in water to remove the $CaCO_3$ leaving pores within the PTFE film. This film was then soaked in a concentrated or dilute solution of polyDADMAC.

7.2 Preparation of porous polyvinylidene fluoride/polyDADMAC AEMs

Porous PVDF membranes were made by dissolving PVDF powder in solvent and then mixing an amount of sodium chloride (salt) into the solution to form a suspension. This suspension was then cast and dried. The dried film was then boiled in water with the intention of removing the salt. However, the salt had become encased within the PVDF film meaning it was unaffected by the boiling water. The most efficient way of removing the salt particles was to gently rub the films on a piece of sand paper. This had the effect of creating a film that had large holes in it rather than fine pores. Nevertheless, the films were then soaked in dilute polyDADMAC solution and dried.

Initially the obtained PVDF/polyDADMAC films were fired at the same temperature reported by Zeng *et al*, which was 190 ^{o}C. However temperatures above and below this were also investigated. Table 7.1 details the impedances and ionic conductivities observed for a number of PVDF/polyDADMAC AEMs.

It may appear as though there is no real pattern that can be seen from these results however one result stands out. All ICs are less than 10 mS cm^{-1} except for the sample thermally treated at 170 ^{o}C whose IC was 12 mS cm^{-1}. This temperature corresponds to the melting temperature of PVDF. PVDF is a semi crystalline polymer meaning it has regions of both amorphous and crystalline character [4]. Amorphous regions mean that the polymer chains are entangled whereas crystalline regions mean that the polymer chains are aligned in an ordered state. Recrystallization from a melt is one way of forming highly crystalline regions [4]. By thermally treating PVDF at its melting temperature, it is hypothesised that some of the amorphous regions within the PVDF were converted to crystalline regions. Now one can deduce that a polymer

containing large areas of crystallinity will be of benefit due to the polymer chains being aligned in an ordered fashion. This would lead to clear pathways for the OH^- to travel through the membrane.

PVDF-PolyDADMAC membrane initial results at room temperature		
Treatment temperature (°C)	**Impedance (Ω)**	**Ionic conductivity (mS cm^{-1})**
150 °C, 10 mins	136.6	0.33
170 °C, 10 mins	4.153	12
190 °C, 10 mins (1st sample)	20.881	2.39
190 °C, 10 mins (2nd sample)	43.896	1.13
190 °C, 20 mins	39.34	1.27
220 °C, 10 mins	61.029	0.81
240 °C, 10 mins	6.608	7.57

Table 7.1: *Room temperature ionic conductivity results for PVDF/polyDADMAC membranes thermally treated at different temperatures.*

However, the ICs of all AEMs shown in table 7.1 decreased as the temperature was increased, indicating that the polyDADMAC was being lost into the water. The AEM test pieces also eventually lost their rigid structure and broke apart. The TGA plot of the PVDF membrane treated at 190 °C is shown in figure 7.2. The plot compares the pre-heat treated sample to the post heat treated sample along with a PVDF baseline. The AEM is more stable after the thermal treatment than the pre-fired membrane yet the polyDADMAC component is still soluble in water. This implies that the heat treatment had the desired effect to a small extent. The thermal treatment temperature

of 190 °C was sufficient to make poly(vinylbenzylammonium chloride) (used by Zeng *et al*) insoluble but may have not been high enough to complete the partial degradation of polyDADMAC. This also seem to indicate that any thermal treatment temperature below 190 °C would also not be sufficient to render the polyDADMAC insoluble in water.

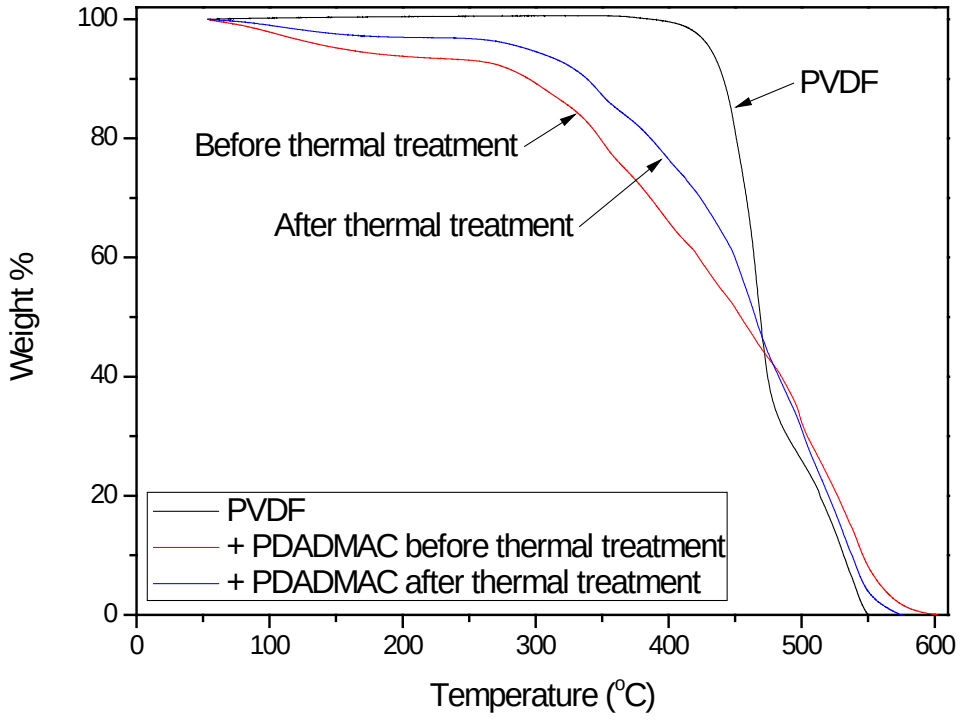

Figure 7.2: *TGA comparison plot of the PVDF/polyDADMAC membrane thermally treated at 190 °C for 10 minutes.*

Figure 7.3 compares the TGA plots for the PVDF-polyDADMAC AEMs thermally treated at 190 °C, 170 °C and 150 °C. This figure supports the theory that all thermal treatment temperatures below 190 °C are insufficient as neither of the lower temperature heat treatments produce a more stable AEM than the 190 °C sample. Thermal treatment temperatures were increased to 220 and 240 °C to further access

whether polyDADMAC could be rendered insoluble, with the results also being shown in table 7.1. These results show that these increases still did not produce an AEM with sufficient IC whilst also highlighting the inconsistency of this technique with two wildly different ICs being observed for two separate samples treated at the same temperature for the same amount of time (190 ^{o}C for 10 minutes).

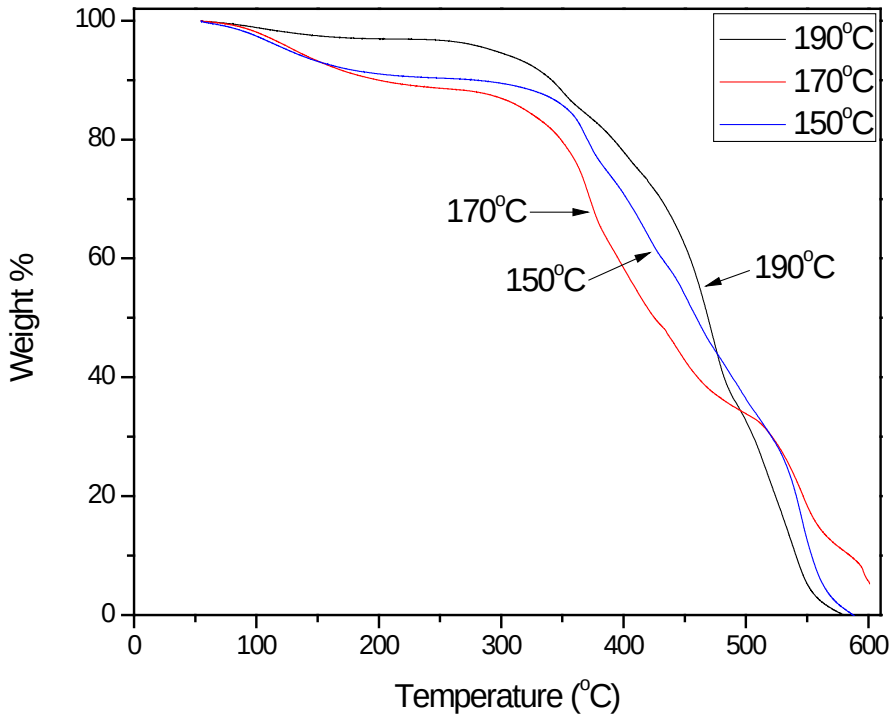

Figure 7.3: *TGA comparison plots for PVDF/PolyDADMAC membranes treated at 190 ^{o}C, 170 ^{o}C and 150 ^{o}C for 10 minutes each. These membranes were prepared using porous PVDF films.*

All AEMs so far had been synthesised using a homemade porous PVDF film as a base (described at the start of this chapter). This technique suffered the same problem observed with the "semi gel" QAPPO AEMs supported on PTFE discussed in section 6.4 of the previous chapter. As the porous bases were dipped into dilute

polyDADMAC, the amount being deposited within the pores would have been extremely small. The reason for this undoubtedly due to the poor porous nature of the homemade PVDF films. As eluded to at the start of this section, the homemade PVDF films were not exactly finely porous but more containing several large holes. This experimental technique was subsequently stopped due to the poor quality of the porous PVDF films.

7.3 Polyvinylidene fluoride or polytetrafluoroethylene /polyDADMAC membranes prepared by polymer blending before casting

7.3.1 Preparation of polyvinylidene fluoride/polyDADMAC blend membranes

Consequently, the next aim was to prepare PVDF/polyDADMAC AEMs from a simple blending technique. Unfortunately PVDF and polyDADMAC share no common solvent making this preparation very difficult. PVDF was dispersed as much as possible in a specific volume of polyDADMAC using high speed mixing and sonication. The dry AEM was thermally treated at 190 ^{o}C for 10 minutes however it did not yield a testable AEM. The AEM was brittle and had uneven PVDF distribution. This uneven nature of the AEM was again undoubtedly due to the preparation method. No milling of the PVDF was undertaken before casting and no dispersion agent was used.

A TG plot was taken for this AEM and is shown in figure 7.4. One observation from this plot compared to those shown in figures 7.2 and 7.3 is the difference in initial weight losses. Figure 7.4 shows a much steeper initial weight loss of over 10% as opposed to only a 2-4% on figures 7.2 and 7.3. This indicates a much higher degree of polyDADMAC loading (due to the first loss being associated with bound water

evaporation) than observed with the porous derivatives discussed in section 7.2. If the two traces from figure 7.4 are compared it can be seen that there is very little difference between the samples before and after thermal treatment. Post thermal treatment, the samples stability appears to be unchanged as the TG curves lie within experimental variability. No clear difference similar to that observed in figures 7.2 and 7.3 can be seen. Again the use of PVDF along with polyDADMAC was stopped.

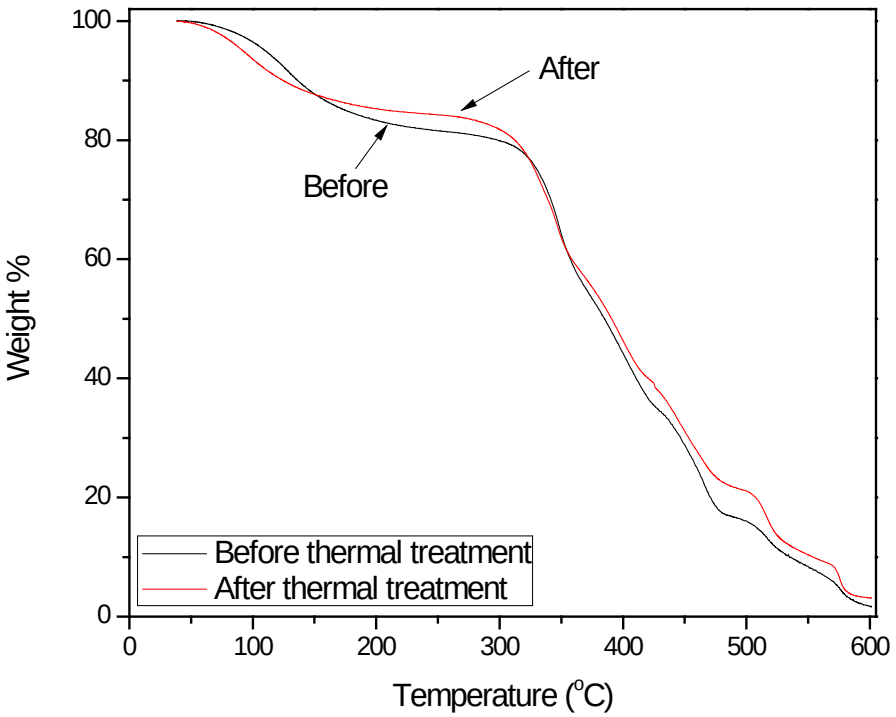

Figure 7.4: *TGA comparison plot of the PVDF/polyDADMAC blend membrane thermally treated at 190 °C for 10 minutes.*

7.3.2 Preparation of polytetrafluoroethylene/polyDADMAC blend membranes

To get around the solvent incompatibility of PVDF and polyDADMAC, a different polymer was selected. Membranes were synthesised using polytetrafluoroethylene

(PTFE) instead of PVDF. Initially, the pre-made porous PTFE filters used in section 6.2.2 of the previous chapter were employed to prepare AEMs analogous to the PVDF derivatives already discussed in section 7.2. No improvement in IC was observed compared to the PVDF derivatives so again this method was quickly abandoned.

As PTFE is commercially available as an emulsion in water, the synthesis of blended membranes (technique 2) was more straightforward. Appropriate amounts of the two components were mixed together, cast and left to dry in air. The initial results of these membranes can be seen in table 7.2.

PTFE-PolyDADMAC mix membrane initial results at RT		
Treatment temperature (ºC)	**Impedance (Ω)**	**Ionic conductivity (mS cm^{-1})**
190 ºC, 10 mins	3.1893 Ω	37.6 mS cm^{-1}
240 ºC, 10 mins	7.4007 Ω	16.2 mS cm^{-1}

Table 7.2: *Ionic conductivity results of PTFE-polyDADMAC blends treated at different temperatures.*

Immediately it can be seen that the initial ICs are much higher than those observed for the PVDF blends. ICs >10 mS cm^{-1} were observed for membranes treated at 190 ºC and 240 ºC. The IC vs temperature plot for the sample treated at 190 ºC is shown in figure 7.5. The IC steadily decreases as the temperature increases which again indicated that these membranes also suffered from polyDADMAC loss at elevated temperatures.

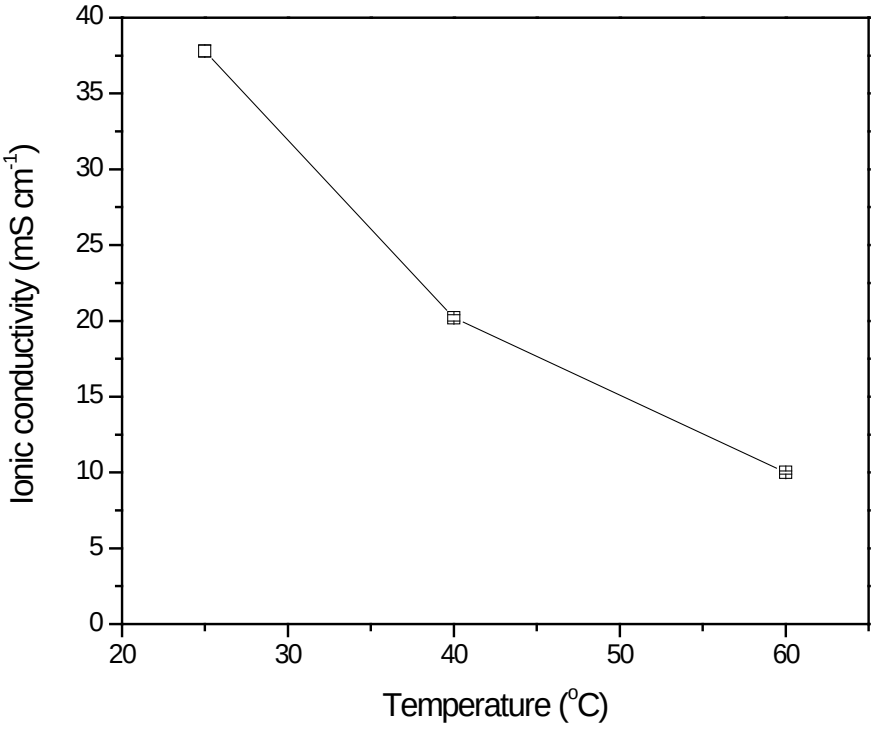

Figure 7.5: *Variation of IC with temperature for the PTFE/polyDADMAC blend membrane fired at 190 °C for 10 mins.*

Figure 7.6 compares the TGA plots of the samples thermally treated at 190 °C and 250 °C for 10 minutes to the non-thermally treated sample. These membrane samples showed very little change from the untreated sample as well as not much initial weight loss. This observation is to some extent contrary to what has been discussed in section 7.2 and 7.3. Whilst the samples in section 7.3.2 (PVDF/polyDADMAC blend membrane) showed very little difference between the treated and untreated samples, the initial weight loss was quite large. Here the initial weight loss is minimal.

As the thermal treatment of the AEM samples at 190 °C and 240 °C did not fully render the polyDADMAC insoluble, a TG investigation of polyDADMAC was performed to obtain a temperature degradation profile which is shown in Figure 7.7.

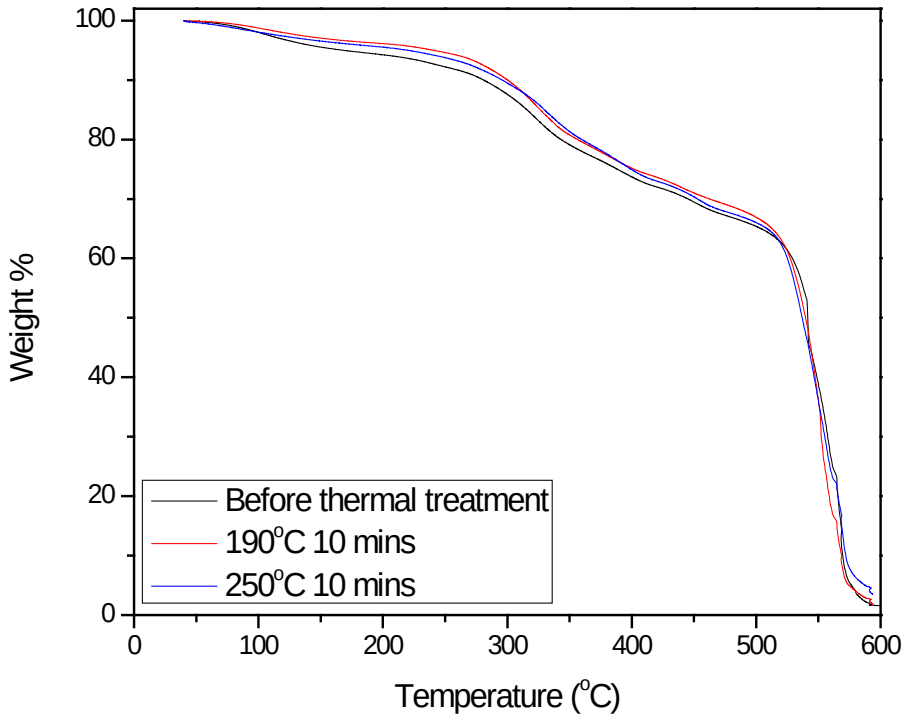

Figure 7.6: *TGA plot comparing the PTFE/polyDADMAC blends thermally treated at 190 °C and 250 °C for 10 minutes to the untreated sample.*

PolyDADMAC shows the initial weight loss attributed to bound water evaporation at 100 °C as normal. However the loss associated with the degradation of the quaternary ammonium groups does not occur until around 300 – 310 °C, with full loss occurring after 350 °C. Therefore the thermal treatments at 190 °C and 240 °C were very much inadequate for trying to degrade some quaternary ammonium groups on polyDADMAC (controlled partial degradation). This data indicates that the bulk of the polyDADMAC would have remained unmodified and therefore still soluble in water. The low ICs observed and low stabilities for all samples presented so far can therefore be attributed to the polyDADMAC leaching from the AEM during testing.

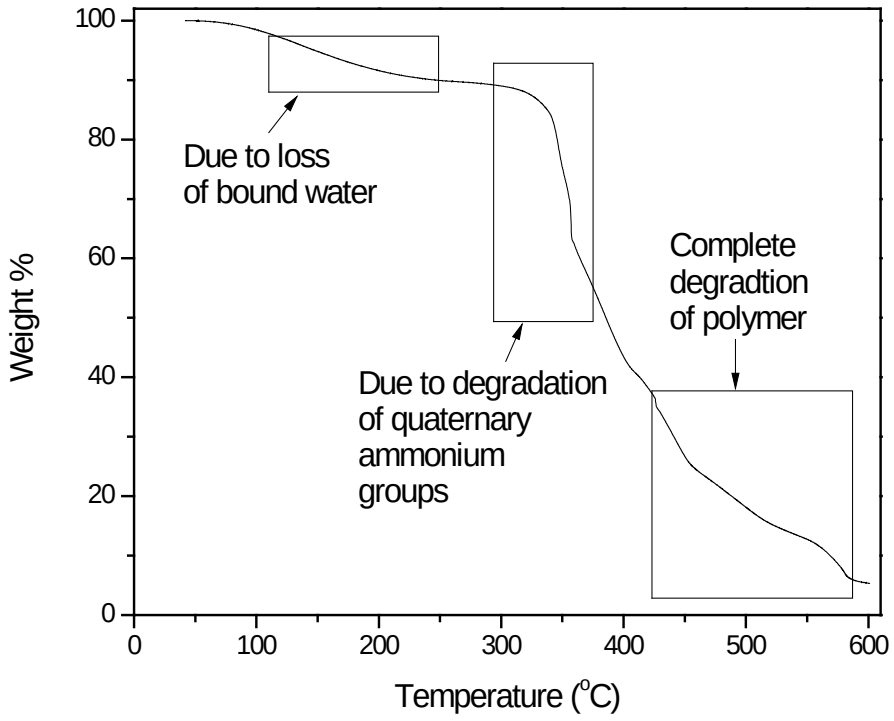

Figure 7.7: *TGA plot of poly(diallyldimethylammonium chloride) (polyDADMAC).*

7.4 Preparation of polyvinyl alcohol/polytetrafluoroethylene/polyDADMAC blend AEMs

7.4.1 Repeat of the preparation of polytetrafluoroethylene/polyDADMAC blend membranes

To investigate the data presented in figure 7.7, the porous PTFE-PDADMAC membranes were repeated with one modification. The porous PTFE membrane was prepared using the method described in point three of the introduction section to this chapter as proposed by Huang *et al* [3]. PVA, PTFE and $CaCO_3$ were blended together and cast into a film. This film was then sintered at 360 ^oC to leave a membrane of PTFE and $CaCO_3$. The PTFE-$CaCO_3$ membrane was then placed in dilute hydrochloric

acid or boiling water to remove the $CaCO_3$ which was confirmed by bubbling coming from the membrane. This porous PTFE membrane was then sonicated in dilute polyDADMAC solution for 30 minutes. Once dry, two samples of this membrane were thermally treated at 300 ^oC (the temperature was increased due to TG data for polyDADMAC indicating the degradation of the quaternary ammonium group did not occur until around 300 ^oC) for 20 and 30 minutes respectively and Figure 7.8 shows the results of these tests.

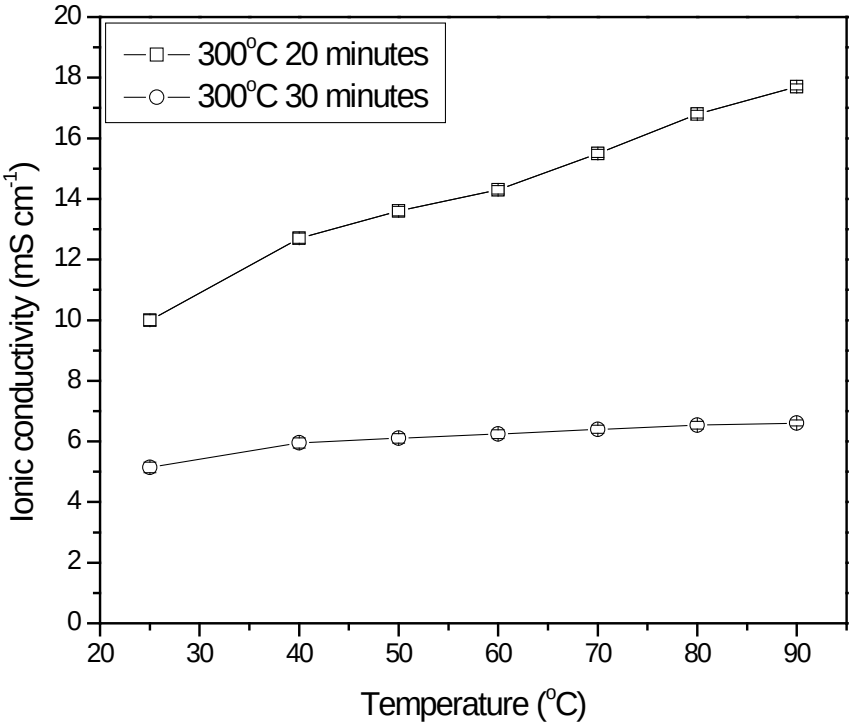

Figure 7.8: *Variation of IC with temperature for the PTFE/polyDADMAC membranes fired at 300 ^oC for 20 and 30 minutes.*

Firstly there is a clear difference between the 20 and 30 minute treatments. The 30 minute treatment yields an IC below 10 mS cm^{-1} so therefore it was discounted. However, the 20 minute treatment not only yielded an IC above 10 mS cm^{-1} but also

an increasing IC with increasing temperature up to 17.7 mS cm^{-1} at 90 ^{o}C. This was the first time this had been observed with any samples using polyDADMAC. Unfortunately the IC of this AEM was not stable at this level at 90 ^{o}C for more than one hour.

7.4.2 Preparation of polyvinyl alcohol/polytetrafluoroethylene/polyDADMAC blend AEMs

The observations that were taken from sections 7.2 and 7.3 were firstly that PTFE was a preferred material to PVDF due to its common solvency with polyDADMAC. Secondly, that straight blends of PTFE and polyDADMAC produced membranes with higher ICs than those prepared from porous PTFE membranes. However all AEMs synthesised (with both PVDF and PTFE) still suffered from polyDADMAC leaching during testing at elevated temperatures. The porous PTFE membrane produced by Huang *et al*'s method [3] had shown some IC improvement however this sample also suffered from polyDADMAC leaching.

In order to try to improve the stability and ionic conductivity of the PTFE/polyDADMAC based membranes, a modification was made to the method proposed by Huang *et al* [3]. Instead of preparing a PVA-PTFE-$CaCO_3$ matrix that was sintered before sonicating with dilute polyDADMAC, a "one pot" synthesis was developed. A mixture of PVA, PTFE and polyDADMAC was prepared and homogenised (no $CaCO_3$ was added). This mixture was then cast in a frame on a glass plate to ensure a uniform thickness of membrane. It was hypothesised that the viscous nature of the PVA would provide a gel for the PTFE and polyDADMAC to disperse evenly and therefore give a more homogeneous membrane.

Three samples were thermally treated at 300 ^{o}C for 20, 30 and 60 minutes with the results of the 20 and 30 minute tests shown in figure 7.9. The sample thermally treated for 60 minutes showed an IC of only 21.4 μS cm^{-1} at room temperature whilst at 90 ^{o}C this IC increased to only 50 μS cm^{-1}. This result implied severe degradation of the polyDADMAC has occurred during the thermal treatment.

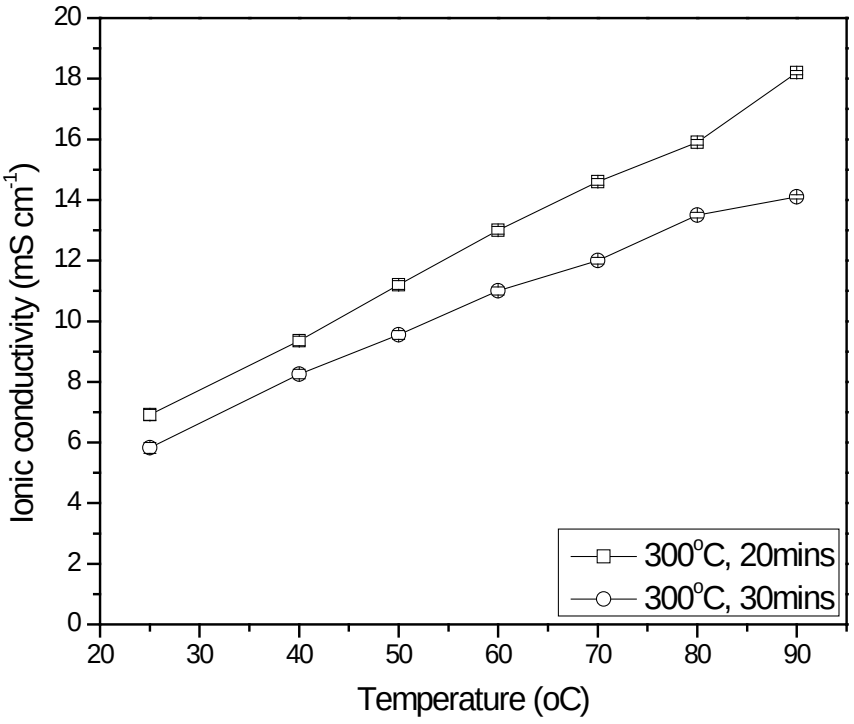

Figure 7.9: *Variation of IC with temperature for the PTFE/PolyDADMAC membrane fired at 300 ^{o}C for 20 and 30 minutes respectively. This membrane was prepared using the modification to Huang et al's method described in the text.*

Compared to the results shown in figure 7.8 (the porous membrane soaked in polyDADMAC), the sample treated for 20 minutes shows a similar IC vs temperature profile. They both increase with increasing temperature up to around 18.2 mS cm^{-1} at

90 ^{o}C. Referring back to figure 7.8 again, the porous sample treated for 30 minutes showed a very low IC compared to the sample treated for 20 minutes. This might indicate that most of the deposited polyDADMAC had either degraded or leached out of the membrane. However the blend sample treated for 30 minutes shows only a marginal decrease in overall performance from that of the sample treated for 20 minutes. The hypothesis of higher polyDADMAC loadings being present in the mix membranes is supported by these results. With a higher loading of polyDADMAC, even a 10 minute increase in thermal treatment time was not enough to effect the IC in any great way. Whereas for the porous membrane derivatives this extra 10 minutes resulted in an unusable sample.

7.5 Attempts to improve the ionic conductivity and stability of polyDADMAC containing membranes

Two problems were encountered with all the polyDADMAC containing AEM samples synthesised so far. The most fundamental problem was that the polyDADMAC was not being rendered insoluble. Secondly the ICs were acceptable but certainly could have done with improving. Improvements to stability could only realistically be achieved by optimising the thermal treatment and length of exposure. Cross-linking processes were limited for these kind of materials due to the chemistry of cross-linking procedures discussed in chapter 4. Cross-linking occurs via the CH_2-Cl functional group of a chloromethylated polymer and more importantly before quaternisation. Since polyDADMAC was being used in its commercially available form there was no way it could be cross-linked. Improvements to IC could be made by increasing the amount of polyDADMAC used or be using a higher molecular weight polyDADMAC

(to provide more functional groups per unit weight). These hypotheses will now be discussed in the next sections.

7.5.1 Increasing the ionic conductivity by increasing the polyDADMAC content of the membranes

All previous samples had been made with a 1:1 weight ratio with respect to PTFE and polyDADMAC. This ratio was increased to 1:3 in favour of polyDADMAC. Figure 7.10 shows the results for the IC vs temperature test for this membrane compared to the 1:1 derivative prepared and discussed in section 7.4.2.

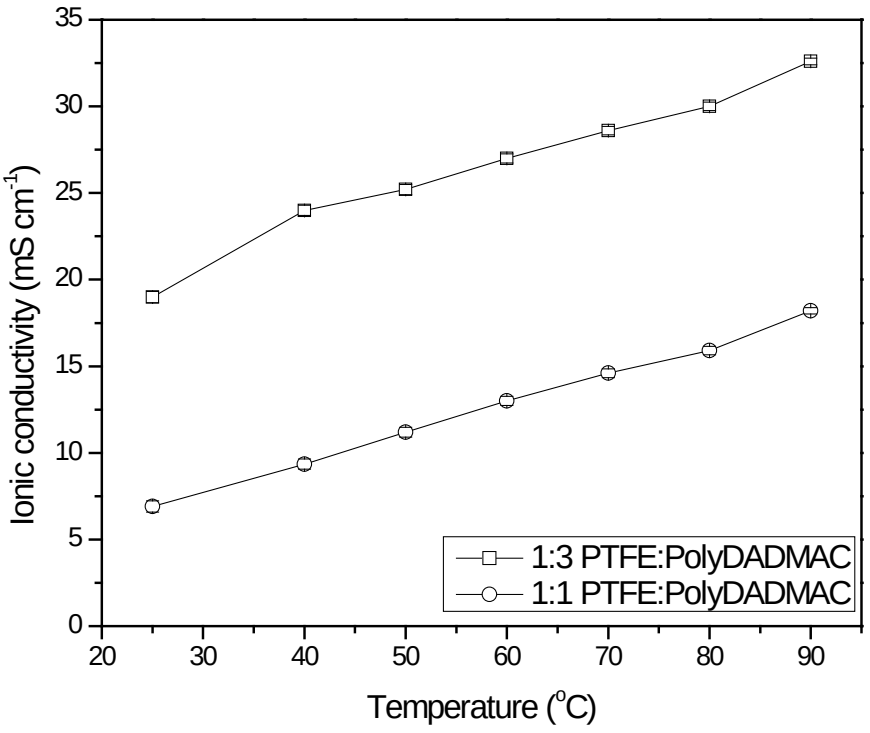

Figure 7.10: *Variation of IC with temperature for the 1:3 weight ratio PTFE/polyDADMAC membrane fired at 300 °C for 20 minutes. The 1:1 weight ratio PTFE/polyDADMAC membrane is also presented for comparison.*

This membrane is roughly twice as conductive as the 1:1 sample. This observation is not unexpected seeing as it contains three times as much polyDADMAC; however the increase in IC is not as high as expected (considering three times as much polyDADMAC was used in synthesis). The membrane was further tested over the course of 24 hours at room temperature to access its IC stability which is shown in figure 7.11. There was a rapid decrease in IC from 32 mS cm^{-1} to 22 mS cm^{-1} at the start of the test. Towards the end of the test, the decrease in IC appears to slow down and even looks as though it is plateauing.

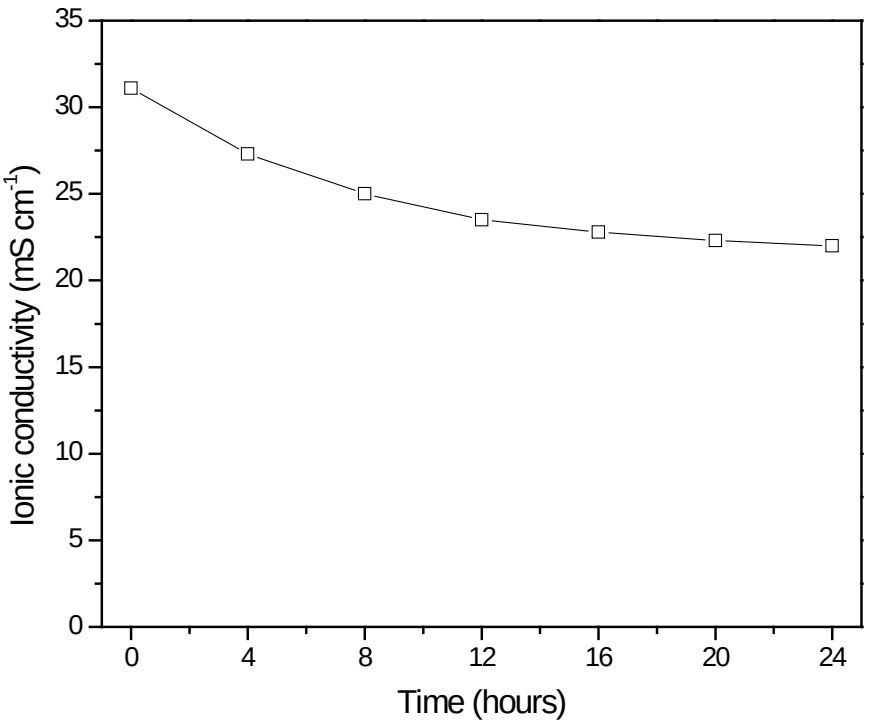

Figure 7.11: *Variation of IC with time for the 1:3 weight ratio PTFE/polyDADMAC membrane fired at 300 °C for 20 minutes over the course of 24 hours. This test was performed at room temperature.*

The rate at which the IC decreases is more than likely due to the higher amount of polyDADMAC present in the AEM to start with (which is then lost into the water due to the leaching effect). However, considering the other results presented so far in this chapter to assume that this indicates that the polyDADMAC is now stable simply by addition of a higher ratio of polyDADMAC would be very naïve.

7.5.2 Increasing the ionic conductivity by using of a higher molecular weight polyDADMAC

The second way of potentially increasing the IC of the membrane samples was to use a higher molecular weight polyDADMAC (HMW-polyDADMAC). The molecular weight of this polyDADMAC was 400,000 – 500,000 grams per mole as opposed to < 100,000 grams per mole as used in other samples in this chapter (Both forms of polyDADMAC that were used in this thesis were bought from Sigma Aldrich). There were no changes to the membrane synthesis procedure. As the PTFE:polyDADMAC weight ratio increase from section 7.5.1 had shown an overall increase in the IC, this modification was continued. The membrane sample was thermally treated at 300 ^{o}C for 20 mins and tested as normal. This membrane showed an IC of 9.37 mS cm^{-1} at room temperature which had decreased to 5 mS cm^{-1} upon increasing the temperature to 60 ^{o}C. A comparison of the TGA data obtained for the HMW-polyDADMAC to the lower molecular weight form is shown in figure 7.12. There appears to be no difference in the second weight loss temperature (post 300 ^{o}C) between the two forms of polyDADMAC. The only difference is that the HMW-polyDADMAC contains a lot more water as its first weight loss is around 10% larger.

As the thermal treatment at 300 ^{o}C did not render the polyDADMAC insoluble in water, the firing temperature was increased by 10 ^{o}C to 310 ^{o}C. The firing time was

kept constant. Figure 7.13 shows the results for this test compared to the results observed for the low molecular weight derivative from section 7.5.1. It can be seen that the IC is roughly 20% higher over the whole temperature range.

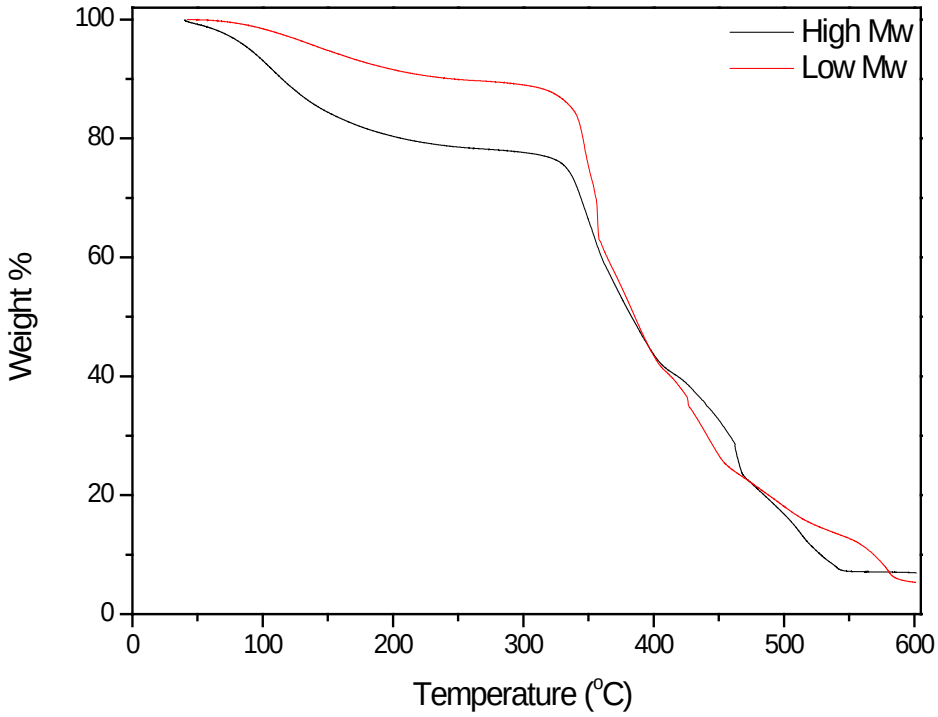

Figure 7.12: *TGA comparison plot between the high and low molecular weight forms of PDADMAC.*

Two more membrane samples (not to be confused with the sample treated at 310 °C for 10 minutes) were thermally treated at 310 °C for 25 and 30 minutes to access their respective ICs. Figure 7.14 shows the results of these tests compared to the initial 20 minute result. A 20 minute firing gives by far the best IC out of the three times. Whilst both increasing the content of polyDADMAC and switching to a HMW reagent succeeded in increasing the IC of all samples tested, it did not help at all with stability.

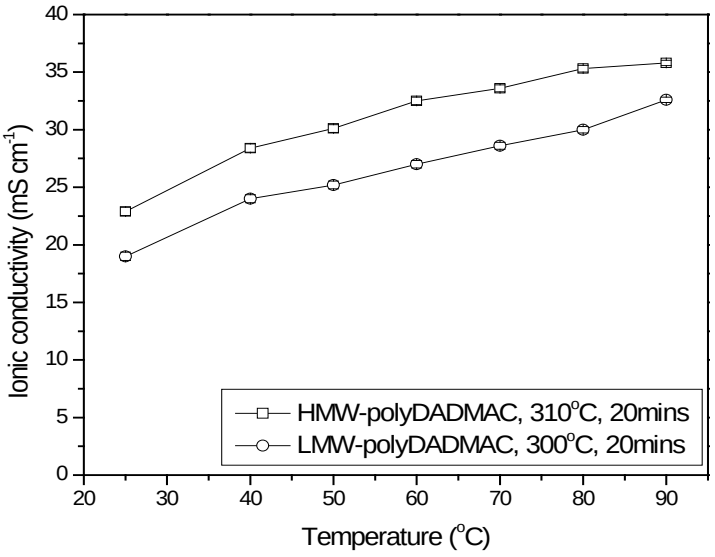

Figure 7.13: *Variation of IC with temperature for the PTFE/HMW-polyDADMAC membrane fired at 310 °C for 20 minutes compared to the low molecular weight derivative fired at 300 °C for 20 minutes.*

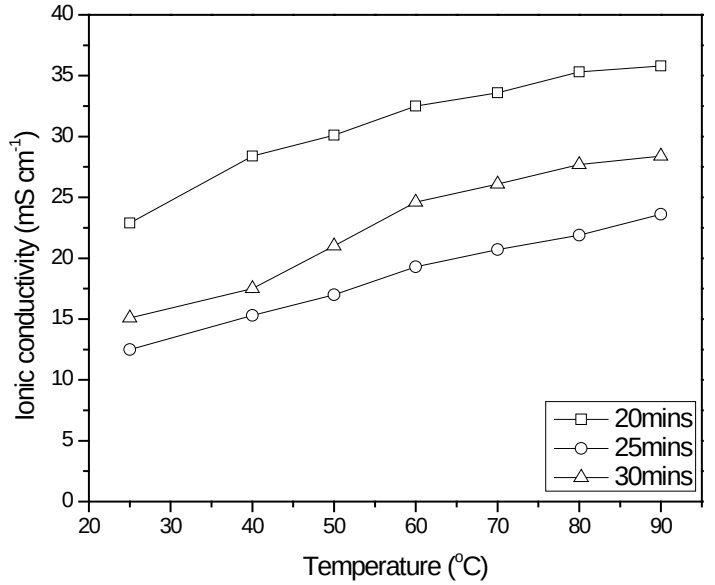

Figure 7.14: *Variation of IC with temperature for the PTFE/HMW-polyDADMAC membrane thermally treated at 310 °C for 20, 25 and 30 minutes.*

All samples tested still suffered declines in IC when tested at any temperature for a sustained period of time which was more than likely due to the polyDADMAC leaching from the AEM sample during testing. A general comment on all the samples prepared in sections 7.5.1 and 7.5.2 would be that in fact the stability may have actually been made worse than previously demonstrated.

7.6 Increasing the membrane stability by cross-linking of AEMs with glutaraldehyde

Cross-linking has been shown to be an effective way of increasing the stability of AEMs discussed in chapter 4. Cross-linking reagents bind to the chloro methyl functional group tethered to the polymer chain forming bridges between the chains. For polyDADMAC containing membranes, cross-linking would need to occur differently due to the water soluble nature of the polyDADMAC and the fact it is used already quaternised. A conventional cross-linking reaction, as discussed in chapter 4, was not able to be performed. Any cross-linking would need to occur between a third polymer with either itself or polyDADMAC.

There has been research conducted on PVA and polyDADMAC hydrogels [5], which relies on cross linking PVA to form an interpenetrating polymer network (IPN). This then traps the polyDADMAC inside the matrix stopping it from dissolving into the water. This idea has been further developed into the preparation of AEMs using a polyDADMAC derivative poly(acrylamide-co-diallyldimethylammonium chloride) [6, 7]. In all cases the method of cross-linking the PVA is the same. PVA is mixed with an appropriate amount of glutaraldehyde along with hydrochloric acid as a catalyst. This reaction is usually performed at 30 ^{o}C [5-7].Cross-linking occurs

between the OH group of the PVA and the CHO group of glutaraldehyde. This reaction has to be done in the presence of the water soluble polymer to allow it to be fully incorporated within the PVA matrix. As most of the previous research was performed using PVA and PA-co-DADMAC only [6, 7] it was decided to extend the idea to our modified procedure that involves PVA, PTFE and polyDADMAC. Before casting, glutaraldehyde was added to the mixture of PVA, PTFE and polyDADMAC in a 1:1 weight ratio with respect to PVA.

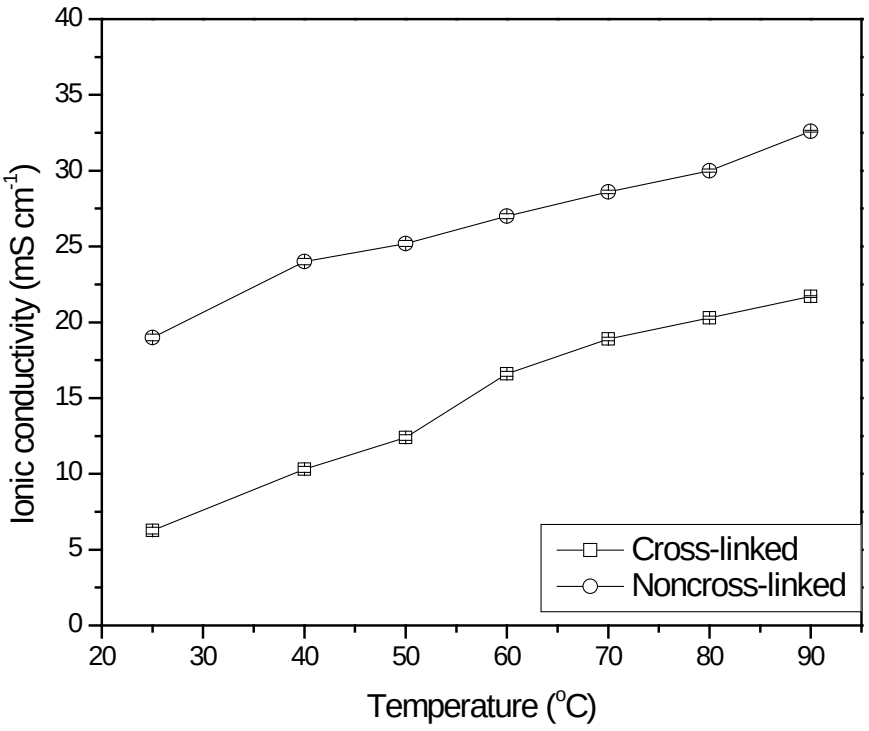

Figure 7.15: *Variation of IC with temperature for the PTFE/HMW-polyDADMAC membrane cross linked with glutaraldehyde and thermally treated at 300 °C for 20 minutes. The noncross-linked sample is also presented for comparison.*

This mixture was then stirred at 30 ºC for 20 mins before casting. Figure 7.15 shows the results for the PVA/PTFE/polyDADMAC membrane cross-linked with glutaraldehyde compared to the noncross-linked derivative.

Over the entire temperature range the IC was slightly lower than the noncross-linked sample. This was expected having in mind the cross-linking effects discussed in chapter 4. For the cross-linked AEMs discussed in chapter 4, the IC decrease was due to the cross-links using up a proportion of the chloromethyl functional groups. This meant that less sites were available for quaternisation and therefore a lower amount of quaternary ammonium groups were added. Here in theory the cross-linking reaction solely involves the PVA so no loss of conducting quaternary ammonium groups on the polyDADMAC should have occurred. The more likely cause for the loss of IC was the leaching of polyDADMAC due to the PVA gel matrix not being sufficiently cross-linked. The IC still increased with increasing temperature so a certain amount of polyDADMAC continued to be trapped.

Due to this performance, the cross-linked membrane sample was tested at room temperature for an extended period of time (figure 7.16). The membrane was stable for the entire 312 hour period giving a consistent IC of 6.5 mS cm^{-1}. Although this IC is relatively low compared to some of those observed in previous chapters, this represents the first time any membrane sample of this type had shown consistent stability for an extended period for time. The membrane was further tested at 40 ºC and 50 ºC for 8 and 50 hours respectively. A stable IC of 9 mS cm^{-1} was observed at

40 ^{o}C as seen in figure 7.17. This represents no increase on the results obtained at room temperature for a much longer time period.

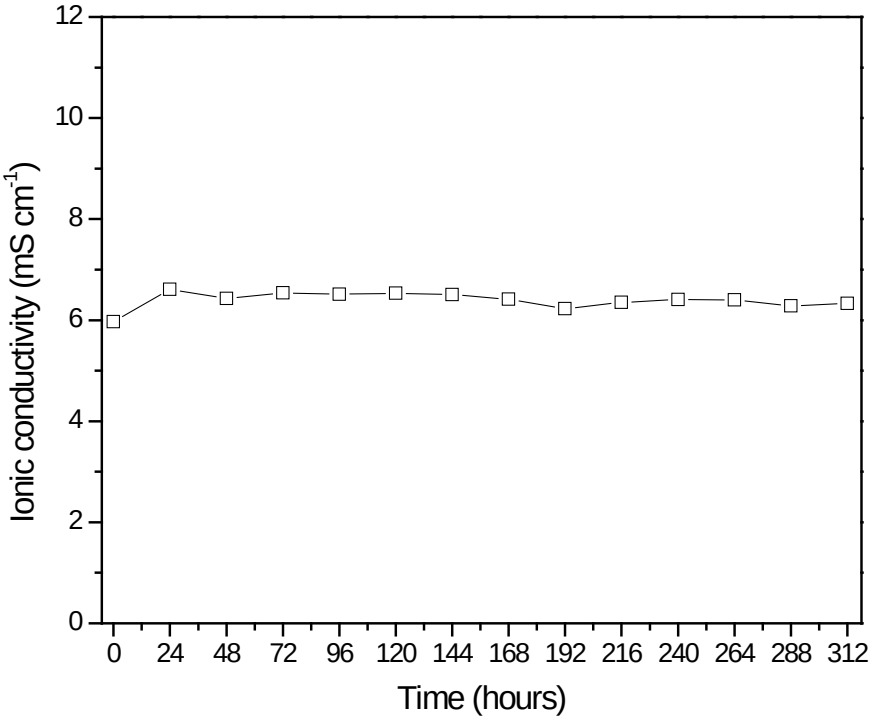

Figure 7.16: *Variation of IC with time for the PVA/PTFE/polyDADMAC blend membrane cross-linked with glutaraldehyde and thermally treated at 300 ^{o}C for 20 minutes. This test was performed at room temperature.*

A small decline from 9 mS cm^{-1} was seen at 50 ^{o}C which is shown in figure 7.18. The lower IC compared to the noncross-linked AEM may be explained in the following way. A certain amount of polyDADMAC was initially successfully trapped within the PVA matrix, however a large amount is lost more or less immediately once placed in water. At room temperature the leaching of polyDADMAC into the testing water is relatively slow. However as the temperature increases, the rate of leaching also

increases meaning the average IC does not change (instead of increasing) as can be seen in figures 7.17 and 7.18.

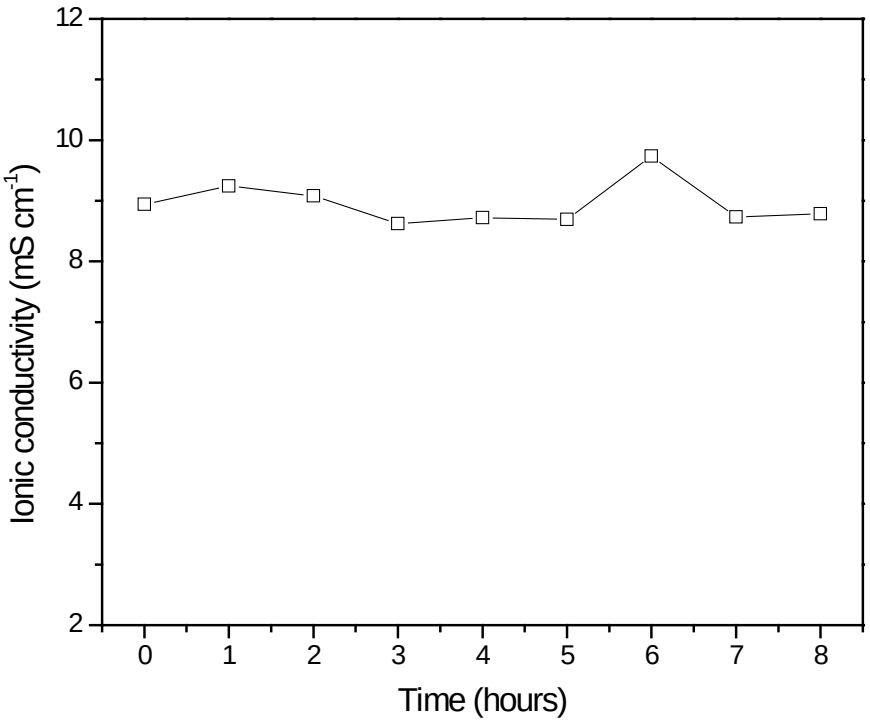

Figure 7.17: *Variation of IC with time for the PVA/PTFE/polyDADMAC blend membrane cross-linked with glutaraldehyde and thermally treated at 300 °C for 20 minutes. This test was performed at 40 °C.*

To overcome the polyDADMAC leaching, a stronger PVA matrix needed to be prepared. The membrane synthesis procedure was repeated with the cross-linking stage being performed at 60 °C (instead of 30 °C) for 20 minutes. Theoretically this temperature increase encourages more cross-links to be formed, creating a stronger gel matrix.

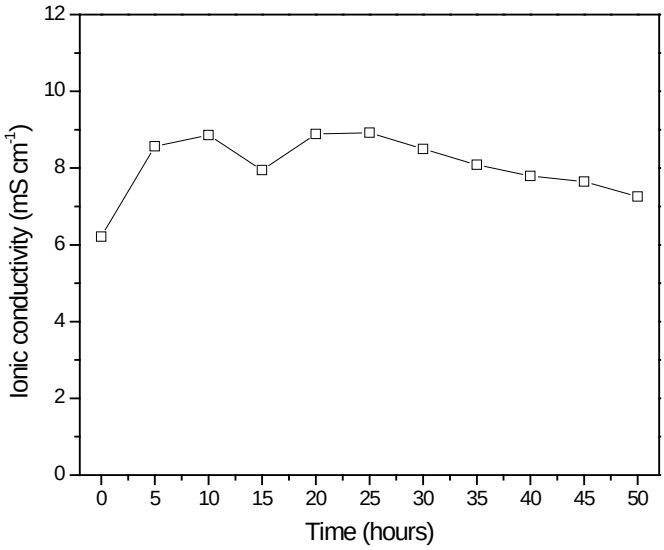

Figure 7.18: *Variation of IC with time for the PVA/PTFE/polyDADMAC blend membrane cross-linked with glutaraldehyde and thermally treated at 300 °C for 20 minutes. This test was performed at 50 °C.*

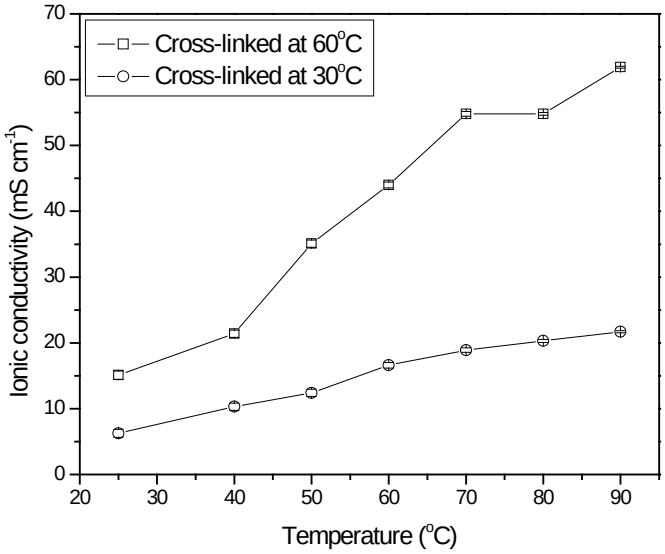

Figure 7.19: *Variation of IC with temperature for the PVA/PTFE/polyDADMAC membrane cross linked with glutaraldehyde at 60 °C and thermally treated at 300 °C for 20 minutes.*

This hypothesis was confirmed via a separate cross-linking experiment that ran for one hour at 60 ^{o}C, in which a large solid mass of unusable PVA/PTFE polymer was formed. The results of the 60 ^{o}C cross-linking procedure are shown in figure 7.19. The IC increases with increasing temperature up to 61.9 mS cm^{-1} at 90 ^{o}C.

This IC is much higher than any IC observed for any membrane sample prepared in this chapter. It was also higher than any ICs observed for the QAPPO or QAPPO/QAPS based membranes discussed in chapter 4, 5 and 6.

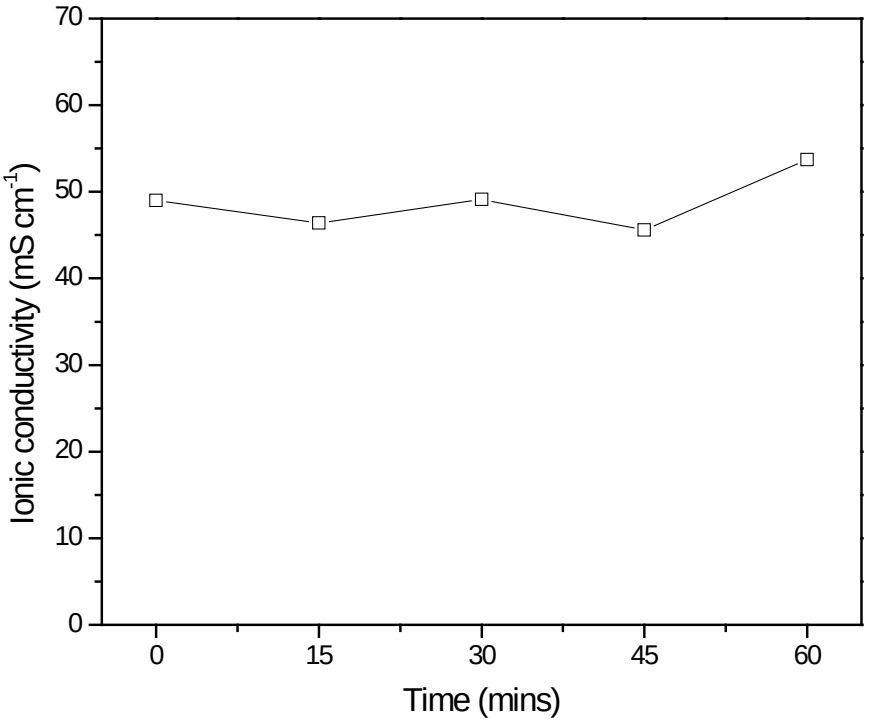

Figure 7.20: *Variation of IC with time for the PVA/PTFE/PDADMAC blend membrane cross-linked with glutaraldehyde at 60 ^{o}C and thermally treated at 300 ^{o}C for 20 minutes. This test was performed at 60 ^{o}C.*

This result shows that a strong PVA gel matrix was formed, fully encasing the polyDADMAC within, leading to no significant loss during testing. The IC (just below 50 mS cm^{-1}) obtained during a 1 hour test at 60 ^{o}C is shown in figure 7.20. The value of IC is stable during this period and this result has highlighted a potential avenue of research for these water soluble materials.

7.7 Conclusions for use of pre-made quaternised polymers in synthesis of AEMs

The aim of this chapter was to prepare a series of AEMs from a commercial water soluble polymeric material, polyDADMAC. This material required no modification other than a counter ion exchange to make it OH- conductive. This preparation method presents a "greener" alternative to the synthesis procedures discussed in chapters 4, 5 and 6 which involve the use and production of hazardous materials.

The AEM production method was based on the research conducted by Zeng et al [1], which involved a thermal degradation of PVBACl to make it insoluble in water whilst still retaining a good level of IC. This hypothesis was applied to polyDADMAC via a number of method variants.

Firstly AEMs were prepared using a porous PVDF membrane model. Porous PVDF membranes prepared in-house were sonicated in polyDADMAC solution and dried. The obtained samples were thermally treated at various temperatures and times and subsequent tests gave no clear pattern or any level of IC worth noting. The polyDADMAC also still remained soluble in water. Straight mixing of PTFE and polyDADMAC gave ICs >10 mS cm^{-1} showing an increase in IC on the porous samples. However the polyDADMAC quickly leached into the water (as it was still soluble) so this IC quickly decreased.

TG analysis of polyDADMAC showed that the degradation process associated with the loss of the trimethylammonium groups did not occur until around 350 ^{o}C. Thermal treatment temperatures were increased with no increase in AEM polyDADMAC stability. Modifications were made to the AEM synthesis method to incorporate PVA which was used to produce a more homogenous membrane. This change enabled the AEM to be thermally treated for longer however this did not decrease the amount of polyDADMAC lost into the water during testing (as it was still soluble in water).

Overall membrane ICs were improved by increasing the PTFE:polyDADMAC weight ratio from 1:1 to 1:3 as well as using a HMW-polyDADMAC which led to a 20% increase in IC. However none of these modifications helped with the main aim of making the polyDADMAC insoluble and the resulting AEM more stable.

The only modification that provided any testing stability was to cross-link the PVA with glutaraldehyde. This produced a matrix that trapped the polyDADMAC preventing it from dissolving into water during testing. When the cross-linking procedure was performed at 60 ^{o}C, an AEM with an IC of 61.9 mS cm^{-1} at 90 ^{o}C was prepared. This AEM produced a stable IC of 50 mS cm^{-1} at 60 ^{o}C for one hour.

7.8 – Chapter 7 references

[1]. R. Zeng, J. Handsel, S. D. Poynton, A. J. Roberts, R. C. T. Slade, H. Herman, D. C. Apperley and J. R. Varcoe, *Energy and Enviromental Science*, (2011), **4**, 4925-28.

[2]. D. Valade, F. Boschet, S. Roualdes and B. Ameduri, *Journal of Polymer Science, Part A: Polymer Chemistry*, (2009), **47**, 2043-58.

[3]. Q. Huang, C. Xiao and X. Hu, *Journal of Applied Polymer Science*, (2012), **124**, E116–E22.

[4]. P. Martins, A. C. Lopes and S. Lanceros-Mendez, *Progress in Polymer Science*, (2014), **39**, 683-706.

[5]. S. J. Kim, S. G. Yoon, Y. M. Lee, K. H. An and S. I. Kim, *Journal of Applied Polymer Science*, (2003), **90**, 1389-92.

[6]. J. Qiao, J. Fu, L. Li, J. Zhang, J. Xie and G. Li, *Solid State Ionics*, (2012), **214**, 6-12.

[7]. J. Qiao, J. Fu, L. Liu, Y. Liu and J. Sheng, *International Journal of Hydrogen Energy*, (2011), 1-10.

Chapter 8 – Implementation of AEMs for the electrolysis of water

Most fuel cells requires hydrogen to operate. Currently this involves having a tank or cylinder of hydrogen within a certain distance of the fuel cell. The logistics of this requires the imposition of a number of safety protocols and associated costs. The electrolysis of water provides a "greener" approach to the continued production of hydrogen from a clean source without the need for any storage.

However the same problems (higher outputs observed by PEMFCs over their alkaline counterparts) encountered for PEMFCs and alkaline PEMFCs apply to water electrolysers with one notable exception. Nafion coupled with platinum catalysts is still the preferred approach [1-4] meaning acidic working environments and high costs. Liquid alkaline environments are unsuitable as they are corrosive and the hydrogen requires purification [1, 3]. However, it has been discovered that by using an alkaline polymer electrolyte membrane, it is in fact more efficient than its liquid counterpart [5]. Similar to the development of APEMFCs though, the major hindrance is the stability and conductivity of the anion exchange membrane [5].

These stability and conductivity issues have been investigated in recent years [6, 7] and the use of alkaline polymer electrolyte in a water electrolysis application was first reported by Xiao *et al* [5]. It is widely accepted that the best catalysts for the hydrogen evolution reaction (HER) that occurs at the cathode and for the oxygen evolution reaction (OER) that occurs at the anode, are the bimetallic catalysts Ni-Mo and Ni-Fe, respectively [2, 5, 8]. Xiao *et al* reported that when using these catalysts the theoretical fuel cell voltage for electrolysis of water was 1.7 V when a current density of 400 mA cm^{-2} was applied at 40 ^{o}C [5]. This calculation however assumes that no voltage losses

are occurring within the cell. This is highly unlikely as voltage losses are expected from the electrode-membrane interfaces. Experimentally Xiao *et al* recorded a voltage of 1.8 – 1.85 V at 70 ^{o}C from an applied current density of 400 mA cm^{-2} [5].

Chapters 4, 5 and 6 detailed various AEMs that showed promising ICs and/or stabilities. A selection of the best performing AEMs were furthered tested for water electrolysis applications using the catalysts discussed previously. The AEMs selected were:

A. QAPPO propylamine cross-linked from chapter 4 section 4.5. This AEM was chosen due to its relatively high IC;
B. QAPPO/QAPS from chapter 5, section 5.2. This AEM was chosen for its high stability along with satisfactory IC;
C. “Semi gel” QAPPO/PVDF 5% from chapter 6, section 6.3.1. This AEM was chosen for its good IC and stability;
D. QAPPO/QAPVBOH 5% from chapter 6, section 6.3.3. This AEM was chosen for its excellent IC.

The QAPPO AEMs cross-linked with hexamethylenetetramine (10%, 20% and 30%) were also initially selected for testing due to their good ICs and stabilities. However these AEMs performed extremely poorly and all cracked under the pressure of the closed cell. In light of this, the results for these AEMs will not be included within this chapter.

Each 1 cm x 1cm membrane sample was subjected to an initial increasing voltage of 1.2 – 1.8 V repeated 5 times with 30 second break in-between. This was followed by a 30 minute constant voltage at 1.2, 1.4, 1.6 and 1.8 V each. This protocol was selected

to access the AEM stability to differing levels of constant electrical stimulus. These tests were followed by a second increasing voltage test to access any changes in the performance. In all tests the corresponding current density was measured. This combination of tests was performed at room temperature, 40 ^{o}C, 60 ^{o}C and 80 ^{o}C for each AEM.

As Xiao *et al* reported that the experimentally observed cell voltage for electrolysis of water was 1.8 – 1.85 V when a current density of 400 mA cm^{-2} was applied at 70 ^{o}C [5], this would be used as the benchmark figure for comparison. However the authors also presented no data at any temperatures other than 70 ^{o}C, meaning only relative comparisons could be made for the tests performed at these temperatures.

A more simplistic observation that would help confirm the successful electrolysis of water was to watch the two “exit” pipes coming from both sides of the cell. If water was successfully being converted to hydrogen and oxygen (which is ultimately the true result that was being sought) then bubbles of gas would emanate from these pipes during the entirety of the testing.

8.1 – Performance of QAPPO propylamine cross-linked AEM in a water electrolysis cell

The room temperature performance for this AEM was very poor as can be seen in figure 8.1. There is very little improvement in I-V performance after constant voltage stability after only observing an output current density of 1 mA cm^{-2} with 1.8 V supply.

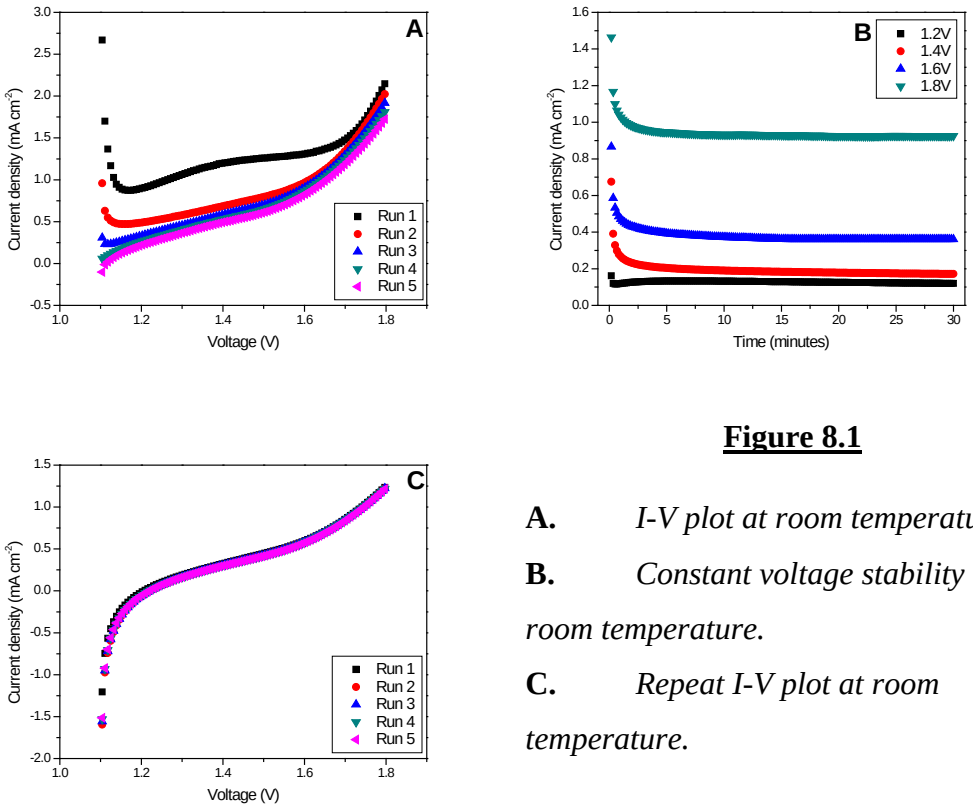

Figure 8.1

A. *I-V plot at room temperature.*

B. *Constant voltage stability test at room temperature.*

C. *Repeat I-V plot at room temperature.*

Figure 8.2 shows a small improvement in performance as the temperature is increased to 40 ^{o}C. Initially there was no change from the performance observed at room temperature however during the constant voltage stability, a voltage of 1.8 V produced an increased current density which fluctuated around 40 mA cm^{-2} (10 times less than the theoretical figure proposed by Xiao *et al* for the electrolysis of water at 40 ^{o}C [5]). The lower voltages did not produce anything more than 10 mA cm^{-2}.

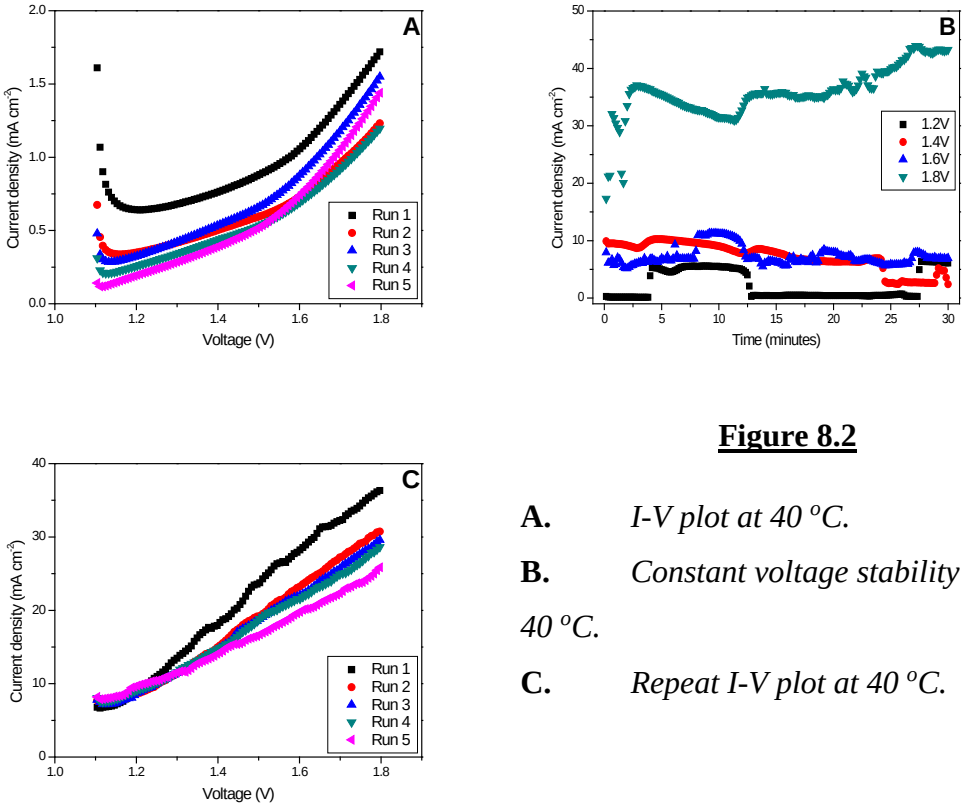

Figure 8.2

A. *I-V plot at 40 °C.*

B. *Constant voltage stability test at 40 °C.*

C. *Repeat I-V plot at 40 °C.*

The observation of 1.8 V producing the best current density was not unexpected as Xiao *et al* had experimentally proven that a voltage of 1.8 – 1.85 V was seen from a current density of 400 mA cm^{-2} [5]. Upon increasing the temperature to 60 °C a further modest increase in current density was observed as shown in figure 8.3. When applying 1.8 V to the cell, instead of a constant current density being observed, the current density increased for the whole 30 minute period which could be attributed to stabilisation of the membrane. However, the current densities observed were still one order of magnitude lower than those identified by Xiao *et al* [5].

When the temperature was raised to 80 °C a much larger change was observed. Initially the I-V plot registered a current density slightly lower than what was shown in figure 8.3 at 60 °C.

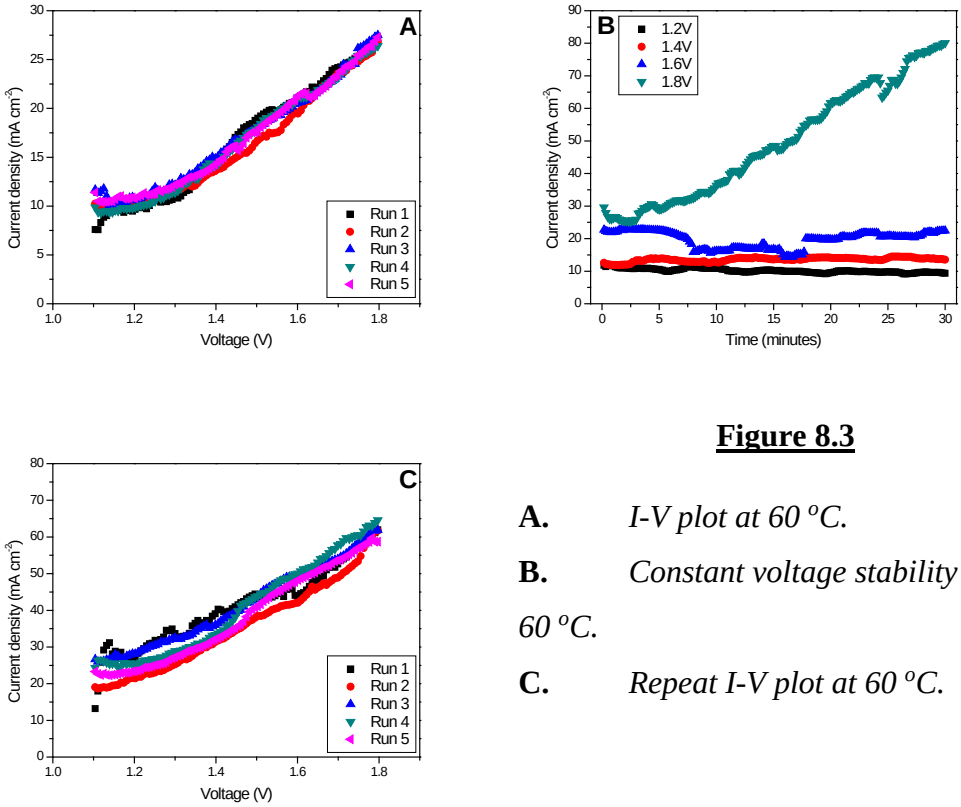

Figure 8.3

A. *I-V plot at 60 °C.*

B. *Constant voltage stability test at 60 °C.*

C. *Repeat I-V plot at 60 °C.*

During the constant voltage stability testing the same pattern as described at 60 °C was observed but on a much larger scale. At 1.8 V the current output steadily increases for 15 minutes, followed by a sharp increase for 5 minutes and finally stabilising at 600 mA cm^{-2} for the last 10 minutes. This result is 200 mA cm^{-2} higher than that observed by Xiao *et al* at the same voltage. This implies that to achieve the 1.8 V per 400 mA cm^{-2} figures, reported by Xiao *et al*, required for successful electrolysis of water a lower voltage than 1.8 V would be required. However their test was performed at 70 °C [5] rather than 80 °C which could partly explain the differences in observed current density. After the stability tests, the I-V results show a slightly lower current density of around 400 mA cm^{-2} at 1.8 V which matches more closely those observed by Xiao *et al*.

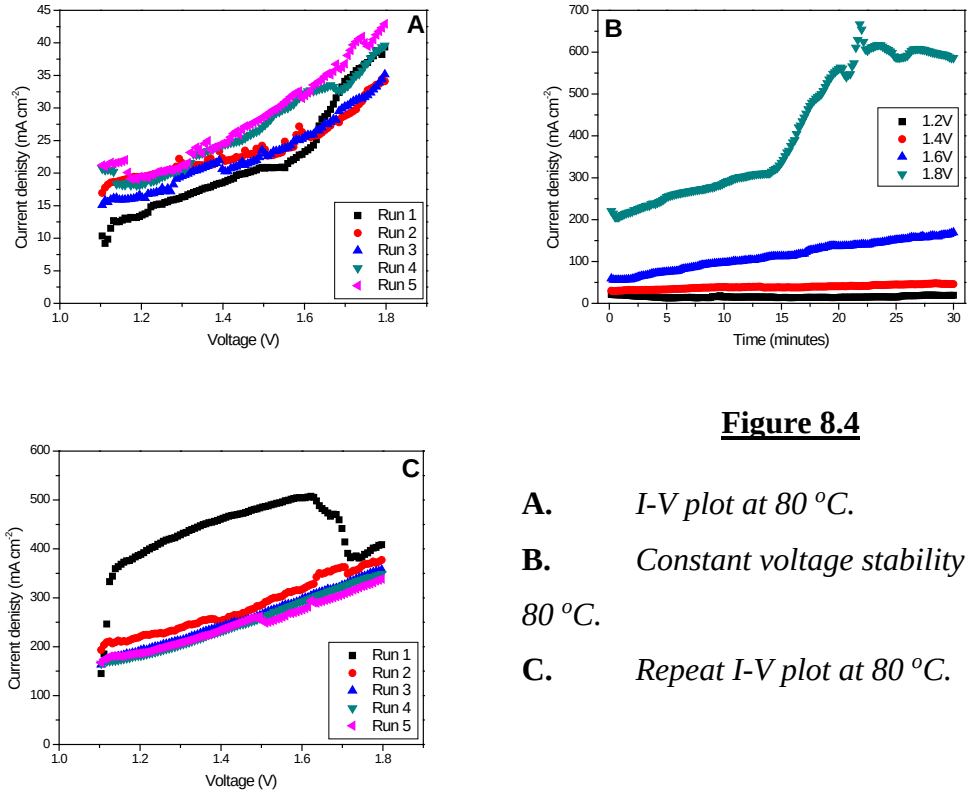

Figure 8.4

A. *I-V plot at 80 °C.*

B. *Constant voltage stability test at 80 °C.*

C. *Repeat I-V plot at 80 °C.*

It was also noted that during the stability stage there were bubbles observed coming from both exit pipes of the fuel cell indicating that a hydrogen and oxygen were being formed. The amount formed was very small (around 1ml per minute of operation during stability at 1.8 V) but nevertheless the electrolysis of water was shown to be successful.

8.2 – Performance of QAPPO/QAPS AEM in a water electrolysis cell

The testing runs at room temperature, 40 °C and 60 °C for this membrane produced extremely poor performances (figures 8.5 – 8.7). The highest current density observed at any point during the three temperature runs was 4 mA cm^{-2}. A reason for this poor performance at these temperatures could be that the OH^- diffusion rate through the membrane was very low.

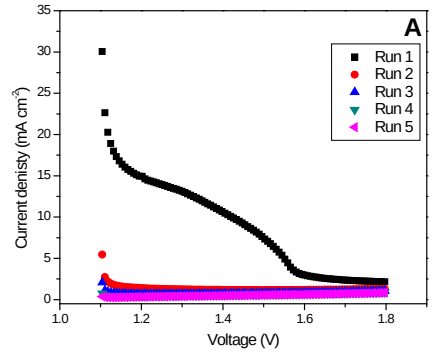

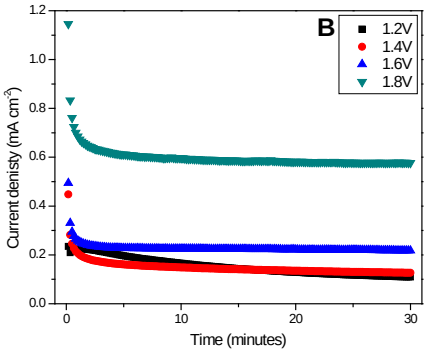

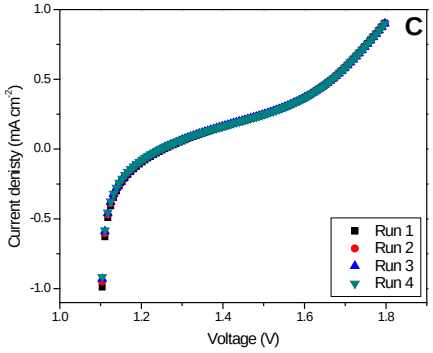

Figure 8.5

A. *I-V plot at room temperature.*

B. *Constant voltage stability test at room temperature.*

C. *Repeat I-V plot at room temperature.*

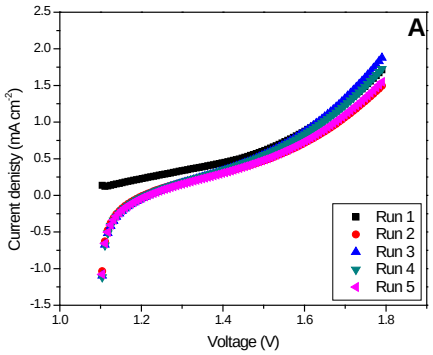

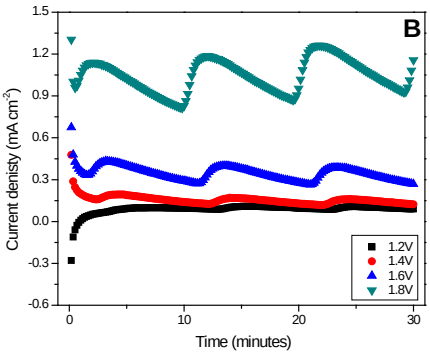

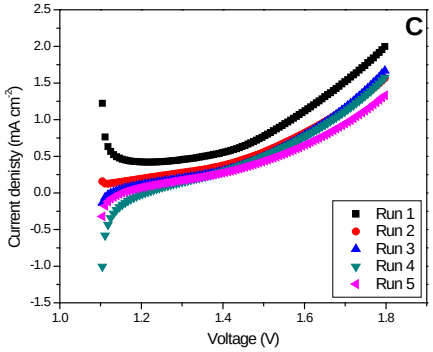

Figure 8.6

A. *I-V plot at 40 ^{o}C.*

B. *Constant voltage stability test at 40 ^{o}C.*

C. *Repeat I-V plot at 40 ^{o}C.*

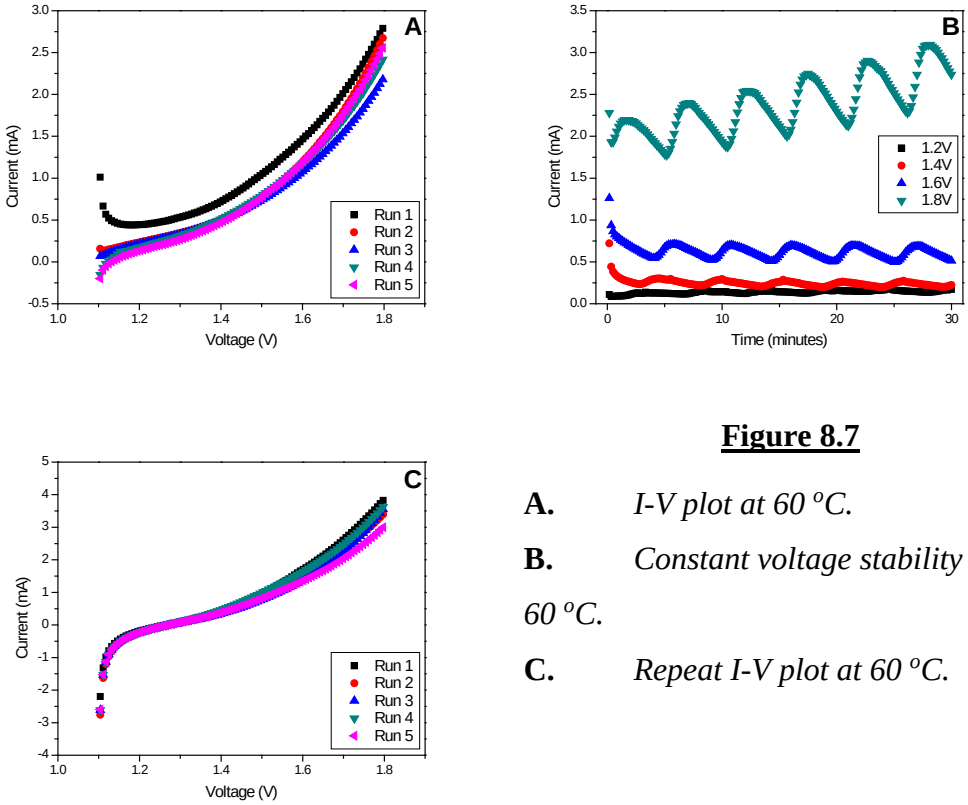

Figure 8.7

A. *I-V plot at 60 ^{o}C.*

B. *Constant voltage stability test at 60 ^{o}C.*

C. *Repeat I-V plot at 60 ^{o}C.*

The functional groups tethered to the polymer chains may not be in a preferred ordered orientation but more in a random placement. This would make it very difficult for the OH^- ions to move through the membrane which in turn would slow down the reactions occurring at both the cathode and anode. The testing performed at 80 ^{o}C is shown in figure 8.8. Although the starting I-V performance was similar to the observed at other temperatures, once again, during the stability test a dramatic increase in current density occurred at a voltage of 1.8 V. At the end of the 30 minute stability test, the current density had almost reached 800 mA cm^{-2}. It was initially believed that the dramatic increase in current density observed at a voltage of 1.8 V could be an experimental artefact, however, a visual inspection of the AEM after opening the cell showed no

damage or punctures to the AEM or catalyst layers. During testing no bubbles were observed coming from the exit pipes of the cell.

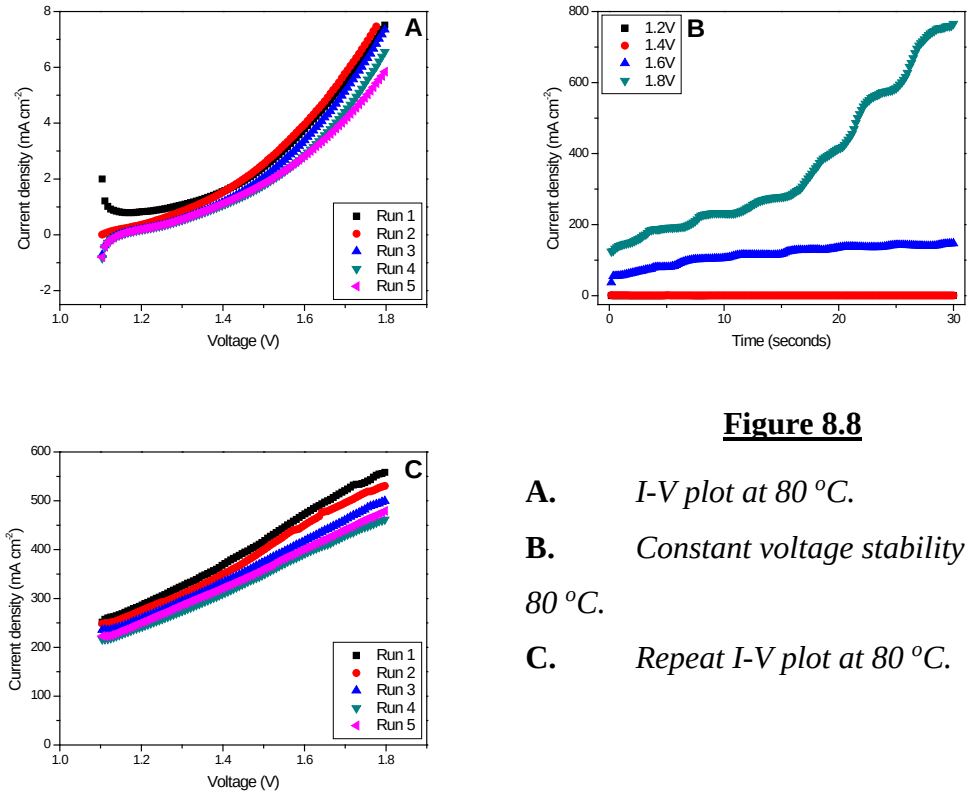

Figure 8.8

A. *I-V plot at 80 °C.*

B. *Constant voltage stability test at 80 °C.*

C. *Repeat I-V plot at 80 °C.*

8.3 – Performance of "semi gel" QAPPO/PVDF 5% AEM in a water electrolysis cell

The tests at room temperature and 40 °C (figures 8.9 and 8.10) for this membrane produced fairly similar results to each other. A good current density of 200 mA cm^{-2} (at RT) and 170 mA cm^{-2} (at 40 °C) were observed when reaching a 1.8 V input. These figures represent around half the amount of current density required for the electrolysis of water at 70 °C as reported by Xiao *et al* [5]. When the temperature was increased to 60 °C, an increase in current density levels was observed as expected (figure 8.11).

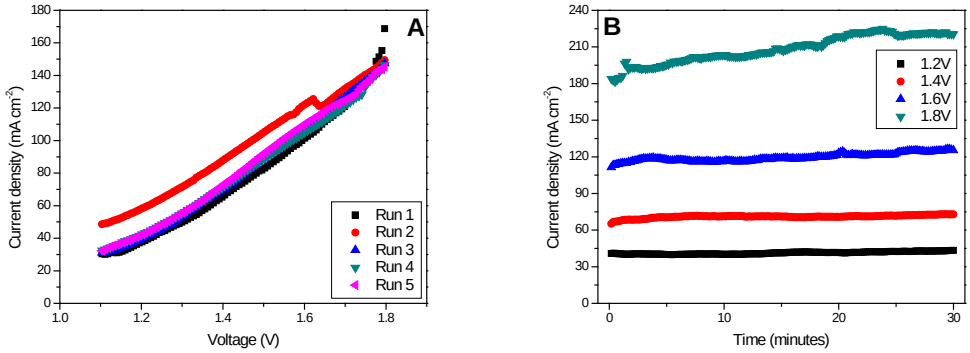

Figure 8.9

A. *I-V plot at room temperature.*

B. *Constant voltage stability test at room temperature.*

C. *Repeat I-V plot at room temperature.*

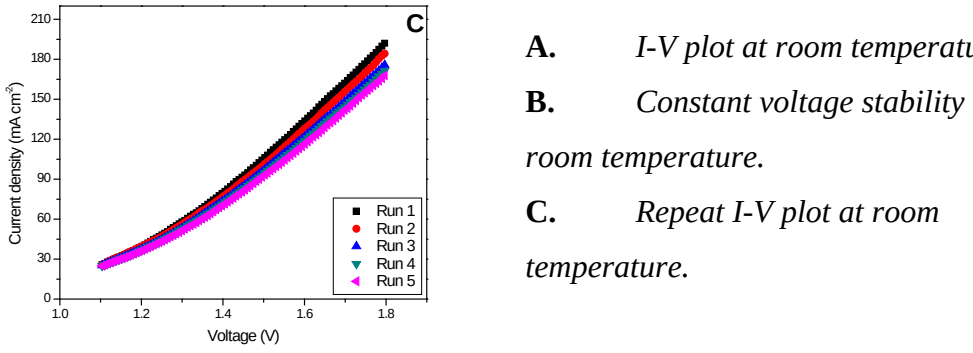

Figure 8.10

A. *I-V plot at 40 ^{o}C.*

B. *Constant voltage stability test at 40 ^{o}C.*

C. *Repeat I-V plot at 40 ^{o}C.*

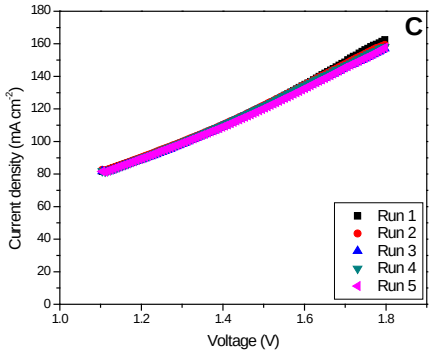

Constant voltages of 1.2 V, 1.4 V and 1.6 V produced good levels of current density of 100 mA cm^2, 200 mA cm^2 and 300 mA cm^2 respectively during which a small amount of bubbling from the cell exit pipes was also observed. However, during the 1.8 V stability test it can be seen from figure 8.11 that the observed current density increases dramatically from 400 mA cm^{-2} to 1200 mA cm^{-2} over the course of 30 minutes. The amount of current being recorded as well as the rate at which it increased over the course of the test at 60 ^oC was wholly unexpected considering the positive results observed at the lower voltages.

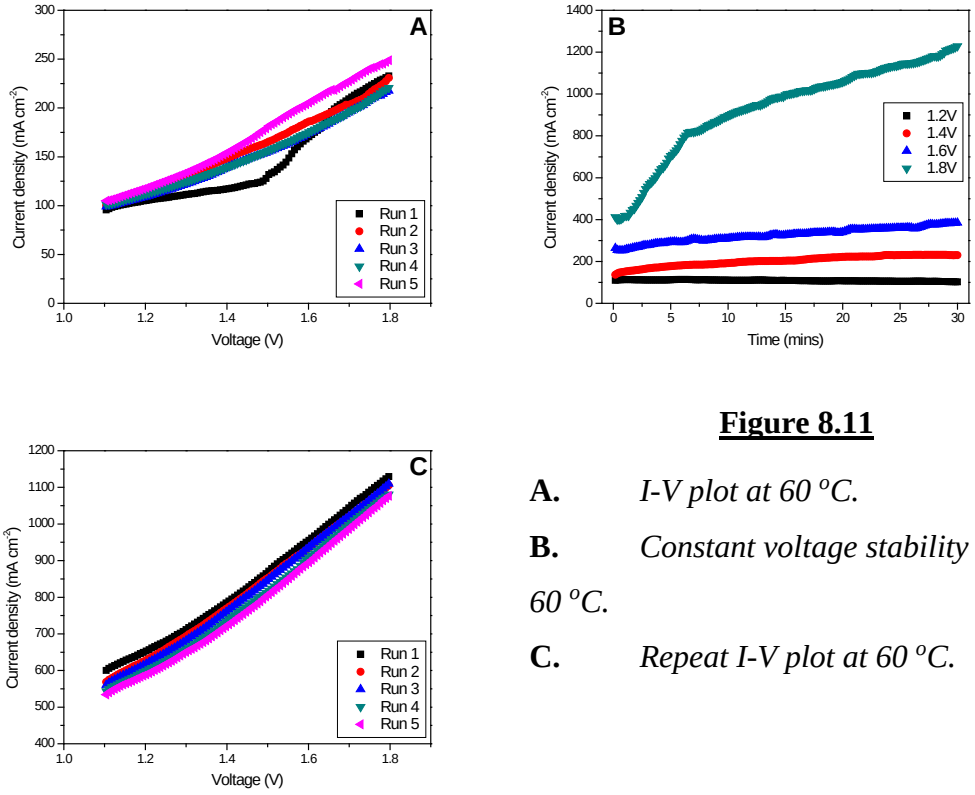

Figure 8.11

A. *I-V plot at 60 ^oC.*

B. *Constant voltage stability test at 60 ^oC.*

C. *Repeat I-V plot at 60 ^oC.*

The same results were also displayed during the 80 ^oC test shown in figure 8.12. The first initial I-V run eventually resulted in 1.8 V producing 1000 mA cm^{-2} current density whilst the 1.2 V and 1.4 V stability runs exhibited stable current densities of

600 mA cm^{-2} and 800 mA cm^{-2} respectively. However, the amount of current being recorded eventually caused the testing run to be ceased when it breached the safety limits that had been set by the software.

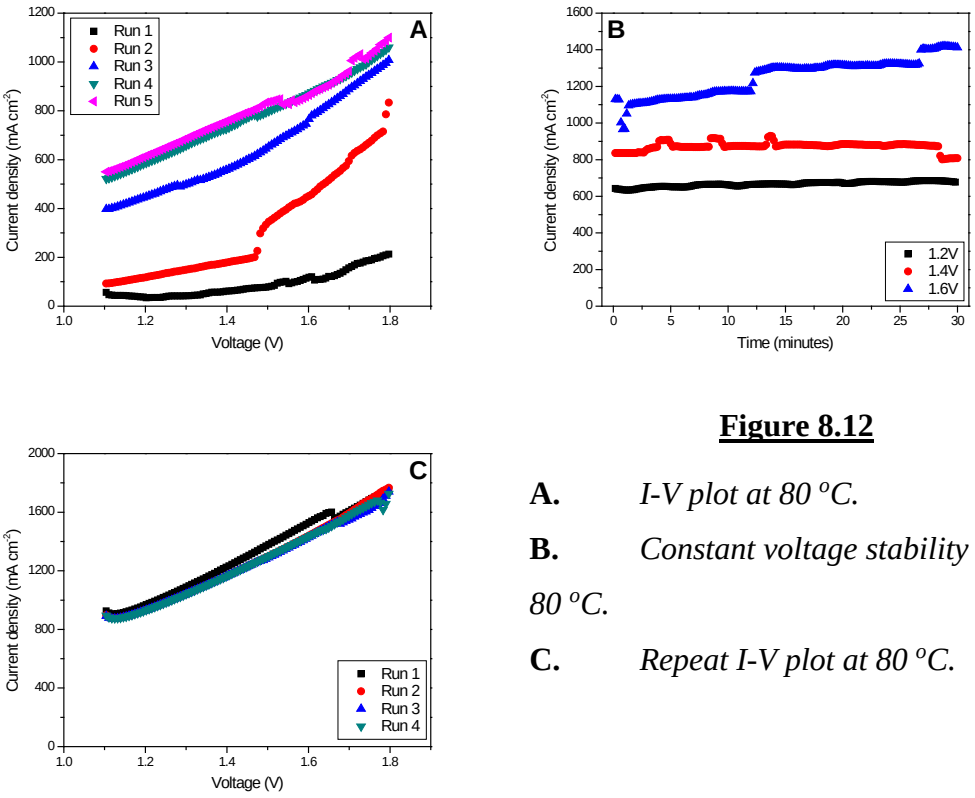

Figure 8.12

A. *I-V plot at 80 °C.*

B. *Constant voltage stability test at 80 °C.*

C. *Repeat I-V plot at 80 °C.*

To try and find an explanation for these results at 80 °C, the testing parameters were switched so that a constant 400 mA cm^{-2} current was applied to the cell and the voltage measured (the same as the test performed by Xiao *et al* [5]). The results of the tests carried out at 60 °C and 80 °C are shown in figure 8.13. At 60 °C, a voltage of between 1.6 – 1.7 V was observed. This voltage seen at 60 °C is similar to the 1.7 V Xiao *et al* reported was the theoretical voltage for water electrolysis at 40 °C when 400 mA cm^{-2} was applied to the cell [5]. At 80 °C, the voltage shown in figure 8.13 is 1.5 V which betters the experimental readings of 1.8 – 1.85 V at 70 °C reported by Xiao *et al*.

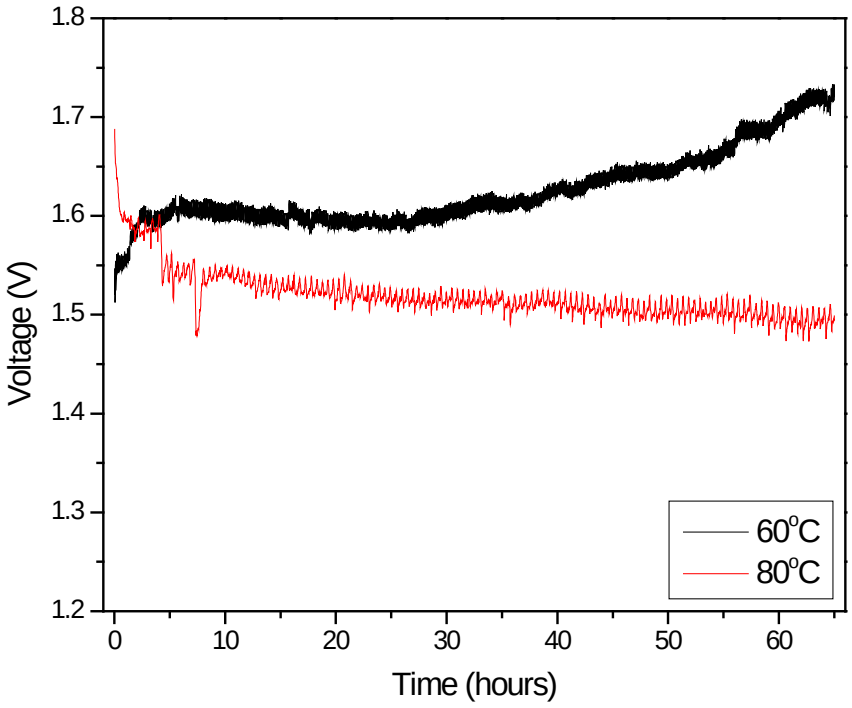

Figure 8.13: *Water electrolysis of QAPPO-PVDF 5% under constant current of 400 mA cm^{-2} for 65 hours.*

It is clear to see that the results presented in figure 8.13 are completely inconsistent with those presented in figures 8.9 – 8.12. PVDF is known to exhibit piezoelectric effects [9]. Piezoelectricity is the gathering of electrical charge by certain materials when mechanical stress is applied or when the temperature changes. When preparing the cell for testing, the AEM and electrodes are sandwiched together and placed between the two cell plates. The cell is then sealed tightly to ensure that no gas or liquid can enter or escape the cell during operation. The AEM separates the two sides of the cell and would be under a high amount of pressure as well as experience increasing temperatures. It is theorised that the 5% PVDF content within the QAPPO/PVDF 5% AEM may have started to accumulate charge due to the high

pressure and temperature within the cell. However, what this reasoning does not explain is the good results observed when testing with a constant current density (figure 8.13). It is clear more work would need to be conducted on this AEM to ascertain which set of results are true.

8.4 – Performance of QAPPO/QAPVBOH 5% AEM in a water electrolysis cell

Similar to the QAPPO/PVDF 5% sample, this AEM produced fairly similar results for the tests performed at room temperature and 40 ^{o}C (figures 8.14 and 8.15). Good stable current densities were observed during the constant voltage stability tests, however during the 60 ^{o}C test the AEM completely disintegrated. When the test was re-done at 60 ^{o}C with a fresh AEM, the same result was observed. This results did not tally with those presented in chapter 6 section 6.2.1.3 which showed the AEM was stable at 90 ^{o}C for 24 hours. The testing conditions within impedance testing are however much less severe with a lot less stress and strain being put upon the AEM. It is assumed that the membrane was in fact made too fragile by the addition of the PVBOH. It was also worth noting that no bubbles were observed coming from the cell exit pipes during the tests.

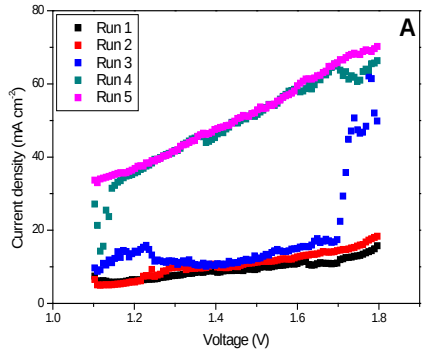

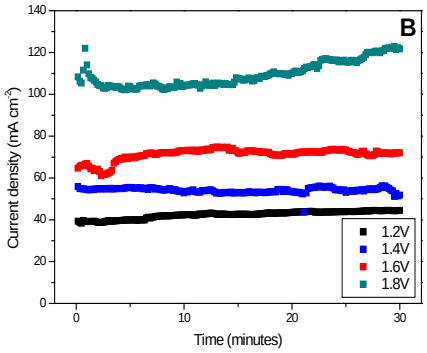

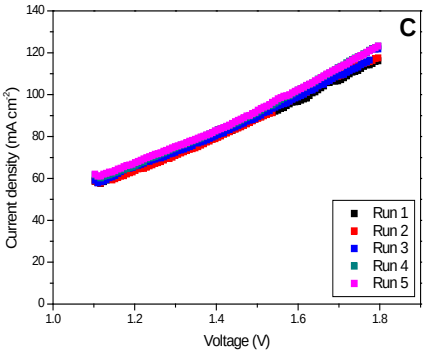

Figure 8.14

A. *I-V plot at room temperature.*

B. *Constant voltage stability test at room temperature.*

C. *Repeat I-V plot at room temperature.*

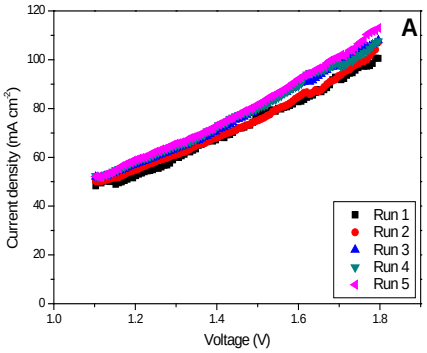

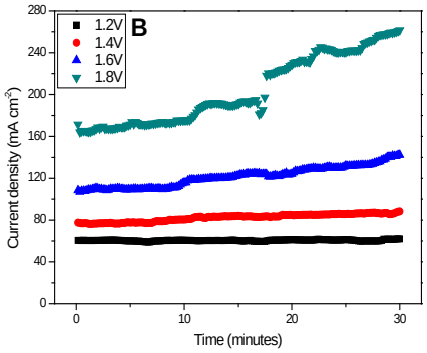

Figure 8.15

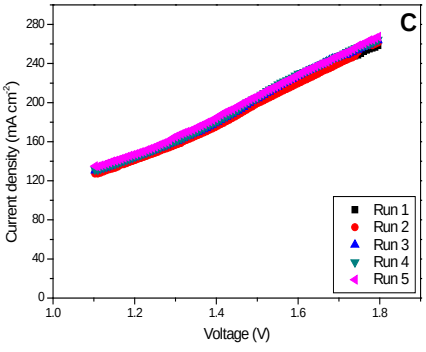

A. *I-V plot at 40 °C.*

B. *Constant voltage stability test at 40 °C.*

C. *Repeat I-V plot at 40 °C.*

8.5 – Chapter 8 references

[1]. J. D. Holladay, J. Hu, D. L. King and Y. Wang, *Catalysis Today*, (2009), **139**, 244-60.

[2]. D. Pletcher and X. Li, *International Journal of Hydrogen Energy*, (2011), **36**, 15089-104.

[3]. P. Millet, R. Ngameni, S. A. Grigoriev, N. Mbemba, F. Brisset, A. Ranjbari and C. Etievant, *International Journal of Energy Research*, (2010), **35**, 5043-52.

[4]. S. A. Grigoriev, P. Millet, S. V. Korobtsev, V. I. Porembskiy, M. Pepic, C. Etievant, C. Puyenchet and V. N. Fateeva, *International Journal of Energy Research*, (2009), **34**, 5986-91.

[5]. L. Xiao, S. Zhang, J. Pan, C. Yang, M. He, L. Zhuang and J. Lu, *Energy and Environmental Science*, (2012), **5**, 7869-71.

[6]. J. Pan, Y. Li, L. Zhang and J. Lu, *Chem. Commun.*, (2010), **46**, 8597-99.

[7]. J. Pan, S. Lu, Y. Li, A. Huang, L. Zhuang and J. Lu, *Advanced Functional Materials*, (2010), **20**, 312-19.

[8]. D. Pletcher, X. Li and S. Wang, *International Journal of Hydrogen Energy*, (2012), **37**, 7429-35.

[9]. H. Kawai, *Japan Journal of Applied Physics*, (1969), **8**, 975-76.

Chapter 9 – Conclusions

The introduction and aims chapter presented a number of criteria that all AEMs should meet in order to be viable materials for alkaline PEMFCs. These criteria are:

i. Thermal stability up to at least 120 ^{o}C;
ii. Mechanical stability, material is able to be hot pressed;
iii. Chemical stability, material is stable in water or alkaline conditions;
iv. High permeation of water but not hydrogen or oxygen;
v. High conduction of OH^- ions.

The three stages of AEM synthesis (chloromethylation, quarternisation and counter ion exchange), all play a role in determining whether the above criteria are met. The polymer that most of the research was conducted on was poly (2,6-dimethyl-1,4-phenylene oxide), PPO. The most difficult stage of the synthesis of PPO based AEMs was the chloromethylation process. It was due to this reason that a part of the research investigated the use of commercially available pre chloromethylated and quaternised polymers.

The stability and IC of all AEMs were investigated and attempts to improve these were also investigated using various experimental ideas. These were:

i. Use of a higher reaction temperature for preparation of CMPPO;
ii. Use of a longer reaction time for preparation of CMPPO;
iii. Use of a chemical cross-linker during the preparation of the AEM;
iv. Addition of inorganic materials during the preparation of the AEM;

9.1 – QAPPO AEM synthesis

Three batches of CMPPO were synthesised with each having a different reaction time, 1 hour, 4 hours and 6 hours. Upon preparation of the quaternised OH^- conductive PPO AEMs, it was found that the AEM prepared from the 6 hour batch of CMPPO produced the AEM with the highest IC. Therefore in terms of IC, the longer reaction time favoured the higher IC.

The counter ion exchange step involved soaking the AEM in 1M KOH. The length of this exchange period was investigated by leaving the AEM in the 1M KOH for one and three days. Three day KOH treatment was shown to detrimentally affect the IC and stability of the AEMs. Due to this evidence a one day KOH treatment was used throughout this work.

In terms of AEM stability a similar pattern was observed. Both the 1 and 4 hour batch of CMPPO produced very unstable AEMs that quickly degraded once 60 ^oC was reached in testing. The 6 hour CMPPO AEM was shown to be stable at 70 ^oC for 500 hours with an IC of 22 mS cm^{-1}. However during testing at 80 ^oC, the IC decreased over the course of 500 hours. The longer reaction time during the chloromethylation process also favours higher stabilities as well as higher ICs.

The enhancement of the stability of AEMs was further investigated by use of chemical cross-linkers. Cross-linkers included diethylamine [1], propylamine and diaminopropane and these were added before the quarternisation step of the AEM preparation. The AEM cross-linked with diethylamine showed a decrease in IC when compared with the non-cross-linked variant. This decrease in IC seems linked to the loss of trimethylammonium groups that are used as cross-linking points between

polymer chains [1]. Despite the decrease in IC, the AEM cross-linked with diethylamine was now testable up to 90 ^{o}C rather than degrading around 60 ^{o}C. The IC further increased during stability testing and eventually was comparable to the non-cross-linked derivative. The diethylamine cross-linked AEM slowly degraded over the course of 210 hours at 90 ^{o}C so the stability was not entirely permanent.

The other cross-linking agents used showed some different and interesting results. Both propylamine and diaminopropane cross-linked AEMs showed an increase in IC compared to the non-cross-linked derivative. During stability testing at 90 ^{o}C, both AEMs showed slight decreases in IC but nevertheless the ICs were still higher than the non-cross-linked variants.

Increasing the reaction temperature of the chloromethylation reaction did not have any beneficial effects on either the IC or stability of the AEMs produced. The increase in temperature made the chloromethylation reaction more difficult, typically producing a thick polymer gel) several times before any success.

These experiments showed that realistically, the only way of synthesising a CMPPO sample capable of producing an AEM with higher IC, was to increase the reaction period of the chloromethylation process. Cross-linking was shown to enhance the stability of the AEMs but they ultimately still remained unstable at 90 ^{o}C. Also, despite some improvements in stability, there were large fluctuations in IC between AEMs.

9.2 – QAPPO/QAPS blend AEMs

Attempts were made to address the stability issues with the QAPPO AEMs highlighted in chapter 4. The aim of using polymer blends was to try and increase the

stability of the AEMs without negatively influencing the IC. This was attempted using two different routes:

i. Running the chloromethylation reaction on the polymer blend ("one pot synthesis");
ii. Synthesising two separate chloromethylated polymers and mixing them together at the ionomer stage before quarternisation.

These ideas were developed based on similar research looking at polymer blends [2]. Polysulphone was researched in one of the first presentations of AEMs for APEMFCs [3]. For this reason it was chosen as the second polymer component.

The AEM produced from the CMPPO and CMPS samples that were prepared via the "one pot" synthesis route, performed very poorly during testing and quickly disintegrated during a stability test at 70 ^{o}C. During the chloromethylation step two reactions are competing, functionalisation and cross-linking. Cross-links are formed at between two points on the polymer chain that have been chloromethylated. It was not possible to control both the degree of functionalisation and the degree of cross-linking when performing the "one pot" synthesis. The results indicate that some functionalisation occurred but very little cross-linking.

The second experimental route (separate chloromethylation followed by blending before quaternisation) produced much better results. The AEM synthesised from the 6 hour batch of CMPPO from chapter 4 was paired with a batch of CMPS prepared previously during an MSc project. It was known that the CMPS was poorly functionalised but highly cross-linked, making it very stable. The resulting combined QAPPO/QAPS AEM was stable at 90 ^{o}C for 1100 hours with a peak IC of 25 mS cm^{-}

^{1} which was equal to the IC observed for the best pure QAPPO AEM. Furthermore, this membrane was also stable in 1M KOH up to 80 ^{o}C before degrading. The total time of testing for this QAPPO/QAPS membrane was 2,178 hours. Polymer blends are usually prepared to produce a material that bears the characteristics of both the materials used to create it. For example, the melting point of a binary polymer blend will typically occur between the two melting points of the pure polymers used. The TG plot for the QAPPO/QAPS membrane showed that its stability was more similar to the stability of the QAPS component whilst still maintaining the good IC of the QAPPO component.

Addition of inorganic materials [4] to the QAPPO/QAPS membrane did not increase the IC by any significant amount. The stability was in fact made worse by their addition.

9.3 – Use of a "semi gel" batch of CMPPO in AEM preparation

Chapters 4 and 5 presented the AEM synthesis process and ways of improving the AEM performance. A conclusion from chapter 4 was that the best way of enhancing the IC and stability of the AEM, was to run the CMPPO synthesis step for a longer period of time. This goal was never achieved as the CMPPO synthesis proved to be very difficult to reproduce. During the CMPPO synthesis, a thick gel was observed at varying times during the reaction. The time at which this gel formed was never the same and the resultant gels were showed to be unusable and had to be discarded. As reported in chapter 6, the success rate for that chapter alone was 1 in 10. Not only was this wasteful and costly, but it also highlights the problems with reproducibility in this synthesis.

No literature was available discussing the chloromethylation synthesis, with regards to when the reaction solution becomes unusable during gel formation. One such CMPPO synthesis run was stopped at the moment the gel was assumed to be forming. Stopping the reaction at this stage yielded a batch of CMPPO with a "semi gel" consistency. A QAPPO AEM formed from this "semi gel" batch of CMPPO showed a peak IC of 27.5 mS cm^{-1} at 90 ^{o}C, higher than any previously prepared QAPPO AEM. The "semi gel" based AEM showed some signs of degradation at 90 ^{o}C over the course of 132 hours.

Stability improvements to the "semi gel" AEM were attempted by using some of the techniques discussed in chapters 4 and 5 to produce blended membranes (using polymer blends). PVDF, PVC and PVBCl were added in 5% amounts similarly to the procedure used to prepare the QAPPO/QAPS AEM (chapter 5). Additions of PVDF and PVBCl managed to make the AEM stable with very minimal impact on the IC, whereas PVC addition stabilised the AEM with a large decrease in IC. A hexamethylenetetramine cross-linking experiment also managed to stabilise the AEM at 90 ^{o}C without any loss of IC.

The successful use of a batch of CMPPO that had seemingly failed ("semi gel" batch), to prepare AEMs with good IC and stability was an entirely unexpected result.

9.4 – Modification of water soluble polymeric materials for use as AEMs

The problems of reproducibility with the QAPPO membranes led to the investigation of commercially available polymeric materials with ammonium chloride groups already incorporated. These materials would provide a "greener" alternative to the hazardous chloromethylation reaction as well as providing a more consistent

molecular weight product. However, one downside of some of these materials was that they are soluble in water. A series of AEMs were prepared using poly(diallyldimethylammonium chloride), based on an experimental procedure reported by Zeng *et al* [5].

Porous PVDF membranes proved to be very ineffective at holding any polyDADMAC whilst thermal treatment temperatures of up to 190 ^{o}C proved incapable of making polyDADMAC insoluble. Common solvent issues prevented PVDF from being mixed with polyDADMAC however, when the porous PVDF was replaced with a porous PTFE membrane as the support, an AEM with good IC was obtained. Nevertheless the stability of these AEMs was very poor.

PTFE:polyDADMAC AEMs were synthesised via a "one pot" synthesis route involving the addition of PVA as binding agent rather than the porous PTFE membrane approach. This modification did not change the IC or stability of the AEM. ICs were improved by incorporating a higher weight ratio of polyDADMAC within the AEM or by using a higher molecular weight polyDADMAC. However, stabilities were unchanged because polyDADMAC remained soluble in water and eventually leached from the membrane with time.

One final series of AEMs focused on forming a cross-linked matrix of PVA which would encase the polyDADMAC within. The PVA was cross-linked with glutaraldehyde during mixing with PTFE and polyDADMAC to form an interpenetrating polymer network (IPN) [6-8]. The AEMs prepared from this procedure were found to be stable at room temperature and 40 ^{o}C. An interpenetrating

polymer network AEM cross-linked at 60 ^{o}C produced an IC peak of 60 mS cm^{-1} and good stability at 60 ^{o}C for 1 hour.

Despite the good final result, the overall conclusion for this section of results (investigation of commercially available quaternised polymers) would be that the results, despite encouraging, were still a bit disappointing. No AEM was stable for a prolonged period of time above 40 ^{o}C. The initial procedure for making the polyDADMAC insoluble involved a partial degradation of the reagent which is not a particularly sensible procedure. Out of the two experimental routes discussed in this section, the cross-linking of PVA provides the most appealing option but more work must be carried out to try and achieve similar stabilities at higher temperatures.

9.5 – Performance of selected AEMs in water electrolysis applications

The main goal of this work was to prepare a variety of AEMs that could work in water electrolysis applications. A selection of the best performing AEMs based on IC and/or stability were accessed for their water electrolysis performance.

9.5.1 – Water electrolysis performance of the QAPPO propylamine cross-linked AEM

This membrane showed a steady increase in performance as the temperature increased. Although at room temperature the current densities were very poor by the end of the test, the AEM exhibited a performance similar to the one reported by Xiao *et al* [9]. A small amount of bubbling was seen coming from the pipes exiting the cell, implying hydrogen and/or oxygen were being formed. The amount of gases being formed was very small, however this visual observation showed that this AEM had some potential.

9.5.2 – Water electrolysis performance of the QAPPO/QAPS AEM

This AEM was the best performing in terms of stability as it was stable at 90 ^{o}C for 1100 hours. On the other hand, its water electrolysis capability was initially very poor. At 80 ^{o}C and with 1.8 V supplied a large increase in current output was observed, however this was coupled with no observation of any gas being emitted from the cell. Either the OH^- ion pathway through the AEM was particularly difficult or the rate of formation was very slow.

9.5.3 – Water electrolysis performance of the "semi gel" QAPPO/PVDF 5% AEM

The initial data obtained for this AEM at room temperature and 40 ^{o}C was very promising (High current densities observed from low input voltages). Nevertheless upon heating to 60 ^{o}C and 80 ^{o}C, large jumps in current density were observed which eventually led to the test being terminated on safety grounds. Usually when the safety parameters have been surpassed it means that either the AEM has ruptured or there are metal components touching each other and causing a short circuit. However, upon inspection of the apparatus and AEM no such fault could be found. When the testing parameters were modified and a constant current applied to this AEM, a better performance over the course of 65 hours than that reported by Xiao *et al* [9] was observed. These two sets of data are contradictory to one another and as sporadic bubbling was observed from the cell further investigation is needed before a final verdict could be made on this AEM.

9.5.4 – Water electrolysis performance of the QAPPO/QAPVBOH 5% AEM

Whilst this AEM showed good IC and stability at 90 ^{o}C, this was not the case within a water electrolysis cell. Good performance was observed at room temperature and 40 ^{o}C. However upon heating to 60 ^{o}C the AEM degraded and the test failed. This observation was confirmed with a second test at 60 ^{o}C with a fresh piece of AEM. No bubbles were observed during this AEMs operation which again suggested a poor performance in terms of water electrolysis.

9.6 – Chapter 9 references

[1]. J. Pan, Y. Li, L. Zhang and J. Lu, *Chem. Commun.*, (2010), **46**, 8597-99.

[2]. J. Wang, R. He and Q. Che, *Journal of Colloid and Interface Science*, (2011), **361**, 219-25.

[3]. S. Lu, J. Pan, A. Huang, L. Zhuang and J. Lu, *Proceedings of the National Academy of Sciences*, (2008).

[4]. R. Vinodh, M. Purushothaman and D. Sangeetha, *International Journal of Hydrogen Energy*, (2011), **36**, 7291-302.

[5]. R. Zeng, J. Handsel, S. D. Poynton, A. J. Roberts, R. C. T. Slade, H. Herman, D. C. Apperley and J. R. Varcoe, *Energy and Enviromental Science*, (2011), **4**, 4925-28.

[6]. S. J. Kim, S. G. Yoon, Y. M. Lee, K. H. An and S. I. Kim, *Journal of Applied Polymer Science*, (2003), **90**, 1389-92.

[7]. J. Qiao, J. Fu, L. Li, J. Zhang, J. Xie and G. Li, *Solid State Ionics*, (2012), **214**, 6-12.

[8]. J. Qiao, J. Fu, L. Liu, Y. Liu and J. Sheng, *International Journal of Hydrogen Energy*, (2011), 1-10.

[9]. L. Xiao, S. Zhang, J. Pan, C. Yang, M. He, L. Zhuang and J. Lu, *Energy and Environmental Science*, (2012), **5**, 7869-71.

Chapter 10 – Future Work

It is clear from the results presented in this work, that there are a number of areas that would benefit from further investigation.

The first area that needs significant further investigation is the chloromethylation of PPO. Whilst the results discussed in chapter 4 show that by increasing the chloromethylation reaction time, the IC and stability increases; what it does not show is the difficulty in achieving those results. Close to 40 chloromethylation reactions were performed during this work, with only 6 "completed" reactions, a success rate of only 15%. A "completed" reaction refers to a batch of CMPPO that was used to create a quaternised AEM. The cause of these failures is not clear, although a number of potential causes could be hypothesised. These include:

1. Temperature – At 50 ^{o}C the competing chloromethylation and cross-linking reactions may not be in equilibrium. The cross-linking reaction appears to be more favoured, as seen by all the thick gels that were observed in this work. A reduction in temperature to 40 ^{o}C or even lower should be looked at and the success rate of the chloromethylation reaction compared to that seen in this work.
2. Paraformaldehyde addition – Before any PPO was added to the reaction vessel, the paraformaldehyde was allowed to stir at 50 ^{o}C for 30 minutes. This was done to ensure that the chloromethylation reaction would start promptly. The abundance of formaldehyde within the reaction vessel upon addition of PPO could have an effect on the speed of the initial reaction.

3. Introduction of moisture or oxygen to reaction system – The chloromethylation reaction had to be performed under anhydrous conditions. Whilst contamination with water was unlikely, the introduction of oxygen was more apparent. The chloromethylation reaction was performed under nitrogen, however it was noticed that a "gel like" build up appeared on the end of the nitrogen line during the reaction. This had the effect of blocking the gas line and limiting the flow of nitrogen into the reaction vessel.

A number of ways were investigated in this work to increase the IC and stability of the synthesised AEMs. This included cross-linking, addition of secondary polymers etc. An increase in reaction time appeared to be the only way that BOTH the IC and stability of the membranes could be increased. Chloromethylation reactions were performed for 1, 4 and 6 hours however reaction times of 8 or even 12 hours should not be disregarded. Once a high performing base QAPPO AEM has been prepared, then cross-linking reactions or addition of secondary polymers may be considered to help further improve the stability, if needed.

A more important result that would need confirming is the one discussed at the start of chapter 6 concerning the "semi gel" batch of CMPPO. This batch produced a QAPPO AEM that exhibited a higher IC and stability at 90 ^{o}C than the QAPPO AEMs produced from both the 4 and 6 hour batches of CMPPO. This was achieved despite the chloromethylation reaction running for only 1 hour. First, this result needs to be re-investigated to confirm that it is reproducible and not simply a "one off". Second, an interesting co-experiment to perform at the same time would be a rheological look at the viscosity of the reaction solution over time. It is clear that the chloromethylation solution thickens over time, as this was the main reason for why the chloromethylation

reaction that yielded the “semi gel” batch of CMPPO, was stopped. A number of identical reactions could be prepared and stopped at different points corresponding to various solution viscosities. A comparison between viscosity and membrane IC/stability could then be sought, to access whether the chloromethylation reactions could be monitored via this route rather than either a set amount of time or by the eye of the researcher.

Another area of further investigation concerns the commercially available quaternised polymer, polyDADMAC. These materials provide a “greener” alternative to the chloromethylation reactions described in this work as they use dangerous chemicals. Whilst the majority of the results presented in chapter 7, failed to achieve the main objective of making polyDADMAC insoluble in water, the cross-linking experiments presented in section 7.6 were very promising. The cross-linking experiments performed at 60 ^{o}C produced membranes with the highest IC observed throughout this thesis. Firstly, a much longer stability test at 60 ^{o}C of at least 500 hours should be performed on this membrane sample to investigate how long the IC of 50 mS cm^{-1} can be maintained for. Secondly, stability tests at 70 ^{o}C, 80 ^{o}C and 90 ^{o}C (dependant on the condition of the membrane) need to also be performed to investigate the IC stabilities at each respective temperature.

To finally conclude, there are a number of avenues that could be investigate to optimise the performance of the AEMs presented in this work, to enable them to be an attractive option to current technologies.

Appendix A – Additional IR spectra – Figure A.1 – Infrared spectrum of PPO

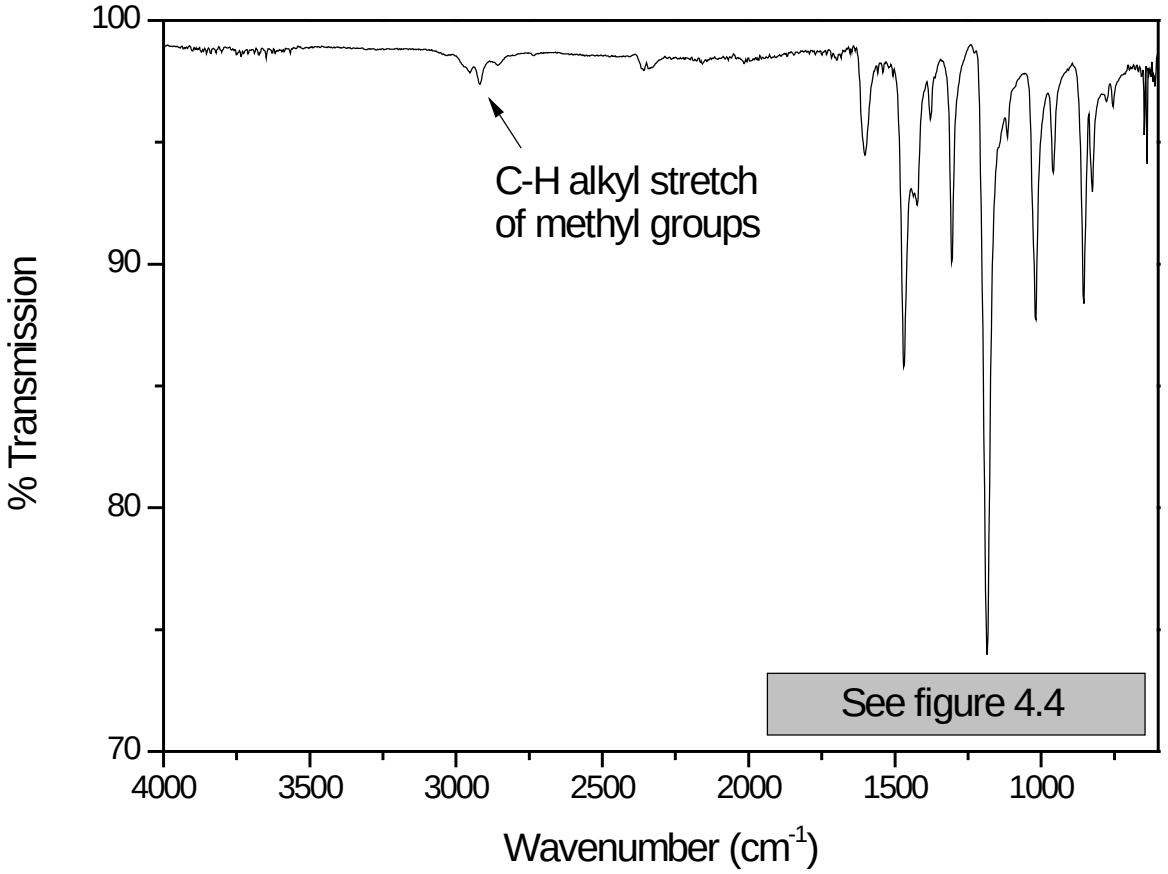

Figure A.2 – Infrared spectrum of CMPPO sample after 1 hour of chloromethylation at 50 ºC

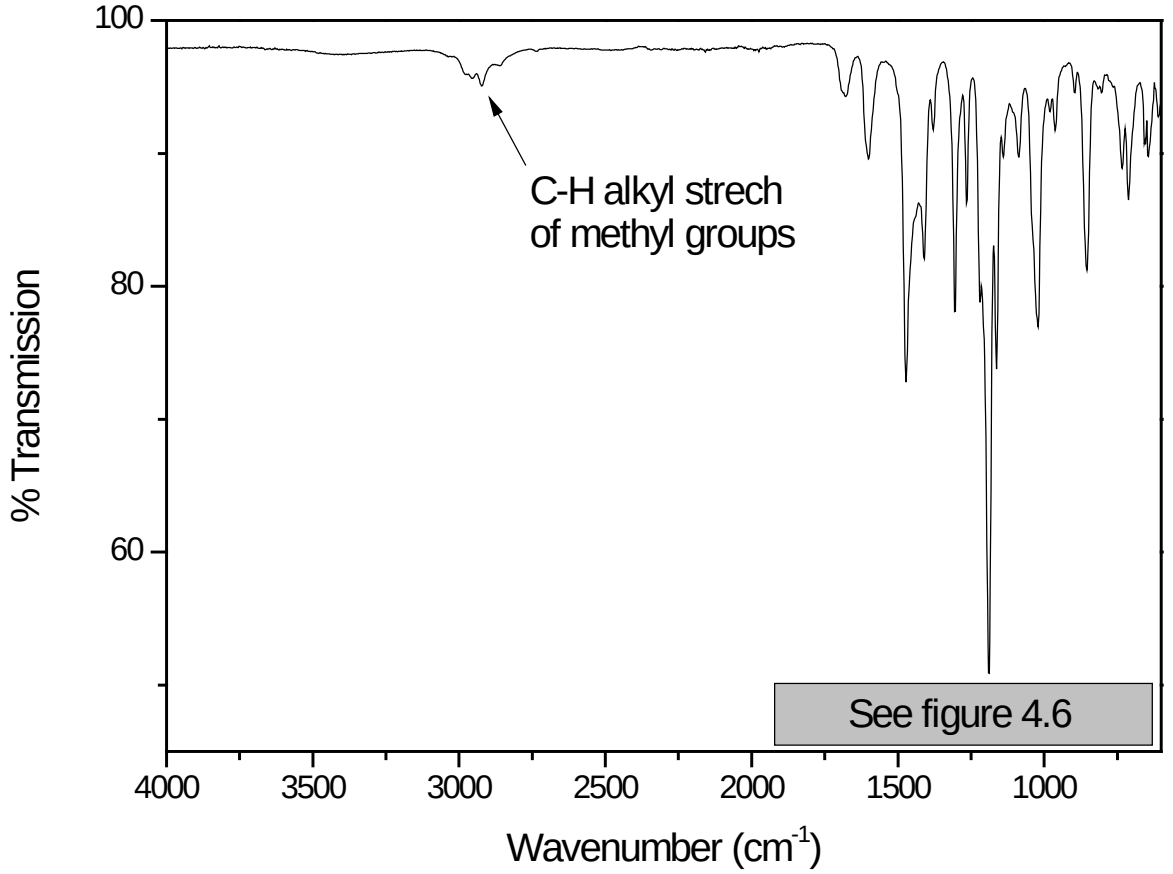

Figure A.3 – Infrared spectrum of QAPPO (1 hour, 50 ºC) immersed 1M KOH for 1 (black) and 3 (red) days

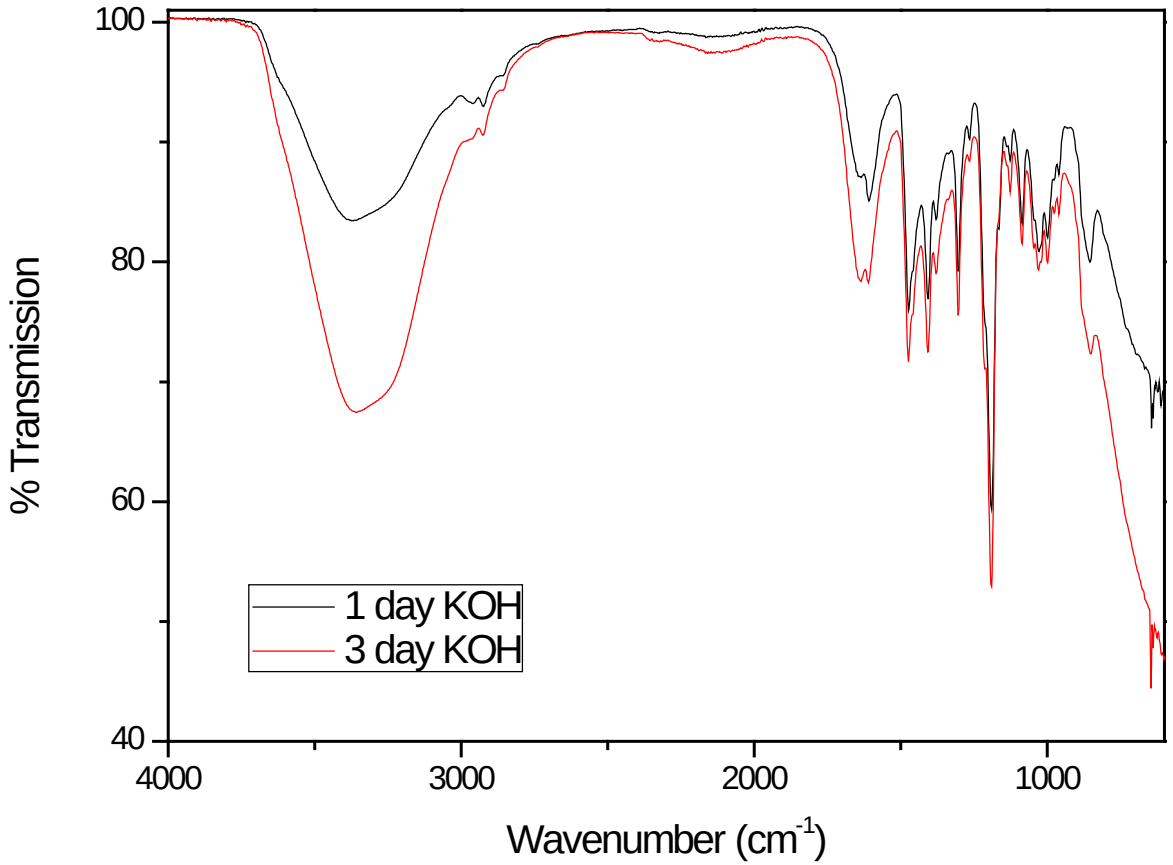

Figure A.4 – Infrared spectrum of CMPPO sample after 2 hours of chloromethylation at 50 ºC

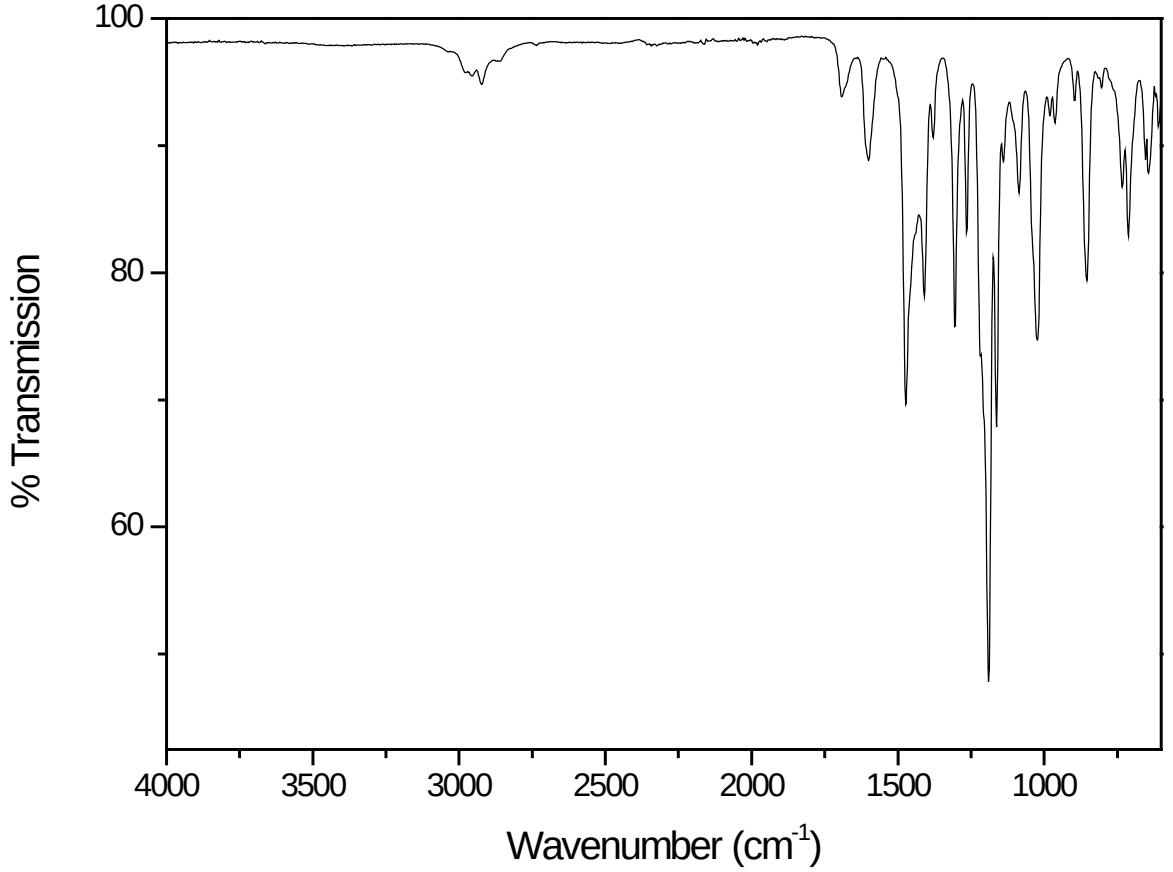

Figure A.5 – Infrared spectrum of CMPPO sample after 3 hours of chloromethylation at 50 ºC

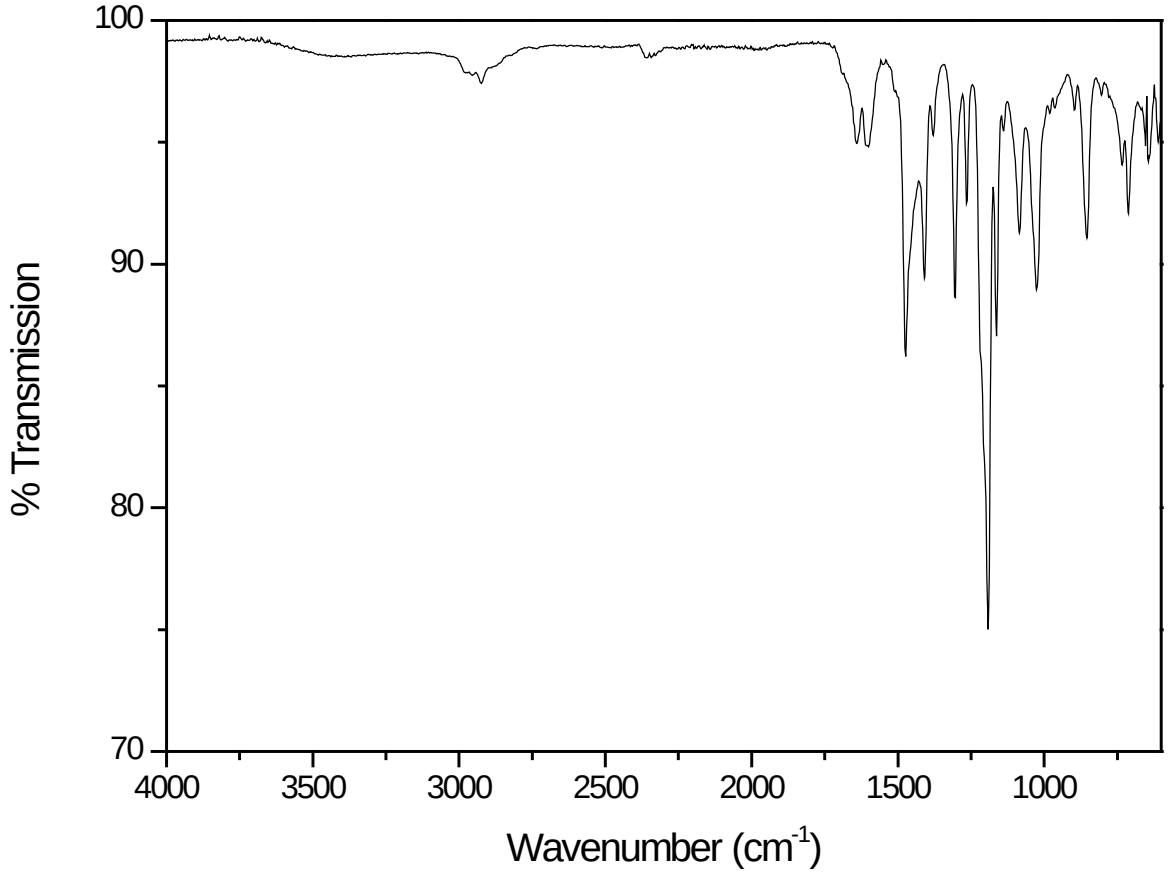

Figure A.6 – Infrared spectrum of CMPPO sample after 4 hours of chloromethylation at 50 ºC

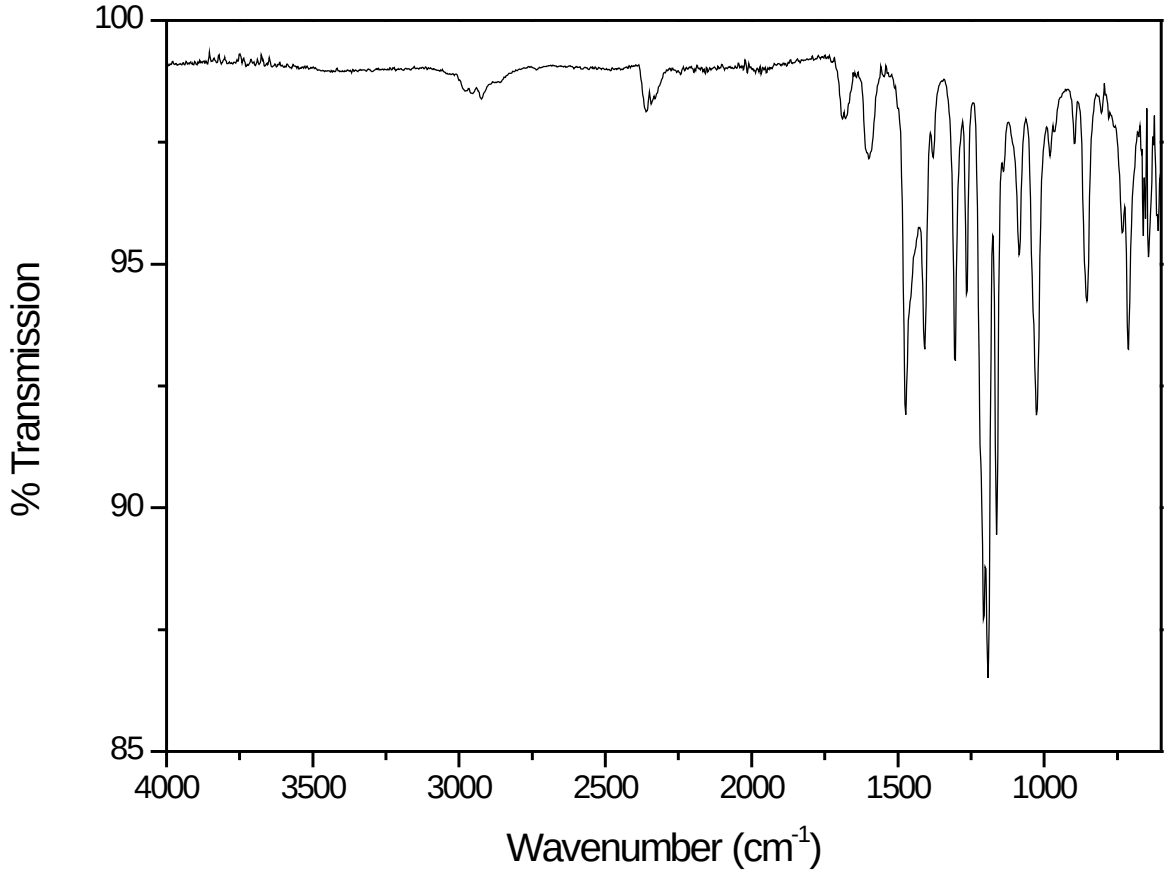

Figure A.7 – Infrared spectrum of QAPPO (4 hr, 50 ºC) before immersion in 1M KOH.

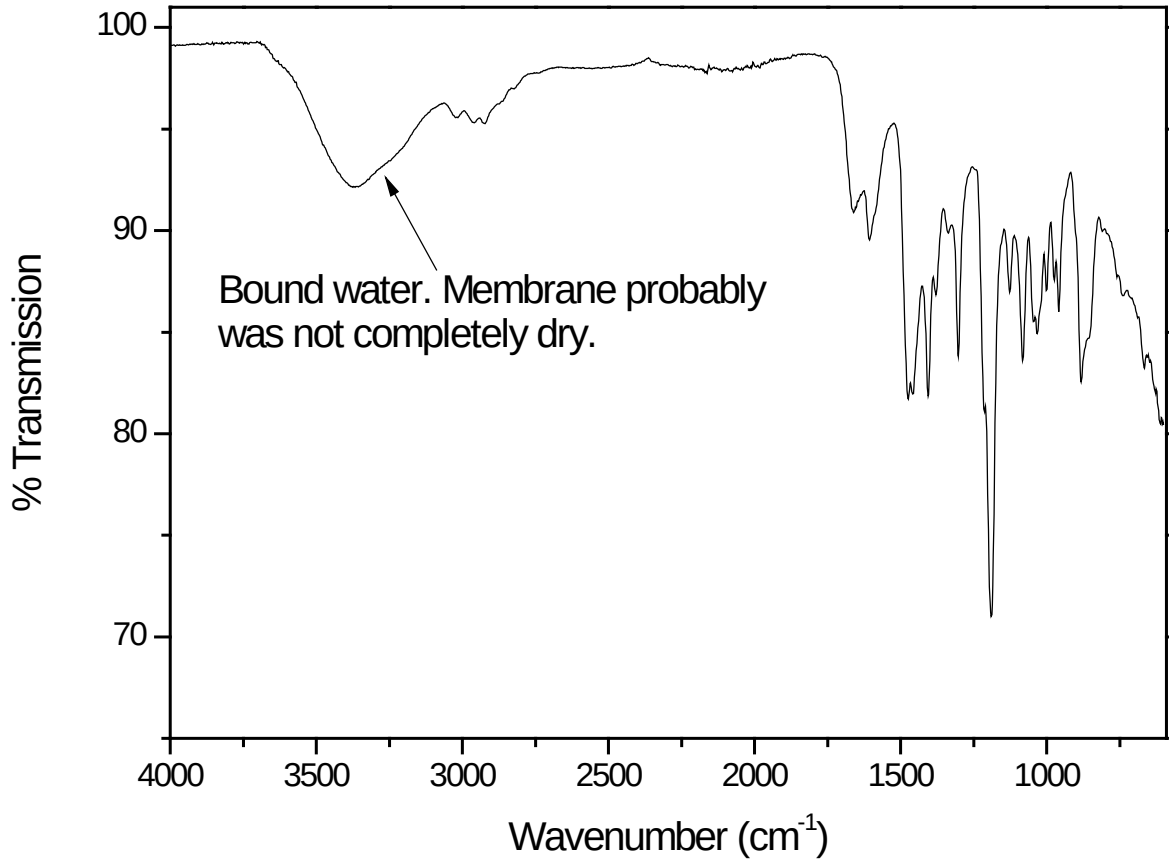

Figure A.8 – Infrared spectrum of QAPPO (4 hour, 50 ºC) after immersion in 1M KOH for 1 (black) and 3 (red) days

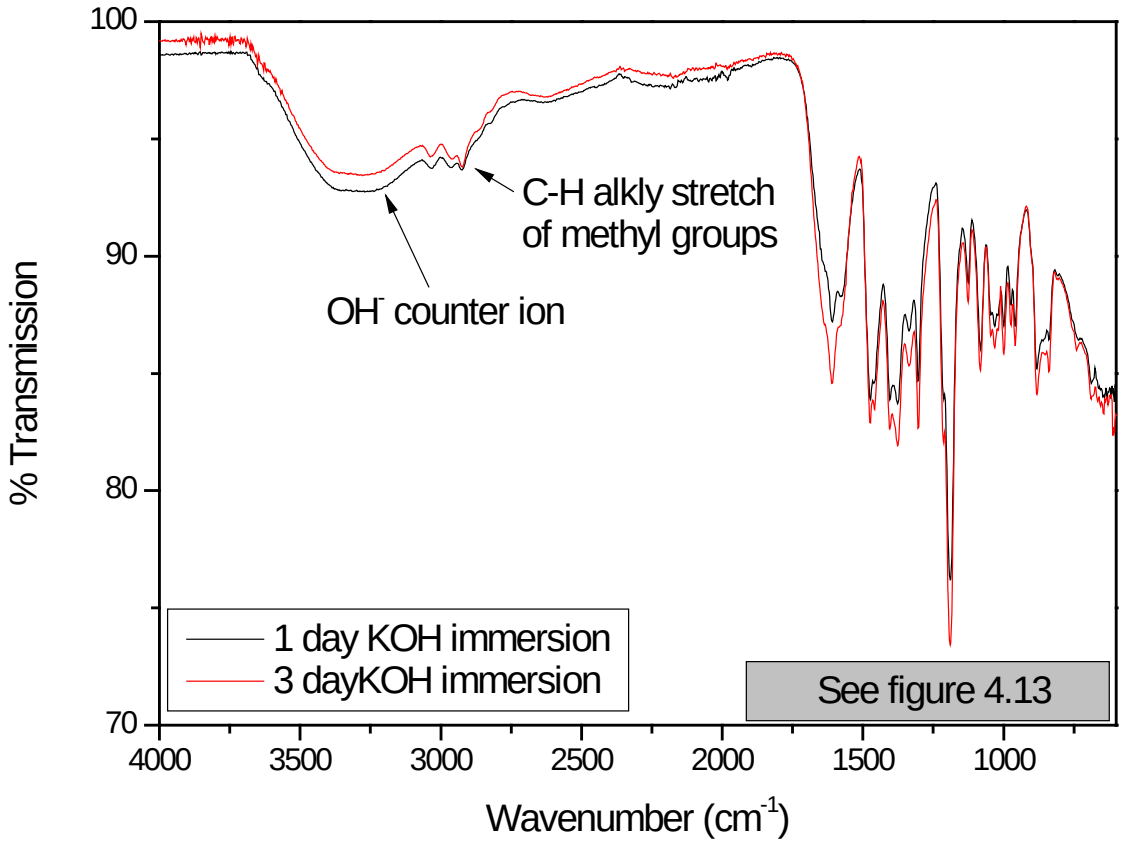

Figure A.9 – Infrared spectrum of QAPPO (4 hour, 50 ºC) cross-linked with diethylamine (1 day in 1M KOH)

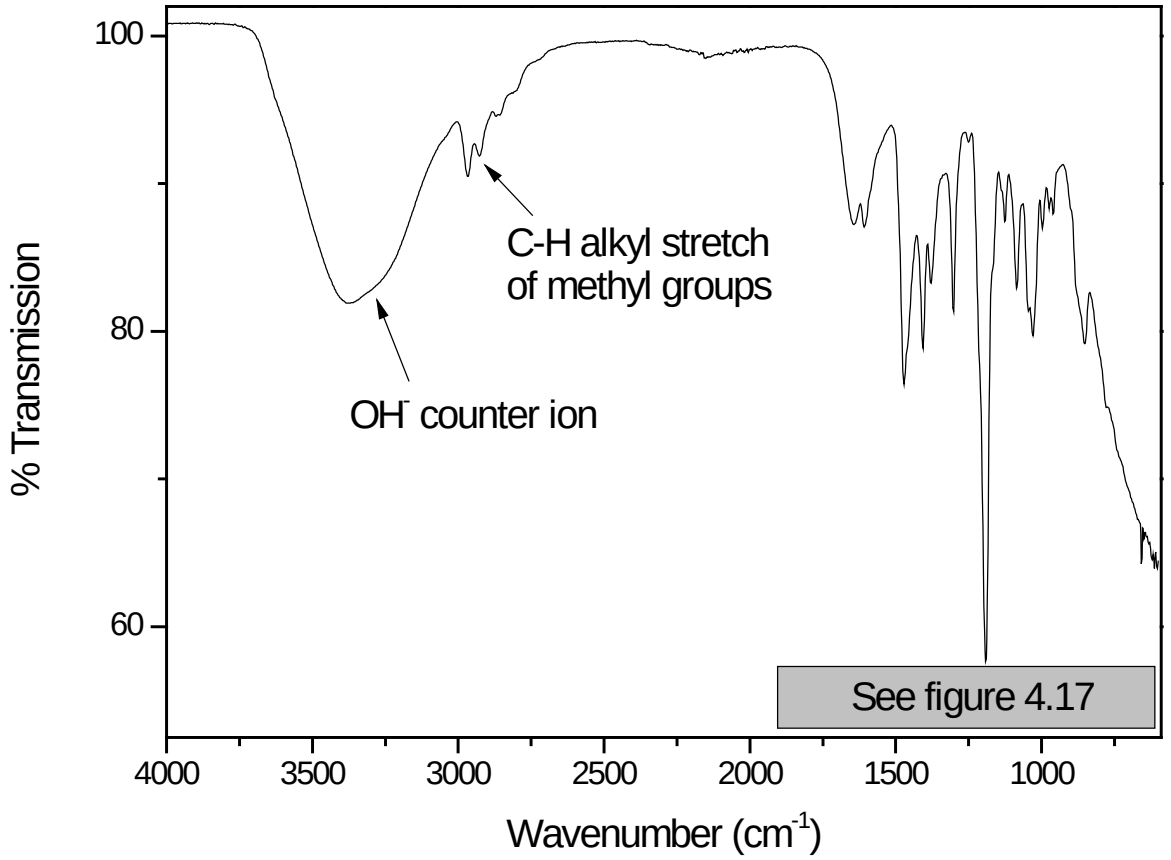

Figure A.10 – Infrared spectrum of QAPPO (4 hr, 50 ºC) cross-linked with diethylamine after a stability test (black) compared to before testing (red, figure A.9)

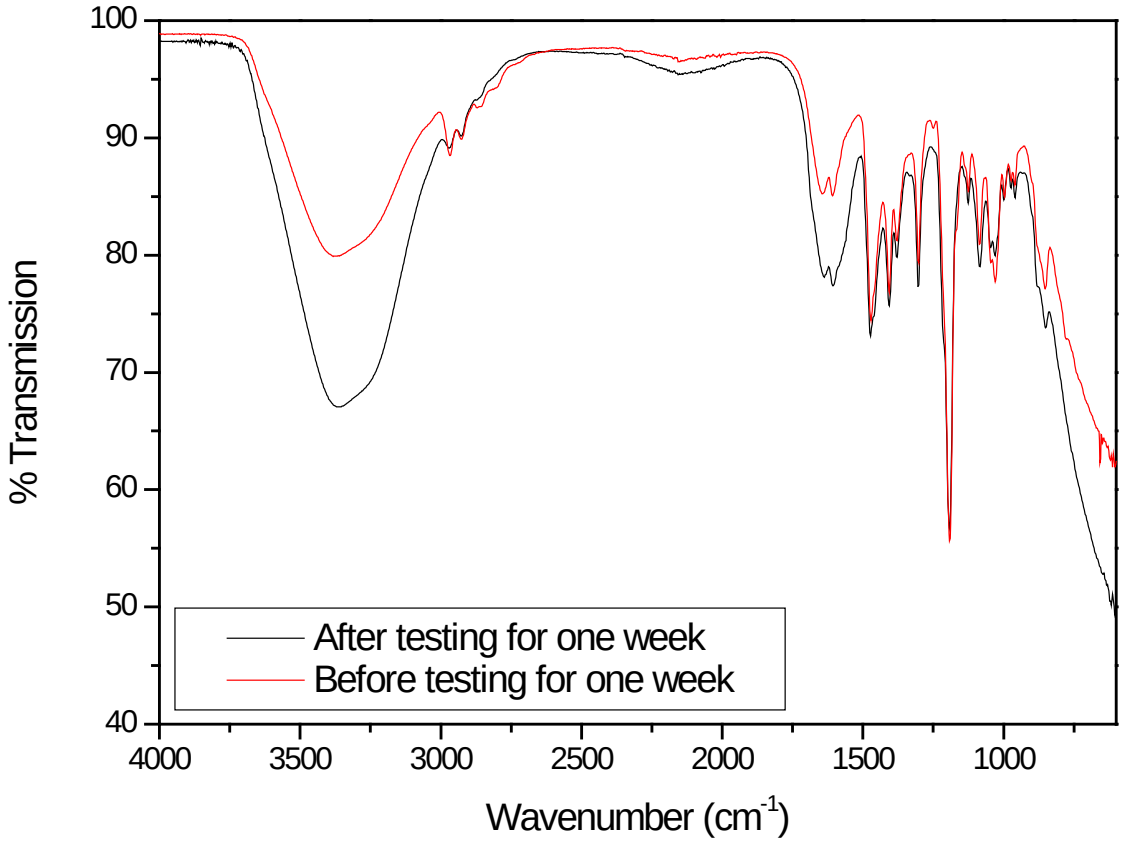

Figure A.11 – Infrared spectrum of over cross-linked CMPPO after 1.5 hours at 60 ºC

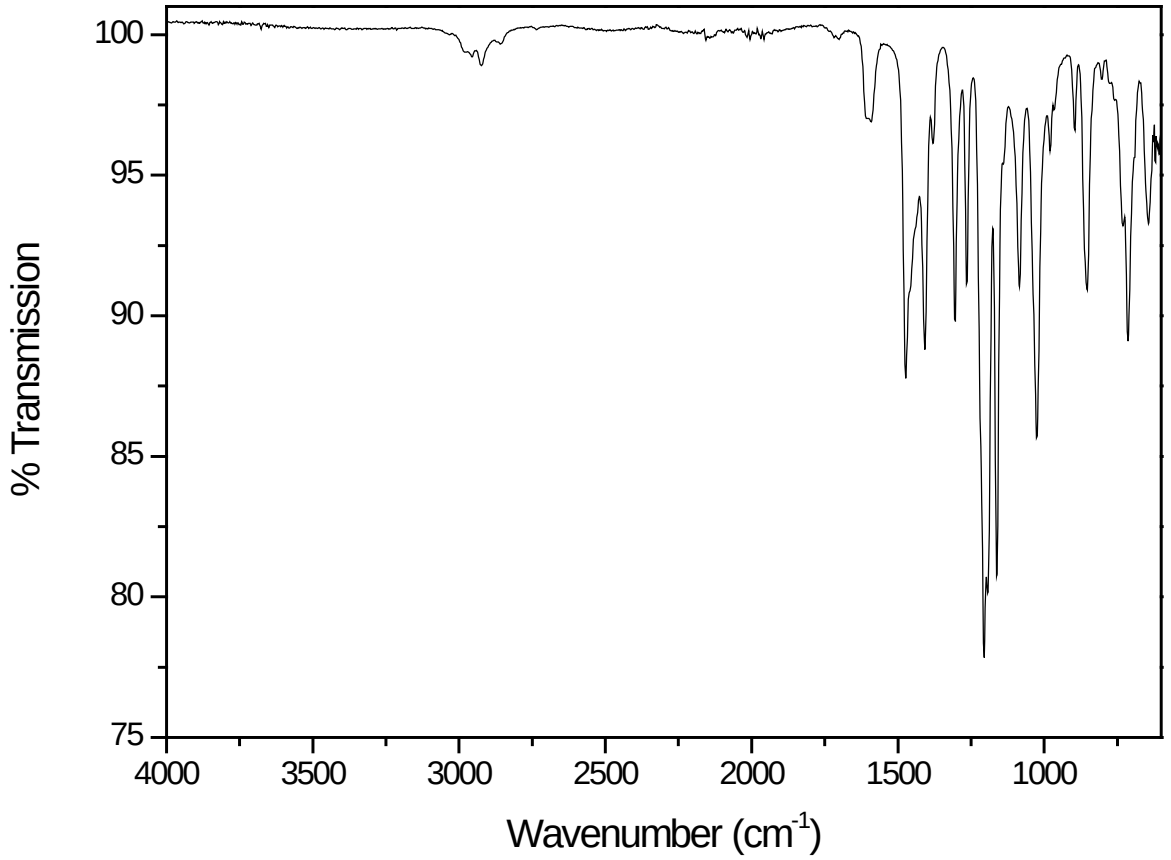

Figure A.12 – Infrared spectrum of CMPPO/CMPS after chloromethylation for 4.5 hours at 50 ºC compared to the batch of CMPPO chloromethylated for 6 hours at 50 ºC.

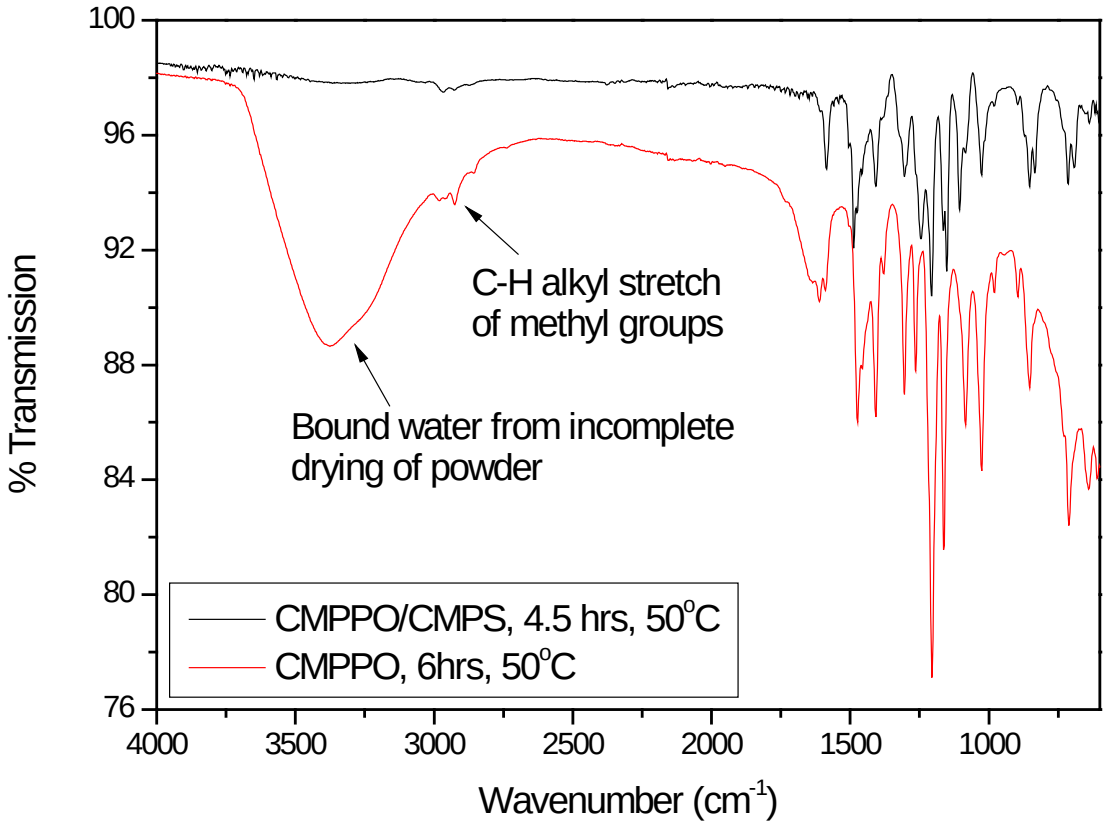

Figure A.13 – Lower section of the infrared spectrum comparison between CMPPO/CMPS after chloromethylation for 4.5 hours at 50 ºC and the batch of CMPPO chloromethylated for 6 hours at 50 ºC.

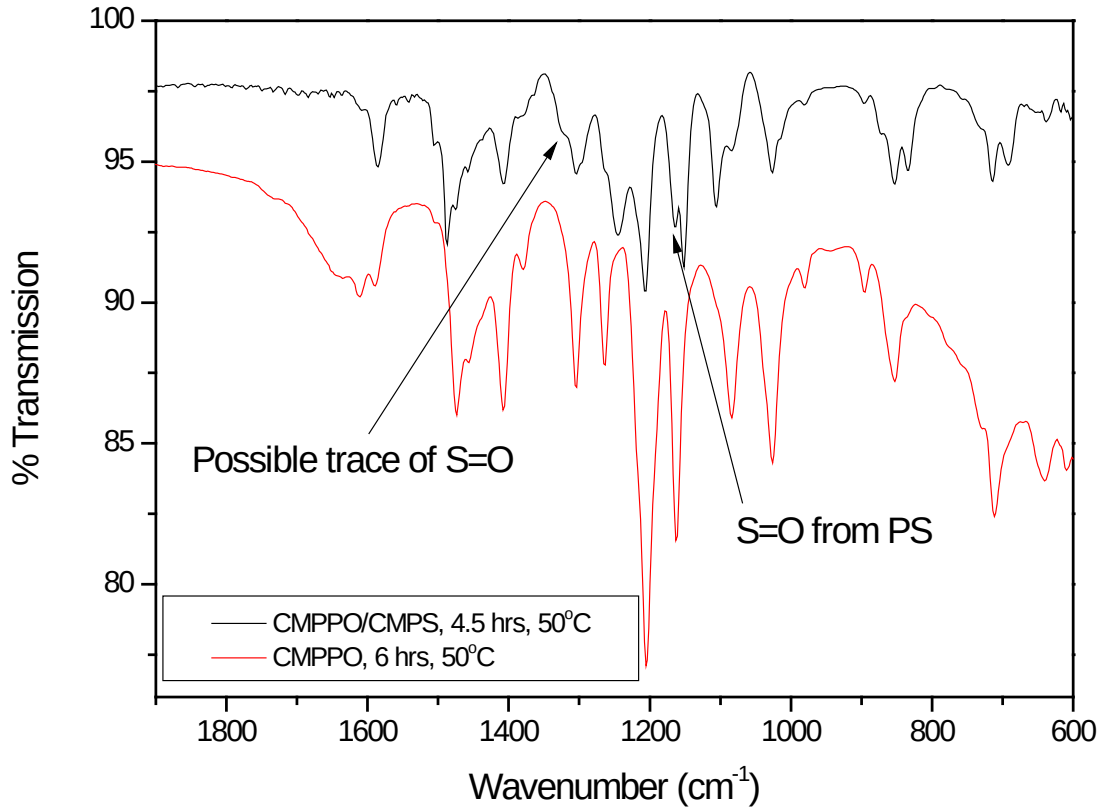

Figure A.14 – Infrared spectrum comparison of PS and CMPS (8 hours, 50 ºC) (MSc project)

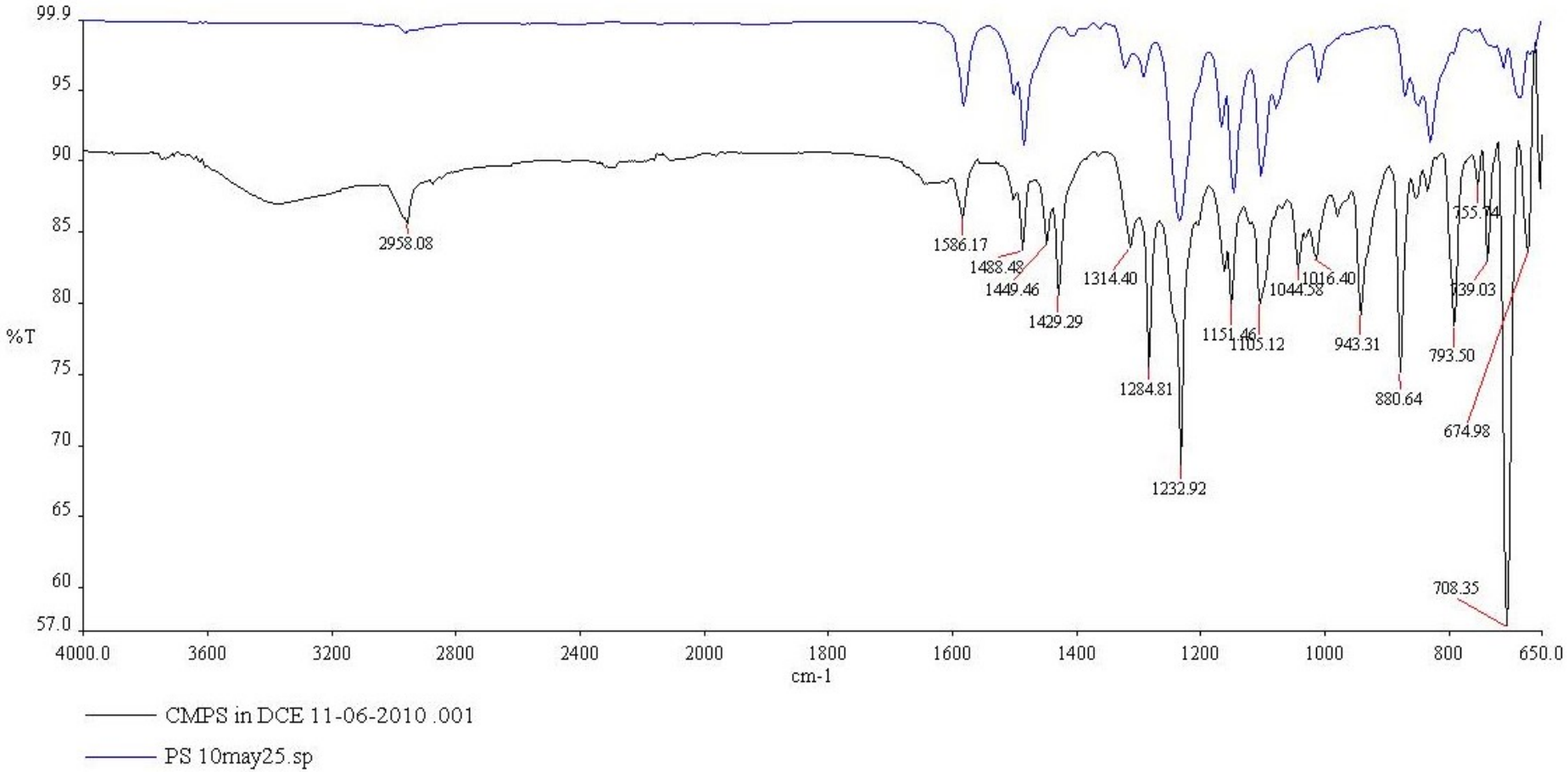

Figure A.15 – Infrared spectrum comparison of QAPS (8 hours, 50 ºC) (MSc project)

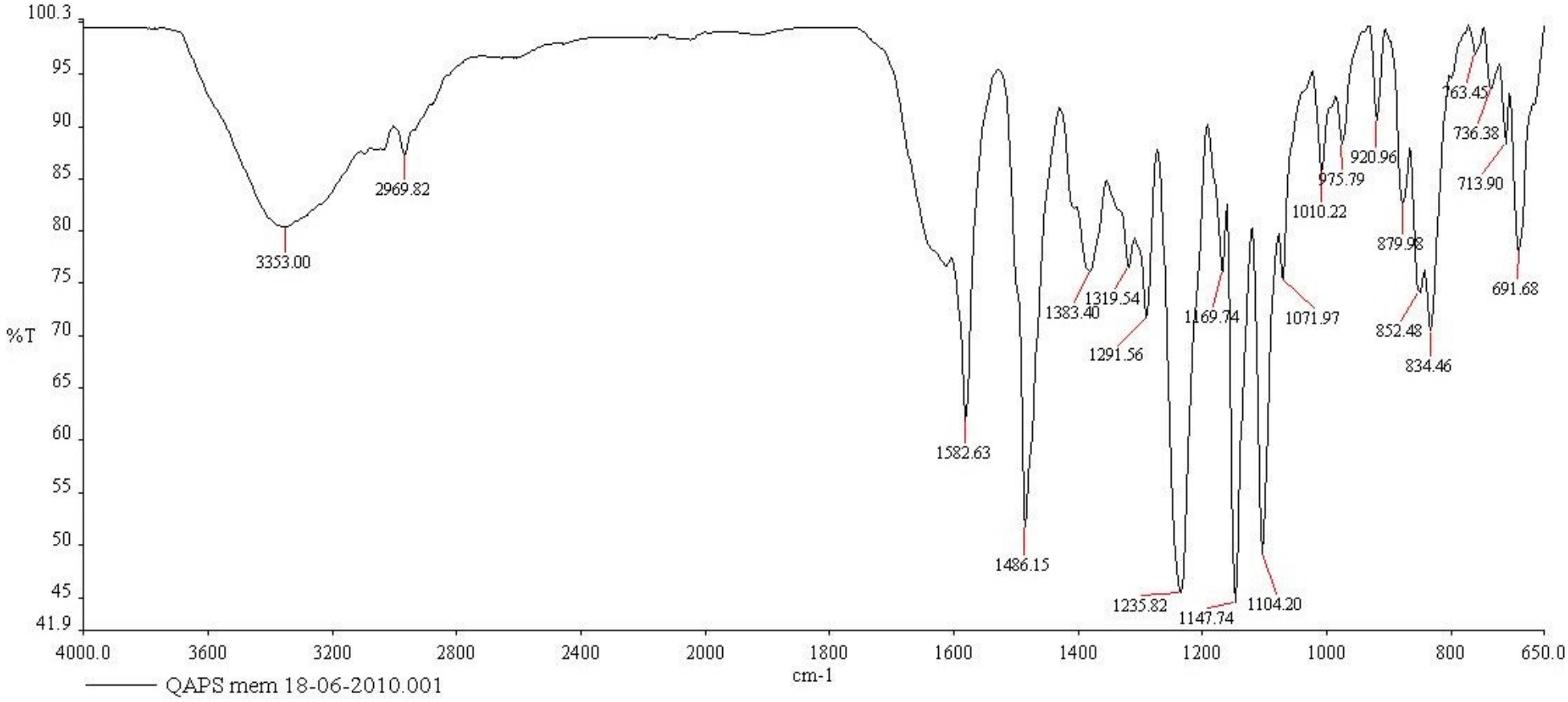

Figure A.16 – Infrared spectrum of QAPPO/QAPS

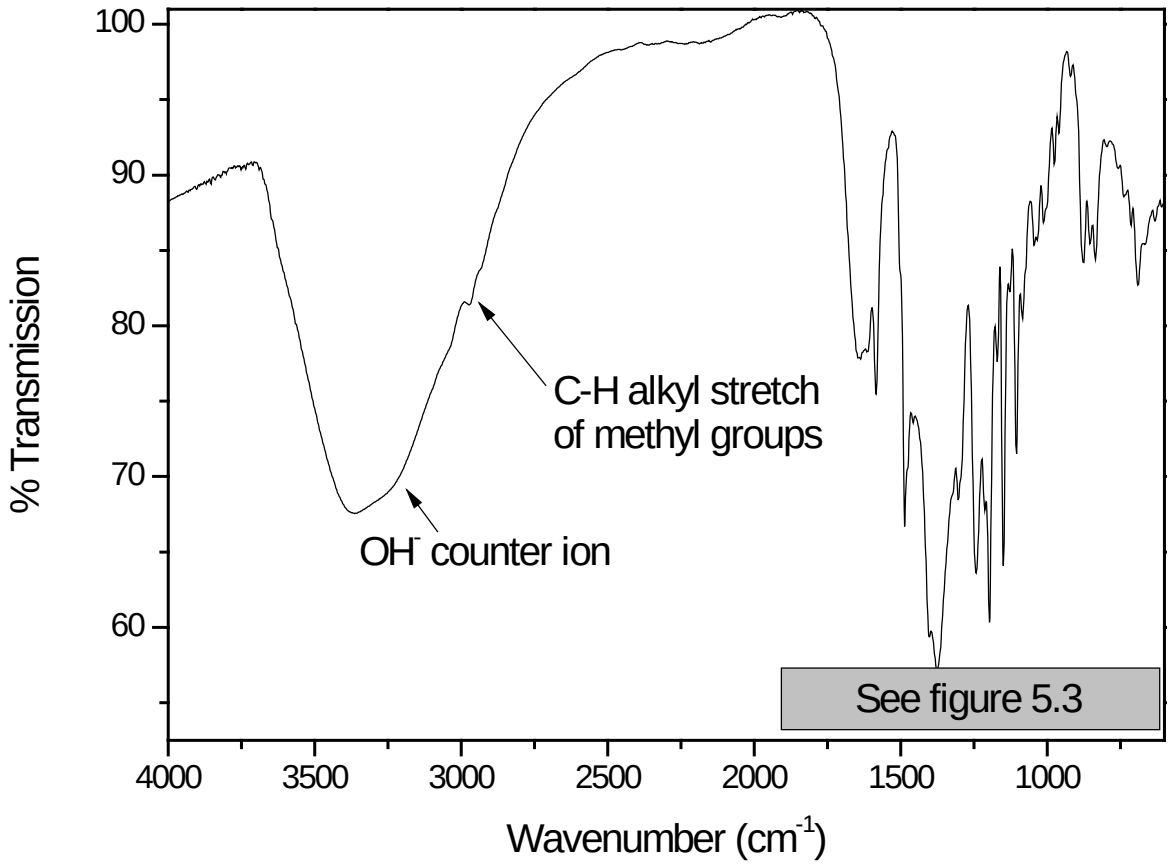

Figure A.17 – Infrared spectrum comparison of QAPPO and QAPPO/PS membranes

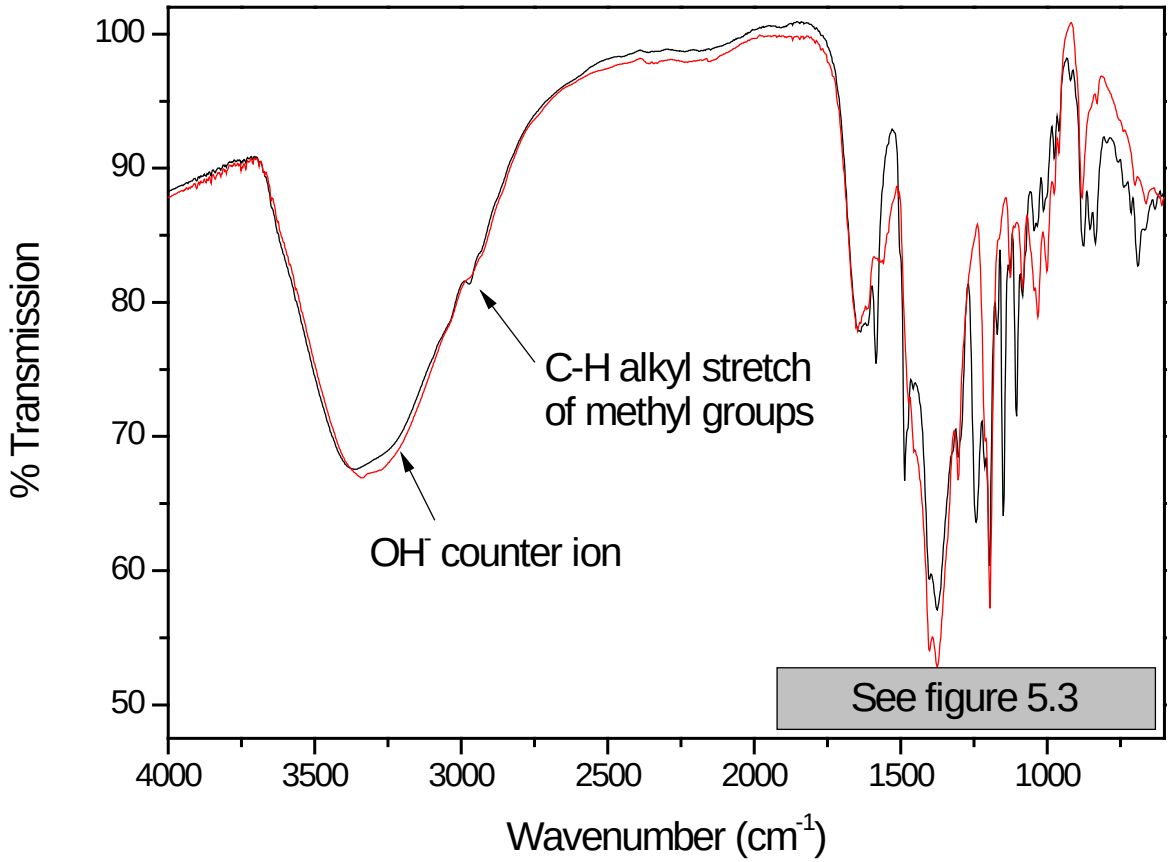

Figure A.18 – Infrared spectrum comparison of "semi gel" QAPPO AEM pre and post immersion in KOH

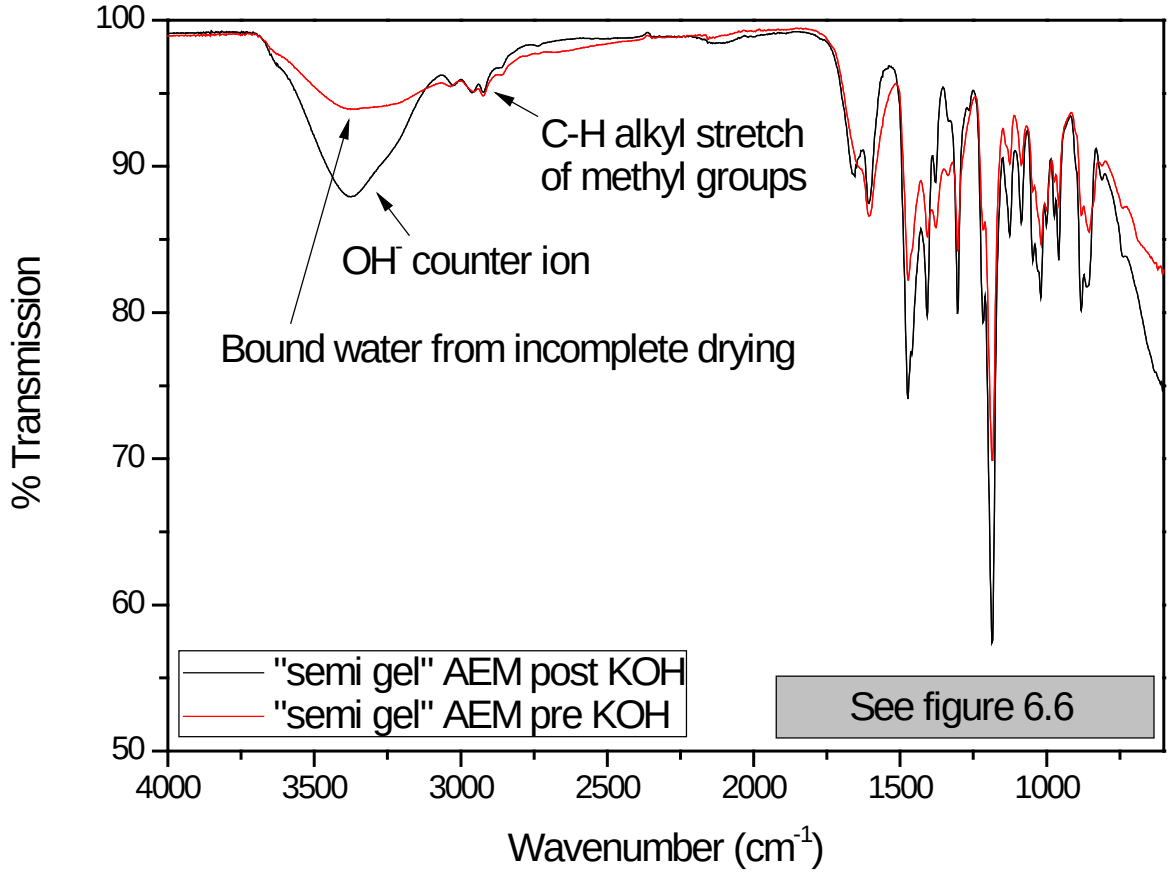

Figure A.19 – Infrared spectrum of "semi gel" QAPPO/PVDF 5% AEM post immersion in KOH

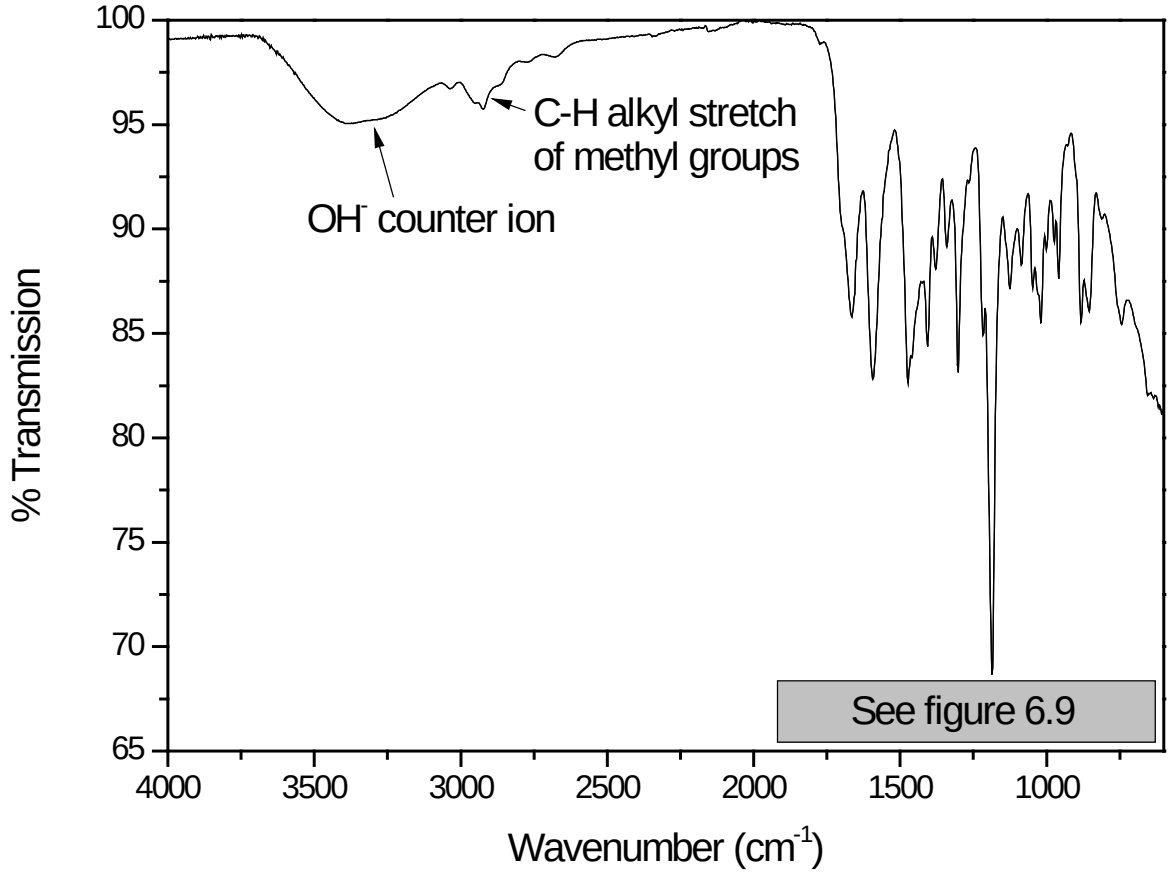

Figure A.20 – Infrared spectrum comparison between the "semi gel" QAPPO supported on PTFE and the unmodified "semi gel" QAPPO AEM.

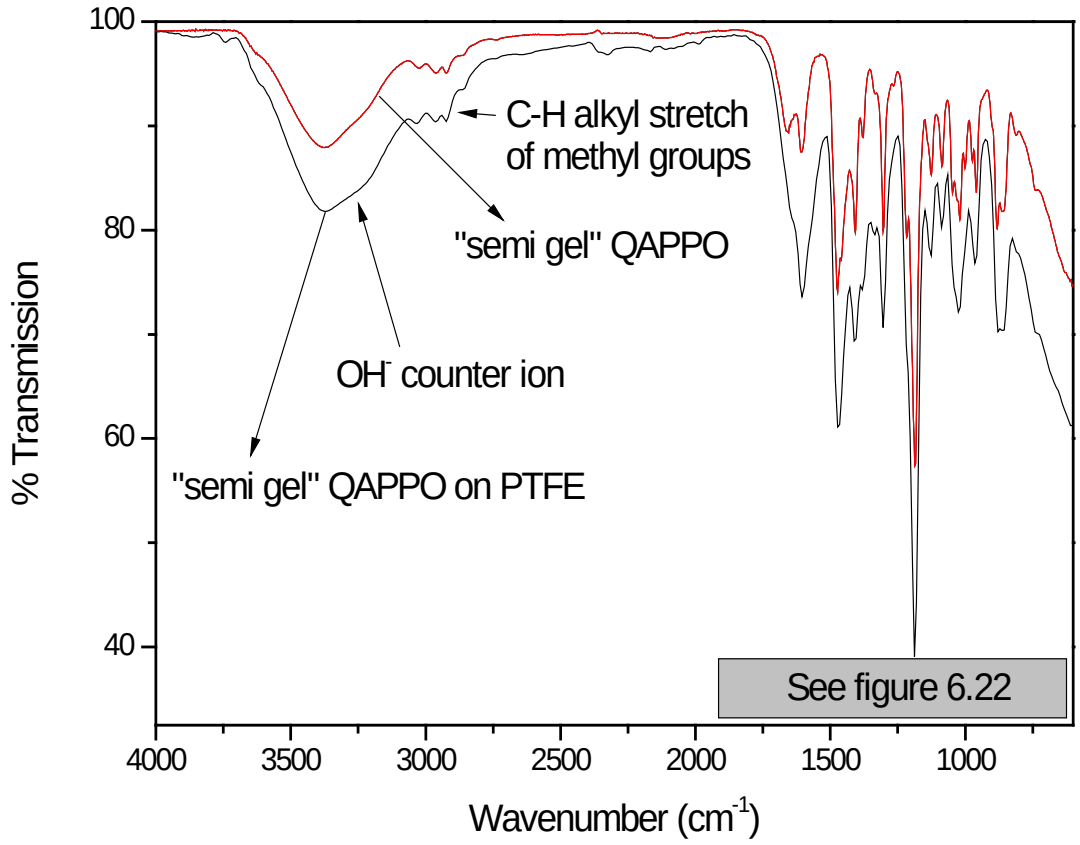

Figure A.21 – Infrared spectrum comparison of "semi gel" QAPPO cross-linked with 10% (blue), 20% (red and 30% (black) of DABCO